

รายงานวิจัยฉบับสมบูรณ์

โครงการการออกแบบและวิเคราะห์ระบบเซลล์เชื้อเพลิงชนิดออกไซด์แข็งสำหรับการผลิต พลังงานไฟฟ้าและความร้อนร่วม

โดย ผู้ช่วยศาสตราจารย์ ดร. อมรชัย อาภรณ์วิชานพ

รายงานวิจัยฉบับสมบูรณ์

โครงการการออกแบบและวิเคราะห์ระบบเซลล์เชื้อเพลิงชนิดออกไซด์แข็งสำหรับการผลิต พลังงานไฟฟ้าและความร้อนร่วม

ผู้วิจัย

สังกัด

ผศ.ดร. อมรชัย อาภรณ์วิชานพ

ภาควิชาวิศวกรรมเคมี คณะวิศวกรรมศาสตร์ จุฬาลงกรณ์มหาวิทยาลัย

สนับสนุนโดยสำนักงานกองทุนสนับสนุนการวิจัย

(ความเห็นในรายงานนี้เป็นของผู้วิจัย สกว. ไม่จำเป็นต้องเห็นด้วยเสมอไป)

บทคัดย่อ

รหัสโครงการ: RSA5480011

ชื่อโครงการ : การออกแบบและวิเคราะห์ระบบเซลล์เชื้อเพลิงชนิดออกไซด์แข็งสำหรับการผลิตพลังงาน

ไฟฟ้าและความร้อนร่วม

ชื่อนักวิจัย: ผู้ช่วยศาสตราจารย์ ดร.อมรชัย อาภรณ์วิชานพ

ภาควิชาวิศวกรรมเคมี คณะวิศวกรรมศาสตร์ จุฬาลงกรณ์มหาวิทยาลัย

E-mail Address: Amornchai.A@chula.ac.th

ระยะเวลาโครงการ : 15 มิถุนายน 2554 – 14 มิถุนายน 2557

งานวิจัยนี้มีวัตถุประสงค์เพื่อวิเคราะห์เชิงทฤษฎีและออกแบบระบบเซลล์เชื้อเพลิงชนิดออกไซด์แข็งเพื่อ ผลิตพลังงานไฟฟ้าและความร้อนร่วม เชื้อเพลิงหมุนเวียนที่สำคัญเช่น ก๊าซชีวภาพ เอทานอล และกลีเซอรอล ถูก นำมาใช้ในการผลิตไฮโดรเจนสำหรับเซลล์เชื้อเพลิง ผลของสภาวะการดำเนินงานที่มีต่อสมรรถนะกระบวนการรี ฟอร์มมิงเชื้อเพลิงถูกศึกษาในแง่ผลได้ของไฮโดรเจน องค์ประกอบของก๊าซผลิตภัณฑ์ที่ได้ การเกิดคาร์บอน สมรรถนะของเซลล์เชื้อเพลิงชนิดออกไซด์แข็งที่ป้อนด้วยก๊าซสังเคราะห์ที่ได้จากกระบวนการรีฟอร์มมิงที่มีการ ป้อนกลับและไม่มีการป้อนกลับก๊าซทิ้งจากขั้วแอโนดถูกวิเคราะห์โดยหลักการเทอร์โมไดนามิก การออกแบบเซลล์ เชื้อเพลิงชนิดออกไซด์แข็งที่เหมาะสมจะพิจารณาจากประสิทธิภาพเชิงไฟฟ้าและความร้อน นอกจากนี้งานวิจัยนี้ ยังได้ศึกษาสมรรถนะของเซลล์เชื้อเพลิงชนิดออกไซด์แข็งที่ทำงานร่วมกับเครื่องกังหันแก๊สและดำเนินการที่ความ ดันสูงโดยมีการนำก๊าซทิ้งจากขั้วแคโทดกลับมาใช้ประโยชน์ การจัดการพลังงานของระบบเซลล์เชื้อเพลิงดังกล่าว จะถูกพิจารณาเพื่อให้เกิดการผลิตกระแสไฟฟ้าสูงสุดและใช้พลังงานความร้อนอย่างมีประสิทธิภาพ

คำหลัก : เซลล์เชื้อเพลิงชนิดออกไซด์แข็ง การผลิตไฮโดรเจน เชื้อเพลิงหมุนเวียน เครื่องรีฟอร์มเมอร์ เครื่อง กังหันแก๊ส การออกแบบกระบวนการ

Abstract

Project Code: RSA5480011

Project Title: Design and analysis of a solid oxide fuel cell system for combined heat and electrical

power generation

Investigator: Assistant Professor Amornchai Arpornwichanop

Department of Chemical Engineering, Faculty of Engineering,

Chulalongkorn University

E-mail Address: Amornchai.A@chula.ac.th

Project Period: 15 June 2011 – 14 June 2014

The aim of this study is to theoretically analyze and design a solid oxide fuel cell (SOFC) system for combined heat and electrical power generation. Several important renewable resources: biogas, ethanol and glycerol, used to produce hydrogen for fuel cell are compared. The effect of operating conditions on the performance of a reforming process is investigated in terms of hydrogen yield, product distribution and carbon formation. The performance of the SOFC system fuelled by synthesis gas derived from the reforming process with non-recycling and recycling of the anode exhaust gas is also investigated based on a thermodynamic analysis. The optimal design of the SOFC system is determined by considering the electrical and thermal efficiencies. Furthermore, the performance of a pressurized SOFC-gas turbine (SOFC-GT) hybrid system with and without a cathode gas recirculation is studied. An energy management of the SOFC-GT system is considered with an aim to achieve the highest electrical generation and efficient thermal energy usage.

Keywords: Solid Oxide Fuel Cell; Hydrogen Production; Renewable Fuels; Reformer; Gas turbine;

Process design

Acknowledgements

The financial support from the Thailand Research Fund on this project is gratefully acknowledged. The author would like to thank the Department of Chemical Engineering, Faculty of Engineering, Chulalongkorn University for providing a good research environment and all the students for their effort and help to complete this project.

Content

Abstract (Thai)	i
Abstract	ii
Acknowledgement	iii
Content	iv
Nomenclature	vi
1. Introduction	1
2. Model of SOFC system	5
2.1. Fuel processor	5
2.2. SOFC model	7
2.3. Gas turbine and compressor	12
2.4. Other units	13
3. Use of different renewable fuels in a steam reformer integrated into a fuel cell: Theoretical analysis and performance comparison	16
3.2. Results and discussion	
3.2.1.Hydrogen production from various fuels	
3.2.2.SOFC system	21
4. Analysis of an Ethanol-Fuelled Solid Oxide Fuel Cell System Using Pa	
4.1. SOFC system	26
4.2. Results and discussion	28
4.2.1.Comparison of SOFC systems with and without anode recycling	
4.2.2.Effects of recirculation ratio and fuel utilization	30
4.2.3.Effects of reformer and SOFC operating temperature	37
4 2 4 Effect of excess air ratio	39

5. Analysis of a pressurized solid oxide fuel cell-gas turbine hybrid power with cathode gas recirculation	-
5.1. Description of SOFC-GT hybrid system	41
5.2. Results and discussion	44
5.2.1.A pressurized SOFC-GT system	44
5.2.2.A pressurized SOFC/GT system with cathode gas recirculation.	49
6. Conclusions	54
7. Project outputs	56
7.1. International Journal publication	56
7.2. International Conferences	57
Reference	60
Appendix	
Appendix A: Publications in international journal	

Nomenclature

 $a_{\rm c}$ activity coefficient of carbon

 $A_{\rm c}$ fuel cell active area (m²)

 $D_{\text{eff,anode}}$ effective gaseous diffusivity through anode (m² s⁻¹)

 $D_{\text{eff.cathode}}$ effective oxygen diffusivity through cathode (m² s⁻¹)

 E^{OCV} open-circuit voltage (V)

 E^0 open-circuit voltage at the standard pressure (V)

 E_{anode} activation energy of anode (kJ mol⁻¹)

 E_{cathode} activation energy of cathode (kJ mol⁻¹)

F Faraday constant (C mol⁻¹)

 \dot{h} enthalpy (kJ mol⁻¹)

 ΔH° standard heat of reaction (kJ mol⁻¹)

j current density (A cm⁻²)

 $j_{0,\text{anode}}$ exchange current density at anode (A m⁻²)

 $j_{0,\text{cathode}}$ exchange current density at cathode (A m⁻²)

 k_{anode} pre-exponential factor of the anode (A m⁻²)

 k_{cathode} pre-exponential factor of cathode (A m⁻²)

 $K_{\rm eq}$ equilibrium constants

LHV_{C,H,OH} low heating value of ethanol (kJ s⁻¹)

n number of electrons transferred

Project: Design and analysis of a solid oxide fuel cell system for combined heat and electrical power generation

Asst. Prof. Amornchai Arpornwichanop, Department of Chemical Engineering, Faculty of Engineering, Chulalongkorn University

 \dot{n} molar flow rate (mol s⁻¹)

 p_i partial pressures of component i (bar)

P operating pressure of SOFC (bar)

 P_{sofc} electrical power output (W)

Q thermal energy (kJ s⁻¹)

R gas constant (kJ mol⁻¹ K⁻¹)

 $R_{\rm ohm}$ total internal resistance (Ω m²)

T temperature (K)

 $U_{\rm f}$ fuel utilization factor

V operating cell voltage (V)

 \dot{z} amount of hydrogen consumed by the electrochemical reaction (mol s⁻¹)

Greek symbols

 α transfer coefficient

 η overpotentials (V)

 λ_{air} excess air ratio

 $\sigma_{\rm anode}$ electronic conductivity of anode (Ω^{-1} m⁻¹)

 σ_{cathode} electronic conductivity of cathode (Ω^{-1} m⁻¹)

 $\sigma_{\text{electrolyte}}$ ionic conductivity of electrolyte ($\Omega^{\text{-1}}$ m⁻¹)

 τ_{anode} thickness of anode (m)

 τ_{cathode} thickness of cathode (m)

 $\tau_{\text{electrolyte}}$ thickness of electrolyte (m)

Project: Design and analysis of a solid oxide fuel cell system for combined heat and electrical power generation

Asst. Prof. Amornchai Arpornwichanop, Department of Chemical Engineering, Faculty of Engineering, Chulalongkorn University

Subscripts

a air channel

conc concentration overpotentials

f fuel channel

i chemical component

j reaction

ohm ohmic loss

r reformer

sofc solid oxide fuel cell

SM steam reforming reaction

TPB three-phase boundary

WGS water gas shift reaction

Chapter 1

Introduction

Fuel cells have been identified as an alternative method to generate power with high efficiency and environmental friendliness when compared to a conventional combustion-based process. Among the various types of fuel cells, the solid oxide fuel cell (SOFC) is the most promising fuel cell technology, as it can be used in a wide range of commercial applications. The high operational temperature of the SOFC (1073–1273 K) results in many advantages; for example, the high-temperature waste heat from a SOFC can be recovered for use in other heat-demanding units in the SOFC system. In addition, different fuels (e.g., methane, methanol, ethanol, etc.) can be directly fed to the SOFC due to the possibility for operation with internal reforming (Patcharavorachot et al., 2010).

Among such renewable fuels, ethanol, biogas and glycerol have received considerable attention (Dou et al., 2009; Mohseni et al., 2012). Ethanol is one of the most attractive raw materials for use in fuel cell hydrogen production because of its non-toxicity and liquid form. Many studies have been devoted to hydrogen production from ethanol (Akande et al., 2006). Sun et al. (2012) studied hydrogen production from ethanol using steam reforming, autothermal reforming and partial oxidation. They found that ethanol steam reforming provides the highest hydrogen yield. A steam-to-ethanol ratio above 6 and temperatures greater than 900 K produce a high hydrogen yield with low carbon monoxide (CO) and carbon formation in the steam reforming environment.

Biogas is also a promising fuel, especially for developing countries. Biogas can be produced by the anaerobic digestion of animal and human waste, agricultural residues,

aquatic weeds and other organic matters and mainly consists of methane (CH₄) and carbon dioxide (CO₂), containing CH₄ up to 60 vol.% (Pandya et al., 1988). To date, use of biogas for hydrogen production process has been widely studied; however, works on the integration of a biogas-based fuel system and a high-temperature fuel cell, such as molten carbonate fuel cells (MCFCs) and solid oxide fuel cells (SOFCs), are quite limited.

Glycerol is another potential fuel for hydrogen production. It is a byproduct of the production of biodiesel, whose consumption is continually increasing. Generally, crude glycerol always contains impurities; however, the purifying process for crude glycerol has a high operational cost and is uneconomic (Demirbas, 2009). The utilization of glycerol for hydrogen production is considered promising (Byrd et al., 2008; Pompeo et al., 2010). For environmental and availability reasons, renewable energy resources have become important alternative fuels in the production of hydrogen.

Many previous works have studied SOFC systems integrated into hydrogen production processes using different fuels. Piroonlerkgul et al. (2008) found that steam is the most suitable reforming agent when biogas is used as fuel. Douvartzides et al. (2004) showed that, in addition to the traditional use of natural gas, ethanol is an attractive fuel for SOFC operation. Tsiakaras and Demin (2001) revealed that the ethanol-fueled SOFCs exhibit the highest theoretical efficiency when operated at 800-1200 K and that the ethanol steam reforming is the most attractive fuel processing system. Farhad et al. (2010) studied biogas-fuelled SOFC systems and observed that the best system thermal and electrical efficiencies can be achieved when the heat generated by an afterburner is used to supply other heat-requiring units in the SOFC system. Because the thermal and electrical efficiencies of SOFC systems depend on the fuel type, the thermal management

Project: Design and analysis of a solid oxide fuel cell system for combined heat and electrical power generation

and performance of SOFC systems using different fuels should be studied in detail to select the best fuel for different SOFC applications.

When considering the operating parameters of SOFC systems, it has been reported that the fuel utilization is the most important parameter affecting the performance of SOFC. A SOFC operated at high fuel utilization can provide high electrical efficiency. However, at high fuel utilization, more hydrogen is consumed by the electrochemical reactions, and the fuel stream at the SOFC fuel channel is thus diluted by steam (Aguiar et al., 2004). A hydrogen deficiency due to the unbalanced fuel flowing through the SOFC causes a larger buildup of nickel oxide (Nehter, 2007) as well as corrosion on the carbon plate (Nishikawa et al., 2008). Therefore, it is reasonable to operate the SOFC at a moderate fuel utilization. Under this condition, the SOFC can produce electrical power together with a high-temperature exhaust gas that contains useful remaining fuel (i.e., hydrogen and carbon monoxide). Typically, the exhaust gases from fuel and air channels are burnt in an afterburner to produce more heat, which is used to preheat the fuel stream and supplied to the steam reformer. Although the combustion of exhaust gases can increase the thermal efficiency of the SOFC system, the fuel stream is utilized inefficiently. To improve the overall SOFC performance, a SOFC system with anode exhaust gas recycling has been proposed in the literatures (Granovskii et al., 2007; Shekhawat et al., 2007; Onda et al., 2003). A portion of anode exhaust gas containing useful fuels, i.e., hydrogen and carbon monoxide, is recirculated to mix with the inlet fuel before it is fed to the reformer, whereas the rest of the anode exhaust gas is burnt with the cathode exhaust gas in the afterburner. Interestingly, it is noteworthy that the steam produced by the electrochemical reaction in the anode exhaust gas can be further used as a reagent for steam reforming and thus the requirement for fresh steam can be reduced (Peter et al., 2002). Shekhawat et al. (2007) demonstrated that the utilization of the anode exhaust gas in the SOFC system integrated with the catalytic partial oxidation of diesel can reduce the carbon formation and increase the hydrogen concentration in the reformate gas. Although the SOFC system with anode exhaust gas recycling was previously studied as mentioned above, there are few studies that investigate in detail the effect of utilizing the anode exhaust gas on the reforming process and the SOFC system performance. This understanding allows for the improvement of the overall SOFC system efficiency.

The aim of this study is to theoretically analyze a SOFC system integrated with a steam reforming process and compare several important renewable resources for hydrogen production: biogas, ethanol and glycerol. The effect of operating conditions on the reformer performance is investigated in terms of hydrogen yield, product distribution and carbon formation. The performance of the SOFC system fuelled by synthesis gas derived from a reforming process with non-recycling and recycling of the anode exhaust gas is also investigated based on a thermodynamic analysis. The optimal design of the SOFC system is determined by considering the electrical and thermal efficiencies. Furthermore, the performance of a pressurized SOFC-GT hybrid system with and without a cathode gas recirculation is studied. An energy management of the SOFC-GT system is considered with an aim to achieve the highest electrical generation and thermal energy usage. Effect of the recirculation ratio of cathode exhaust gas on the system efficiency is also investigated.

Project: Design and analysis of a solid oxide fuel cell system for combined heat and electrical power generation

Chapter 2

Model of SOFC system

2.1 Fuel processor

The main reactions that occur in the steam reformer fed by ethanol as an example fuel for hydrogen production are shown below (Freni et al., 1996):

$$C_2H_5OH + H_2O \leftrightarrow 4H_2 + 2CO \tag{1}$$

$$CO + H_2O \leftrightarrow H_2 + CO_2 \tag{2}$$

$$CO + 3H_2 \leftrightarrow CH_4 + H_2O \tag{3}$$

The equilibrium composition of the synthesis gas at the outlet of the steam reformer can be determined based on a thermodynamic analysis using a stoichiometric approach. The equilibrium constants of each reaction (Eqs. (1)-(3)) can be written as:

$$K_{\text{eq,SE}} = \frac{p_{\text{CO,r}}^2 p_{\text{H}_2,\text{r}}^4}{p_{\text{C}_2\text{H}_5\text{OH},\text{r}} p_{\text{H}_2\text{O},\text{r}}}$$
(4)

$$K_{\text{eq,WGS}} = \frac{p_{\text{CO}_2,r} p_{\text{H}_2,r}}{p_{\text{CO},r} p_{\text{H}_2,r}}$$
 (5)

$$K_{\text{eq,MR}} = \frac{p_{\text{CH}_4,r} p_{\text{H}_2\text{O,r}}}{p_{\text{CO,r}} p_{\text{H}_2,r}^3}$$
 (6)

where $K_{\text{eq},j}$ represents the equilibrium constant associated with reaction j and $p_{i,r}$ is the partial pressure of component i in the steam reformer.

The equilibrium constants of all the reactions can be determined by the Van't Hoff equation:

$$\frac{d\ln K}{dT} = \frac{\Delta H^{\circ}}{RT^2} \tag{7}$$

The molar flow rates of each component in the ethanol steam reformer are given by the following expressions:

$$n_{\text{EtOH,r}} = a - x_1 \tag{8}$$

$$n_{\text{H-O.r}} = b + c - x_1 - x_2 + x_3 \tag{9}$$

$$n_{\rm H_2,r} = d + 4x_1 + x_2 - 3x_3 \tag{10}$$

$$n_{\text{CO}_{x}} = g + 2x_{1} - x_{2} - x_{3} \tag{11}$$

$$n_{\rm CH_4,r} = m + x_3 \tag{12}$$

$$n_{\text{CO}_2,r} = e + x_2 \tag{13}$$

$$n_{\text{total,r}} = \sum_{i=1}^{6} n_i = a + b + c + d + e + g + m + 4x_1 - 2x_3$$
 (14)

where x_1 , x_2 and x_3 are the extent of reactions of Eqs. (1)–(3) and a and b represent the inlet feed flows of ethanol and water fed to the steam reformer, respectively. When recycling the anode exhaust gas, c, d, e, g and m represent the inlet recycle flows of water, hydrogen, carbon dioxide, carbon monoxide and methane to the steam reformer, respectively.

The following three reactions, i.e., the Boudouard reaction (Eq. (15)), methane cracking (Eq. (16)) and CO reduction (Eq. (17)), are the most probable reactions that can lead to the formation of carbon in the ethanol reforming system:

$$2CO \leftrightarrow CO_2 + C$$
 (15)

$$CH_4 \leftrightarrow 2H_2 + C$$
 (16)

$$CO + H_2 \leftrightarrow H_2O + C$$
 (17)

In this study, the carbon formation is examined by using a thermodynamic analysis that considers the Boudouard reaction because it presents the lowest value of the Gibbs free energy. The possibility of the carbon formation is determined by the value of the carbon activity, defined as:

$$a_{\rm c} = \frac{K_{\rm b} p_{\rm CO,r}^2}{p_{\rm CO,r}}$$
 (18)

where a_c is the activity coefficient of carbon and K_b represents the equilibrium constant for the Boudouard reaction. If the carbon activity is greater than unity, the system is not in equilibrium and carbon formation is present. When the carbon activity equals to unity, the system is in equilibrium. Finally, when the carbon activity is less than unity, the formation of carbon is thermodynamically impossible in the system. It is noted that the carbon activity is only the indicator for determining the presence of carbon in the system and thus the amount of carbon formation cannot be examined.

The heat required for the steam reformer operation can be computed from the energy balance equation around the reformer:

$$Q_{SR} = (\sum_{o} \dot{n}_{8} \dot{h}_{8}) - (\sum_{i} \dot{n}_{7} \dot{h}_{7})$$
(19)

2.2 SOFC model

The synthesis gas obtained from the ethanol steam reformer consists of CH₄, H₂, H₂O, CO, and CO₂ and is fed to a fuel channel of the SOFC. Because the SOFC is operated at high temperatures, a steam reforming reaction of methane (Eq. (20)) and a water gas shift reaction (Eq. (21)) can occur within the SOFC stack. Furthermore, the use of Ni–cermet as the anode can provide sufficient activity for the steam reforming reaction.

Steam reforming:
$$CH_4 + H_2O \leftrightarrow CO + 3H_2$$
 (20)

Project: Design and analysis of a solid oxide fuel cell system for combined heat and electrical power generation

/

Water gas shift:
$$CO + H_2O \leftrightarrow CO_2 + H_2$$
 (21)

Hydrogen is produced from the ethanol steam reformer as well as from the methane reforming and water gas-shift reactions on the anode side and is consumed by the oxidation reaction (Eq. (22)) to generate steam and electrons. Oxygen in the air that is fed at the cathode side is reduced to oxygen ions (Eq. (23)) that migrate through the electrolyte. The overall electrochemical reaction occurring within the SOFC is shown in Eq. (24). The electrons flow from the anode to the cathode to produce direct-current electricity.

Anode:
$$H_2 + O^{2-} \rightarrow H_2O + 2e^{-}$$
 (22)

Cathode:
$$0.5O_2 + 2e^- \rightarrow O^{2-}$$
 (23)

Overall reaction:
$$H_2 + 0.5O_2 \rightarrow H_2O$$
 (24)

The molar flow rates of each component at the SOFC outlet can be determined based on the reaction equilibrium. The relationships between the thermodynamic equilibrium constants and gaseous components for the steam reforming and water gas shift reactions in the SOFC stack are shown in Eqs. (25) and (26), respectively.

$$K_{\text{eq,SM}} = \frac{p_{\text{CO,sofc}} p_{\text{H}_2,\text{sofc}}^3}{p_{\text{CH}_4,\text{sofc}} p_{\text{H}_2\text{O,sofc}}}$$
(25)

$$K_{\text{eq,WGS}} = \frac{p_{\text{CO}_2,\text{sofc}} p_{\text{H}_2,\text{sofc}}}{p_{\text{CO},\text{sofc}} p_{\text{H}_2,\text{sofc}}}$$
(26)

where $p_{i,sofe}$ is the partial pressure of species i at the SOFC outlet.

For the SOFC operation, hydrogen is consumed by the electrochemical reaction (\dot{z}). The consumption of hydrogen is related to a fuel utilization factor ($U_{\rm f}$) and the inlet gas compositions, as expressed in Eq. (27).

$$U_{\rm f} = \frac{\dot{z}}{(4\dot{n}_{\rm CH_A} + \dot{n}_{\rm H_A} + \dot{n}_{\rm CO})} \tag{27}$$

The current density (j) generated by the fuel cell involves the decrease of hydrogen by the electrochemical reaction at the anode side (Eq. (28)):

$$j = \frac{2F\dot{z}}{A_c} \tag{28}$$

where F is the Faraday constant and $A_{\rm c}$ is the fuel cell active area.

The theoretical open-circuit voltage or the reversible cell voltage computed by the difference between the thermodynamic potentials of the electrode reactions can be expressed by the Nernst equation:

$$E^{\text{OCV}} = E^{0} - \frac{RT}{2F} \ln(\frac{P_{\text{H}_{2}\text{O}}}{P_{\text{H}_{2}}P_{\text{O}_{2}}^{0.5}})$$
 (29)

where E^0 is the open-circuit voltage at standard pressure and is a function of the operating temperature, expressed as:

$$E^{0} = 1.253 - 2.4516 \times 10^{-4} T(K) \tag{30}$$

The operating cell voltage or actual fuel cell voltage (V) is always lower than its open-circuit voltage due to the internal voltage losses encountered in real fuel cell operation (Eq. (31)). There are three dominant voltage losses, which are the function of the temperature, current density and substance concentrations.

$$V = E - \eta_{\text{act}} - \eta_{\text{ohm}} - \eta_{\text{conc}}$$
(31)

Ohmic losses (η_{ohm}) occur due to the resistance to the flow of ions in the electrolyte and the resistance to the flow of electrons through the electrodes and current collectors. This loss is linearly correlated with the voltage drop and current density (Eq. (32)).

$$\eta_{\rm ohm} = jR_{\rm ohm} \tag{32}$$

where R_{ohm} is the internal resistance, which depends on the conductivity and thickness of the individual layers as shown below:

$$R_{\text{Ohm}} = \frac{\tau_{\text{anode}}}{\sigma_{\text{anode}}} + \frac{\tau_{\text{electrolyst}}}{\sigma_{\text{electrolyst}}} + \frac{\tau_{\text{cathode}}}{\sigma_{\text{cathode}}}$$
(33)

where $au_{\rm anode}$, $au_{\rm cathode}$ and $au_{\rm electrolyte}$ are the thickness of the anode, cathode and electrolyte layers, respectively. $au_{\rm anode}$ and $au_{\rm cathode}$ are the electronic conductivity of the anode and cathode, respectively, and $au_{\rm electrolyte}$ is the ionic conductivity of the electrolyte.

The concentration overpotentials (η_{conc}) are caused by a decrease in the substances at the surface of the electrodes due to the resistance to mass transport. These overpotentials become significant at high current densities because the rate of hydrogen consumption at the reaction sites is higher than that of diffusion of the reactant through the porous electrode to the reaction sites (Aguiar et al., 2004; Patcharavorachot et al., 2008). These overpotentials can be expressed as:

$$\eta_{\text{conc}} = \eta_{\text{conc,anode}} + \eta_{\text{conc,cathode}}$$
(34)

$$\eta_{\text{conc,anode}} = \frac{RT}{2F} \ln \left(\frac{p_{\text{H}_2\text{O,TPB}} p_{\text{H}_2,f}}{p_{\text{H}_2\text{O,f}} p_{\text{H}_2,\text{TPB}}} \right)$$
(35)

$$\eta_{\text{conc,cathode}} = \frac{RT}{4F} \ln \left(\frac{p_{O_2,a}}{p_{O_{2,\text{TPB}}}} \right)$$
 (36)

The partial pressures of H_2 , H_2O , and O_2 at the three-phase boundaries can be determined by using a gas transport model in porous media as shown in the following expressions:

$$p_{\rm H_2,TPB} = p_{\rm H_2,f} - \frac{RT\tau_{\rm anode}}{2FD_{\rm eff, anode}} j \tag{37}$$

$$p_{\rm H_2O,TPB} = p_{\rm H_2O,f} + \frac{RT\tau_{\rm anode}}{2FD_{\rm eff,anode}} j$$
(38)

Project: Design and analysis of a solid oxide fuel cell system for combined heat and electrical power generation

$$p_{\text{O}_2,\text{TPB}} = P - \left(P - p_{\text{O}_2,a}\right) \exp\left(\frac{RT\tau_{\text{cathode}}}{4FD_{\text{eff,cathode}}P}j\right)$$
(39)

where P is the operating SOFC pressure, $D_{\rm eff,anode}$ is the effective gaseous diffusivity through the anode (considered to be a binary gas mixture of H_2 and H_2O) and $D_{\rm eff,cathode}$ is the effective oxygen diffusivity through the cathode (considered to be a binary gas mixture of O_2 and O_2).

The activation overpotentials ($\eta_{\rm act}$) are caused by the sluggishness of the electrochemical reaction at the electrode surfaces. The activation overpotentials can be determined by the non-linear Butler–Volmer equation as follows:

$$j = j_{0,\text{anode}} \left[\frac{p_{\text{H}_2,\text{TPB}}}{p_{\text{H}_2,\text{f}}} \exp\left(\frac{\alpha nF}{RT} \eta_{\text{act,anode}}\right) - \frac{p_{\text{H}_2\text{O},\text{TPB}}}{p_{\text{H}_2\text{O},\text{f}}} \exp\left(-\frac{(1-\alpha)nF}{RT} \eta_{\text{act,anode}}\right) \right]$$

$$(40)$$

$$j = j_{0,\text{cathode}} \left[\exp \left(\frac{\alpha nF}{RT} \eta_{\text{act,cathode}} \right) - \exp \left(-\frac{(1-\alpha)nF}{RT} \eta_{\text{act,cathode}} \right) \right]$$
(41)

where α is the transfer coefficient (usually considered to be 0.5), n is the number of electrons transferred in the single elementary rate-limiting reaction step represented by the Butler–Volmer equation and $j_{0,\text{cathode}}$ and $j_{0,\text{anode}}$ are the exchange current density at the cathode and the anode, which depend on the operating temperature as shown in Eqs. (42) and (43), respectively.

$$j_{0,\text{cathode}} = \frac{RT}{nF} k_{\text{cathode}} \exp\left(-\frac{E_{\text{cathode}}}{RT}\right)$$
 (42)

$$j_{0,\text{anode}} = \frac{RT}{nF} k_{\text{anode}} \exp\left(-\frac{E_{\text{anode}}}{RT}\right)$$
(43)

where $E_{\rm cathode}$ and $E_{\rm anode}$ represent the activation energies at the anode and the cathode, which are equal to 137 and 140 kJ mol⁻¹, respectively, and $k_{\rm cathode}$ and $k_{\rm anode}$ denote the preexponential factors, which are 2.35 x 10^{11} and 6.54 x 10^{11} Ω^{-1} m⁻², respectively (Aguiar et al., 2004).

The electrical power output ($P_{\rm sofe}$) is obtained when a current is drawn from the fuel cell, defined as:

$$P_{\text{sofe}} = I \times V_{\text{actual}} = j \times V_{\text{actual}} \times A_{\text{c}} \tag{44}$$

where V_{actual} represents the actual voltage and I is the current flowing through the fuel cell.

In this study, the SOFC is operated under adiabatic condition; therefore, the air flowing through the SOFC is employed to control the fuel cell temperature. The air inlet temperature can be calculated from the energy balance around the fuel cell, given as:

$$(\sum_{i} \dot{n}_{9} \dot{h}_{9}) + (\sum_{i} \dot{n}_{11} \dot{h}_{11}) - (\sum_{o} \dot{n}_{12} \dot{h}_{12}) - (\sum_{o} \dot{n}_{13} \dot{h}_{13}) - P_{sofc} = 0$$

$$(45)$$

2.3 Gas turbine and compressor

The exhaust gas from the SOFC stack is fed to the gas turbine in order to generate more power. The power produced by the gas turbine and the power consumed by the air compressor can be computed from the energy balances around the gas turbine and the compressor as follows:

$$P_{t} = \sum_{i} (\dot{n}_{i,t}^{\text{in}} \dot{h}_{i,t}^{\text{in}}) - \sum_{i} (\dot{n}_{i,t}^{\text{out}} \dot{h}_{i,t}^{\text{out}})$$
(46)

$$P_{c} = \sum_{i} (\dot{n}_{i,c}^{in} \dot{h}_{i,c}^{in})_{out} - \sum_{i} (\dot{n}_{i,c}^{in} \dot{h}_{i,c}^{in})_{in}$$
(47)

The net electric power output of the gas turbine section can be expressed as:

$$P_{\rm gt} = (P_{\rm t} - P_{\rm c}) \eta_{\rm m} \eta_{\rm g} \tag{48}$$

Project: Design and analysis of a solid oxide fuel cell system for combined heat and electrical power generation

where $P_{\rm t}$ is the power obtained from the gas turbine, P_c is the power consumed by the compressor and η_m and η_g are the mechanical and generator efficiencies, respectively.

The temperature of the gas turbine and compressor outlet gases can be determined based on the isentropic efficiency (Eqs. (49)-(50)).

$$T_{t}^{\text{out}} = T_{t}^{\text{in}} \left(1 - \eta_{t} \left(1 - \left(\frac{p_{t}^{\text{out}}}{p_{t}^{\text{in}}} \right)^{\frac{\gamma - 1}{\gamma}} \right) \right)$$

$$(49)$$

$$T_{\rm c}^{\rm out} = T_{\rm c}^{\rm in} \left(1 + \frac{1}{\eta_c} \left(\left(\frac{p_{\rm c}^{\rm out}}{p_{\rm c}^{\rm in}} \right)^{\frac{\gamma - 1}{\gamma}} - 1 \right) \right)$$
 (50)

where γ is the ratio of the specific heat capacities at the constant pressure and volume.

2.4 Other units

2.4.1 Vaporizers

Ethanol and water are converted from the liquid to the gas phase in the vaporizer.

The required heat for the operation of the vaporizer can be expressed as:

$$Q_{\text{vap,C}_2H_5OH} = (\sum_{o} \dot{n}_2 \dot{h}_2) - (\sum_{i} \dot{n}_1 \dot{h}_1)$$
 (51)

$$Q_{\text{vap,H}_2O} = (\sum_{i} \dot{n}_4 \dot{h}_4) - (\sum_{i} \dot{n}_3 \dot{h}_3)$$
 (52)

2.4.2 Pre-heaters

As seen in Fig. 1, the SOFC system has three pre-heaters that are used to preheat the feed stream of ethanol and steam, the synthesis gas obtained from the reformer and the air fed to the SOFC. The heat required for these pre-heaters can be determined by the following equations:

$$Q_{\text{preheater},1} = \left(\sum_{\alpha} \dot{n}_{7} \dot{h}_{7}\right) - \left(\sum_{\alpha} \dot{n}_{6} \dot{h}_{6}\right) \tag{53}$$

$$Q_{\text{preheater,2}} = \left(\sum_{0} \dot{n}_{9} \dot{h}_{9}\right) - \left(\sum_{i} \dot{n}_{8} \dot{h}_{8}\right) \tag{54}$$

$$Q_{\text{preheater,3}} = \left(\sum_{o} \dot{n}_{11} \dot{h}_{11}\right) - \left(\sum_{i} \dot{n}_{10} \dot{h}_{10}\right) \tag{55}$$

2.4.3 Mixer

For the SOFC system with anode exhaust gas recycling, the recirculated gas stream is mixed with the fresh fuel feed in a mixer. The outlet temperature of the mixer can be calculated from the energy balance around the mixer, expressed as:

$$(\sum_{i} \dot{n}_{5} \dot{h}_{5}) + (\sum_{i} \dot{n}_{14} \dot{h}_{14}) - (\sum_{a} \dot{n}_{6} \dot{h}_{6}) = 0$$
(56)

2.4.4 After-burner

The residue flue gas from the anode outlet stream and the unused oxidant gas from the cathode are mixed and burnt in an afterburner. The combustion reactions that occur in the afterburner can be written as follows:

Hydrogen combustion:
$$H_2 + 0.5O_2 \rightarrow H_2O$$
 (57)

Carbon monoxide combustion:
$$CO + 0.5O_2 \rightarrow CO_2$$
 (58)

For the non-recycling SOFC system, the exit temperature of the afterburner can be calculated from the energy balance on the afterburner as:

$$\left(\sum_{i} \dot{n}_{12} \dot{h}_{12}\right) + \left(\sum_{i} \dot{n}_{13} \dot{h}_{13}\right) - \left(\sum_{o} \dot{n}_{14} \dot{h}_{14}\right) = 0 \tag{59}$$

For the SOFC system with anode exhaust gas recycling, the portion of the anode flue gas that is not recycled to the reformer is fed into the afterburner. The exit temperature of the afterburner outlet is calculated by solving the following equation:

$$\left(\sum_{i} \dot{n}_{12} \dot{h}_{12}\right) + \left(\sum_{i} \dot{n}_{15} \dot{h}_{15}\right) - \left(\sum_{i} \dot{n}_{16} \dot{h}_{16}\right) = 0 \tag{60}$$

The performance parameters of the SOFC system are considered in terms of the electrical efficiency (η_{el}) and the thermal efficiency (η_{th}), which are defined as:

$$h_{el} = \frac{P_{\text{sofc}}}{\dot{n}_{\text{C,H,OH}} L H V_{\text{C,H,OH}}}$$
(61)

$$h_{th} = \frac{Q_{rec} - Q_{use}}{\dot{n}_{C_2H_3OH} LHV_{C_2H_3OH}}$$
(62)

where $\dot{n}_{\rm C_2H_5OH}$ is the inlet ethanol molar flow rate, $LHV_{\rm C_2H_5OH}$ is the lower heating value of ethanol, $Q_{\rm rec}$ is the thermal energy obtained from the SOFC system (the reference temperature is 100 °C) and $Q_{\rm use}$ is the total thermal energy used in the SOFC system.

Chapter 3

Use of different renewable fuels in a steam reformer integrated into a solid oxide

fuel cell: Theoretical analysis and performance comparison

Hydrogen production from renewable energy resources has received significant attention with advances in fuel cell technology. The fuel type and operational reforming conditions directly affect fuel cell electricity generation. This study analyzes the theoretical performance of a solid oxide fuel cell (SOFC) integrated with a steam reforming process using three different renewable fuels: ethanol, glycerol and biogas. The effects of key steam reformer operating parameters on the hydrogen production for SOFCs are investigated. The performances of SOFC systems run on different fuels are compared in terms of electrical and thermal efficiencies.

3.1 Fuel processor and SOFC integrated system

Fig. 1 shows the external reformer and SOFC integrated system, which comprises heat exchangers, fuel processor, SOFC and afterburner. Steam and fuel are mixed, then preheated at operating reforming temperatures and sent to the steam reformer, where a synthesis gas (hydrogen-rich gas) is produced. Next, the synthesis gas is preheated at the desired temperature and then fed to the SOFC. Air is also compressed and preheated before being fed to the SOFC. The SOFC produces electrical power and steam via the electrochemical reaction of hydrogen and oxygen in air. In general, SOFCs cannot be operated at complete fuel utilization; thus, the residual fuel is combusted in an afterburner to generate heat for use in other heat-requiring units in the SOFC system, such as a reformer and fuel and air preheaters (dash line in Fig. 1).

In this study, biogas, ethanol and glycerol are considered the potential fuels to produce hydrogen for SOFC systems. Biogas is composed of 60 mol% methane and 40 mol% carbon dioxide. To analyze the theoretical performance of the SOFC system, it is assumed that the system is run under steady-state conditions and that all gases behave as ideal gases. Furthermore, heat losses from individual components in the SOFC system are negligible and the operating pressure and temperature of the reformer and the SOFC are constant. The considered SOFC is planar and described by a one-dimensional model, which is operated at a constant cell voltage along the cell coordinate.

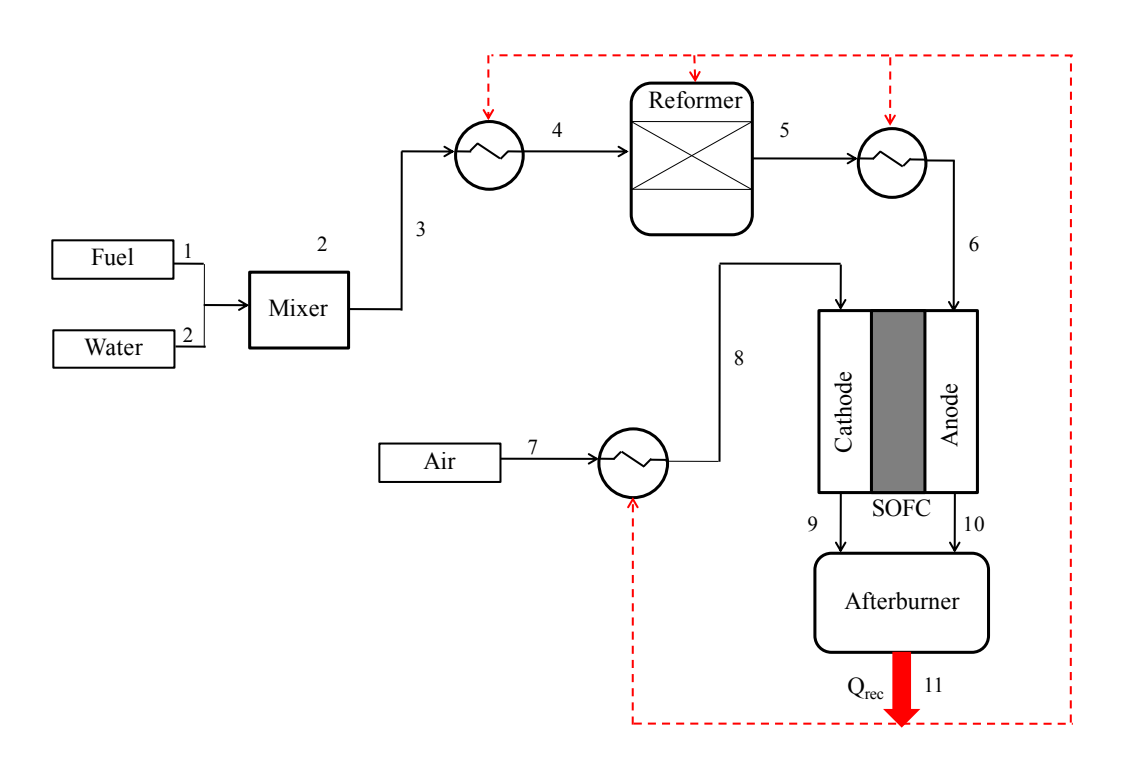


Fig. 1 Schematic of an SOFC system integrated with a fuel processor.

3.2 Results and discussion

3.2.1 Hydrogen production from various fuels

In this section, hydrogen production via steam reforming using ethanol, biogas and glycerol as fuels is investigated. Fig. 2 shows the effect of operating temperature on hydrogen production from the steam reforming of these three fuels. The results show a similar trend for each fuel type; this behavior is also observed for other fuels, such as methane and methanol. An increase in the reforming temperature enhances the hydrogen yield due to the endothermicity of the steam reforming reaction. Ethanol and glycerol provide a higher hydrogen yield than does biogas. At atmospheric pressure, glycerol provides a slightly higher hydrogen yield than ethanol below 973 K. When the steam reformer is operated at high pressure, glycerol produces more hydrogen than ethanol below 1033 K. The operating pressure does not affect the hydrogen yield above 1073 K.

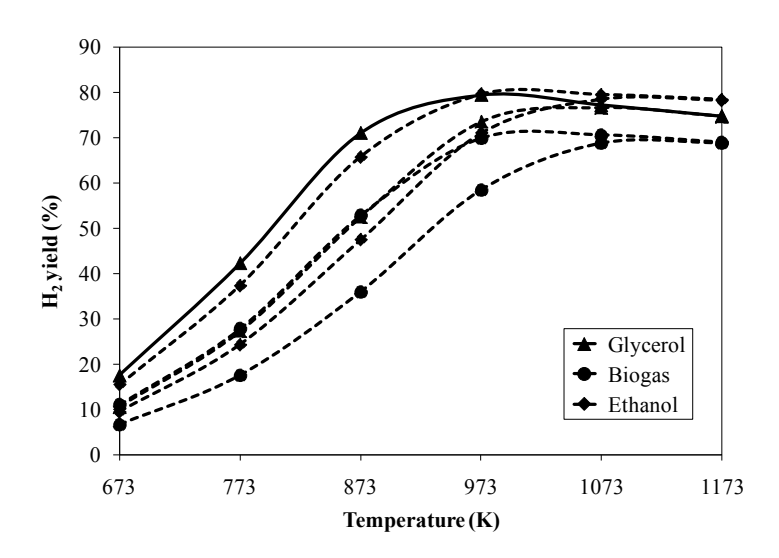


Fig. 2 Effect of reforming temperature on H_2 yield at S/C = 2:1 and pressures of 1 bar (solid line) and 3 bar (dashed line)

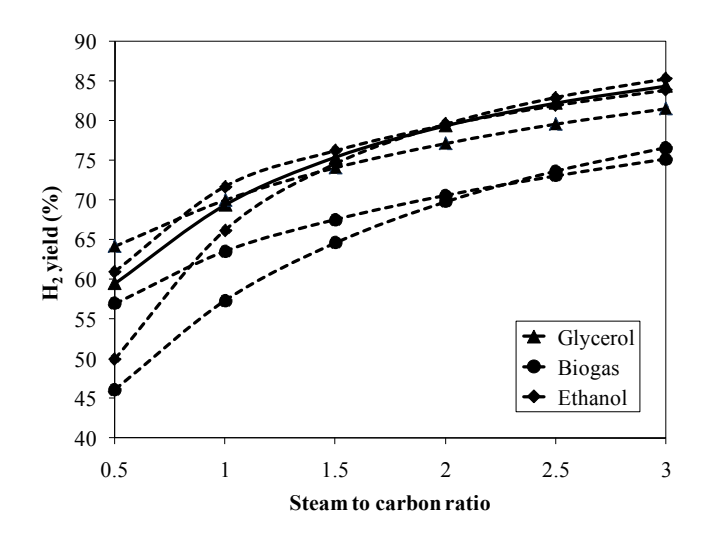


Fig. 3 Effect of S/C ratio on H_2 yield (P = 1 bar): T = 973 K (solid line) and T = 1073 K (dashed line).

Fig. 3 shows the effect of the steam-to-carbon (S/C) ratio on hydrogen yield at a pressure of 1 bar. At a low S/C ratio, glycerol produces more hydrogen than ethanol does. However, ethanol gives the highest hydrogen yield for higher S/C ratios. The use of biogas provides the lowest hydrogen yield throughout the operational range studied. Fig. 4 shows the ratio of the amount of gaseous product to that of hydrogen produced from the steam reforming of glycerol, ethanol and biogas at a temperature of 973 K and an S/C ratio of 2. The glycerol reforming process yields the highest CO₂ concentration because glycerol has a hydrogen-to-carbon ratio lower than other fuels. The results also indicate that when ethanol is used as a fuel, less CO is produced. The presence of CO may cause the formation of carbon in the steam reforming process and the SOFC.

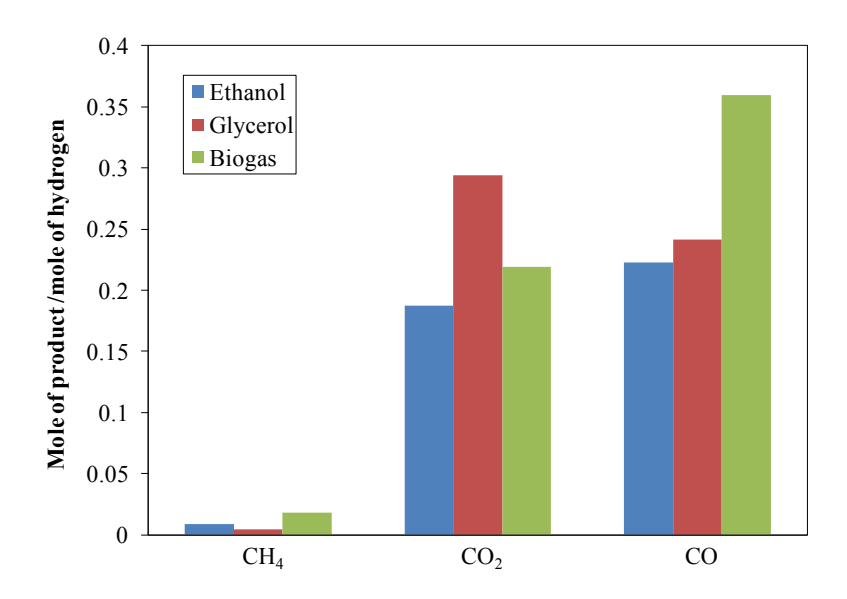


Fig. 4 Product distribution from the steam reforming of glycerol, ethanol and biogas (T = 973 K and S/C = 2).

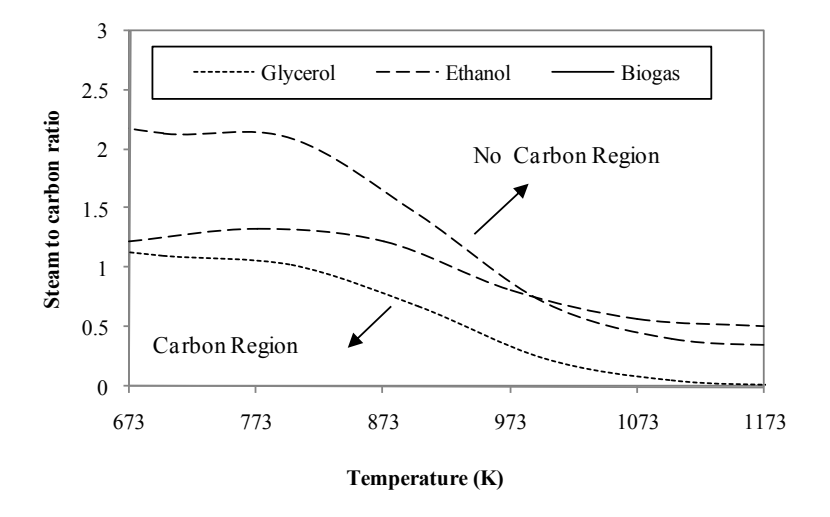


Fig. 5 Carbon boundary of various fuels

Fig. 5 shows the carbon formation boundary when glycerol, ethanol and biogas are used to produce hydrogen. The carbon formation tendencies of the different fuels are similar, being lower for high-temperature operation and high S/C ratios. Because the steam reforming of biogas generates more carbon monoxide, shifting the Boudouard reaction towards the products, this process must be performed at a higher temperature and S/C ratio to avoid carbon formation. Although the amount of carbon monoxide generated

by the steam reformer fuelled by ethanol is lower than that fuelled by glycerol, ethanol

reforming exhibits a higher carbon formation tendency than glycerol reforming because

glycerol has a higher oxygen-to-carbon ratio than ethanol. Thus, glycerol is more likely

than ethanol to be reformed to CO and CO₂ rather than carbon.

3.3.2 SOFC system

Next, the performance of the SOFC fed by the synthesis gas obtained from the

steam reforming of ethanol, glycerol and biogas is investigated. The power output of the

SOFC system is specified at 150 kW. Fig. 6 presents the fraction of the heat duty required

for each unit in the SOFC systems. The air preheater requires the most heat input, 79-81%

of the overall heat consumption of the SOFC system, compared to other heat-requiring

units. SOFCs are usually operated at high temperatures, and the electrochemical reaction

is an exothermic reaction. These factors cause a temperature gradient in the SOFC stack.

Therefore, excess air is required to maintain the SOFC temperature at a suitable level.

The steam reformer also requires a large amount of energy.

Project: Design and analysis of a solid oxide fuel cell system for combined heat and electrical power generation

21

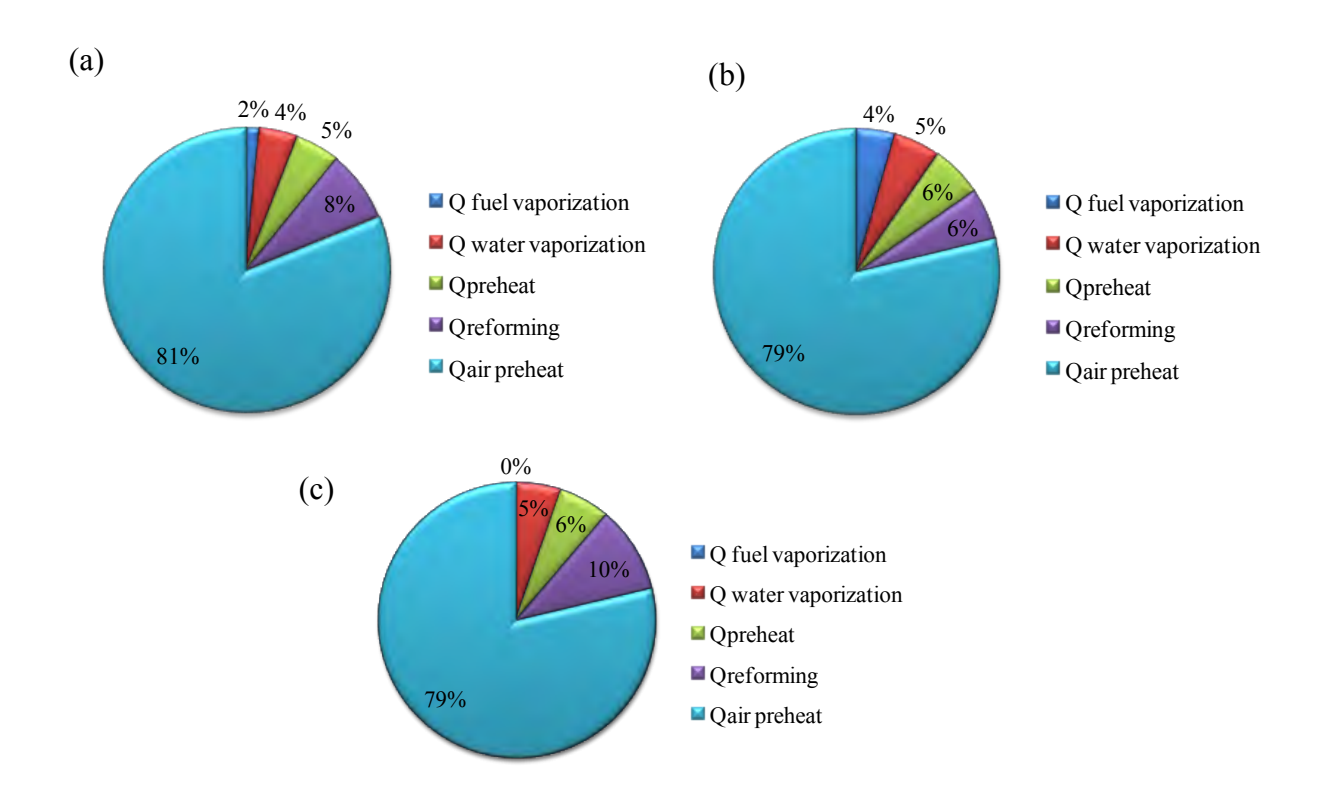


Fig. 6 Distribution of energy consumption in an SOFC system fed by different fuels: (a) ethanol, (b) glycerol and (c) biogas.

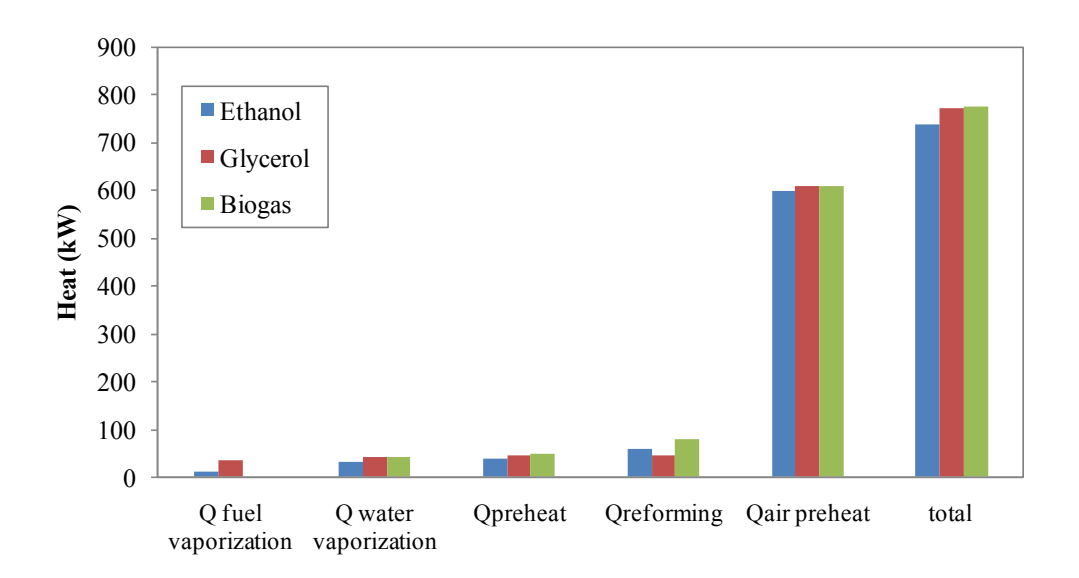


Fig. 7 Energy required by each unit of an SOFC system for different fuel feeds.

The energy consumptions for each unit of the SOFC system are compared in Fig. 7 for different fuels. The results indicate that the SOFC system run on biogas requires the most external energy, whereas the ethanol-fueled SOFC system requires the least energy. Biogas reforming requires the most energy (77.9 kW) because the high CO₂ content in biogas promotes a reverse water gas shift reaction, which is an endothermic reaction. Although the energy requirement of the glycerol steam reforming is lower, more heat is needed for the evaporator due to the high boiling point of glycerol (561.9 K).

Fig. 8 shows the SOFC stack efficiency and the thermal and electrical efficiencies of the SOFC systems supplied by different fuels. As observed in the figure, the SOFC system fuelled by ethanol gives the best performance in terms of the SOFC stack efficiency, the electrical efficiency and the thermal efficiency due to the superior performance of the ethanol steam reformer compared that of other fuels, which translates into the greatest hydrogen production. The ethanol-fuelled SOFC system can achieve an electrical efficiency of 51 %, whereas the electrical efficiencies of the glycerol- and biogas-fuelled SOFC systems are 49% and 32%, respectively. The use of biogas as a fuel for the SOFC system provides the worst electrical efficiency because biogas mainly consists of carbon dioxide, which dilutes the hydrogen fuel fed into the SOFC stack. This dilution lowers the reversible cell voltage and increases the concentration and activation overpotentials in the SOFC. The efficiency of the SOFC stack is fairly independent of fuel type (42-43%). The SOFC system fed by biogas shows the lowest thermal efficiency at the desired power output of 150 kW because a large amount of heat is lost to preheat carbon dioxide in the biogas feed.

Project: Design and analysis of a solid oxide fuel cell system for combined heat and electrical power generation

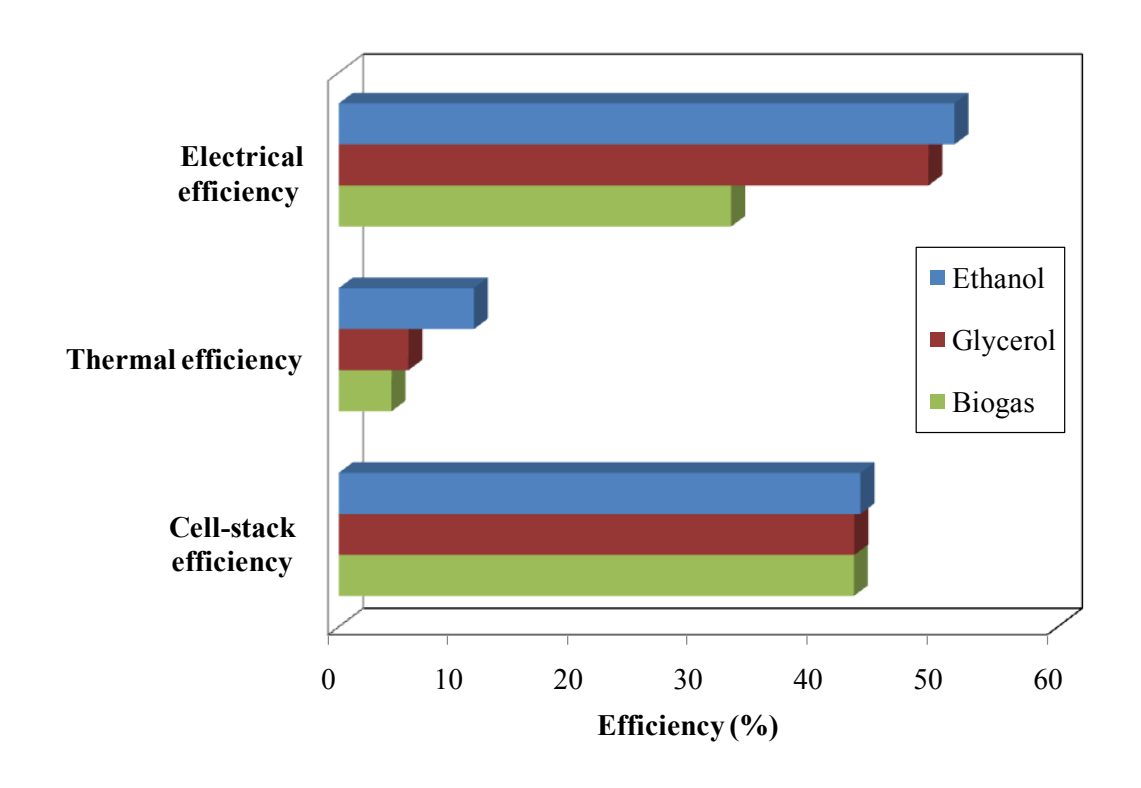


Fig. 8 Efficiencies of the SOFC systems with different type of fuels.

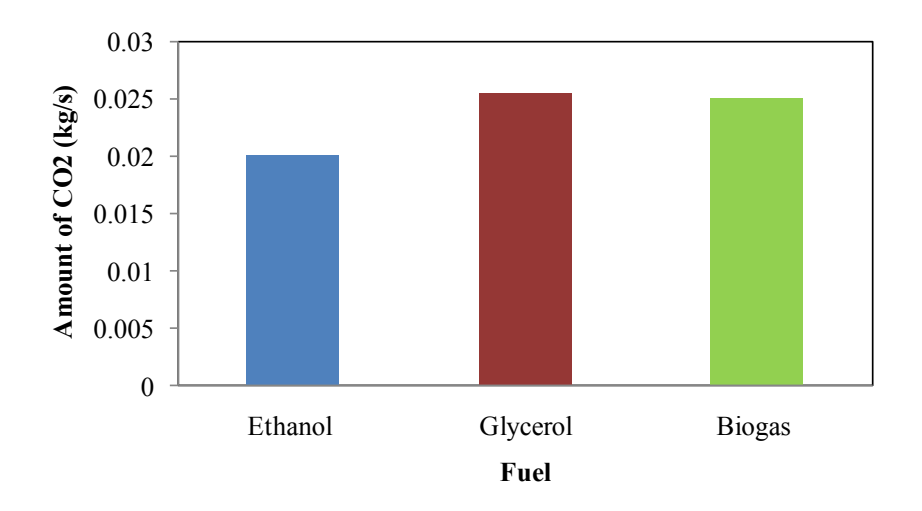


Fig. 9 CO₂ released from SOFC systems with different fuels.

Fig. 9 presents the amount of carbon dioxide released from the SOFC system at a power output of 150 kW. The SOFC system fed by ethanol minimizes the emission of

carbon dioxide, whereas the glycerol-fuelled SOFC system produces the most carbon dioxide. The carbon dioxide emission of the ethanol-fed SOFC system is less than that of the other systems by 21.76% (glycerol) and 19.97% (biogas). The simulation study indicates that ethanol is the most suitable of the three renewable fuels studied for use in an SOFC system integrated with an external steam reformer. The use of ethanol as fuel provides the greatest SOFC stack efficiency, system electrical efficiency and thermal efficiency and the least carbon dioxide emission. When biogas is used as a fuel for SOFC, the use of a purification unit is suggested to remove carbon dioxide from the biogas, thereby improving both the thermal and electrical system efficiencies.

Chapter 4

Analysis of an Ethanol-Fuelled Solid Oxide Fuel Cell System Using Partial Anode

Exhaust Gas Recirculation

This chapter presents an analysis of a solid oxide fuel cell (SOFC) system

integrated with an ethanol reforming process. The recycling of the anode exhaust gas in

the integrated SOFC system is considered to improve its performance. The required

conditions to prevent carbon formation in the ethanol reformer are also examined.

4.1 SOFC system

Figs. 1a and 1b show schematics of the ethanol steam reformer and the SOFC

integrated system with and without the recycle of the anode exhaust gas, respectively.

Both the SOFC systems consist of a vaporizer, heat exchanger, fuel processor, SOFC

stack and afterburner. First, ethanol and water are separately fed into the vaporizer and

then sent to the heat exchanger to be preheated to the desired operating temperature of the

reformer. The ethanol and steam then undergo the steam reforming reaction at the

reformer to produce a synthesis gas. The obtained synthesis gas is preheated before being

fed to the SOFC stack where the hydrogen in the synthesis gas reacts with oxygen in air

to produce electrical power via an electrochemical reaction. The residue fuel in the SOFC

outlet stream is combusted in the afterburner and the heat thus generated can be used for

the heat-requiring units in the SOFC system. In the case where the anode exhaust gas is

recycled (Fig. 1b), a portion of the anode exhaust gas is recycled to the reformer. The

steam generated by the electrochemical reaction can be used as a reforming reagent,

26

Project: Design and analysis of a solid oxide fuel cell system for combined heat and electrical power generation

whereas the residue of carbon monoxide in the anode exhaust gas can further react with steam via the water gas-shift reaction to produce more hydrogen in the steam reformer.

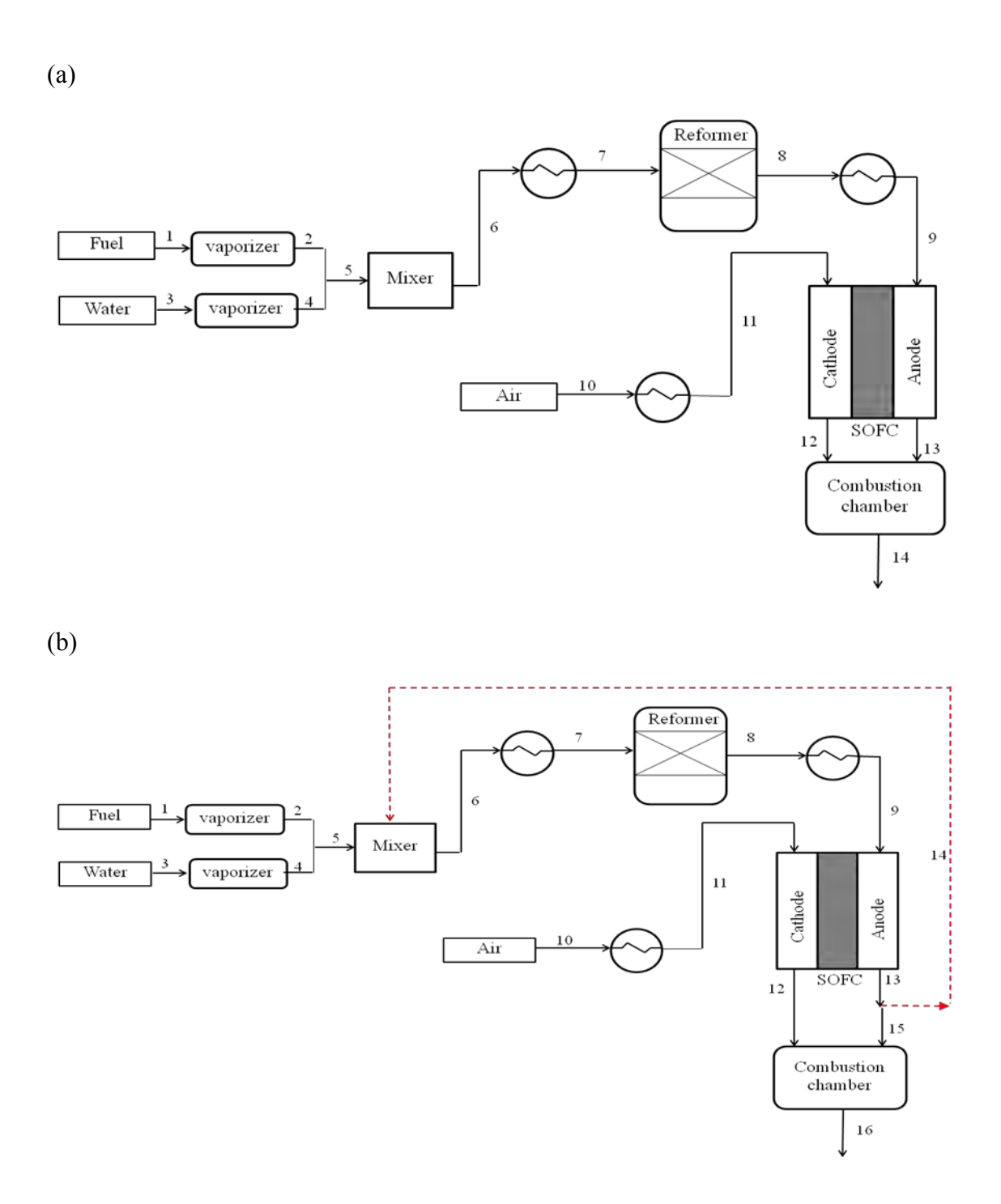


Fig. 1. Schematic of the SOFC systems integrated with an external ethanol steam reformer: (a) no recirculation and (b) anode exhaust gas recirculation.

4.2 Results and discussion

4.2.1 Comparison of SOFC systems with and without anode exhaust gas recycling

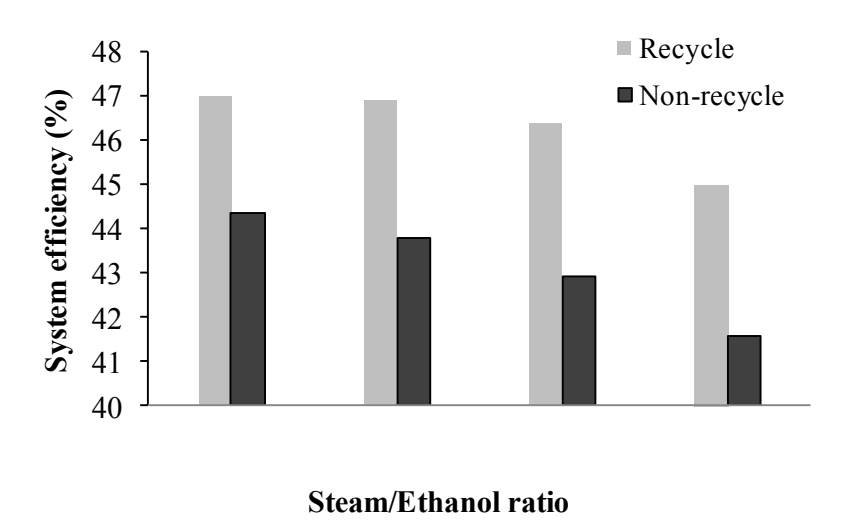
The performances of the SOFC system with and without recycling the anode exhaust gas are first analyzed under nominal conditions. The steam and ethanol fed to the ethanol steam reformer are fixed at the ratio of 1.5. The results show that the electrical performance of the SOFC system with the anode gas recycling is 46.16%, which is higher than that without the anode gas recycle (42.87%). Table 1 shows the heat duty needed in each unit of both SOFC systems. The energy requirements for the ethanol processor section of the SOFC system with and without the anode exhaust gas recirculation are 397.10 and 634.18 kW, respectively. The recirculation of the anode gas reduces the energy required by the fuel processor (37.4% reduction). In addition, it is observed that all of the steam required for the steam reformer is recovered by the anode exhaust gas recirculation (the recirculation ratio = 0.6), and this can save the energy supplied to the water vaporizer. However, the total energy requirements of the two SOFC systems are not different. The SOFC with anode gas recirculation can produce more electrical power and thus requires a high air supply to maintain the temperature of the SOFC. This results in high energy consumption in the air pre-heater. It is noted that since the power required to drive the blower for the anode exhaust gas recycling has slight effect on the SOFC system, it is negligible in calculating the electrical efficiency of the SOFC system.

Fig. 2 shows a comparison of the SOFC system performance when not recycling and recycling the anode exhaust gas at different steam-to-ethanol feed ratios. The simulation results clearly show that the SOFC system with anode exhaust gas recycling provides higher electrical and thermal efficiencies than that without recycling the anode exhaust gas. In the case of the SOFC system with anode exhaust gas recirculation, it is found that the molar flow rates of hydrogen and carbon monoxide in the SOFC feed

stream increase. As a result, the current density generated by the SOFC is more produced, resulting in higher electrical and thermal efficiencies.

Table 1 Heat duty of each unit in the SOFC systems with and without anode exhaust gas recirculation

Heat exchangers	Heat duty (kW)	
	SOFC System without recycling the anode-exhaust gas	SOFC System with recycling the anode-exhaust gas
Ethanol vaporizer	49.12	49.12
Water vaporizer	167.88	-
Pre-heating gas before reformer	152.04	33.18
Pre-heating gas before SOFC	30.44	47.61
Reformer	234.70	267.19
Air pre-heater	1503.94	1731.53
Total	2138.1	2128.63





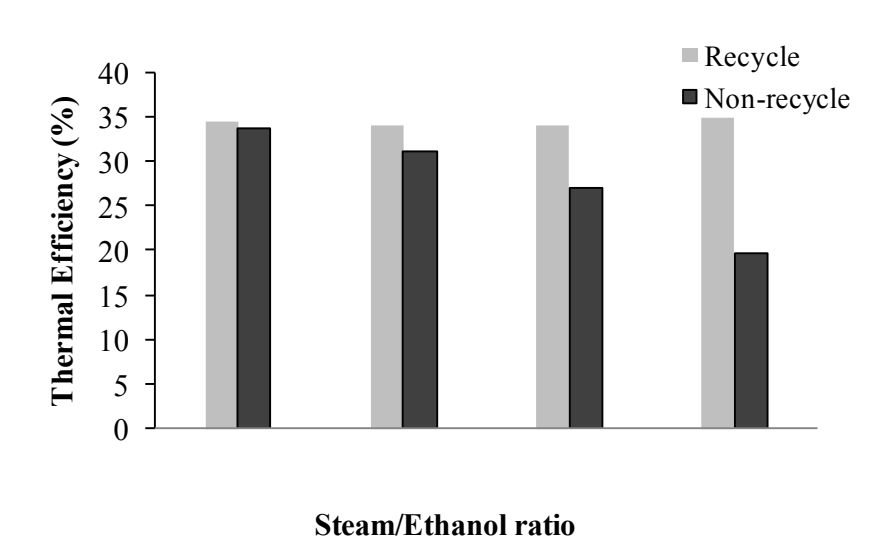


Fig. 2. Performance of the SOFC systems with and without recycling the anode exhaust gas at different steam-to-ethanol ratios: (a) electrical efficiency and (b) thermal efficiency.

4.2.2 Effects of recirculation ratio and fuel utilization

It is well known that a crucial problem of ethanol steam reforming is caused by the formation of carbon (graphite), which could lead to the deactivation of the catalyst and increased pressure drops in the reformer. To avoid carbon formation, the suitable operating temperature and steam-to-carbon ratio should be determined. In general, a

steam reforming reaction needs to be fed with excess steam to increase hydrogen

production and to reduce the carbon monoxide. The presence of carbon monoxide will

promote carbon formation via the Boudouard reaction. Furthermore, the tendency of

carbon formation decreases as the reforming temperature increases due to the exothermic

nature of the Boudouard reaction. However, operation of the steam reformer at a high

temperature with more steam addition results in a high operating cost.

Fig. 3 presents the effect of the recirculation ratio of the anode exhaust gas on the

reformer temperature and steam-to-carbon ratio required to avoid carbon formation at

different fuel utilizations. It is noted that the fuel utilization affects the gaseous

composition of the residual gas exiting from the SOFC anode, whereas the recirculation

ratio indicates the amount of the steam, which is generated by the electrochemical

reaction, that is recycled to the ethanol steam reforming section.

As seen in Fig. 3a, the reforming temperature required to suppress the tendency of

carbon formation is reduced when the SOFC is operated at the higher recirculation ratio

and fuel utilization. The higher recirculation ratio increases the recycle of the steam to the

ethanol reformer. Furthermore, at high fuel utilization, more steam is also generated from

the SOFC stack. These factors lead to an increase in the steam-to-carbon ratio of the

reformer feed (Fig. 3b). From the simulation result, when the SOFC system with anode

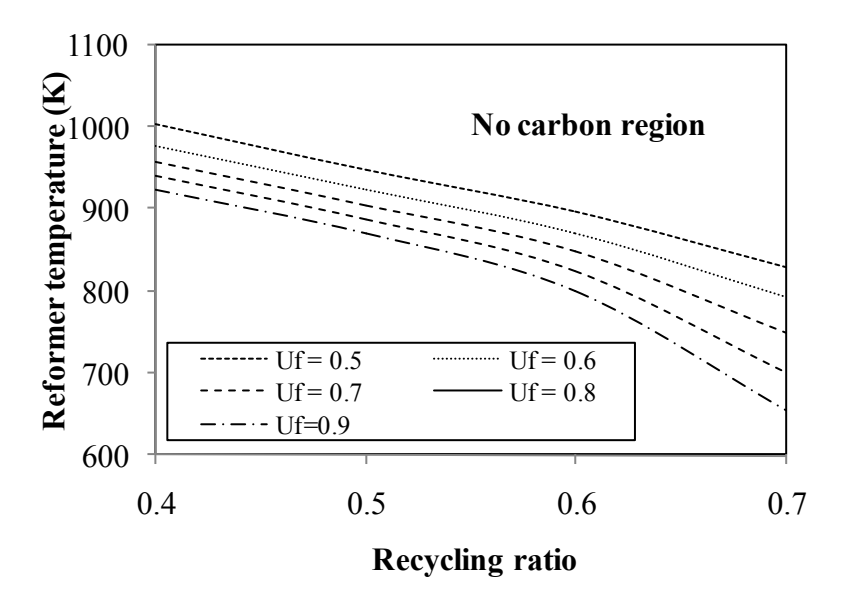
exhaust gas recycling is operated at a low fuel utilization of 0.6 and recirculation ratio of

0.4, the reforming temperature should be higher than 970 K to prevent the formation of

31

carbon in the ethanol reformer.

Project: Design and analysis of a solid oxide fuel cell system for combined heat and electrical power generation



(b)

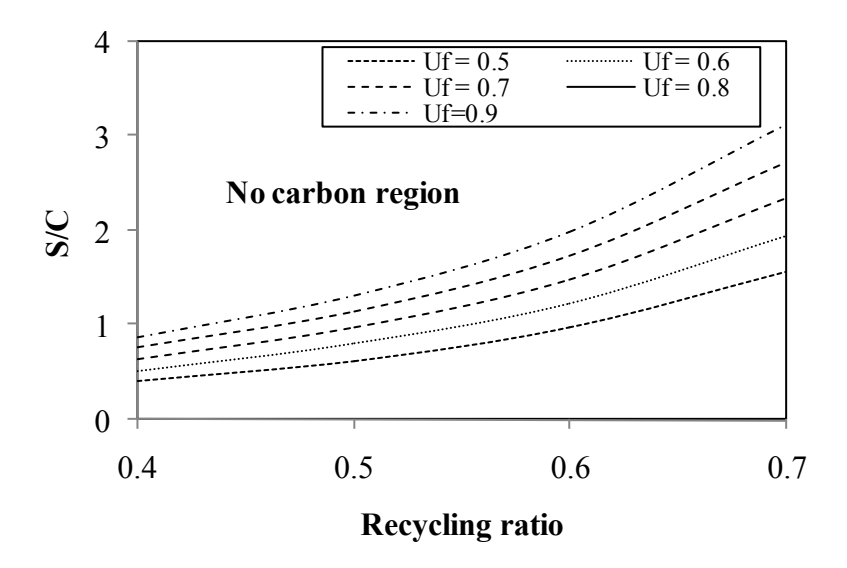


Fig. 3. Effect of the recirculation ratio of the anode exhaust gas at different fuel utilizations on the requirement of (a) the reformer temperature and (b) the steam-to-carbon ratio, to avoid a carbon formation.

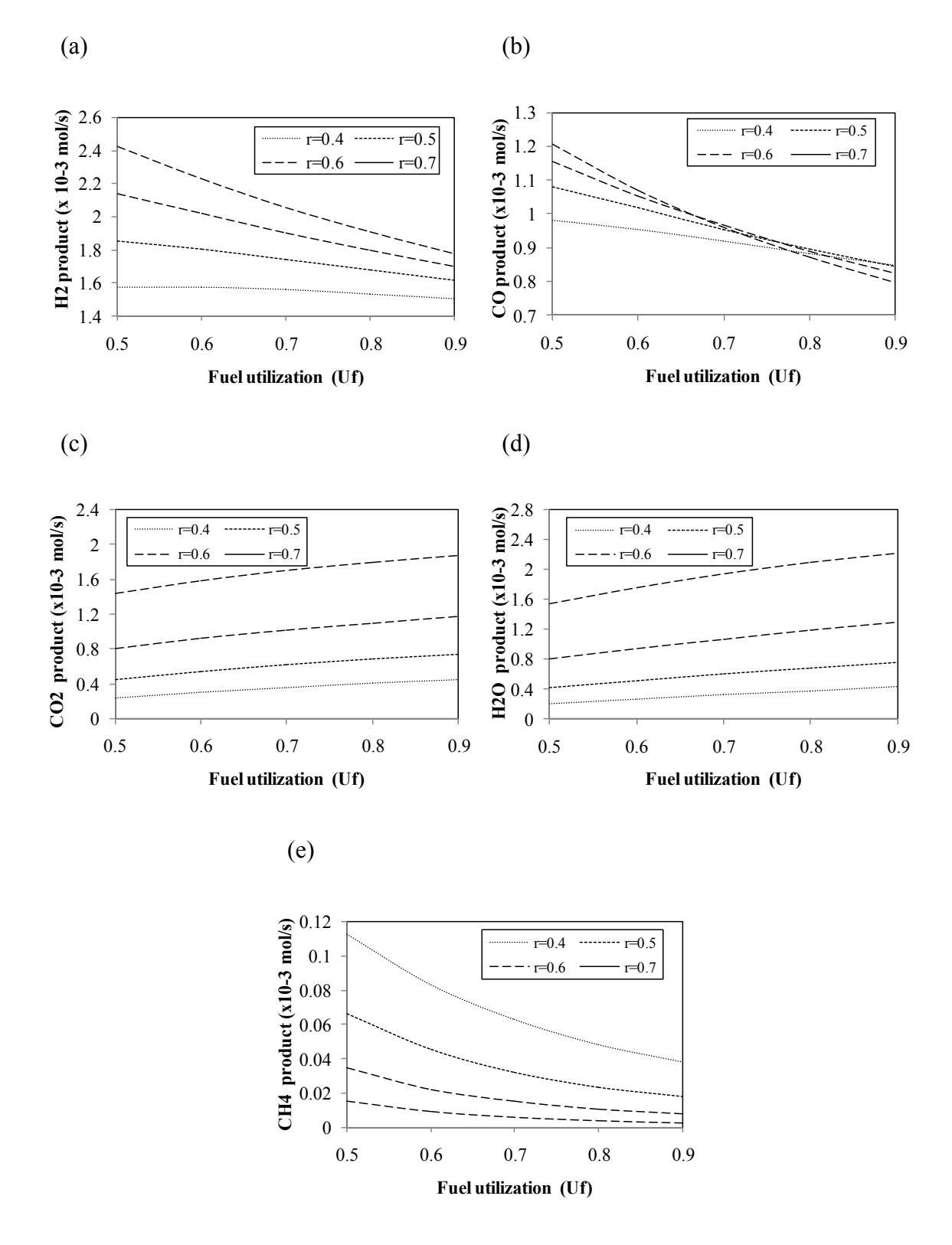


Fig. 4. Effect of fuel utilization on the composition of the synthesis gas obtained from the ethanol steam reformer at different recirculation ratios.

Figs. 4a-e shows the molar flow rates of hydrogen, carbon monoxide, carbon dioxide, steam and methane at the outlet of the ethanol reformer as functions of the recirculation ratio and fuel utilization. As expected, the amount of hydrogen and carbon monoxide decreases as the fuel utilization of the SOFC increases, whereas carbon dioxide and steam increase because the electrochemical and water gas shift reactions in the SOFC are more pronounced. The results show that an increase in the recirculation ratio increases the flow rates of the steam, carbon dioxide, carbon monoxide and hydrogen. However, at high fuel utilization, the carbon monoxide flow rate decreases when the recirculation ratio increases. At these conditions, more steam is recycled to the reformer, promoting the water gas shift reaction. It is noted that when the SOFC is operated at a high fuel utilization and recirculation ratio, a higher steam content in the anode exhaust gas and also a decrease in the content of methane at the reformer outlet is observed due to an increase in the reverse methanation reaction.

The influences of the fuel utilization and recirculation ratio on the current density, cell voltage, power density and electrical and thermal efficiencies are shown in Fig. 6. It can be seen that increasing the fuel utilization and the recirculation ratio cause the SOFC to generate more current density (Fig. 5a). When the SOFC is operated at higher fuel utilization, more hydrogen is consumed to produce electricity, while increasing the recirculation ratio of the anode exhaust gas leads to an increase in the molar flow rate of fuel to the SOFC. However, it is found that the operating cell voltage decreases with the increments of fuel utilization and recirculation ratio (Fig. 5b). This is mainly due to a significant increase of steam in the anode exhaust gas as the fuel utilization and recirculation ratio increase. Although a higher amount of steam promotes the ethanol reforming reaction, an excess of steam results in a dilution of the hydrogen required for

the electrochemical reaction. This leads to a significant decrease in the open-circuit

voltage and an increase in the concentration loss.

Figs. 5c and d show that at low fuel utilization (0.5-0.6), the power density and

electrical efficiency of SOFC increase with the increasing recirculation ratio. As the

anode exhaust gas consists of a higher unreacted fuel content due to the low fuel

utilization, an increase in the recirculation ratio results in an increase in hydrogen at the

SOFC anode inlet, improving the SOFC performance in terms of current density, power

density and electrical efficiency. However, the power density and the SOFC electrical

efficiency decrease when increasing the recirculation ratio at high fuel utilization. Even

though an increase in the fuel utilization results in more current density generated, the

increased recirculation ratio causes a significant decrease in the fuel cell voltage. This

implies that at high fuel utilization, the decrease in the fuel cell voltage has a strong

impact on the power density and electrical efficiency, compared with an increase in the

current density.

Considering the thermal efficiency of the SOFC system (Fig. 5e), when the SOFC

is operated at low fuel utilization, an increase in the recirculation ratio decreases the

thermal efficiency. Operation of the SOFC at a high recirculation ratio lowers the amount

of the exhaust gas sent to the afterburner; therefore, the heat generated from the

afterburner for use in the SOFC system will decrease. However, the thermal efficiency

can be enhanced when the SOFC system is operated at a higher recirculation ratio and

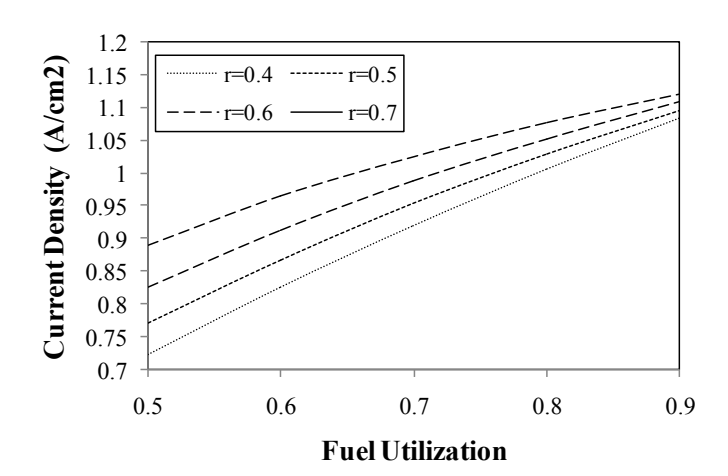
higher fuel utilization. This is mainly because the significant increase of steam recycled to

the ethanol reformer reduces the demand of energy for generating steam and preheating

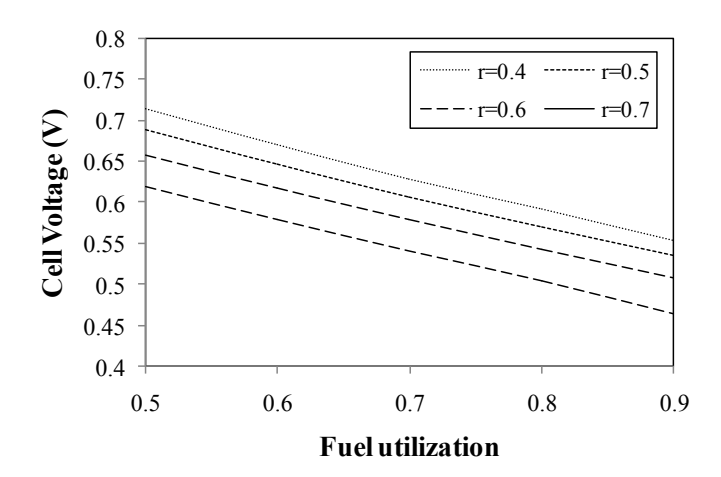
35

fuel stream.

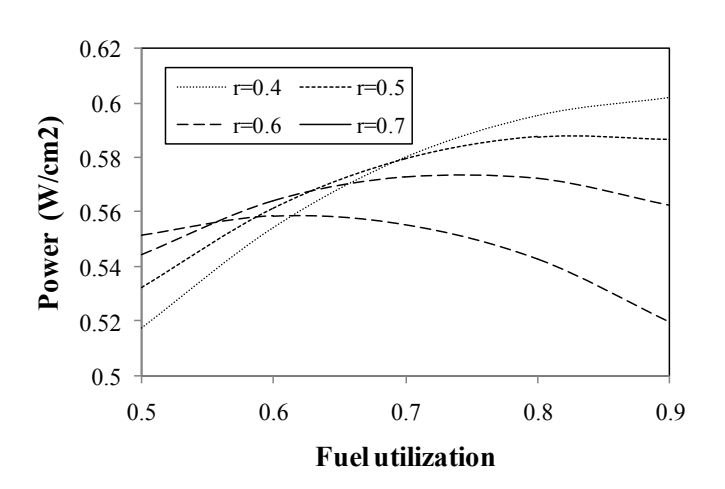
Project: Design and analysis of a solid oxide fuel cell system for combined heat and electrical power generation



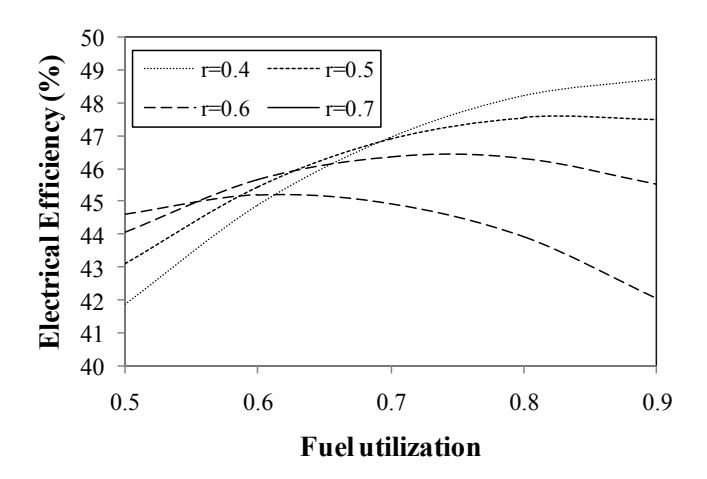
(b)



(c)



(d)



(e)

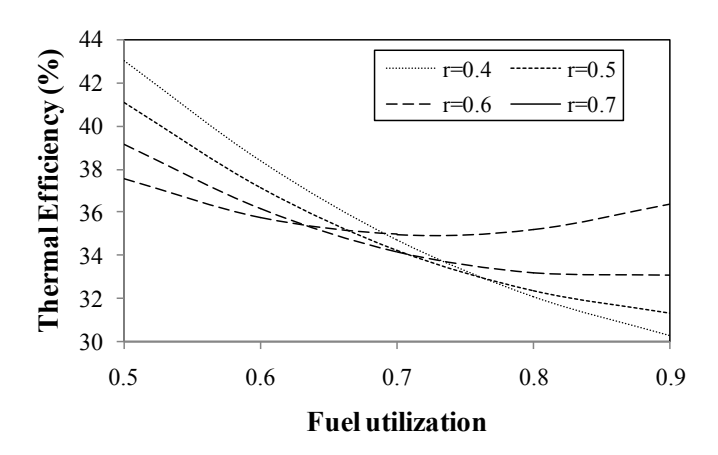


Fig. 5. Effect of fuel utilization on the SOFC system performance at different recirculation ratios: (a) current density, (b) fuel cell voltage, (c) power density, (d) electrical efficiency, and (e) thermal efficiency.

4.2.3 Effects of reformer and SOFC operating temperature

The effect of the reformer temperatures on the electrical efficiency when the SOFC is operated at temperature of 1073 K is shown in Fig. 6. The electrical efficiency of the SOFC system with the anode gas recirculation considerably increases when increasing the reformer temperature. As the ethanol steam reforming is favored in operation at high

temperatures, the increase in produced hydrogen promotes the electrochemical reaction in the SOFC stack, and thus, the electrical efficiency of SOFC is enhanced. However, an increase in the recirculation ratio results in a lower SOFC electrical efficiency. The degradation of the SOFC performance is obviously noticed when the reformer is operated at unsuitable temperatures. This lowers the production of hydrogen fuel for the SOFC. In addition, at a high recirculation of the anode exhaust gas, more steam is added to the SOFC, thereby decreasing the fuel cell voltage and the electrical efficiency.

Fig. 7 presents the electrical efficiency of the SOFC system as a function of the SOFC operating temperatures when the reformer is operated at temperature of 973 K. It can be seen that the electrical efficiency increases as the operating temperature of SOFC increases. An increase in the SOFC operating temperature can improve its performance because the rate of the electrochemical reaction is more pronounced. In addition, at elevated temperatures, the ohmic and activation losses are also reduced. Therefore, the more current density is generated, leading to the increased electrical efficiency.

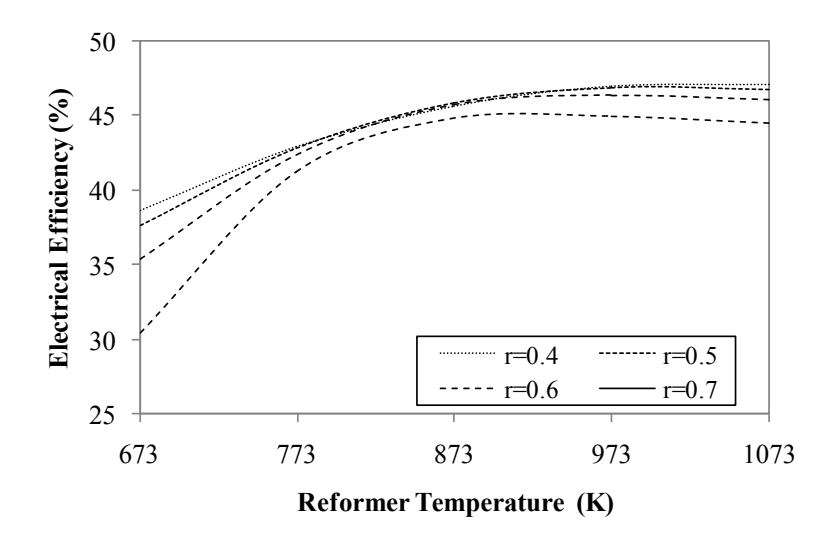


Fig. 6. Effect of the reformer operating temperature on the electrical efficiency of the SOFC system at different recirculation ratios.

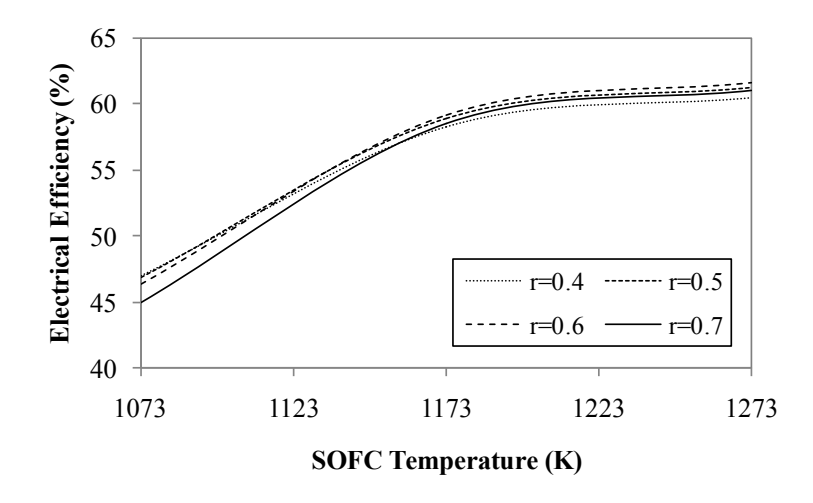
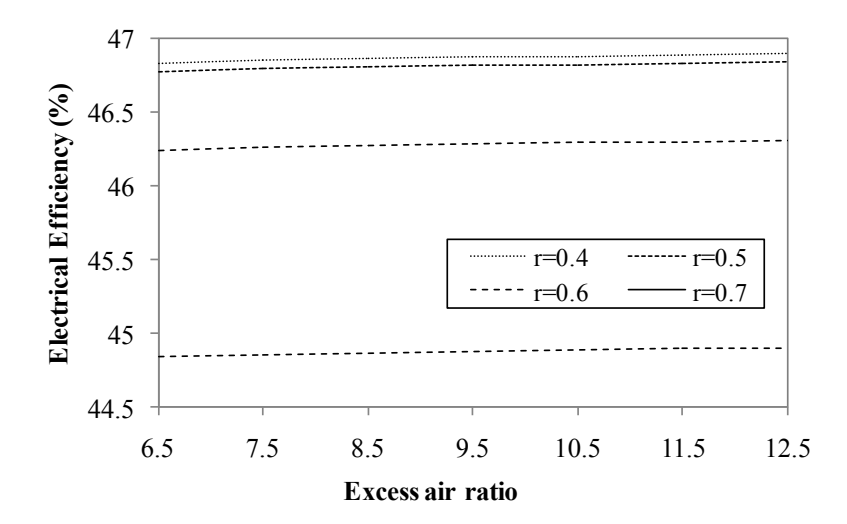


Fig. 7. Effect of the SOFC operating temperature on the electrical efficiency of the SOFC system at different recirculation ratios.

4.2.4 Effect of excess air ratio

The influence of the excess air ratio on the system's electrical and thermal efficiencies at different recirculation ratios is presented in Figs. 8a and 8b, respectively. The excess air ratio has a slight effect on the system electrical efficiency but a larger effect on the system thermal efficiency. The thermal efficiency sharply drops when the SOFC system is operated at a high excess air ratio owing to an increased requirement of the heat duty of the air pre-heater.



(b)

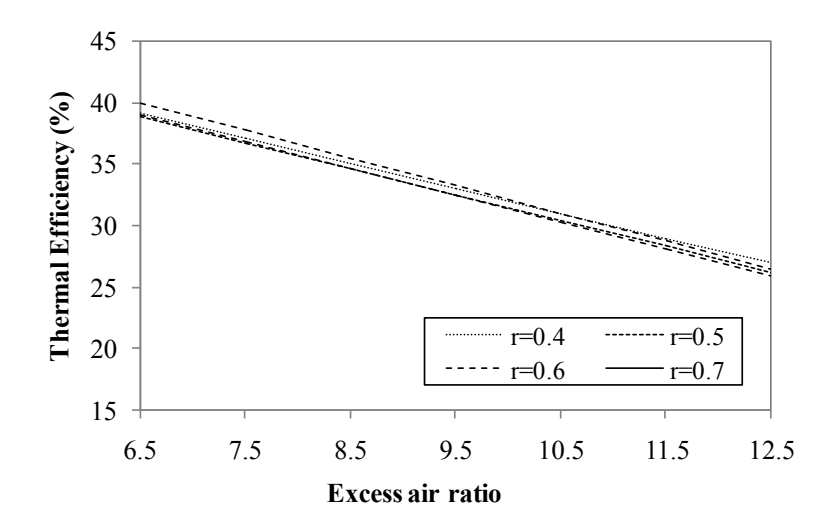


Fig. 8. Effect of the excess air ratio on (a) the electrical efficiency and (b) the thermal efficiency of the SOFC system at different recirculation ratios.

Chapter 5

Analysis of a pressurized solid oxide fuel cell-gas turbine hybrid power system with cathode gas recirculation

A pressurized solid oxide fuel cell-gas turbine hybrid system (SOFC-GT system) has been received much attention for a distributed power generation due to its high efficiency. When considering an energy management of the system, it is found that a heat input is highly required to preheat air before being fed to the SOFC stack. The recirculation of a high-temperature cathode exhaust gas is probably an interesting option to reduce the requirement of an external heat for the SOFC-GT system. This study aims to analyze the pressurized SOFC-GT hybrid system fed by ethanol with the recycle of a cathode exhaust gas via a simulation study. Effect of important operating parameters on the electrical efficiency and heat management of the system is investigated.

5.1 Description of SOFC-GT hybrid system

The schematic diagram of a pressurized SOFC-GT hybrid system is illustrated in Fig. (1a). The system consists of a pump, evaporator, heat exchanger, fuel processor, SOFC, combustor, gas turbine and compressor. The steam and ethanol are pumped and then vaporized in the evaporator. The mixture of ethanol and steam is preheated to a desired temperature and converted into a synthesis gas in the steam reformer. The synthesis gas is preheated and fed into the SOFC. Hydrogen in the synthesis gas reacts with oxygen in the compressed air to produce electrical power and steam via the electrochemical reaction. In general, SOFC cannot be operated at the full utilization of

fuel. As a result, the residue fuel in the SOFC outlet stream is combusted in the combustor and the obtained exhaust gas is then fed into the gas turbine to generate more electricity. Due to its high temperature, the gas turbine outlet can be used as a heat source for other heat-requiring units. The heat management of the SOFC system can reduce the requirement of an external heat. Fig. 1(b) shows the SOFC-GT hybrid system in which a portion of the cathode exhaust gas is recycled to mix with the compressed fresh air via a blower. The retrofitted SOFC-GT hybrid system would minimize the energy requirement of the air pre-heater.

(a)

Fuel vaporizer Mixer Soft Combustion chamber Air

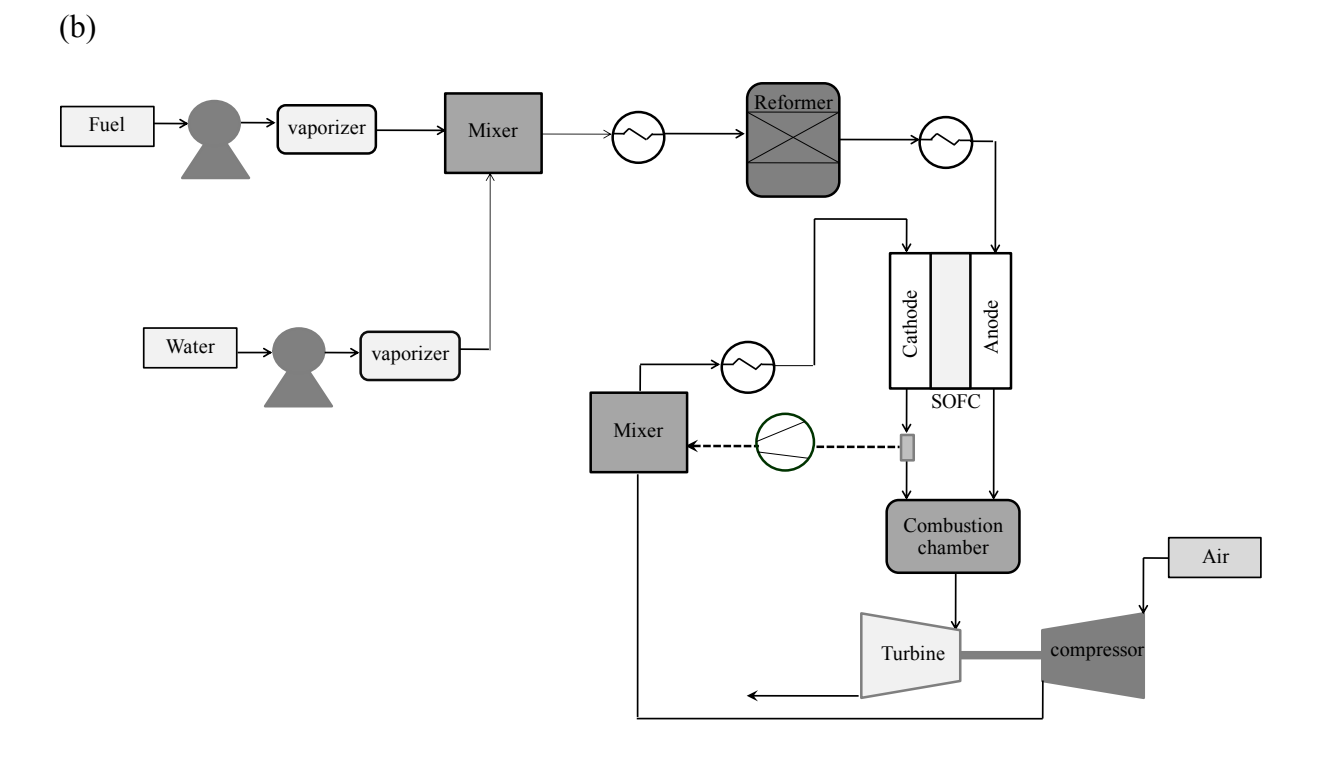


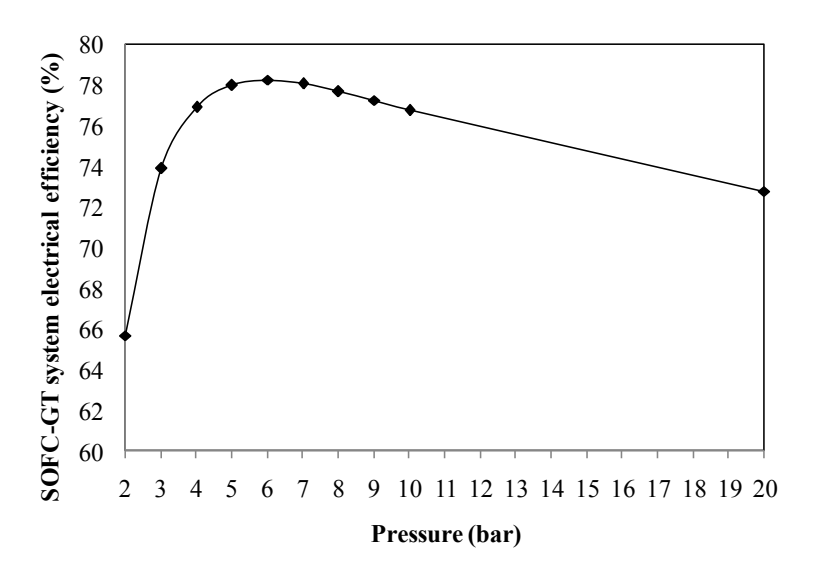
Fig. 1 Schematic diagram of an ethanol-fuelled SOFC system integrated with gas turbine:

(a) a conventional SOFC-GT system and (b) a SOFC-GT system with cathode gas recirculation.

5.2 Results and discussion

5.2.1 A pressurized SOFC-GT system

Firstly, the performance of a pressurized SOFC-GT hybrid system is analyzed. Fig. 2a shows the effect of the operating pressure on the electrical efficiency of the SOFC-GT system, whereas its effect on the SOFC electrical efficiency and the power ratio of gas turbine to SOFC (PGT/PSOFC) is given in Fig. 2b. It can be seen that the system efficiency is considerably improved when increasing the operating pressure from 2 to 4 bar. This is because the SOFC and GT can generate more electrical power; the PGT/PSOFC ratio increases with increasing the operating pressure (Fig. 2b). The increased pressure increases the partial pressure of H₂ in the fuel channel and O₂ in the air channel. In addition, the transport of gases to the electrolyte-electrode interfaces is improved, thereby reducing the concentration losses. These factors lead to the improvement of fuel cell performance. However, it is found that the system efficiency decreases when the operating pressure is higher than 6 bar. This is caused by that the compressor consumes more power at the high pressure operation, while the power produced by the GT slightly increases. As a result, the pressurized SOFC-GT hybrid system should not be operated at a higher pressure. Moreover, the high pressure operation of the SOFC system causes a faster fuel cell degradation and higher capital cost. From Fig. 2a, the SOFC-GT system gives the maximum electrical efficiency of 78.27 % when operated at the pressure of 6 bar. The SOFC generates the power output at 60-75 % of the overall power produced by the SOFC-GT system.



(b)

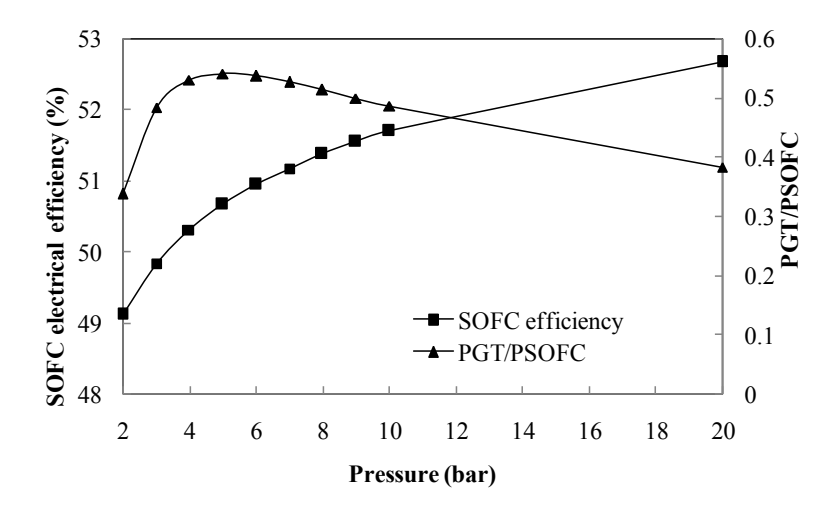


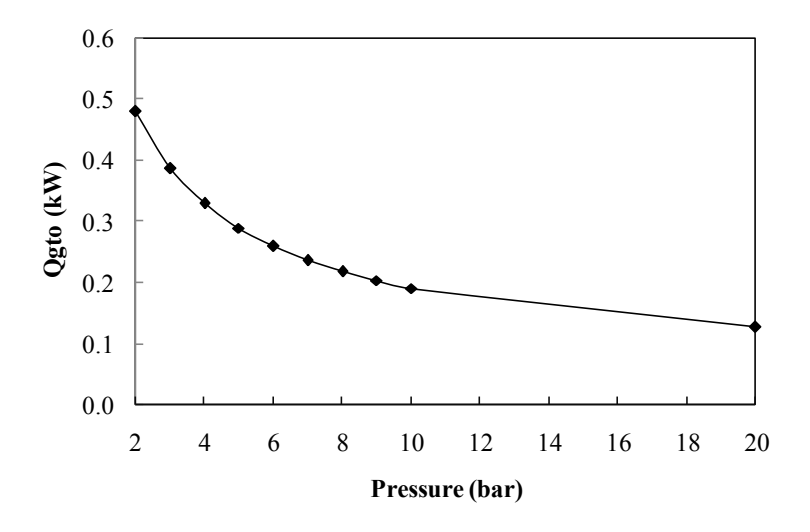
Fig. 2 Effect of operating pressure on the conventional SOFC-GT hybrid system: (a) system electrical efficiency and (b) SOFC electrical efficiency and power ratio of GT to SOFC.

When considering the GT operation, although the temperature of the GT outlet gas decrease, it is still high enough and is considered a useful heat source for supplying to other heat-requiring units within the SOFC system. Fig. 3a shows the effect of the

operating pressure of the SOFC system on the thermal energy of the GT outlet gas, which is calculated based on the reference temperature of 100 °C. It is found that the thermal energy of the GT outlet gas reduces when the SOFC system is operated at a higher pressure. This thermal energy depends on the inlet gas flow to the GT, the GT inlet temperature and the operating pressure of the GT. Fig. 3b shows the relation of the operating pressure to the GT outlet temperature and the excess air ratio. The results indicate that the temperature of the GT outlet decreases with increasing the operating pressure. Furthermore, the excess air needed for supplying to the SOFC is lower when the SOFC system is run at a higher pressure, leading to a decrease in the flow rate of gas fed into the GT.

Regarding the energy management of the SOFC-GT hybrid system, the thermal energy in the turbine exhaust gas is generally utilized for pre-heating air fed to the SOFC. However, this study focuses on the use of this remaining thermal energy for supplying to all other heat-requiring units in order to reduce the requirement of the external heat. Fig. 4 shows the impact of the operating pressure on the residual energy calculated from the thermal energy of the GT exhaust gas subtracted by the system heat requirement. The negative value of the residual energy indicates that the thermal energy from the GT outlet gas is insufficient to supply the SOFC system and thus the external heat is needed. It is found that an increase in the operating pressure reduces the external heat requirement because the ethanol steam reformer needs less energy. It is noted that when operated at the pressure of 20 bar, the SOFC-GT system can be operated at a self-sustainable condition where the external heat is unnecessary; however, at high pressure operation, a low system electrical efficiency is obtained.

Project: Design and analysis of a solid oxide fuel cell system for combined heat and electrical power generation



(b)

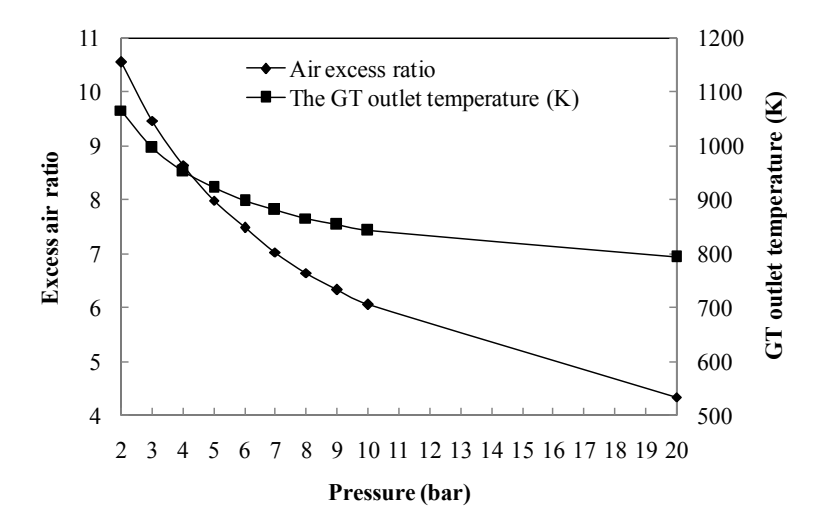


Fig. 3 Effect of operating pressure on (a) thermal energy of the GT outlet gas (Qgto) and (b) excess air ratio and GT outlet temperature (the conventional SOFC-GT hybrid system).

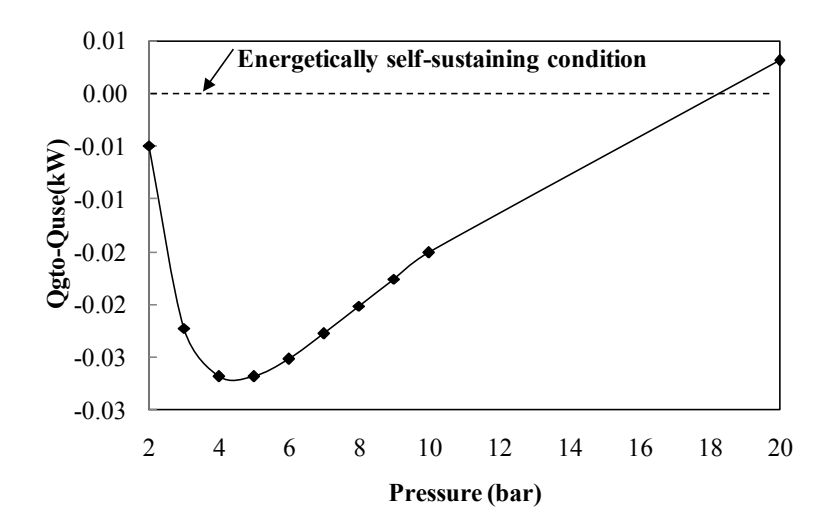


Fig. 4 Effect of operating pressure on the remaining energy of the GT exhaust gas (the conventional SOFC-GT hybrid system).

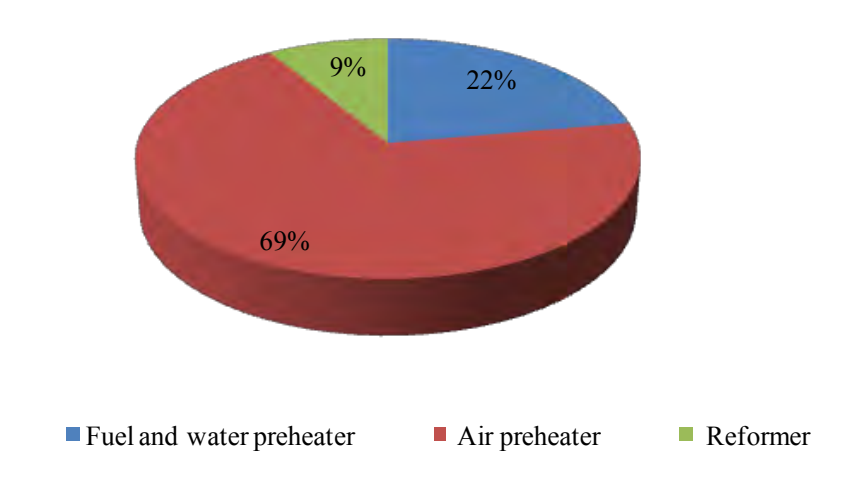


Fig. 5 Distribution of heat used in the conventional SOFC-GT hybrid system (P = 6 bar).

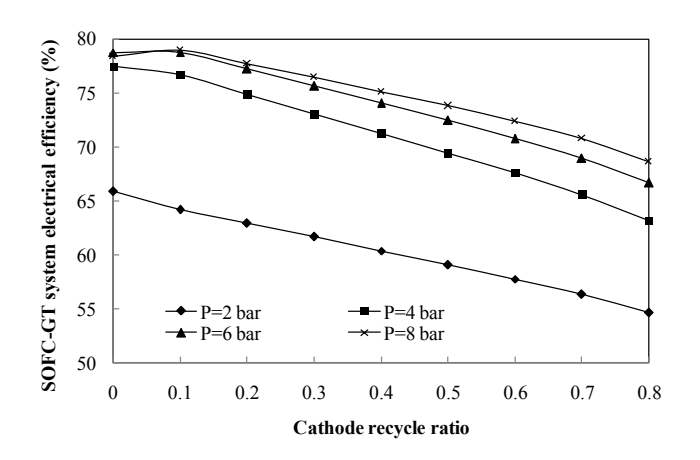
Fig. 5 shows the energy requirement in each part of the pressurized SOFC-GT hybrid system. It can be divided into three parts, namely the energy used for pre-heating air, pre-heating fuel and water and ethanol steam reformer. The air pre-heating unit consumes the highest energy; it takes about 65-74% of the overall energy consumption of the SOFC-GT system. Therefore, if the energy used for the air pre-heater operation can be

reduced, the requirement of the external heat for supplying to the SOFC system would be minimized and the energy management of the system would be probably better.

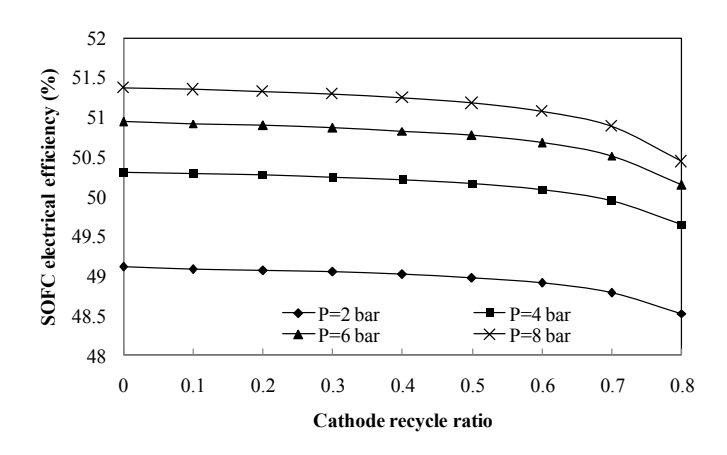
5.2.2 A pressurized SOFC/GT system with cathode gas recirculation

In the previous section, it was found that most thermal energy consumption in the SOFC system is caused by the air pre-heater. To improve the system performance, a portion of the cathode exhaust gas is recycled and then mixed with a fresh air feed to reduce a heat duty of the air pre-heater. Regarding the system electrical efficiency, the pressurized SOFC-GT hybrid system is studied under a pressure range of 2-8 bar. The influence of a recirculation ratio of the cathode exhaust gas at different operating pressures on the system electrical efficiency, SOFC electrical efficiency and the PGT/PSOFC ratio is illustrated in Figs. 6a-c, respectively. The system electrical efficiency decreases with increasing the recirculation ratio of the cathode exhaust gas at all the operating pressure considered, and the SOFC efficiency and the PGT/PSOFC ratio show similar trends. The results also indicate that the recirculation ratio has impact on the performance of the GT more than the SOFC. The electrical efficiency of the SOFC slightly declines with increasing the recirculation ratio of the cathode exhaust gas (0.1-0.7); however, the decrement of the SOFC efficiency is obviously observed at the recirculation ratio of higher than 0.7. This is because the oxygen feed is diluted when increasing the recirculation ratio and consequently, a larger concentration loss in the SOFC appears. An increase in the cathode gas recycle also decreases the PGT/PSOFC ratio as the gas inlet flow to the GT drop and thus the GT power is less generated.

Project: Design and analysis of a solid oxide fuel cell system for combined heat and electrical power generation Asst. Prof. Amornchai Arpornwichanop, Department of Chemical Engineering,



(b)



(c)

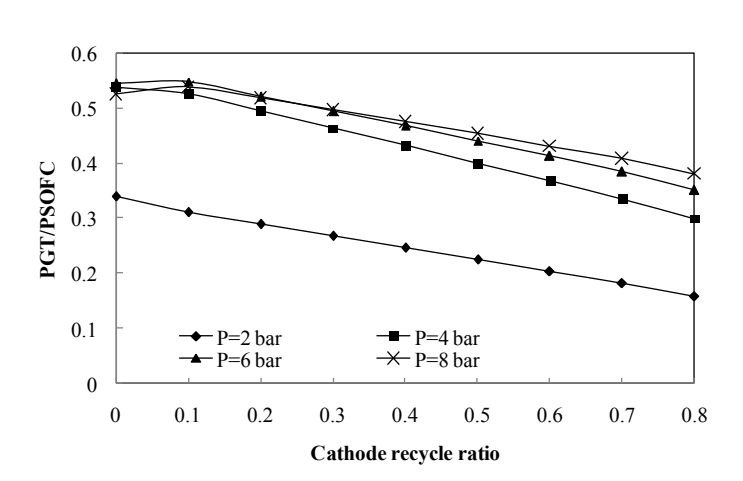


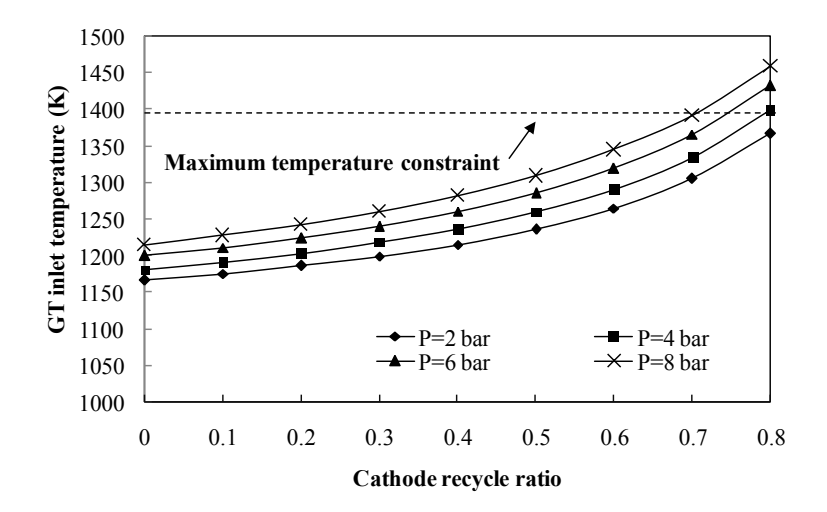
Fig. 6 Effect of recirculation ratio of cathode gas on the SOFC-GT hybrid system with cathode gas recirculation at different operating pressure: (a) system electrical efficiency, (b) SOFC electrical efficiency and (c) power ratio of GT to SOFC.

Fig. 7 shows the variations in the GT inlet temperature and the thermal energy of the GT outlet gas as a function of the recirculation ratio of the cathode gases at different operating pressures. An increase in the cathode gas recycle results in the elevated temperature of the GT inlet because the air stream fed to the combustor decreases while the fuel in the anode exhaust gas is still constant. It is noted that the fuel utilization of the SOFC is kept constant at 70% in all case studies. Although the increased temperature of the GT inlet enhances the performance of the GT, the GT inlet temperature should not exceed the endurance limit of GT materials. In general, the maximum GT inlet temperature is 1400 K [27]. Taking this constraint into consideration, the cathode recirculation ratio should not be higher than 0.7-0.8, depending on the operating pressure (Fig. 8a). When considering the thermal energy of the GT exhaust gas (Fig. 8b), it decreases with the increased recirculation ratio because a decrease in the GT inlet feed flow has more effect on the thermal energy of the GT outlet gas than an increase in the GT inlet temperature.

Fig. 8 shows the effect of the cathode gas recirculation on the residual thermal energy of the SOFC-GT system. When the system is operated at a higher recirculation of the cathode gas, it is found that the SOFC system generates the thermal energy higher than its consumption. This result indicates a possibility of the SOFC-GT system with cathode gas recirculation to be operated at the self-sustainable condition. At high recirculation ratio of the cathode exhaust gas, the requirement of the fresh air fed to the SOFC reduces, resulting in the decreased heat duty of the air pre-heater. Because the recirculation of the cathode gas has a positive effect on the thermal management of the pressurized SOFC-GT hybrid system but decreases the system electrical efficiency. Therefore, the recirculation ratio of the cathode exhaust gas should be carefully selected. In this study, it is found that the pressurized SOFC-GT hybrid system should be operated

at pressure of 6 bar because the highest electrical efficiency can be achieved and the cathode gas recirculation ratio of 0.3 is selected. At this condition, the SOFC system can be self-sustainable and the system electrical efficiency slightly decreases (3 %).

(a)



(b)

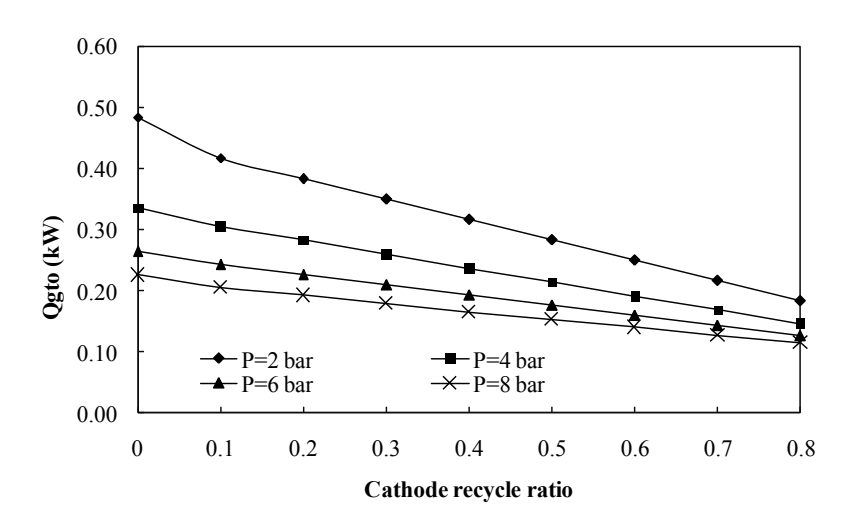


Fig. 7 Effect of recirculation ratio of cathode gas on (a) the GT inlet temperature and (b) the thermal energy of the GT outlet gas (the SOFC-GT hybrid system with cathode gas recirculation).

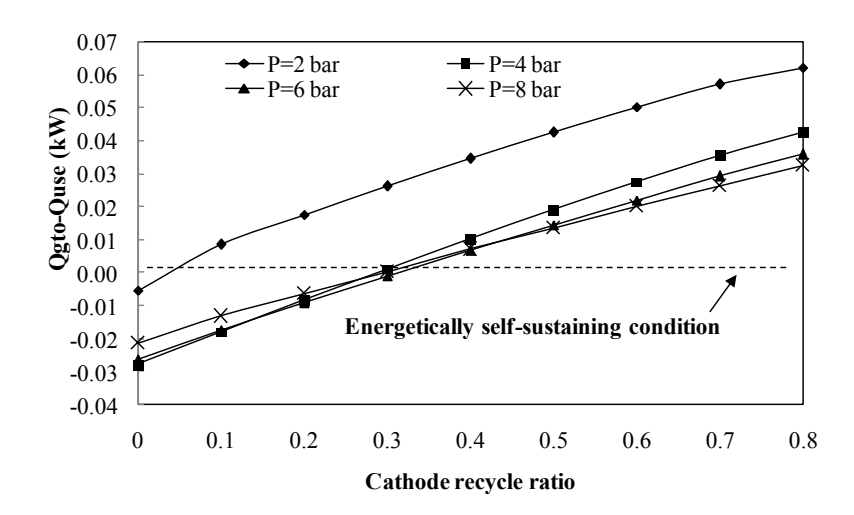


Fig. 8 Effect of recirculation ratio of cathode-off gas on the residual energy from the outlet GT energy (the SOFC-GT hybrid system with cathode gas recirculation).

Chapter 6

Conclusions

6.1 Use of different renewable fuels in a steam reformer integrated into a solid oxide

fuel cell: Theoretical analysis and performance comparison

The performance and efficiency of a steam reforming process and solid oxide fuel

cell (SOFC) integrated system is theoretically analyzed in this study. Different renewable

fuels, i.e., glycerol, ethanol and biogas, were applied to generate hydrogen for SOFC. The

results showed that ethanol can produce the most hydrogen at an operating temperature of

1073 K. The utilization of glycerol for hydrogen production shows the least tendency

toward carbon formation. The SOFC system supplied by biogas requires the most energy

and has the lowest electrical and thermal efficiencies. Ethanol is a suitable fuel for the

SOFC system; it has the highest electrical and thermal efficiencies of the three fuels, and

it has low carbon dioxide emission.

6.2 Analysis of an ethanol-fuelled solid oxide fuel cell system using partial anode

exhaust gas recirculation

The performance analysis of a SOFC system fuelled by ethanol is presented in this

work. An electrochemical model of the SOFC and an equilibrium model of ethanol steam

reforming are employed to simulate the SOFC system. The performance of two SOFC

systems with and without anode exhaust gas recirculation is compared. The results

indicate that the SOFC system with anode exhaust gas recycling provides higher electrical

and thermal efficiencies than that of a non-recycling SOFC system. It is found that the

Project: Design and analysis of a solid oxide fuel cell system for combined heat and electrical power generation

tendency of carbon formation in the ethanol steam reformer decreases with an increasing

recirculation ratio and fuel utilization in the SOFC stack. At low fuel utilization, the

electrical efficiency of the SOFC system increases with the increasing recirculation ratio

while the thermal efficiency decreases. The performances of the SOFC system show an

opposite trend at high fuel utilization operation. Therefore, the recirculation ratio must be

carefully selected. Furthermore, the electrical efficiency of the SOFC system can be

enhanced when the ethanol reformer and SOFC stack are operated at high temperatures.

6.3 Analysis of a pressurized solid oxide fuel cell-gas turbine hybrid power system

with cathode gas recirculation

A pressurized solid oxide fuel cell and gas turbine hybrid system (SOFC-GT) fed

by ethanol is studied. The performance of the SOFC system in terms of the electrical

efficiency and thermal management is analyzed with respect to the operating pressure and

recycle ratio of a cathode exhaust gas. The simulation results show that the optimal

operating pressure of the pressurized SOFC system is in a range of 4-6 bar. Under this

condition, the system can achieve the highest electrical efficiency, whereas the

recuperation of the waste heat from the GT exhaust gas is minimized. The recirculation of

the cathode exhaust gas in the SOFC system can reduce the external heat requirement of

an air pre-heater. However, the electrical efficiency of the SOFC system with cathode gas

recycling is lower than the conventional SOFC system. In addition, it is found that the

SOFC system with cathode gas recycling can be operated at a self-sustainable condition.

55

Project: Design and analysis of a solid oxide fuel cell system for combined heat and electrical power generation

Chapter 7

Project outputs

7.1 International Journal publication

- 1. Saebea, D., Patcharavorachot, Y. and Arpornwichanop, A. (2012). Analysis of an ethanol-fuelled solid oxide fuel cell system using partial anode exhaust gas recirculation. Journal of Power Sources, 208, 120-130. (IF-2012 = 4.675)
- Authayanun, S., Wiyaratn, W., Assabumrungrat, S. and Arpornwichanop, A. (2013). Theoretical analysis of a glycerol reforming and high-temperature PEMFC integrated system: Hydrogen production and system efficiency. Fuel, 105, 345-352. (IF-2012 = 3.357)
- 3. Saebea, D., Authayanun, S., Patcharavorachot, Y., Paengjuntuek, W. and Arponwichanop, A. (2013). Use of different renewable fuels in a steam reformer integrated into a solid oxide fuel cell: Theoretical analysis and performance comparison. Energy, 51, 305-313. (IF-2012 = 3.651)
- Saebea, D., Patcharavorachot, Y., Assabumrungrat, S. and Arpornwichanop, A.
 (2013). Analysis of a pressurized solid oxide fuel cell-gas turbine hybrid power system with cathode gas recirculation. International Journal of Hydrogen Energy, 38, 4748-4759. (IF-2012 = 3.548)
- Authayanun, S., Mamlouk, M., Scott, K. and Arpornwichanop, A. (2013).
 Comparison of high-temperature and low-temperature polymer electrolyte membrane fuel cell systems with glycerol reforming process for stationary applications. Applied Energy, 109, 192-201. (IF-2012 = 4.781)

- Chutichai, B., Authayanun, S., Assabumrungrat, S. and Arpornwichanop, A.
 (2013). Performance analysis of an integrated biomass gasification and
 PEMFC system: Hydrogen and power generation. Energy, 55, 98-106. (IF-2012 = 3.651)
- Arpornwichanop, A. and Patcharavorachot, Y. (2013). Investigation of a proton-conducting SOFC with internal autothermal reforming of methane.
 Chemical Engineering Research and Design, 91, 1508-1516. (IF-2012 = 1.927)
- 8. Tippawan, P. and Arpornwichanop, A. (2014). Energy and exergy analysis of an ethanol reforming process for solid oxide fuel cell applications. Bioresource Technology, 157, 231-239. (IF-2012 = 4.750)
- 9. Authayanun, S., Saebea, D., Patcharavorachot, Y. and Arpornwichanop, A. (2014). Effect of different fuel options on performance of high-temperature PEMFC (proton exchange membrane fuel cell) systems. Energy, 68, 989-997. (IF-2012 = 3.651)

7.2 International Conferences

- Saebea, D., Patcharavorachot, Y., Assabumrungrat, S., Arpornwichanop, A. (2011). Design of a solid oxide fuel cell-gas turbine hybrid power system with cathode gas recycling. The 6th Asia Pacific Chemical Reaction Engineering Symposium (APCRE'11), Sep. 18-21, 2011, Beijing, China. (The Excellent Poster Presentation Award)
- 2. Saebea, D., Authayanun, S., Patcharavorachot, Y., Paengjuntuek, W. and Arpornwichanop, A. (2012). Performance analysis of SOFC systems integrated with steam reforming of different renewable fuels. International

- Conference on Renewable Energies and Power Quality (ICREPQ'12). Mar. 28-30, 2012, Santiago de Compostela, Spain.
- Saebea, D., Magistri, L., Massardo, A. and Arpornwichanop, A. (2012).
 Design and heat recovery of pressurized SOFC/GT hybrid systems. Grove
 Fuel Cells Conference 2012, April 11-12, 2012, Berlin, Germany.
- Tippawan, P. and Arpornwichanop, A. (2012). Energy and exergy analyses of hydrogen production from different ethanol reforming processes. XX International Conference on Chemical Reactors (CHEMREACTOR-20), Dec. 3-7, 2012, Luxembourg.
- Jienkulsawad, P., Saebea, D., Patcharavorachot, Y., Assabumrungrat, S. and Arpornwichanop, A. (2013). Effect of fluid properties on performance of solid oxide fuel cell: Isothermal and non-isothermal operations. Pure and Applied Chemistry International Conference (PACCON2013), Jan. 23-25, 2013, Chon Buri, Thailand.
- 6. Tippawan, P., Saebea, D., Patcharavorachot, Y. and Arpornwichanop, A. (2013). Performance improvement of a solid oxide fuel cell system with a two-step ethanol steam reforming process using CO2 sorbent. 9th European Congress of Chemical Engineering (ECCE9), April 21-25, 2013, The Hague, The Netherlands.
- Authayanun, S., Aunsup, P., Im-orb, K. and Arpornwichanop A. (2013).
 Systematic analysis of proton electrolyte membrane fuel cell systems integrated with biogas reforming process. 16th Conference Process Integration,
 Modelling and Optimisation for Energy Saving and Pollution Reduction (PRES'13), Sep. 29-Oct. 2, 2013, Rhodes, Greece.

- 8. Saebea, D., Patcharavorachot, Y., Authayanun, S. and Appornwichanop, A. (2013). Design of energy recuperation in a solid oxide fuel cell-gas turbine hybrid power system. Fifth European Fuel Cell Technology & Applications Conference (EFC 2013), Dec. 11-13, 2013, Rome, Italy.
- Mahisanan, C. and Arpornwichanop, A. (2014). Performance analysis of a solid oxide fuel cell and oxyfuel combustion integrated system. Pure and Applied Chemistry International Conference 2014 (PACCON2014), Jan. 8-10, 2014, Khon Kaen, Thailand.

References

- Aguiar P, Adjiman CS, Brandon NP. Anode-supported intermediate temperature direct internal reforming solid oxide fuel cell. I: model-based steady-state performance. J. Power Sources 138 (2004) 120-136.
- Akande A, Aboudheir A, Idem R, Dalai A. Kinetic modeling of hydrogen production by the catalytic reforming of crude ethanol over a co-precipitated Ni-Al₂O₃ catalyst in a packed bed tubular reactor. Int J Hydrogen Energy 31 (2006) 1707–1715.
- Byrd AJ, Pant KK, Gupta RB. Hydrogen production from glycerol by reforming in supercritical water over Ru/Al₂O₃ catalyst. Fuel 87 (2008) 2956–2960.
- Demirbas A. Biodiesel from waste cooking oil via base catalytic and supercritical methanol transesterification. Energy Convers Manage 50 (2009) 923–927.
- Dou B, Dupont V, Rickett G, Blakeman N, Williams PT, Chen H, Ding Y, Ghadiri M, Hydrogen production by sorption-enhanced steam reforming of glycerol. Bioresour Technol 100 (2009) 3540–3547.
- Douvartzides SL, Coutelieris FA, Tsiakaras PE. On the systematic of ethanol fed SOFC-based electricity generating system in terms of energy and exergy. J Power Sources 114 (2004) 203–212.
- Farhad S, Hamdullahpur F, Yoo Y. Performance evaluation of different configurations of biogas-fuelled SOFC micro-CHP systems for residential applications. Int J Hydrogen Energy 35 (2010) 3758–3768.
- Freni S, Maggio G, Cavallaro S. Ethanol steam reforming in a molten carbonate fuel cell: a thermodynamic approach. J. Power Sources 62 (1996) 67–73.

- Granovskii M, Dincer I, Rosen MA. Performance comparison of two combined SOFC–gas turbine systems. J. Power Sources 165 (2007) 307–314.
- Mohseni F, Magnusson M, Görling M, Alvfors P. Biogas from renewable electricity Increasing a climate neutral fuel supply. Appl Energy 90 (2012) 11–16.
- Nehter P. A high fuel utilizing solid oxide fuel cell cycle with regard to the formation of nickel oxide and power density. J. Power Sources 164 (2007) 252–259.
- Nishikawa H, Sasou H, Kurihara R, Nakamura S, Kano A, Tanaka K, Aoki T, Ogami Y. High fuel utilization operation of pure hydrogen fuel cells. Int. J. Hydrogen Energy 33 (2008) 6262–6269.
- Onda K, Iwanari T, Miyauchi N, Ito K, Ohba T, Sakaki Y, Nagata S. Cycle Analysis of Combined Power Generation by Planar SOFC and Gas Turbine Considering Cell Temperature and Current Density Distributions. J. Electrochem. Soc. 150 (2003) A1569-1576.
- Pandya JD, Ghosh KK, Rastogi SK. A phosphoric acid fuel cell coupled with biogas. Energy 13 (1988) 383–388.
- Patcharavorachot Y, Arpornwichanop A, Chuachuensuk A. Electrochemical study of a planar solid oxide fuel cell: Role of support structures. J. Power Sources 177 (2008) 254–261.
- Patcharavorachot Y, Paengjuntuek W, Assabumrungrat S, Arpornwichanop A. Performance evaluation of combined solid oxide fuel cells with different electrolytes. Int. J. Hydrogen Energy 35 (2010) 4301–4310.
- Piroonlerkgul P, Assabumrungrat S, Laosiripojana N, Adesina AA. Selection of appropriate fuel processor for biogas-fuelled SOFC system. Chem Eng J 140 (2008) 341–351.

- Pompeo F, Santori G, Nichio NN. Hydrogen and/or syngas from steam reforming of glycerol: Study of platinum catalysts. Int J Hydrogen Energy 35 (2010) 8912–8920.
- Peter R, Dahl R, Kluttgen U, Plam C, Stolten D. Internal reforming of methane in solid oxide fuel cell systems. J. Power Sources 106 (2002) 238-244.
- Sun S, Yan W, Sun P, Chen J. Thermodynamic analysis of ethanol reforming for hydrogen production. Energy 44 (2012) 911–924.
- Tsiakaras P, Demin A. Thermodynamic analysis of a solid oxide fuel cell system fuelled by ethanol. J Power Sources 102 (2001) 210–217.

Appendix A

Publications in international journal

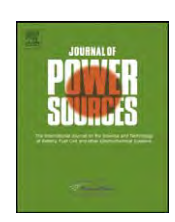
- 1. Saebea, D., Patcharavorachot, Y. and Arpornwichanop, A. (2012). Analysis of an ethanol-fuelled solid oxide fuel cell system using partial anode exhaust gas recirculation. Journal of Power Sources, 208, 120-130. (IF-2012 = 4.675)
- 2. Authayanun, S., Wiyaratn, W., Assabumrungrat, S. and Arpornwichanop, A. (2013). Theoretical analysis of a glycerol reforming and high-temperature PEMFC integrated system: Hydrogen production and system efficiency. Fuel, 105, 345-352. (IF-2012 = 3.357)
- 3. Saebea, D., Authayanun, S., Patcharavorachot, Y., Paengjuntuek, W. and Arponwichanop, A. (2013). Use of different renewable fuels in a steam reformer integrated into a solid oxide fuel cell: Theoretical analysis and performance comparison. Energy, 51, 305-313. (IF-2012 = 3.651)
- 4. Saebea, D., Patcharavorachot, Y., Assabumrungrat, S. and Arpornwichanop, A. (2013). Analysis of a pressurized solid oxide fuel cell-gas turbine hybrid power system with cathode gas recirculation. International Journal of Hydrogen Energy, 38, 4748-4759. (IF-2012 = 3.548)
- 5. Authayanun, S., Mamlouk, M., Scott, K. and Arpornwichanop, A. (2013). Comparison of high-temperature and low-temperature polymer electrolyte membrane fuel cell systems with glycerol reforming process for stationary applications. Applied Energy, 109, 192-201. (IF-2012 = 4.781)
- 6. Chutichai, B., Authayanun, S., Assabumrungrat, S. and Arpornwichanop, A. (2013). Performance analysis of an integrated biomass gasification and PEMFC system: Hydrogen and power generation. Energy, 55, 98-106. (IF-2012 = 3.651)
- 7. Arpornwichanop, A. and Patcharavorachot, Y. (2013). Investigation of a proton-conducting SOFC with internal autothermal reforming of methane. Chemical Engineering Research and Design, 91, 1508-1516. (IF-2012 = 1.927)
- 8. Tippawan, P. and Arpornwichanop, A. (2014). Energy and exergy analysis of an ethanol reforming process for solid oxide fuel cell applications. Bioresource Technology, 157, 231-239. (IF-2012 = 4.750)
- 9. Authayanun, S., Saebea, D., Patcharavorachot, Y. and Arpornwichanop, A. (2014). Effect of different fuel options on performance of high-temperature PEMFC (proton exchange membrane fuel cell) systems. Energy, 68, 989-997. (IF-2012 = 3.651)

S-S-WIER ELSEVIER

Contents lists available at SciVerse ScienceDirect

Journal of Power Sources

journal homepage: www.elsevier.com/locate/jpowsour



Analysis of an ethanol-fuelled solid oxide fuel cell system using partial anode exhaust gas recirculation

Dang Saebea^a, Yaneeporn Patcharavorachot^a, Amornchai Arpornwichanop^{a,b,*}

- ^a Department of Chemical Engineering, Faculty of Engineering, Chulalongkorn University, Bangkok 10330, Thailand
- ^b Computational Process Engineering, Chulalongkorn University, Bangkok 10330, Thailand

ARTICLE INFO

Article history:
Received 3 December 2011
Received in revised form 5 February 2012
Accepted 7 February 2012
Available online 15 February 2012

Keywords: Solid oxide fuel cell Anode exhaust gas recycle Ethanol reforming Performance analysis

ABSTRACT

This paper presents an analysis of a solid oxide fuel cell (SOFC) system integrated with an ethanol reforming process. The recycling of the anode exhaust gas in the integrated SOFC system is considered to improve its performance. The results indicate that under the same operating conditions, the SOFC system operated with the recycle of the anode exhaust gas has higher electrical and thermal efficiencies than a non-recycling SOFC system. The required conditions to prevent carbon formation in the ethanol reformer are also examined. When the SOFC system with anode exhaust gas recycling is operated at a higher recirculation ratio and fuel utilization, the carbon formation can be reduced, which in turn decreases the reformer operating temperature. However, the recirculation ratio has to be carefully selected because an increase in the recirculation ratio has an adverse impact on the electrical efficiency of the SOFC system. In addition, the results show that the electrical efficiency depends on the fuel utilization of the SOFC. At low fuel utilization (0.5–0.6), the electrical efficiency increases as the recirculation ratio increases. In contrast, when the SOFC is operated at a higher fuel utilization (>0.6), an increase in the recirculation ratio results in a decrease in the electrical efficiency.

© 2012 Elsevier B.V. All rights reserved.

1. Introduction

Fuel cells have been identified as an alternative method to generate power with high efficiency and environmental friendliness when compared to a conventional combustion-based process. Among the various types of fuel cells, the solid oxide fuel cell (SOFC) is the most promising fuel cell technology, as it can be used in a wide range of commercial applications. The high operational temperature of the SOFC (1073–1273 K) results in many advantages; for example, the high-temperature waste heat from a SOFC can be recovered for use in other heat-demanding units in the SOFC system. In addition, different fuels (e.g., methane, methanol, ethanol, etc.) can be directly fed to the SOFC due to the possibility for operation with internal reforming [1].

In general, natural gas is widely used as the fuel for SOFC applications. However, liquid fuels such as ethanol, methanol and gasoline have been recommended for use in automotive applications or auxiliary power units [2–4]. In comparison with other feedstocks, ethanol is considered an economically attractive green

E-mail address: Amornchai.A@chula.ac.th (A. Arpornwichanop).

fuel as it can be derived renewably from several biomass sources, including energy plants and agriculture residues [5]. In addition, it presents several advantages for fuel cell applications; that is, it has a relatively high hydrogen content and is easy to store, handle and transport safely due to its lower toxicity and volatility [6]. Douvartzides et al. [7] presented a thermodynamic and economic analysis of the electricity generation of SOFCs using various fuels. The results showed that the use of ethanol to produce hydrogen for SOFCs is a very promising option. When ethanol is considered as the primary fuel, it is possible to be internally reformed into a hydrogen-rich gas (synthesis gas) within a fuel cell stack (referred to as an internal reforming SOFC, or IR-SOFC) because the operating temperature of the SOFC is in the same range as that of the reforming reactions. However, it was reported that the direct feed of ethanol to the SOFC stack is not appropriate due to the easy degradation of the Ni/YSZ catalyst at the anode by carbon formation, which leads to the loss of fuel cell performance and poor durability [8]. In order to avoid this problem, the implementation of an external reforming system is a potentially better option because the higher content of hydrogen that is obtained from the conversion of ethanol via a steam reforming process can be introduced to the SOFC stack [9]. Nevertheless, because the steam reforming reaction involves a highly endothermic reaction, the SOFC system with external reforming requires a high external heat source and efficient energy management.

^{*} Corresponding author at: Department of Chemical Engineering, Faculty of Engineering, Chulalongkorn University, Bangkok 10330, Thailand. Tel.: +66 2 218 6878; fax: +66 2 218 6877.

Nomenclature

activity coefficient of carbon a_c fuel cell active area (m²) A_{c} D_{eff,anode} effective gaseous diffusivity through $(m^2 s^{-1})$ D_{eff,cathode} effective oxygen diffusivity through cathode $(m^2 s^{-1})$ **E**OCV open-circuit voltage (V) E^0 open-circuit voltage at the standard pressure (V) Eanode activation energy of anode (kJ mol^{-1}) activation energy of cathode ($k \text{I} \text{ mol}^{-1}$) Ecathode Faraday constant ($C \text{ mol}^{-1}$) h enthalpy (kJ mol^{-1}) standard heat of reaction (kJ mol⁻¹) ΔH° current density (A m⁻²) exchange current density at anode (A m⁻²) $j_{0,\mathrm{anode}}$ exchange current density at cathode (A m⁻²) $j_{0,\mathrm{cathode}}$ pre-exponential factor of the anode (A m⁻²) $k_{\rm anode}$ pre-exponential factor of cathode (A m⁻²) $k_{\rm cathode}$ equilibrium constants K_{eq} $LHV_{C_2H_5OH}$ low heating value of ethanol (kJ s $^{-1}$) number of electrons transferred n molar flow rate ($mol s^{-1}$) 'n partial pressures of component *i* (bar) p_i operating pressure of SOFC (bar) P_{sofc} electrical power output (W) Q thermal energy (kJ s $^{-1}$) gas constant ($kJ \, mol^{-1} \, K^{-1}$) R $R_{\rm ohm}$ total internal resistance (Ω m²) temperature (K) fuel utilization factor $U_{\rm f}$ operating cell voltage (V) ż amount of hydrogen consumed by the electrochemical reaction ($mol s^{-1}$) Greek symbols transfer coefficient overpotentials (V) η λ_{air} excess air ratio electronic conductivity of anode (Ω^{-1} m⁻¹) $\sigma_{
m anode}$ electronic conductivity of cathode (Ω^{-1} m⁻¹) $\sigma_{cathode}$ $\sigma_{electrolyte}$ ionic conductivity of electrolyte ($\Omega^{-1} \, m^{-1}$)

 $au_{
m anode}$ thickness of anode (m) thickness of cathode (m) $\tau_{\rm cathode}$ $\tau_{electrolyte}$ thickness of electrolyte (m)

Subscripts

air channel a

concentration overpotentials conc

fuel channel f

i chemical component

reaction ohm ohmic loss reformer

sofc solid oxide fuel cell SM steam reforming reaction TPB three-phase boundary WGS water gas shift reaction

When considering the operating parameters of SOFC systems, it has been reported that the fuel utilization is the most important parameter affecting the performance of SOFC. A SOFC operated at high fuel utilization can provide high electrical efficiency. However,

at high fuel utilization, more hydrogen is consumed by the electrochemical reactions, and the fuel stream at the SOFC fuel channel is thus diluted by steam [10]. A hydrogen deficiency due to the unbalanced fuel flowing through the SOFC causes a larger buildup of nickel oxide [11] as well as corrosion on the carbon plate [12]. Therefore, it is reasonable to operate the SOFC at a moderate fuel utilization. Under this condition, the SOFC can produce electrical power together with a high-temperature exhaust gas that contains useful remaining fuel (i.e., hydrogen and carbon monoxide). Typically, the exhaust gases from fuel and air channels are burnt in an afterburner to produce more heat, which is used to preheat the fuel stream and supplied to the steam reformer. Although the combustion of exhaust gases can increase the thermal efficiency of the SOFC system, the fuel stream is utilized inefficiently. To improve the overall SOFC performance, a SOFC system with anode exhaust gas recycling has been proposed in the literatures [13–15]. A portion of anode exhaust gas containing useful fuels, i.e., hydrogen and carbon monoxide, is recirculated to mix with the inlet fuel before it is fed to the reformer, whereas the rest of the anode exhaust gas is burnt with the cathode exhaust gas in the afterburner. Interestingly, it is noteworthy that the steam produced by the electrochemical reaction in the anode exhaust gas can be further used as a reagent for steam reforming and thus the requirement for fresh steam can be reduced [16]. Shekhawat et al. [14] demonstrated that the utilization of the anode exhaust gas in the SOFC system integrated with the catalytic partial oxidation of diesel can reduce the carbon formation and increase the hydrogen concentration in the reformate gas. Although the SOFC system with anode exhaust gas recycling was previously studied as mentioned above, there are few studies that investigate in detail the effect of utilizing the anode exhaust gas on the reforming process and the SOFC system performance. This understanding allows for the improvement of the overall SOFC system efficiency.

In this study, the performance of a SOFC system fuelled by synthesis gas derived from an ethanol reforming process with nonrecycling and recycling of the anode exhaust gas is investigated based on a thermodynamic analysis. The optimal design of the SOFC system is determined by considering the electrical and thermal efficiencies. In addition, the influences of the fuel utilization and recirculation ratio of the anode exhaust gas on the carbon formation in the ethanol steam reformer and on the system efficiency are investigated to justify the benefit of using the anode exhaust gas recycling.

2. Model of SOFC system

2.1. SOFC system

Fig. 1a and b shows schematics of the ethanol steam reformer and the SOFC integrated system with and without the recycle of the anode exhaust gas, respectively. Both the SOFC systems consist of a vaporizer, heat exchanger, fuel processor, SOFC stack and afterburner. First, ethanol and water are separately fed into the vaporizer and then sent to the heat exchanger to be preheated to the desired operating temperature of the reformer. The ethanol and steam then undergo the steam reforming reaction at the reformer to produce a synthesis gas. The obtained synthesis gas is preheated before being fed to the SOFC stack where the hydrogen in the synthesis gas reacts with oxygen in air to produce electrical power via an electrochemical reaction. The residue fuel in the SOFC outlet stream is combusted in the afterburner and the heat thus generated can be used for the heat-requiring units in the SOFC system. In the case where the anode exhaust gas is recycled (Fig. 1b), a portion of the anode exhaust gas is recycled to the reformer. The steam generated by the electrochemical reaction can be used as

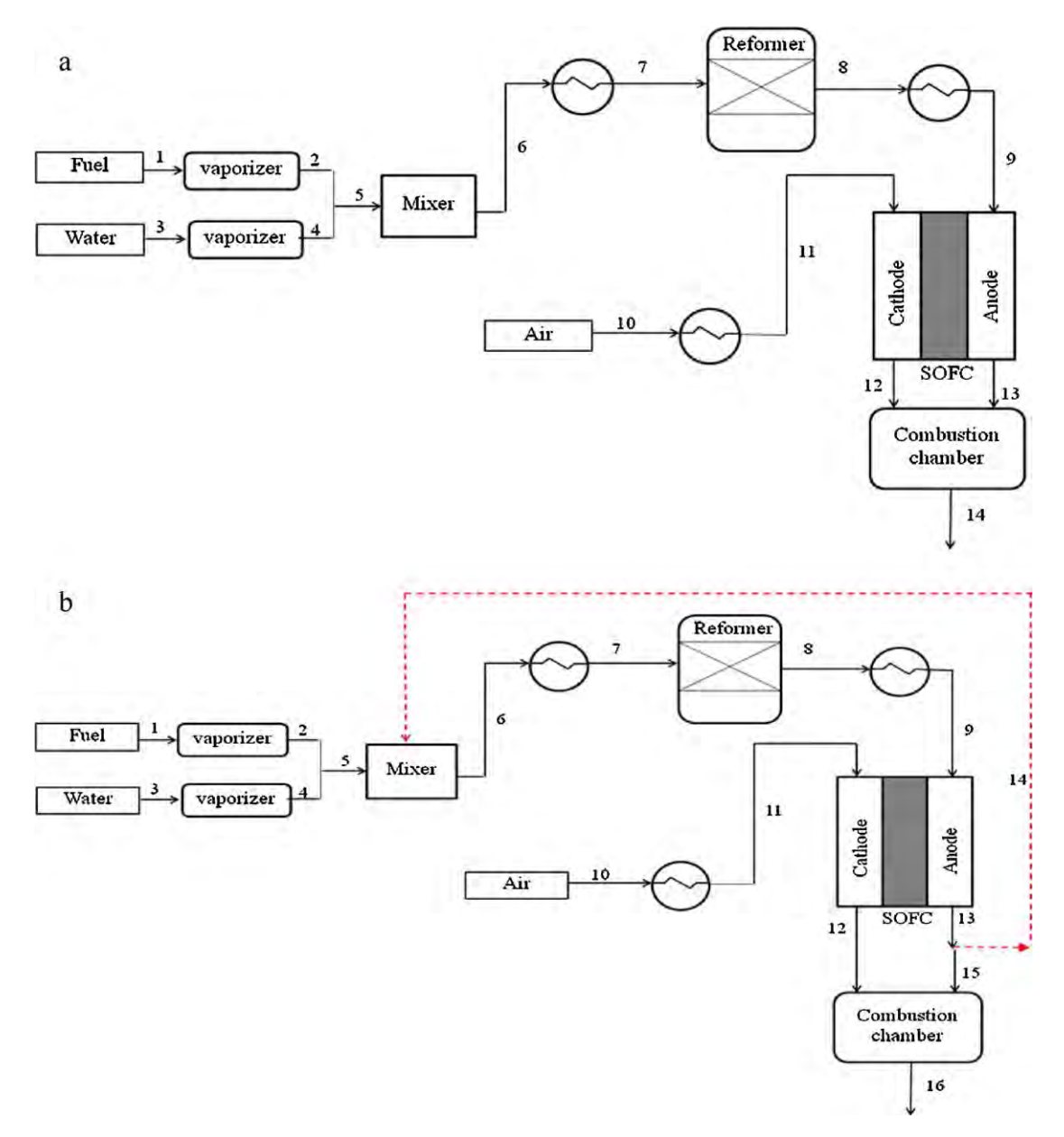


Fig. 1. Schematic of the SOFC systems integrated with an external ethanol steam reformer: (a) no recirculation and (b) anode exhaust gas recirculation.

a reforming reagent, whereas the residue of carbon monoxide in the anode exhaust gas can further react with steam via the water gas-shift reaction to produce more hydrogen in the steam reformer.

The following assumptions have been made for modeling the ethanol steam reforming and SOFC integrated system: (i) heat losses from each unit in the SOFC system are negligible, (ii) all gases behave as ideal gases, and (iii) the temperatures of the system are kept constant.

2.2. Fuel processor

The main reactions that occur in the ethanol steam reformer for hydrogen production are as follows [17]:

$$C_2H_5OH + H_2O \leftrightarrow 4H_2 + 2CO \tag{1}$$

$$CO + H_2O \leftrightarrow H_2 + CO_2 \tag{2}$$

$$CO + 3H_2 \leftrightarrow CH_4 + H_2O \tag{3}$$

The equilibrium composition of the synthesis gas at the outlet of the steam reformer can be determined based on a thermodynamic analysis using a stoichiometric approach. The equilibrium constants of each reaction (Eqs. (1)–(3)) can be written as:

$$K_{\text{eq,SE}} = \frac{p_{\text{CO,r}}^2 p_{\text{H_2,r}}^4}{p_{\text{C_2H_5OH,r}} p_{\text{H_2O,r}}}$$
(4)

$$K_{\text{eq,WGS}} = \frac{p_{\text{CO}_2,r}p_{\text{H}_2,r}}{p_{\text{CO}_r}p_{\text{H}_2\text{O},r}}$$
 (5)

$$K_{\text{eq,MR}} = \frac{p_{\text{CH}_4,r} p_{\text{H}_2\text{O,r}}}{p_{\text{CO,r}} p_{\text{H}_2,r}^3}$$
 (6)

where $K_{\rm eq,j}$ represents the equilibrium constant associated with reaction j and $p_{i,r}$ is the partial pressure of component i in the steam reformer.

The equilibrium constants of all the reactions can be determined by the Van't Hoff equation:

$$\frac{d\ln K}{dT} = \frac{\Delta H^{\circ}}{RT^2} \tag{7}$$

The molar flow rates of each component in the ethanol steam reformer are given by the following expressions:

$$n_{\text{EtOH,r}} = a - x_1 \tag{8}$$

$$n_{\rm H_2O,r} = b + c - x_1 - x_2 + x_3 \tag{9}$$

$$n_{\rm H_2,r} = d + 4x_1 + x_2 - 3x_3 \tag{10}$$

$$n_{\text{CO,r}} = g + 2x_1 - x_2 - x_3 \tag{11}$$

$$n_{\text{CH}_{A,\Gamma}} = m + \chi_3 \tag{12}$$

$$n_{\mathrm{CO}_2,\mathrm{r}} = e + x_2 \tag{13}$$

$$n_{\text{total,r}} = \sum_{i=1}^{6} n_i = a + b + c + d + e + g + m + 4x_1 - 2x_3$$
 (14)

where x_1, x_2 and x_3 are the extent of reactions of Eqs. (1)–(3) and a and b represent the inlet feed flows of ethanol and water fed to the steam reformer, respectively. When recycling the anode exhaust gas, c, d, e, g and m represent the inlet recycle flows of water, hydrogen, carbon dioxide, carbon monoxide and methane to the steam reformer, respectively.

The following three reactions, i.e., the Boudouard reaction (Eq. (15)), methane cracking (Eq. (16)) and CO reduction (Eq. (17)), are the most probable reactions that can lead to the formation of carbon in the ethanol reforming system:

$$2CO \leftrightarrow CO_2 + C \tag{15}$$

$$CH_4 \leftrightarrow 2H_2 + C$$
 (16)

$$CO + H_2 \leftrightarrow H_2O + C \tag{17}$$

In this study, the carbon formation is examined by using a thermodynamic analysis that considers the Boudouard reaction because it presents the lowest value of the Gibbs free energy. The possibility of the carbon formation is determined by the value of the carbon activity, defined as:

$$a_{\rm c} = \frac{K_{\rm b} p_{\rm CO,r}^2}{p_{\rm CO_2,r}} \tag{18}$$

where $a_{\rm c}$ is the activity coefficient of carbon and $K_{\rm b}$ represents the equilibrium constant for the Boudouard reaction. If the carbon activity is greater than unity, the system is not in equilibrium and carbon formation is present. When the carbon activity equals to unity, the system is in equilibrium. Finally, when the carbon activity is less than unity, the formation of carbon is thermodynamically impossible in the system. It is noted that the carbon activity is only the indicator for determining the presence of carbon in the system and thus the amount of carbon formation cannot be examined.

The heat required for the steam reformer operation can be computed from the energy balance equation around the reformer:

$$Q_{SR} = \left(\sum_{o} \dot{n}_8 \dot{h}_8\right) - \left(\sum_{i} \dot{n}_7 \dot{n}_7\right) \tag{19}$$

2.3. SOFC model

The synthesis gas obtained from the ethanol steam reformer consists of CH_4 , H_2 , H_2O , CO, and CO_2 and is fed to a fuel channel of the SOFC. Because the SOFC is operated at high temperatures, a steam reforming reaction of methane (Eq. (20)) and a water gas shift reaction (Eq. (21)) can occur within the SOFC stack. Furthermore,

the use of Ni-cermet as the anode can provide sufficient activity for the steam reforming reaction.

Steam reforming:
$$CH_4 + H_2O \leftrightarrow CO + 3H_2$$
 (20)

Water gas shift:
$$CO + H_2O \leftrightarrow CO_2 + H_2$$
 (21)

Hydrogen is produced from the ethanol steam reformer as well as from the methane reforming and water gas-shift reactions on the anode side and is consumed by the oxidation reaction (Eq. (22)) to generate steam and electrons. Oxygen in the air that is fed at the cathode side is reduced to oxygen ions (Eq. (23)) that migrate through the electrolyte. The overall electrochemical reaction occurring within the SOFC is shown in Eq. (24). The electrons flow from the anode to the cathode to produce direct-current electricity.

Anode:
$$H_2 + O^{2-} \rightarrow H_2O + 2e^-$$
 (22)

Cathode:
$$0.50_2 + 2e^- \rightarrow 0^{2-}$$
 (23)

Overall reaction:
$$H_2 + 0.50_2 \rightarrow H_2O$$
 (24)

The molar flow rates of each component at the SOFC outlet can be determined based on the reaction equilibrium. The relationships between the thermodynamic equilibrium constants and gaseous components for the steam reforming and water gas shift reactions in the SOFC stack are shown in Eqs. (25) and (26), respectively.

$$K_{\text{eq,SM}} = \frac{p_{\text{CO,sofc}} p_{\text{H_2,sofc}}^3}{p_{\text{CH_4,sofc}} p_{\text{H_2O,sofc}}}$$
(25)

$$K_{\text{eq,WGS}} = \frac{p_{\text{CO}_2,\text{sofc}}p_{\text{H}_2,\text{sofc}}}{p_{\text{CO},\text{sofc}}p_{\text{H}_2,\text{sofc}}}$$
(26)

where $p_{i,sofc}$ is the partial pressure of species i at the SOFC outlet.

For the SOFC operation, hydrogen is consumed by the electrochemical reaction (\dot{z}). The consumption of hydrogen is related to a fuel utilization factor ($U_{\rm f}$) and the inlet gas compositions, as expressed in Eq. (27).

$$U_{\rm f} = \frac{\dot{z}}{(4\dot{n}_{\rm CH_4} + \dot{n}_{\rm H_2} + \dot{n}_{\rm CO})} \tag{27}$$

The current density (j) generated by the fuel cell involves the decrease of hydrogen by the electrochemical reaction at the anode side (Eq. (28)):

$$j = \frac{2F\dot{z}}{A_{\rm c}} \tag{28}$$

where F is the Faraday constant and A_c is the fuel cell active area.

The theoretical open-circuit voltage or the reversible cell voltage computed by the difference between the thermodynamic potentials of the electrode reactions can be expressed by the Nernst equation:

$$E^{\text{OCV}} = E^0 - \frac{RT}{2F} \ln \left(\frac{P_{\text{H}_2\text{O}}}{P_{\text{H}_2} P_{\text{O}_2}^{0.5}} \right)$$
 (29)

where E^0 is the open-circuit voltage at standard pressure and is a function of the operating temperature, expressed as:

$$E^0 = 1.253 - 2.4516 \times 10^{-4} \ T \ (K) \tag{30}$$

The operating cell voltage or actual fuel cell voltage (V) is always lower than its open-circuit voltage due to the internal voltage losses encountered in real fuel cell operation (Eq. (31)). There are three dominant voltage losses, which are the function of the temperature, current density and substance concentrations.

$$V = E - \eta_{\text{act}} - \eta_{\text{ohm}} - \eta_{\text{conc}}$$
 (31)

Ohmic losses (η_{ohm}) occur due to the resistance to the flow of ions in the electrolyte and the resistance to the flow of electrons

through the electrodes and current collectors. This loss is linearly correlated with the voltage drop and current density (Eq. (32)).

$$\eta_{\text{ohm}} = jR_{\text{ohm}} \tag{32}$$

where $R_{\rm ohm}$ is the internal resistance, which depends on the conductivity and thickness of the individual layers as shown below:

$$R_{\rm Ohm} = \frac{\tau_{\rm anode}}{\sigma_{\rm anode}} + \frac{\tau_{\rm electrolyst}}{\sigma_{\rm electrolyst}} + \frac{\tau_{\rm cathode}}{\sigma_{\rm cathode}}$$
 (33)

where $au_{
m anode}$, $au_{
m cathode}$ and $au_{
m electrolyte}$ are the thickness of the anode, cathode and electrolyte layers, respectively. $au_{
m anode}$ and $au_{
m cathode}$ are the electronic conductivity of the anode and cathode, respectively, and $au_{
m electrolyte}$ is the ionic conductivity of the electrolyte.

The concentration overpotentials (η_{conc}) are caused by a decrease in the substances at the surface of the electrodes due to the resistance to mass transport. These overpotentials become significant at high current densities because the rate of hydrogen consumption at the reaction sites is higher than that of diffusion of the reactant through the porous electrode to the reaction sites [10,18]. These overpotentials can be expressed as:

$$\eta_{\text{conc}} = \eta_{\text{conc,anode}} + \eta_{\text{conc,cathode}}$$
(34)

$$\eta_{\text{conc,anode}} = \frac{RT}{2F} \ln \left(\frac{p_{\text{H}_2\text{O,TPB}} p_{\text{H}_2,f}}{p_{\text{H}_2\text{O,f}} p_{\text{H}_2,\text{TPB}}} \right)$$
(35)

$$\eta_{\text{conc,cathode}} = \frac{RT}{4F} \ln \left(\frac{p_{\text{O}_2,a}}{p_{\text{O}_2,\text{TPB}}} \right)$$
 (36)

The partial pressures of H_2 , H_2O , and O_2 at the three-phase boundaries can be determined by using a gas transport model in porous media as shown in the following expressions:

$$p_{\rm H_2,TPB} = p_{\rm H_2,f} - \frac{RT\tau_{\rm anode}}{2FD_{\rm eff,anode}} j \tag{37}$$

$$p_{\rm H_2O,TPB} = p_{\rm H_2O,f} + \frac{RT\tau_{\rm anode}}{2FD_{\rm eff,anode}} j \tag{38}$$

$$p_{O_2,TPB} = P - (P - p_{O_2,a}) \exp\left(\frac{RT\tau_{cathode}}{4FD_{eff,cathode}} I\right)$$
(39)

where P is the operating SOFC pressure, $D_{\rm eff,anode}$ is the effective gaseous diffusivity through the anode (considered to be a binary gas mixture of H_2 and H_2O) and $D_{\rm eff,cathode}$ is the effective oxygen diffusivity through the cathode (considered to be a binary gas mixture of O_2 and O_2).

The activation overpotentials (η_{act}) are caused by the sluggishness of the electrochemical reaction at the electrode surfaces. The activation overpotentials can be determined by the non-linear Butler–Volmer equation as follows:

$$j = j_{0,\text{anode}} \left[\frac{p_{\text{H}_2,\text{TPB}}}{p_{\text{H}_2,\text{f}}} \exp\left(\frac{\alpha nF}{RT} \eta_{\text{act,anode}}\right) - \frac{p_{\text{H}_2,\text{O,TPB}}}{p_{\text{H}_2,\text{O,f}}} \exp\left(-\frac{(1-\alpha)nF}{RT} \eta_{\text{act,anode}}\right) \right]$$
(40)

$$j = j_{0,\text{cathode}} \left[\exp\left(\frac{\alpha nF}{RT} \eta_{\text{act,cathode}}\right) - \exp\left(-\frac{(1-\alpha)nF}{RT} \eta_{\text{act,cathode}}\right) \right]$$
(41)

where α is the transfer coefficient (usually considered to be 0.5), n is the number of electrons transferred in the single elementary rate-limiting reaction step represented by the Butler–Volmer equation and $j_{0,\text{cathode}}$ and $j_{0,\text{anode}}$ are the exchange current density at the

cathode and the anode, which depend on the operating temperature as shown in Eqs. (42) and (43), respectively.

$$j_{0,\text{cathode}} = \frac{RT}{nF} k_{\text{cathode}} \exp\left(-\frac{E_{\text{cathode}}}{RT}\right)$$
 (42)

$$j_{0,\text{anode}} = \frac{RT}{nF} k_{\text{anode}} \exp\left(-\frac{E_{\text{anode}}}{RT}\right)$$
 (43)

where $E_{\rm cathode}$ and $E_{\rm anode}$ represent the activation energies at the anode and the cathode, which are equal to 137 and 140 kJ mol⁻¹, respectively, and $k_{\rm cathode}$ and $k_{\rm anode}$ denote the pre-exponential factors, which are 2.35×10^{11} and $6.54\times 10^{11}~\Omega^{-1}$ m⁻², respectively [10].

The electrical power output (P_{sofc}) is obtained when a current is drawn from the fuel cell, defined as:

$$P_{\text{sofc}} = I \times V_{\text{actual}} = j \times V_{\text{actual}} \times A_{\text{c}} \tag{44}$$

where $V_{\rm actual}$ represents the actual voltage and I is the current flowing through the fuel cell.

In this study, the SOFC is operated under adiabatic condition; therefore, the air flowing through the SOFC is employed to control the fuel cell temperature. The air inlet temperature can be calculated from the energy balance around the fuel cell, given as:

$$\left(\sum_{i} \dot{n}_{9} \dot{h}_{9}\right) + \left(\sum_{i} \dot{n}_{11} \dot{h}_{11}\right) - \left(\sum_{o} \dot{n}_{12} \dot{h}_{12}\right) - \left(\sum_{o} \dot{n}_{13} \dot{h}_{13}\right) - P_{\text{sofc}} = 0$$
(45)

2.4. Other units

2.4.1. Vaporizers

Ethanol and water are converted from the liquid to the gas phase in the vaporizer. The required heat for the operation of the vaporizer can be expressed as:

$$Q_{\text{vap,C}_2\text{H}_5\text{OH}} = \left(\sum_{o} \dot{n}_2 \dot{h}_2\right) - \left(\sum_{i} \dot{n}_1 \dot{h}_1\right) \tag{46}$$

$$Q_{\text{vap,H}_2O} = \left(\sum_o \dot{n}_4 \dot{h}_4\right) - \left(\sum_i \dot{n}_3 \dot{h}_3\right) \tag{47}$$

2.4.2. Pre-heaters

As seen in Fig. 1, the SOFC system has three pre-heaters that are used to preheat the feed stream of ethanol and steam, the synthesis gas obtained from the reformer and the air fed to the SOFC. The heat required for these pre-heaters can be determined by the following equations:

$$Q_{\text{preheater},1} = \left(\sum_{o} \dot{n}_7 \dot{n}_7\right) - \left(\sum_{i} \dot{n}_6 \dot{n}_6\right) \tag{48}$$

$$Q_{\text{preheater,2}} = \left(\sum_{o} \dot{n}_9 \dot{n}_9\right) - \left(\sum_{i} \dot{n}_8 \dot{n}_8\right) \tag{49}$$

$$Q_{\text{preheater,3}} = \left(\sum_{o} \dot{n}_{11} \dot{h}_{11}\right) - \left(\sum_{i} \dot{n}_{10} \dot{h}_{10}\right)$$
 (50)

2.4.3. Mixer

For the SOFC system with anode exhaust gas recycling, the recirculated gas stream is mixed with the fresh fuel feed in a mixer. The

Table 1Values of the structural parameters for the planar SOFC.

Cell length, L (m)	0.4
Cell width, W (m)	0.1
Fuel channel height, $h_{\rm f}$ (mm)	1
Air channel height, ha (mm)	1
Anode thickness, $\tau_{\text{anode}}(\mu\text{m})$	500
Cathode thickness, τ_{cathode} (μ m)	50
Electrolyte thickness, $\tau_{\text{electrolyte}}$ (μ m)	20

outlet temperature of the mixer can be calculated from the energy balance around the mixer, expressed as:

$$\left(\sum_{i} \dot{n}_{5} \dot{h}_{5}\right) + \left(\sum_{i} \dot{n}_{14} \dot{h}_{14}\right) - \left(\sum_{o} \dot{n}_{6} \dot{h}_{6}\right) = 0 \tag{51}$$

2.4.4. After-burner

The residue flue gas from the anode outlet stream and the unused oxidant gas from the cathode are mixed and burnt in an afterburner. The combustion reactions that occur in the afterburner can be written as follows:

$$\mbox{Hydrogen combustion}: \ \ \mbox{H}_2 + 0.5\mbox{O}_2 \rightarrow \mbox{H}_2\mbox{O} \eqno(52)$$

Carbon monoxide combustion:
$$CO + 0.5O_2 \rightarrow CO_2$$
 (53)

For the non-recycling SOFC system, the exit temperature of the afterburner can be calculated from the energy balance on the afterburner as:

$$\left(\sum_{i} \dot{n}_{12} \dot{h}_{12}\right) + \left(\sum_{i} \dot{n}_{13} \dot{h}_{13}\right) - \left(\sum_{o} \dot{n}_{14} \dot{h}_{14}\right) = 0 \tag{54}$$

For the SOFC system with anode exhaust gas recycling, the portion of the anode flue gas that is not recycled to the reformer is fed into the afterburner. The exit temperature of the afterburner outlet is calculated by solving the following equation:

$$\left(\sum_{i} \dot{n}_{12} \dot{h}_{12}\right) + \left(\sum_{i} \dot{n}_{15} \dot{h}_{15}\right) - \left(\sum_{o} \dot{n}_{16} \dot{h}_{16}\right) = 0 \tag{55}$$

The performance parameters of the SOFC system are considered in terms of the electrical efficiency ($\eta_{\rm el}$) and the thermal efficiency ($\eta_{\rm th}$), which are defined as:

$$\eta_{\rm el} = \frac{P_{\rm sofc}}{\dot{n}_{\rm C_2H_5OH} LHV_{\rm C_2H_5OH}} \tag{56}$$

$$\eta_{\text{th}} = \frac{Q_{\text{rec}} - Q_{\text{use}}}{\dot{n}_{C_2 H_5 \text{OH}} L H V_{C_2 H_5 \text{OH}}}$$
 (57)

where $\dot{n}_{C_2H_5OH}$ is the inlet ethanol molar flow rate, $LHV_{C_2H_5OH}$ is the lower heating value of ethanol, Q_{rec} is the thermal energy obtained from the SOFC system (the reference temperature is $100\,^{\circ}C$) and Q_{use} is the total thermal energy used in the SOFC system.

2.5. Solution approach

The performance of the SOFC system with non-recycling and recycling of the anode exhaust gas is analyzed based on the SOFC system model mentioned in the previous section. The proposed model consists of a set of nonlinear algebraic equations and was coded and solved by using MATLAB. Tables 1–3 list the parameters of the SOFC geometry, material properties and operating conditions for the SOFC system under nominal conditions [1,10,18]. The SOFC model was verified with the experimental data of Zhao and Virkar [19] to ensure its reliability. The values of the operating parameters used for model validation are presented in Table 4. The comparison of the model prediction with the experimental

Table 2Values of the kinetic and material property parameters for the SOFC.

Pre-exponential factor of anode exchange current density, k_{anode} (A m ⁻²)	6.54×10^{11}
Pre-exponential factor of cathode exchange current density, $k_{cathode}$ (A m ⁻²)	2.35×10^{11}
Activation energy of anode exchange current density, Eagode (k mol ⁻¹)	140
Activation energy of cathode exchange current density, E _{cathode} (k mol ⁻¹)	137
Anode diffusion coefficient, $D_{\text{eff,anode}}$ (m ² s ⁻¹)	3.66×10^{-5}
Cathode diffusion coefficient, $D_{\text{eff,cathode}}$ (m ² s ⁻¹)	1.37×10^{-5}
Anode electrical conductivity, $\sigma_{\rm anode}~(\Omega^{-1}~{\rm m}^{-1})$	$\frac{4.2\times10^7}{T}$ exp $\left(\frac{-1200}{T}\right)$
Cathode electrical conductivity, $\sigma_{\mathrm{cathode}}$ $(\Omega^{-1}\mathrm{m}^{-1})$	$\frac{9.5\times10^7}{T}\exp\left(\frac{-1150}{T}\right)$
Electrolyte ionic conductivity, $\sigma_{\rm electrolyte}$ $(\Omega^{-1}~{\rm m}^{-1})$	$33.4\times10^3\exp\left(\frac{-10300}{T}\right)$

Table 3Values of the operating conditions for the SOFC system under nominal conditions.

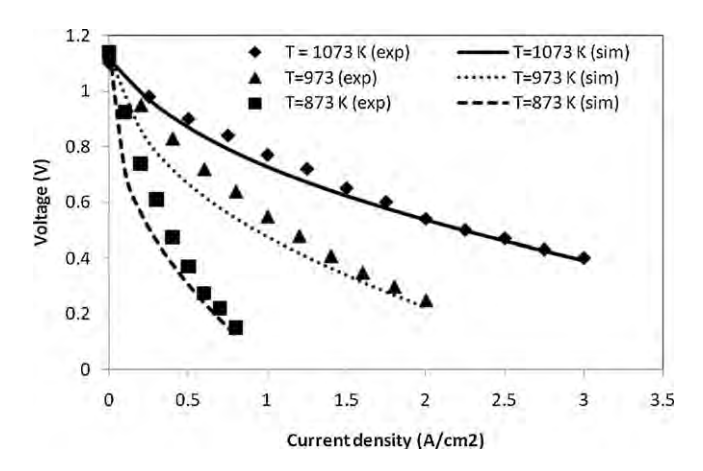
Pre-reformer unit	
Operating temperature, $T_{\rm r}$ (K)	973 K
Operating pressure, $P_{\rm r}$ (bar)	1
Molar flow of ethanol (mol s ⁻¹)	1
Solid oxide fuel cell unit	
Operating temperature, T_{sofc} (K)	1073
Operating pressure, P_{sofc} (bar)	1
Air composition	$21\% O_2$, $79\% N_2$
Fuel utilization	0.7
Excess air ratio	8.5
SOFC pressure drop (%)	2
Operating pressure, $P_{\rm r}$ (bar) Molar flow of ethanol (mol s ⁻¹) Solid oxide fuel cell unit Operating temperature, $T_{\rm sofc}$ (K) Operating pressure, $P_{\rm sofc}$ (bar) Air composition Fuel utilization Excess air ratio	1 21% O ₂ , 79% N ₂ 0.7 8.5

data regarding the operating voltage of the SOFC at different current densities and operating temperatures is shown in Fig. 2. It can be seen that the model prediction shows a good agreement with the experimental data of the SOFC operated under the temperature range used in this study. The model parameters may differ from the experiment as they are taken from different sources and this factor causes the error between the model prediction and experimental data; however, this error can be reasonably acceptable.

For the simulations of the SOFC system with anode exhaust gas recycling, an iterative approach is employed: the recycle stream (i.e., the composition of the anode exhaust gas) is assumed to be variable and the SOFC system model is solved until the assumed variables are recalculated. This procedure is repeated until the difference in the values of the assumed and calculated variables satisfies a desired accuracy (10^{-6}) .

Table 4Values of the input parameters used in the model validation [19].

Operating temperature, T_{sofc} (K)	873, 973, 1073
Operating pressure, P_{sofc} (bar)	1
Air composition	21% O ₂ , 79% N ₂
Fuel composition	$97\% H_2, 3\% H_2O$
Cell dimensions	
Cell length, L (m)	0.4
Cell width, W(m)	0.1
Fuel channel height, h_f (mm)	1
Air channel height, h_a (mm)	1
Anode thickness, τ_{anode} (μ m)	1000
Cathode thickness, τ_{cathode} (μ m)	20
Electrolyte thickness, $\tau_{\text{electrolyte}}$ (μ m)	8



 $\begin{tabular}{ll} Fig. 2. Comparison between the model predictions and experimental results of Zhao and Virkar [19]. \end{tabular}$

3. Results and discussion

3.1. Comparison of SOFC systems with and without anode exhaust gas recycling

The performances of the SOFC system with and without recycling the anode exhaust gas are first analyzed under nominal conditions. The steam and ethanol fed to the ethanol steam reformer are fixed at the ratio of 1.5. The results show that the electrical performance of the SOFC system with the anode gas recycling is 46.16%, which is higher than that without the anode gas recycle (42.87%). Table 4 shows the heat duty needed in each unit of both SOFC systems. The energy requirements for the ethanol processor section of the SOFC system with and without the anode exhaust gas recirculation are 397.10 and 634.18 kW,

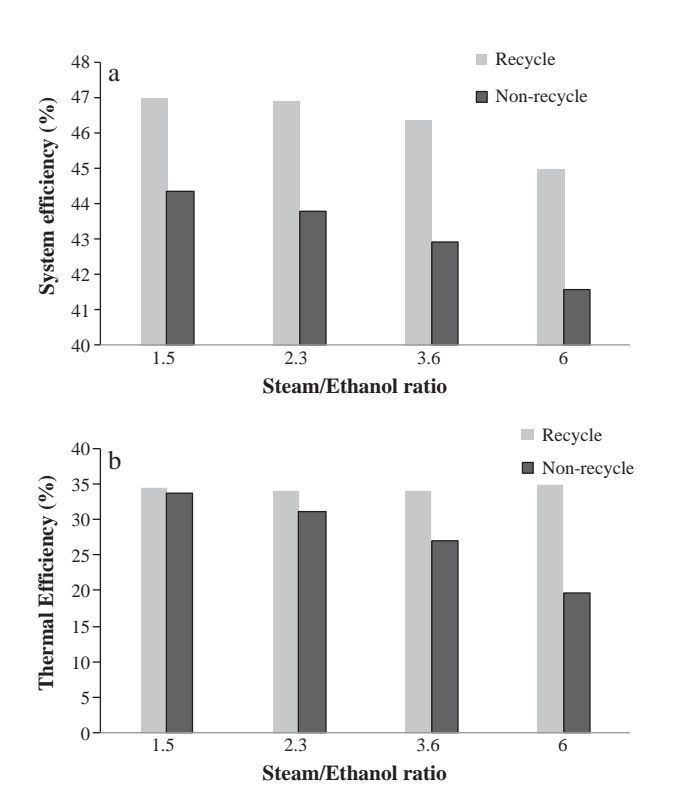
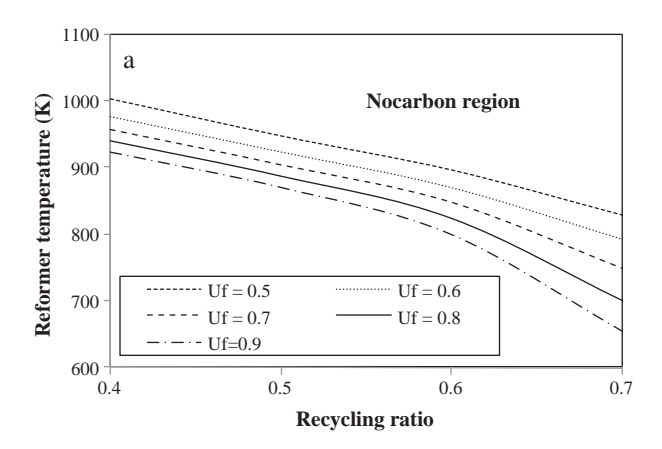


Fig. 3. Performance of the SOFC systems with and without recycling the anode exhaust gas at different steam-to-ethanol ratios: (a) electrical efficiency and (b) thermal efficiency.



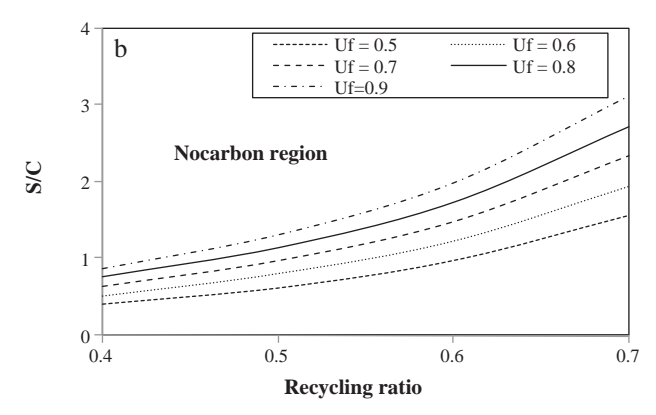


Fig. 4. Effect of the recirculation ratio of the anode exhaust gas at different fuel utilizations on the requirement of (a) the reformer temperature and (b) the steam-to-carbon ratio, to avoid a carbon formation.

respectively. The recirculation of the anode gas reduces the energy required by the fuel processor (37.4% reduction). In addition, it is observed that all of the steam required for the steam reformer is recovered by the anode exhaust gas recirculation (the recirculation ratio = 0.6), and this can save the energy supplied to the water vaporizer. However, the total energy requirements of the two SOFC systems are not different. The SOFC with anode gas recirculation can produce more electrical power and thus requires a high air supply to maintain the temperature of the SOFC. This results in high energy consumption in the air pre-heater. It is noted that since the power required to drive the blower for the anode exhaust gas recycling has slight effect on the SOFC system, it is negligible in calculating the electrical efficiency of the SOFC system.

Fig. 3 shows a comparison of the SOFC system performance when not recycling and recycling the anode exhaust gas at different steam-to-ethanol feed ratios. The simulation results clearly show that the SOFC system with anode exhaust gas recycling provides higher electrical and thermal efficiencies than that without recycling the anode exhaust gas. In the case of the SOFC system with anode exhaust gas recirculation, it is found that the molar flow rates of hydrogen and carbon monoxide in the SOFC feed stream increase. As a result, the current density generated by the SOFC is more produced, resulting in higher electrical and thermal efficiencies.

Considering the effect of the steam-to-ethanol feed ratio, the electrical performance of both SOFC systems decreases when increasing the steam-to-ethanol feed ratio. This can be explained by a dilution of the hydrogen fed to the SOFC. Unlike the electrical efficiency, when more steam is added, the thermal efficiency of the SOFC system operated with a recycle of the anode exhaust gas slightly increases because the load of steam generation is reduced.

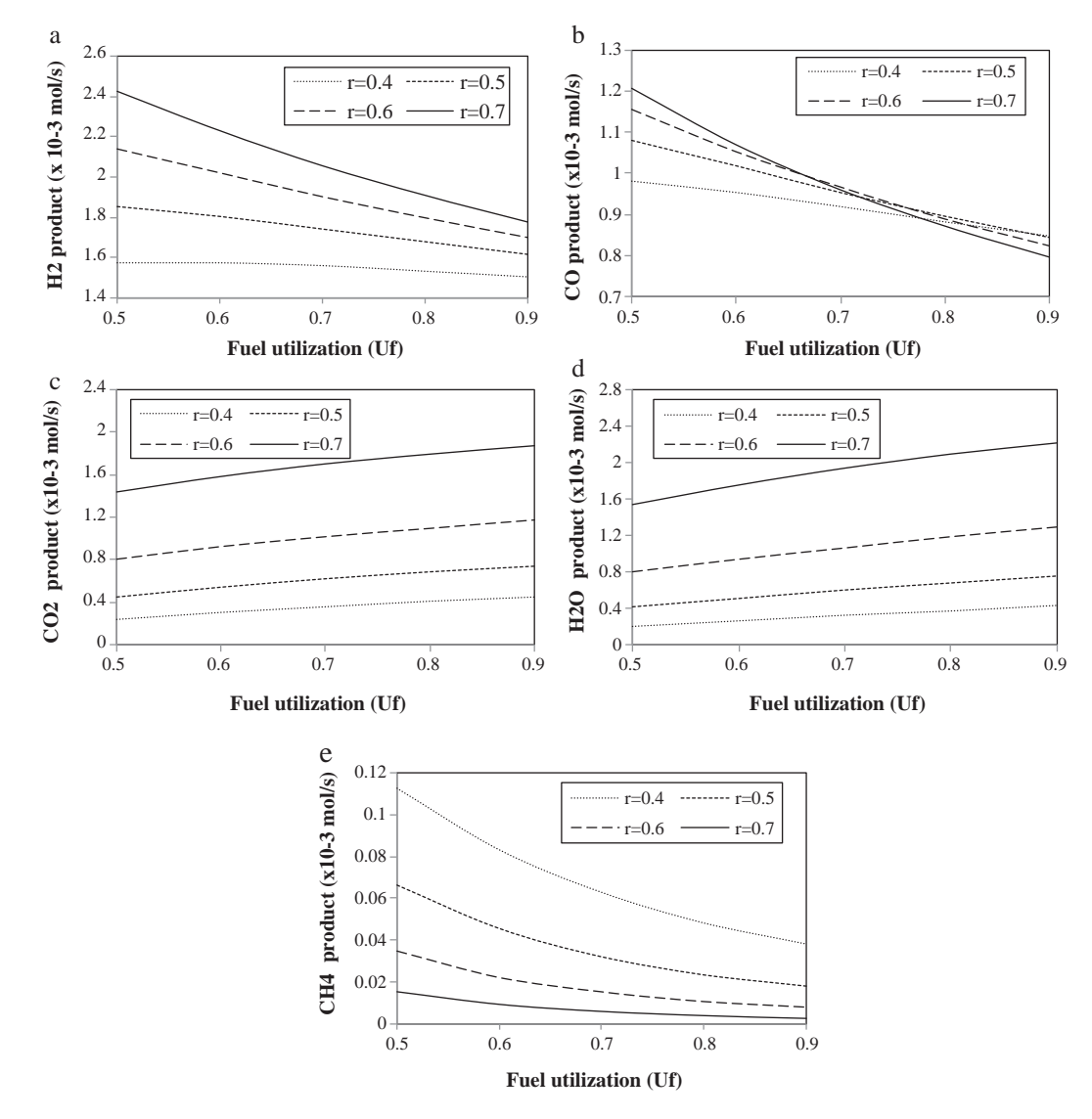


Fig. 5. Effect of fuel utilization on the composition of the synthesis gas obtained from the ethanol steam reformer at different recirculation ratios.

In addition, the high-temperature recycling gas reduces the external heat load for the SOFC feed pre-heater. In contrast, for the conventional SOFC system, an increase in the steam-to-ethanol ratio leads to a higher energy requirement for evaporating and preheating feed the steam, and thus the thermal efficiency is significantly decreased.

3.2. Effects of recirculation ratio and fuel utilization

It is well known that a crucial problem of ethanol steam reforming is caused by the formation of carbon (graphite), which could lead to the deactivation of the catalyst and increased pressure drops in the reformer. To avoid carbon formation, the suitable operating temperature and steam-to-carbon ratio should be determined. In general, a steam reforming reaction needs to be fed with excess steam to increase hydrogen production and to reduce the carbon monoxide. The presence of carbon monoxide will promote carbon formation via the Boudouard reaction (Eq. (15)). Furthermore, the tendency of carbon formation decreases as the reforming temperature increases due to the exothermic nature of the Boudouard reaction. However, operation of the steam reformer at a high temperature with more steam addition results in a high operating cost (Table 5).

Fig. 4 presents the effect of the recirculation ratio of the anode exhaust gas on the reformer temperature and steam-to-carbon ratio required to avoid carbon formation at different fuel utilizations. It is noted that the fuel utilization affects the gaseous composition of the residual gas exiting from the SOFC anode, whereas the recirculation ratio indicates the amount of the steam,

Table 5Heat duty of each unit in the SOFC systems with and without anode exhaust gas recirculation.

Heat exchangers	Heat duty (kW)		
	SOFC system without recycling the anode-exhaust gas	SOFC system with recycling the anode-exhaust gas	
Ethanol vaporizer	49.12	49.12	
Water vaporizer	167.88	_	
Pre-heating gas before reformer	152.04	33.18	
Pre-heating gas before SOFC	30.44	47.61	
Reformer	234.70	267.19	
Air pre-heater	1503.94	1731.53	
Total	2138.1	2128.63	

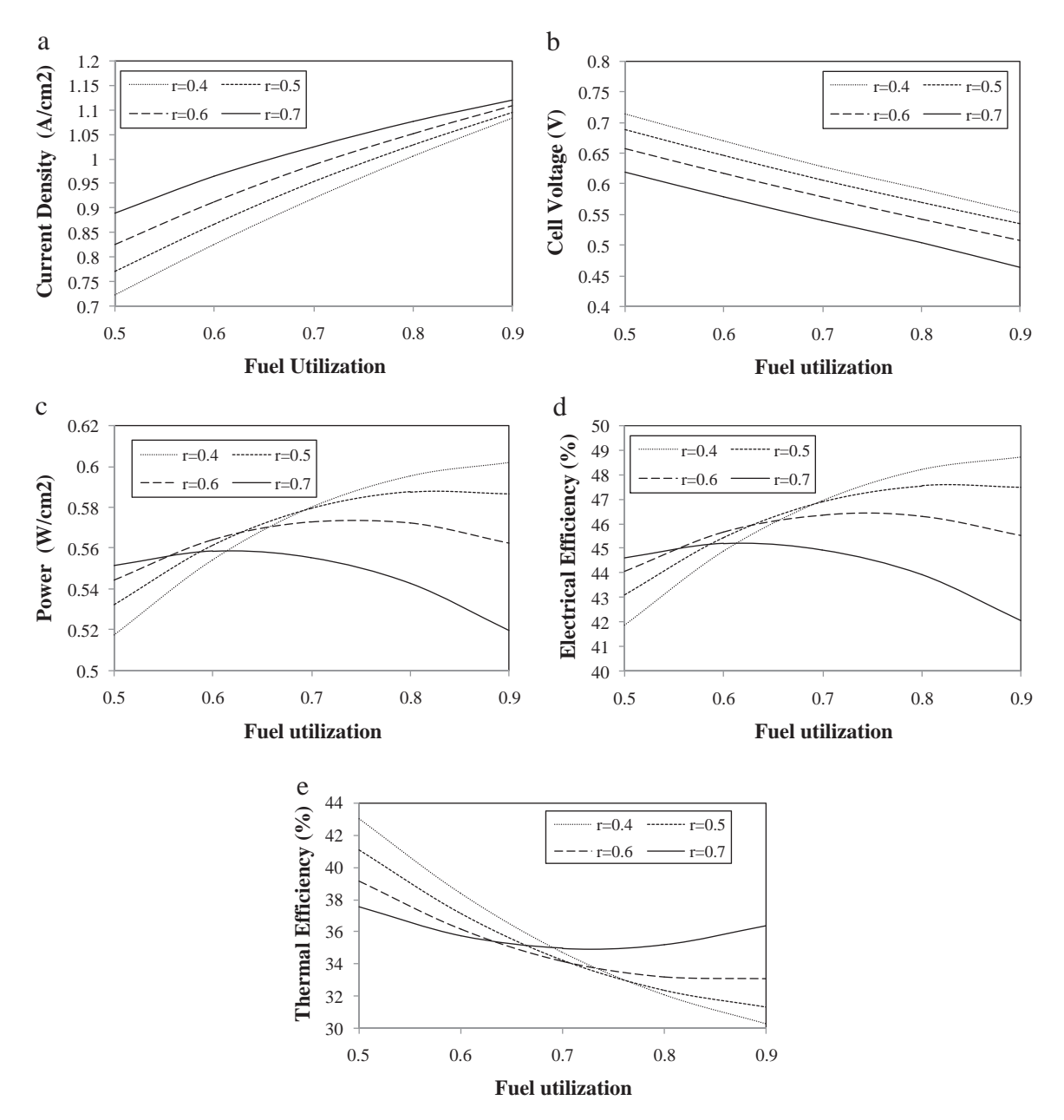


Fig. 6. Effect of fuel utilization on the SOFC system performance at different recirculation ratios: (a) current density, (b) fuel cell voltage, (c) power density, (d) electrical efficiency, and (e) thermal efficiency.

which is generated by the electrochemical reaction, that is recycled to the ethanol steam reforming section.

As seen in Fig. 4a, the reforming temperature required to suppress the tendency of carbon formation is reduced when the SOFC is operated at the higher recirculation ratio and fuel utilization. The higher recirculation ratio increases the recycle of the steam to the ethanol reformer. Furthermore, at high fuel utilization, more steam is also generated from the SOFC stack. These factors lead to an increase in the steam-to-carbon ratio of the reformer feed (Fig. 4b). From the simulation result, when the SOFC system with anode exhaust gas recycling is operated at a low fuel utilization of 0.6 and recirculation ratio of 0.4, the reforming temperature should be higher than 970 K to prevent the formation of carbon in the ethanol reformer.

Fig. 5a-e shows the molar flow rates of hydrogen, carbon monoxide, carbon dioxide, steam and methane at the outlet of the ethanol reformer as functions of the recirculation ratio and

fuel utilization. As expected, the amount of hydrogen and carbon monoxide decreases as the fuel utilization of the SOFC increases, whereas carbon dioxide and steam increase because the electrochemical and water gas shift reactions in the SOFC are more pronounced. The results show that an increase in the recirculation ratio increases the flow rates of the steam, carbon dioxide, carbon monoxide and hydrogen. However, at high fuel utilization, the carbon monoxide flow rate decreases when the recirculation ratio increases. At these conditions, more steam is recycled to the reformer, promoting the water gas shift reaction. It is noted that when the SOFC is operated at a high fuel utilization and recirculation ratio, a higher steam content in the anode exhaust gas and also a decrease in the content of methane at the reformer outlet is observed due to an increase in the reverse methanation reaction.

The influences of the fuel utilization and recirculation ratio on the current density, cell voltage, power density and electrical and

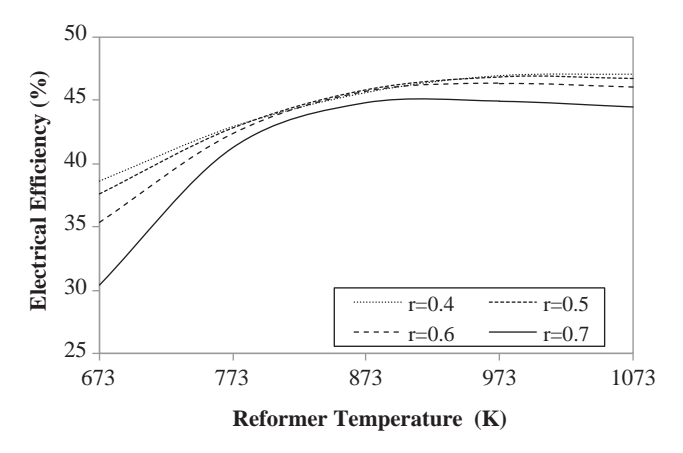


Fig. 7. Effect of the reformer operating temperature on the electrical efficiency of the SOFC system at different recirculation ratios.

thermal efficiencies are shown in Fig. 6. It can be seen that increasing the fuel utilization and the recirculation ratio cause the SOFC to generate more current density (Fig. 6a). When the SOFC is operated at higher fuel utilization, more hydrogen is consumed to produce electricity, while increasing the recirculation ratio of the anode exhaust gas leads to an increase in the molar flow rate of fuel to the SOFC. However, it is found that the operating cell voltage decreases with the increments of fuel utilization and recirculation ratio (Fig. 6b). This is mainly due to a significant increase of steam in the anode exhaust gas as the fuel utilization and recirculation ratio increase. Although a higher amount of steam promotes the ethanol reforming reaction, an excess of steam results in a dilution of the hydrogen required for the electrochemical reaction. This leads to a significant decrease in the open-circuit voltage and an increase in the concentration loss.

Fig. 6c and d shows that at low fuel utilization (0.5–0.6), the power density and electrical efficiency of SOFC increase with the increasing recirculation ratio. As the anode exhaust gas consists of a higher unreacted fuel content due to the low fuel utilization, an increase in the recirculation ratio results in an increase in hydrogen at the SOFC anode inlet, improving the SOFC performance in terms of current density, power density and electrical efficiency. However, the power density and the SOFC electrical efficiency decrease when increasing the recirculation ratio at high fuel utilization. Even though an increase in the fuel utilization results in more current density generated, the increased recirculation ratio causes a significant decrease in the fuel cell voltage. This implies that at high fuel utilization, the decrease in the fuel cell voltage has a strong impact on the power density and electrical efficiency, compared with an increase in the current density.

Considering the thermal efficiency of the SOFC system (Fig. 6e), when the SOFC is operated at low fuel utilization, an increase in the recirculation ratio decreases the thermal efficiency. Operation of the SOFC at a high recirculation ratio lowers the amount of the exhaust gas sent to the afterburner; therefore, the heat generated from the afterburner for use in the SOFC system will decrease. However, the thermal efficiency can be enhanced when the SOFC system is operated at a higher recirculation ratio and higher fuel utilization. This is mainly because the significant increase of steam recycled to the ethanol reformer reduces the demand of energy for generating steam and preheating fuel stream.

3.3. Effects of reformer and SOFC operating temperature

The effect of the reformer temperatures on the electrical efficiency when the SOFC is operated at temperature of 1073 K is shown in Fig. 7. The electrical efficiency of the SOFC system with

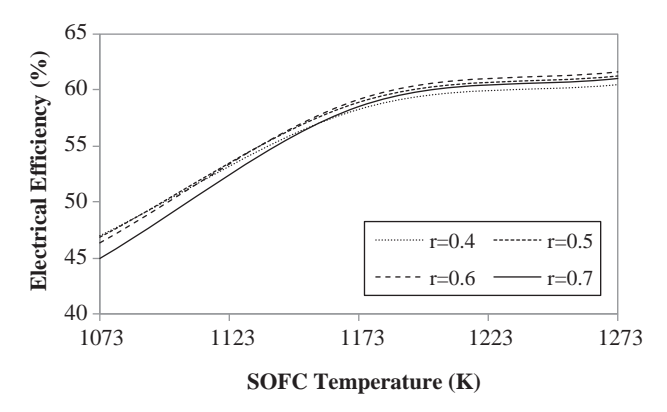
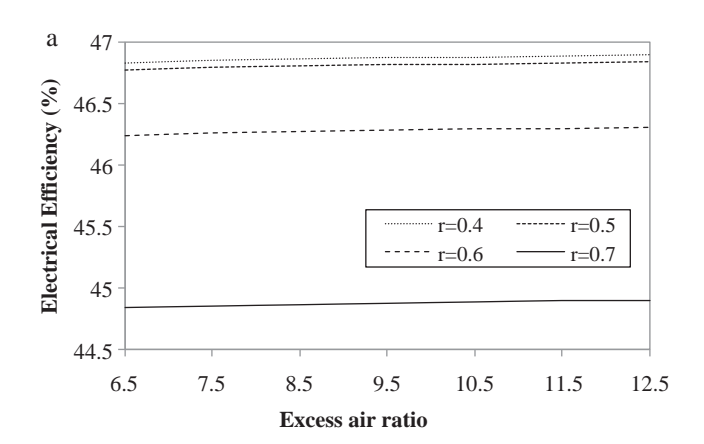


Fig. 8. Effect of the SOFC operating temperature on the electrical efficiency of the SOFC system at different recirculation ratios.

the anode gas recirculation considerably increases when increasing the reformer temperature. As the ethanol steam reforming is favored in operation at high temperatures, the increase in produced hydrogen promotes the electrochemical reaction in the SOFC stack, and thus, the electrical efficiency of SOFC is enhanced. However, an increase in the recirculation ratio results in a lower SOFC electrical efficiency. The degradation of the SOFC performance is obviously noticed when the reformer is operated at unsuitable temperatures. This lowers the production of hydrogen fuel for the SOFC. In addition, at a high recirculation of the anode exhaust gas, more steam is added to the SOFC, thereby decreasing the fuel cell voltage and the electrical efficiency.

Fig. 8 presents the electrical efficiency of the SOFC system as a function of the SOFC operating temperatures when the reformer is



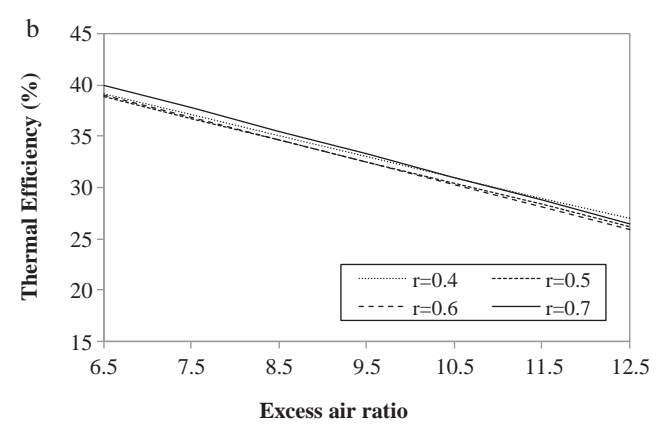


Fig. 9. Effect of the excess air ratio on (a) the electrical efficiency and (b) the thermal efficiency of the SOFC system at different recirculation ratios.

operated at temperature of 973 K. It can be seen that the electrical efficiency increases as the operating temperature of SOFC increases. An increase in the SOFC operating temperature can improve its performance because the rate of the electrochemical reaction is more pronounced. In addition, at elevated temperatures, the ohmic and activation losses are also reduced. Therefore, the more current density is generated, leading to the increased electrical efficiency.

3.4. Effect of excess air ratio

The influence of the excess air ratio on the system's electrical and thermal efficiencies at different recirculation ratios is presented in Fig. 9a and b, respectively. The excess air ratio has a slight effect on the system electrical efficiency but a larger effect on the system thermal efficiency. The thermal efficiency sharply drops when the SOFC system is operated at a high excess air ratio owing to an increased requirement of the heat duty of the air pre-heater.

4. Conclusions

The performance analysis of a SOFC system fuelled by ethanol is presented in this work. An electrochemical model of the SOFC and an equilibrium model of ethanol steam reforming are employed to simulate the SOFC system. The performance of two SOFC systems with and without anode exhaust gas recirculation is compared. The results indicate that the SOFC system with anode exhaust gas recycling provides higher electrical and thermal efficiencies than that of a non-recycling SOFC system. It is found that the tendency of carbon formation in the ethanol steam reformer decreases with an increasing recirculation ratio and fuel utilization in the SOFC system increases with the increasing recirculation ratio while the thermal efficiency decreases. The performances of the SOFC system show an opposite trend at high fuel utilization operation. Therefore, the recirculation ratio must be carefully selected. Furthermore, the

electrical efficiency of the SOFC system can be enhanced when the ethanol reformer and SOFC stack are operated at high temperatures.

Acknowledgements

Support from the Thailand Research Fund and the Higher Education Research Promotion and National Research University Project of Thailand, Office of the Higher Education Commission (EN280A) is gratefully acknowledged.

D. Saebea would like to thank the Office of the Higher Education Commission, Thailand for their grant support under the program "Strategic Scholarships for Frontier Research Network for the Joint Ph.D. Program Thai Doctoral degree" for this research.

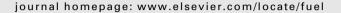
References

- Y. Patcharavorachot, W. Paengjuntuek, S. Assabumrungrat, A. Arpornwichanop, Int. J. Hydrogen Energy 35 (2010) 4301–4310.
- [2] A. Perna, Int. J. Hydrogen Energy 32 (2007) 1811-1819.
- [3] M. Santin, A. Traverso, L. Magistri, Appl. Energy 86 (2009) 2204–2212.
- [4] M.D. Falco, Fuel 90 (2011) 739-747.
- [5] J. Comas, F. Marino, M. Laborde, N. Amadeo, Chem. Eng. J. 98 (2004) 61-68.
- [6] L.E. Arteaga, L.M. Peralta, V. Kafarov, Y. Casas, E. Gonzales, Chem. Eng. J. 136 (2008) 256–266.
- [7] S.L. Douvartzides, F.A. Coutelieris, P.E. Tsiakaras, J. Power Sources 114 (2003) 203–212.
- [8] N. Laosiripojana, S. Assabumrungrat, I. Power Sources 163 (2007) 943–951.
- [9] D. Cocco, V. Tola, Energy 34 (2008) 2124–2130.
- [10] P. Aguiar, C.S. Adjiman, N.P. Brandon, J. Power Sources 138 (2004) 120–136.
- [11] P. Nehter, J. Power Sources 164 (2007) 252-259.
- [12] H. Nishikawa, H. Sasou, R. Kurihara, S. Nakamura, A. Kano, K. Tanaka, T. Aoki, Y. Ogami, Int. J. Hydrogen Energy 33 (2008) 6262–6269.
- [13] M. Granovskii, I. Dincer, M.A. Rosen, J. Power Sources 165 (2007) 307–314.
- [14] D. Shekhawat, D.A. Berry, T.H. Gardner, D.J. Haynes, J.J. Spivey, J. Power Sources 168 (2007) 447–483.
- [15] K. Onda, T. Iwanari, N. Miyauchi, K. Ito, T. Ohba, Y. Sakaki, S. Nagata, J. Electrochem. Soc. 150 (2003) A1569–A1576.
- [16] R. Peter, R. Dahl, U. Kluttgen, C. Plam, D. Stolten, J. Power Sources 106 (2002) 238–244.
- [17] S. Freni, G. Maggio, S. Cavallaro, J. Power Sources 62 (1996) 67–73.
- [18] Y. Patcharavorachot, A. Arpornwichanop, A. Chuachuensuk, J. Power Sources 177 (2008) 254–261.
- [19] F. Zhao, A.F. Virkar, J. Power Sources 141 (2005) 79–95.



Contents lists available at SciVerse ScienceDirect

Fuel





Theoretical analysis of a glycerol reforming and high-temperature PEMFC integrated system: Hydrogen production and system efficiency

Suthida Authayanun ^a, Wisitsree Wiyaratn ^b, Suttichai Assabumrungrat ^a, Amornchai Arpornwichanop ^{a,c,*}

- ^a Department of Chemical Engineering, Faculty of Engineering, Chulalongkorn University, Bangkok 10330, Thailand
- b Department of Production Technology Education, Faculty of Industrial Education and Technology, King Mongkut's University of Technology Thonburi, Bangkok 10140, Thailand
- ^c Computational Process Engineering, Chulalongkorn University, Bangkok 10330, Thailand

HIGHLIGHTS

- ▶ A performance of a glycerol processing and HT-PEMFC integrated system is analyzed.
- ▶ Glycerol shows higher hydrogen production and lower carbon formation than methane.
- ▶ Increases in the fuel utilization and reformer temperature can improve the HT-PEMFC system efficiency.
- ▶ Water obtained from the HT-PEMFC is sufficient to supply to the steam reformer.
- ▶ External heat is required to maintain the steam reforming to achieve high system efficiency at high fuel utilization.

ARTICLE INFO

Article history: Received 14 February 2012 Received in revised form 12 July 2012 Accepted 13 July 2012 Available online 28 July 2012

Keywords: High-temperature PEMFC Fuel processor Glycerol Hydrogen production Theoretical analysis

ABSTRACT

The aim of this study is to theoretically analyze the performance and efficiency of a glycerol processing and high-temperature proton exchange membrane fuel cell (HT-PEMFC) integrated system. Glycerol is considered a renewable fuel source for hydrogen production. In comparison with methane, glycerol shows a better performance in terms of high hydrogen production and low possibility to carbon formation. However, the content of CO_2 in the reformate gas and its dilution effect as well as the energy required for the glycerol processor should be concerned. When considering the operation of the glycerol processor for HT-PEMFCs, the reformer temperature (T_R) has a significant influence on hydrogen content in the reformate gas, whereas the steam-to-carbon ratio (S/C) affects hydrogen production slightly. In addition, the content of CO in the reformate gas satisfies the required constraint for HT-PEMFC operation. The performance and efficiency of the glycerol reforming process and HT-PEMFCs integrated system are evaluated by considering a heat recovery and a water balance.

© 2012 Elsevier Ltd. All rights reserved.

1. Introduction

A hydrogen production is an important process in chemical and petrochemical industries because hydrogen can be used as a reactant to produce various valuable products. In addition, hydrogen is considered an important energy carrier for the future as it can be used in fuel cells to generate electricity through electrochemical reactions without a release of pollution gases. Apart from natural gas, renewable resources such as biomass, ethanol and biogas, are potential feedstock for hydrogen production [1–3]. Recently, the production of biodiesel, which is a promising alternative fuel derived from vegetable oils, has been received considerable attention.

E-mail address: Amornchai.A@chula.ac.th (A. Arpornwichanop).

As a result, glycerol as a major by-product of the biodiesel production is highly generated. To date, a number of studies have been performed to find useful applications of glycerol, especially in cosmetic, pharmaceutical and food industries. Alternatively, the use of glycerol as a renewable fuel for hydrogen production is also an attractive option, leading to a sustainable hydrogen production process.

A proton exchange membrane fuel cell (PEMFC) is regarded as an effective electrical generator for automobile, residential and portable applications. Due to a low temperature operation, PEMFC can quick start. Other advantages include low weight and volume, and high power density. In general, PEMFC can run on the reformate gas or the synthesis gas derived from a fuel processor. However, to avoid a catalyst poisoning problem, the reformate gas must be highly purified to reduce the amount of carbon monoxide (CO) to be less than 10 ppm, thereby requiring a sophisticated purification process of hydrogen feedstock [4]. This causes a large scale of

^{*} Corresponding author at: Department of Chemical Engineering, Faculty of Engineering, Chulalongkorn University, Bangkok 10330, Thailand. Tel.: +66 2 2186878; fax: +66 2 2186877.

Nomenclature P_{O_2} reference concentration (mol m⁻³) partial pressure of O₂ (Pa) C_{ref} gas constant ($J \text{ mol}^{-1} \text{ K}^{-1}$) oxygen concentration (mol m⁻³) R c_{O_2} cell voltage (V) reformer temperature (K) E_{cell} T_{R} reversible cell potential (V) cell temperature (K) E_r $T_{\rm cell}$ F Faraday constant (C mol⁻¹) fuel utilization current density (A cm⁻²) exchange current density (A cm⁻²) i_0 Greek letter electrode thickness (m) l_d transfer coefficient membrane thickness (m) activation loss (V) l_m η_{act} lower heating value (kJ mol⁻¹) LHV fuel cell efficiency η_{FC} molar flow of H_2 (gmol s⁻¹) fuel processing efficiency $\dot{m}_{\rm H_2}$ η_{FP} molar flow of fuel (gmol s⁻¹) $\dot{m}_{ m fuel}$ $\eta_{\rm conc}$ concentration loss (V) pressure (Pa) ohmic loss (V) $\eta_{\rm ohmic}$ power density (W cm⁻²) P_{FC} system efficiency $\eta_{\rm sys}$ P_{H_2} partial pressure of H₂ (Pa) $P_{\rm H_2O}$ partial pressure of H₂O (Pa)

the hydrogen production process and requires a high operational cost. Another important problem on the PEMFC operation is a water management due to its low operating temperatures and the characteristics of membrane. To avoid the dry-out condition of a polymer membrane, the hydrogen fuel needs to be saturated with water. However, the excess water may cause flooding in a cathode gas diffusion layer, which blocks oxygen to transport to a catalyst layer, resulting in a drop of PEMFC performance.

In order to solve the problem mentioned above, a high-temperature PEMFC (HT-PEMFC) operated at the temperature of 100-200 °C has been developed. Under a high temperature operation, the extent of CO that adsorbs on Pt catalyst in the HT-PEM-FC reduces, resulting in a high tolerance of CO. Li et al. [5] demonstrated that the HT-PEMFC can tolerate CO up to 3% at the temperature of 200 °C and generate the electricity at 0.8 A/ cm² with the voltage losses lower than 10 mV. Das et al. [6] reported that the CO poisoning problem of the PEMFC operated at high temperatures is less than at low temperatures. It was found that when the PEMFC is operated at the temperature of 180 °C or above, the reforming gas with 2-5%CO can be used with the insignificant loss of cell performance. Due to the high CO tolerance of HT-PEMFC, it is also possible to use the reformate gas directly from reformers without requiring CO removal processes. This could make a design and operating conditions of the fuel processor for HT-PEMFCs differ from conventional PEMFCs. Furthermore, the higher operating temperature of PEMFCs also increases the electrochemical reaction rates at the anode and cathode and simplifies a water management within PEMFCs. When PEMFCs are operated at the temperature above 100 °C, water only presents in the vapor phase. For this reason, the flooding problem is solved and the transport of water is easy to balance.

In the past, many researchers concentrated on a conventional low-temperature PEMFC (LT-PEMFC) system integrated with a fuel processor and various types of fuels such as methane, ethanol, methanol and biodiesel, were considered [7–10]. There are limited investigations concerning about the analysis of a HT-PEMFC system. Korsgaard et al. [11] developed a dynamic model of the HT-PEMFC system operated on the reformed natural gas and the heat and power cogeneration of the system was considered. Pan et al. [12] studied the methanol reformer integrated with HT-PEMFC system and found that the reformate gas from the reforming of methanol can be directly used in HT-PEMFC without a further requirement of the CO removal unit.

The objective of this study is to investigate the performance of the HT-PEMFC integrated with a fuel processor, taking into account heat and water balances. To develop and encourage a hydrogen production from renewable resources, glycerol obtained from biodiesel production is employed to produce hydrogen for the HT-PEMFC system. The performance of a glycerol steam reforming process is analyzed based on a thermodynamic study in terms of carbon formation boundary, fuel consumption and product distribution. Comparison between the use of glycerol and methane for hydrogen production is also made. The reformate gas produced from the glycerol steam reforming process integrated with a water gas shift reactor is fed into HT-PEMFC and its electrical efficiency is analyzed. The possibility of using waste heat and water from the HT-PEMFC to support the reforming process is also studied to understand the overall HT-PEMFC integrated system.

2. Steam reforming process

The steam reforming is a thermochemical process which is used to convert hydrocarbon fuels to hydrogen for use in fuel cells. Due to its equilibrium and exothermic natures, the steam reformer is generally operated under high temperature and excess steam conditions. However, more CO content is pronounced at high temperature operation and thus a water gas shift unit is applied to eliminate CO in the reformate gas before it is fed to the HT-PEMFC. It is noted that owing to the high CO tolerance of HT-PEMFCs, a preferential oxidation process is unnecessary to further purify the reformate gas. Therefore, the fuel processing subsystem considered in this study consists of a steam reformer as a hydrogen production unit and a water gas shift reactor as a CO removal unit.

In the case of using glycerol and methane for hydrogen production, the overall steam reforming reactions is represented by Eq. (1) and Eq. (2), respectively. For a water gas shift (WGS) unit, the reaction occurring is given in Eq. (3).

$$C_3H_8O_3 + 3H_2O \leftrightarrow 3CO_2 + 7H_2$$
 (1)

$$CH_4 + 2H_2O \leftrightarrow 3H_2 + CO_2$$
 (2)

$$CO + H_2O \leftrightarrow CO_2 + H_2 \tag{3}$$

$$CO + 3H_2 \leftrightarrow CH_4 + H_2O \tag{4}$$

$$2CO \leftrightarrow CO_2 + C \tag{5}$$

$$CH_4 \leftrightarrow 2H_2 + C$$
 (6)

$$CO + H_2 \leftrightarrow H_2O + C \tag{7}$$

The possible side reactions of the steam reforming are water gas shift (Eq. (3)), methanation reactions (Eq. (4)) and carbon formation (Eqs. (5)–(7)), and thus the components appeared in the steam reforming system are C₃H₈O₃, CH₄, H₂, CO, CO₂, C and H₂O. The equilibrium composition of the reformate gas obtained from the steam reforming of glycerol is calculated based on a thermodynamic analysis. In this study, an equilibrium reactor model in HYSYS simulator [13] is used to model the steam reformer. The validation of the glycerol reforming model is given by comparing with experimental data reported by Profeti et al. [14]. The results shown in Fig. 1 indicate that the model prediction and experimental data of the product distribution obtained from the glycerol steam reformer is in a good agreement. For the CO removal unit, the WGS reactor is also modelled as an equilibrium reactor and its operating temperature is specified at 473.15 K [15].

The efficiency of a fuel processing process ($\eta_{\rm FP}$) can be determined by the following expression:

$$\eta_{FP} = \frac{LHV_{H_2} \times (\dot{m}_{H_2})}{LHV_{fuel} \times (\dot{m}_{fuel}) + \text{External heat required}}$$
(8)

where $\dot{m}_{\rm H_2}$ is the molar flow rate of $\rm H_2$ and $\dot{m}_{\rm fuel}$ is the molar flow rate of fuel used for producing hydrogen. The external heat used to maintain the glycerol reformer at the isothermal condition and to preheat reactant is determined from the difference between the overall heat required for the glycerol steam reforming process and the heat recovered from the hot reformate gas.

3. High-temperature proton exchange membrane fuel cell (HT-PEMFC)

Operation of PEMFC at high temperatures can solve both CO poisoning and water management problems. The increased temperature results in a lower CO coverage on the anode catalyst (Pt) surface. Furthermore, water produced from the electrochemical reaction is appeared in the vapor phase and thus there is no flooding problem in a gas diffusion layer at the cathode side. In general, a fuel cell voltage ($E_{\rm cell}$) is always smaller than a theoretical voltage due to the presence of irreversible losses. $E_{\rm cell}$ can be calculated from the reversible cell potential (E_r), the maximum voltage that can be achieved by a fuel cell, and the various voltage losses as:

$$E_{\text{cell}} = E_r - (\eta_{\text{act}} + \eta_{\text{ohmic}} + \eta_{\text{conc}})$$
 (9)

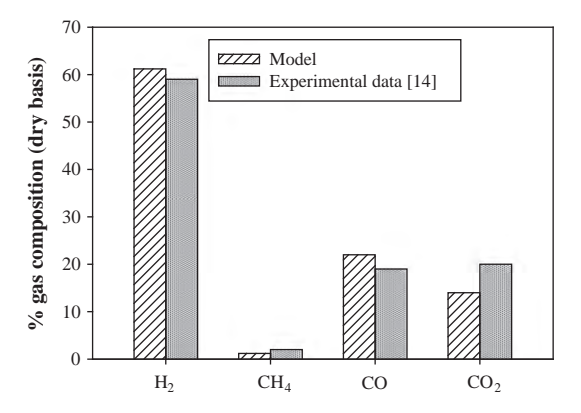


Fig. 1. Validation of the equilibrium reactor model used to predict gaseous products of the glycerol steam reformer (steam-to-glycerol ratio = 3 and T = 950 K).

where $\eta_{\rm act}$ is the activation loss, $\eta_{\rm ohmic}$ is the ohmic loss and $\eta_{\rm conc}$ is the concentration loss.

The reversible cell potential could be described by the Nernst equation [16]:

$$E_r = 1.184 - 0.00023(T - 298) + \frac{RT}{2F} ln \left(\frac{P_{H_2} P_{O_2}^{0.5}}{P_{H_2O}} \right) \eqno(10)$$

where R is the universal gas constant, F is the Faraday constant, T is the operating temperature (K), and $P_{\rm H_2}$, $P_{\rm H_2O}$ and $P_{\rm O_2}$ are the partial pressures of $\rm H_2$, $\rm H_2O$ and $\rm O_2$, respectively.

The activation loss is calculated from the Tafel equation (Eq. (11)). Due to the high CO tolerance of HT-PEMFC and a higher hydrogen oxidation reaction rate at the anode, compared to the oxygen reaction rate at the cathode, the anode activation loss is neglected. The cathode activation loss of the HT-PEMFC can be calculated from the correlation and parameters reported by Shamardina et al. [17].

$$i = i_0 \left(\frac{c_{0_2}}{c_{ref}}\right) exp\left(\frac{\eta_{act} \alpha F}{RT}\right) \tag{11}$$

The ohmic losses are caused by a resistance to the flow of ions through the membrane and a resistance to the flow of electrons through the electrically conductive fuel cell components. These losses for the HT-PEMFC can be expressed from the correlation proposed by Cheddie et al. [18] as:

$$\eta_{\text{ohmic}} = i \left(\frac{l_m}{\kappa_m} + \frac{2l_d}{\sigma_d} \right) \tag{12}$$

The concentration loss can be calculated from a limiting current density (i_L) as shown in Eq. (13). The limiting current density is the maximum current density that fuel cell can be reached.

$$\eta_{\rm conc} = \frac{RT}{nF} \ln \left(\frac{i_L}{i_L - i} \right) \tag{13}$$

The HT-PEMFC model mentioned above is solved by Matlab. In order to verify the reliability of the HT-PEMFC model used in this study, the polarization curve obtained from the model prediction and experimental data [17] when the HT-PEMFC is run on pure hydrogen and air and operated at the temperature of 433 K is compared in Fig. 2 and the simulation results agree very well with the experimental data.

To evaluate the performance of the HT-PEMFC, the power density (P_{FC}) and the thermal efficiency as given in Eqs. (14), (15) are determined.

$$P_{FC} = iE_{cell} \tag{14}$$

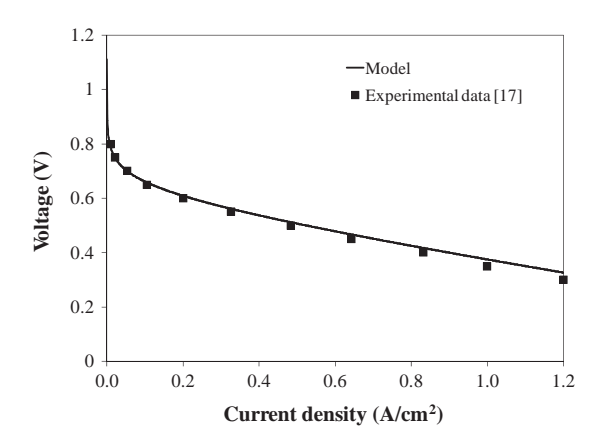


Fig. 2. Comparison of polarization curve obtained from the model prediction and experimental data [17] (pure hydrogen and air operation and cell temperature of 433 K)

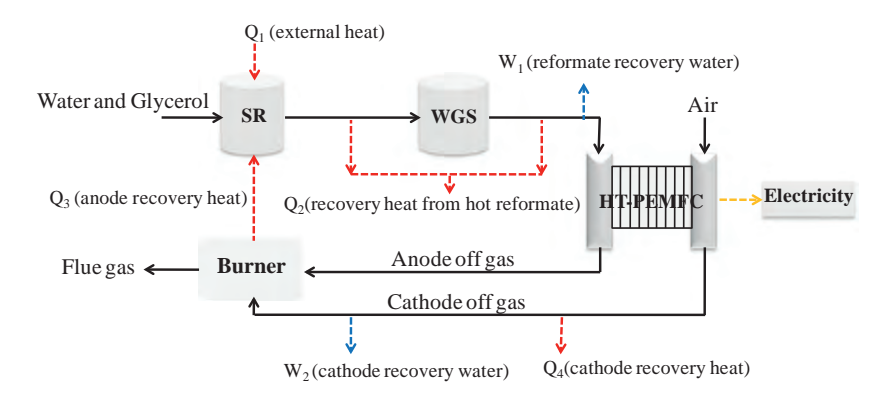


Fig. 3. Schematic diagram of the glycerol processor and HT-PEMFC integrated system.

$$\eta_{FC} = \frac{P_{FC} \cdot U_f}{\dot{m}_{H_2} \cdot LHV_{H_2}} \tag{15}$$

where $m_{\rm H_2}$ is the hydrogen molar flow rate which is used in electrochemical reaction and U_f is the fuel utilization, which is defined by the ratio of consumed hydrogen to supplied hydrogen.

Fig. 3 shows a fuel processor and HT-PEMFC integrated system. The fuel processor consists of a steam reformer and a water gas shift (WGS) unit. The system efficiency can be defined as follows:

$$\eta_{\text{sys}} = \frac{P_{\text{FC}}}{\dot{m}_{\text{fuel}} \times LHV_{\text{fuel}} + \text{External heat}(Q_1)}$$
 (16)

It is noted that the external heat (Q_1) is required to maintain the system (including heat for vaporizing and preheating reactant and water) and can be calculated from of the overall required heat for the reforming process and the overall heat recovered from the HT-PEMFC system (Eq. (17))

External heat (Q_1) = Overall required heat
$$- \mbox{Overall recovered heat}(Q_2+Q_3 \\ + Q_4) \eqno(17)$$

where Q_2 is the heat recovered from the hot reformate gas and Q_3 and Q_4 are the heat recovered from the anode and cathode off gases of the HT-PEMFC, respectively.

4. Results and discussion

In this study, glycerol is used as a green and renewable fuel for hydrogen production via a steam reforming process. The reforming of glycerol is compared with that of methane, which is presently a primary fuel for hydrogen production process. The reforming process consists of a steam reformer and a water gas shift reactor unit. The latter unit is employed to reduce the CO content to the level that satisfies the required specification of the reformate gas for HT-PEMFC. Thermodynamic analysis is performed to determine the equilibrium composition of the reformate gas. The carbon formation, fuel consumption and gaseous product distribution are key factors to be considered. Finally, the performance and efficiency of the combined glycerol reforming process and HT-PEMFC is presented.

4.1. Hydrogen production: glycerol and methane

Carbon formation is an important problem in a reforming process. In general, the reforming temperature and steam-to-carbon (S/C) feed ratio are controlled to avoid the presence of carbon in the reformer. Fig. 4 shows the boundary of carbon formation when glycerol and methane are reformed to hydrogen. The region below

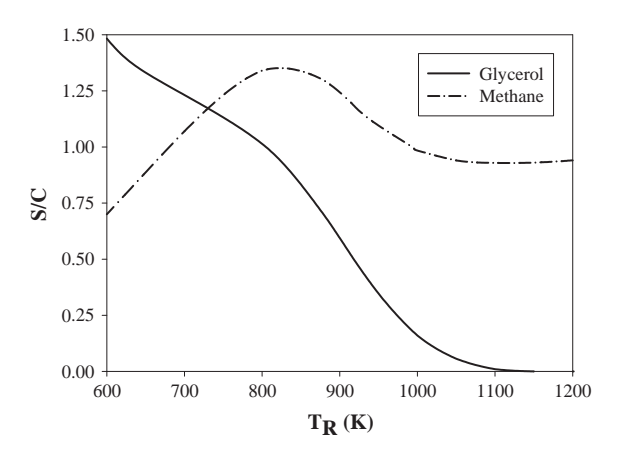


Fig. 4. Boundary of carbon formation.

the boundary line is the area where the formation of carbon is possible. The results show that at a lower reforming temperature, glycerol requires more steam than methane to inhibit the formation of carbon; however, the opposite trend is observed when the steam reformer is operated under high temperatures ($T_R > 730 \text{ K}$).

Next, the performance of the steam reformer for hydrogen production from glycerol is evaluated and compared with methane. Fig. 5 shows that at the same hydrogen production rate, the amount of glycerol fed to the steam reformer is lower than that of methane. This can be explained by a higher hydrogen atom in the glycerol molecule. When the steam reformer is operated at a

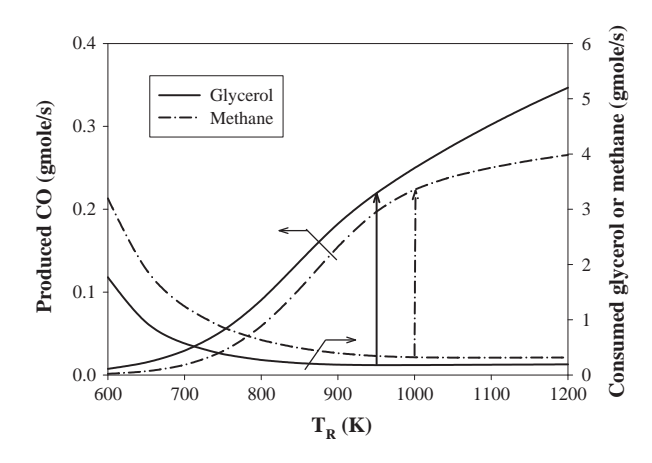


Fig. 5. Fuel consumption and CO generation of the steam reformer (H_2 produced = 1 gmole/s, S/C = 2).

higher temperature, an amount of glycerol or methane fed to the reformer is less required. For the glycerol steam reforming, the optimal operating temperature (providing the maximum hydrogen content) is 950 K, whereas it is 1000 K for the methane steam reforming. It is also found that the amount of CO produced from the glycerol reforming is higher than that from methane, especially at high temperatures. However, under the optimal operating temperature, the content of CO produced from the steam reforming of glycerol and methane is approximately the same. In general, CO has a direct impact on the activity of Pt catalyst in PEMFC. For a low-temperature PEMFC operated at a temperature range of 60-80 °C, a purification unit such as a preferential oxidation process, is further needed to remove CO from the reformate gas. If the reformate gas has a higher fraction of CO, the loss of hydrogen through the oxidation reaction of hydrogen in the preferential oxidation process may be occurred. Therefore, the CO content has an indirect effect on the amount of hydrogen containing in the reformate gas.

Fig. 6 shows the comparison of glycerol and methane steam reforming processes in terms of the product distribution and the fuel consumption when the steam reformer is operated at the steam-to-carbon ratio of 2 and optimal operating temperature. The result indicates that the consumption of glycerol is less than that of methane at the same level of hydrogen production. It is noted that the amount of CO₂ generated should also be taken into consideration because it decreases the fraction of hydrogen in the reformate gas. Fig. 7 shows the mole fraction of the reformate gas obtained from the reformer. The reforming of methane provides higher hydrogen fraction than that of glycerol because less amount of CO₂ is generated. It should be noted that the hydrogen fraction has a direct impact on the fuel cell performance.

The total energy requirement for operation of the steam reformer running on glycerol and methane is investigated and the results are shown in Table 1. The energy required for the steam reforming process accounts for the heat of vaporization, the sensible heat to heat up reactants to the desired temperature and the heat needed for maintaining the reformer at an isothermal operation. It is observed that the glycerol processor requires a higher external energy for hydrogen production. The main energy consumption of the glycerol reformer is caused by the heat to vaporize and preheat the reactant.

From the simulation results mentioned above, glycerol shows the potential of fuel for hydrogen production in terms of low possibility to carbon formation and high hydrogen yield. In addition, it is the renewable energy resource and thus becomes the competitive fuel when compared with methane. Furthermore, the use of glycerol to produce a high-value added product could reduce a biodiesel production cost.

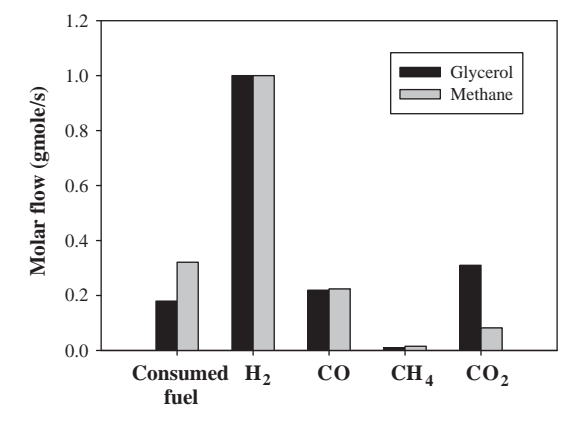


Fig. 6. Product distribution and fuel consumption of the steam reformer (S/C = 2, $T_R = 950 \text{ K}$ (glycerol) and 1000 K (methane)).

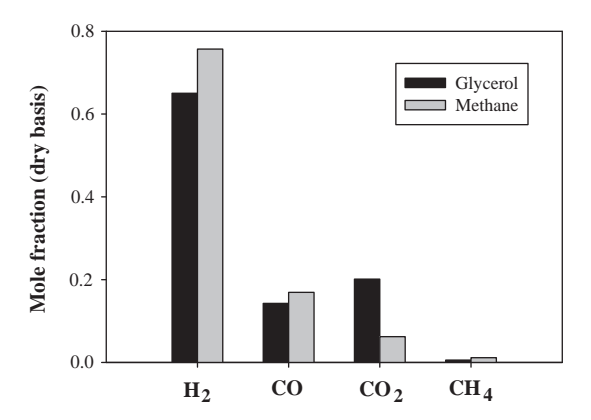


Fig. 7. Mole fraction of the product obtained from the steam reformer (S/C = 2, $T_R = 950 \text{ K}$ (glycerol) and 1000 K (methane)).

Table 1Energy requirements for the steam reforming of glycerol and methane.

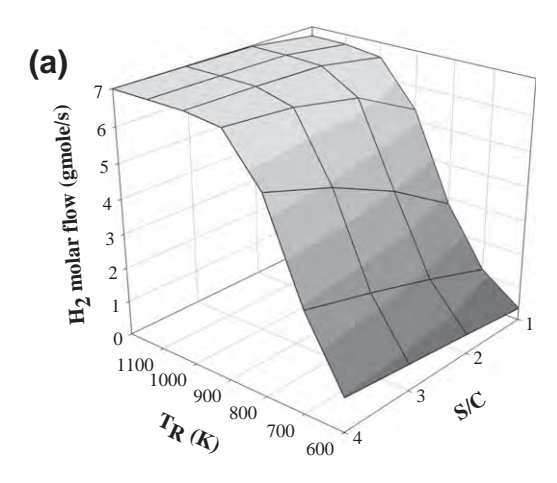
	Glycerol	Methane
Condition		
$T_{\rm R}$ (K)	950	1000
S/C	2	2
Energy (kW)		
Latent heat		
-Glycerol	14.96	=
-Water	42.71	26.18
Sensible heat	69.04	31.00
Required heat for reformer	36.69	69.45
Total heat requirement	163.40	126.63

4.2. Glycerol reforming process for HT-PEMFC

For HT-PEMFCs, a further CO purification process in the fuel processor such as a preferential oxidation, a methanation or a membrane separation, can be eliminated because the reformate gas with a higher CO content can be directly employed for electricity generation. Therefore, the glycerol reforming process (GRP) comprising of a reformer and a water gas shift unit is examined in this work. Fig. 8a shows the amount of hydrogen obtained from the GRP operated under different temperatures (T_R) and steam-to-carbon (S/C) ratios. The results indicate that the reformer temperature is the key factor to improve the hydrogen production, whereas the S/C ratio has a slight effect. When the GRP is operated under the S/C ratio of higher than 2 and the temperature of higher than 1000 K, the production of hydrogen is kept constant. It is found that the highest amount of hydrogen obtained from the GRP is very close to its maximum value based on the reaction stoichiometry in Eq. (7).

Fig. 8b shows the content of CO in the reformate gas when the reformer is operated at different temperatures and steam-to-carbon (S/C) ratios. It is found that at S/C > 2, the CO flowing out from the water gas shift unit in the GRP is lower than 0.5% for all operating reformer temperatures. Increases in the S/C ratio and the reformer temperature over such the conditions have an insignificant effect on the CO content. At S/C < 2, the operating temperature of the reformer affects the presence of CO; however, its concentration satisfies the desired specification of the reformate gas for HT-PEM-FC. As a result, the reformate gas obtained from the GRP can be directly fed to the HT-PEMFC without further purification.

The thermal efficiency of the GRP is demonstrated in Fig. 9. The reformer operating temperature and S/C are the critical factor in achieving a high efficiency of the GRP. Although operation of the reformer with high S/C ratio provides more hydrogen content, it



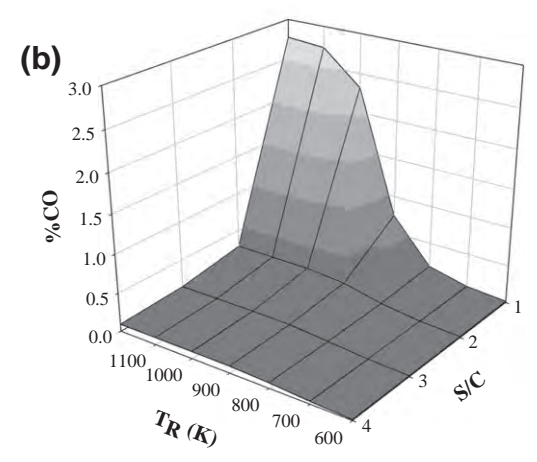


Fig. 8. (a) Hydrogen molar flow and (b) %CO in the reformate gas (dry basis) at different temperatures and S/C ratios.

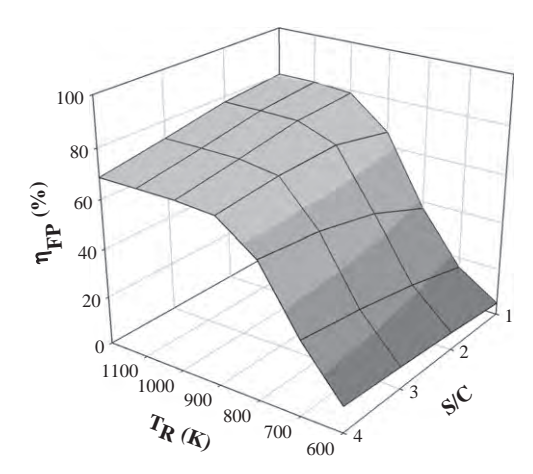


Fig. 9. Efficiency of the glycerol reforming process at different temperatures and S/C ratios.

leads to a large energy consumption and thus decreases the efficiency of the GRP. The highest efficiency is about 80% at the S/C of 1-2 and the temperature of 1000-1200 K.

4.3. Glycerol reforming process and HT-PEMFC integrated system

In this section, the performance of the GRP and HT-PEMFC integrated system is analyzed. The reformate fed to the HT-PEMFC is derived from the product gas of the glycerol steam reformer operated at

Table 2Model parameters used for simulation of the HT-PEMFC [17].

Parameters	Value	Unit
Fuel cell temperature (T_{cell})	433	K
Operating pressure at anode (P_a)	101.325	kPa
Operating pressure at anode (P_c)	101.325	kPa
Faraday constant (F)	96485	$C \text{ mol}^{-1}$
Gas constant (R)	8.31	$\rm J~mol^{-1}~K^{-1}$
Transfer coefficient (α)	0.8	-
Reference concentration (c_{ref})	28	$\mathrm{mol}~\mathrm{m}^{-3}$
Exchange current density (i_0)	0.25	${ m A~m^{-2}}$
Ionic conductivity ($\kappa_{ m m}$)	3.8	${ m S}~{ m m}^{-1}$
Electrical conductivity (σ_d)	220	${ m S}~{ m m}^{-1}$
Membrane thickness (l_m)	6×10^{-5}	m
Electrode thickness (l_d)	4×10^{-4}	m
Lower heating value of glycerol (LHV glycerol)	1564.9	kJ mol ⁻¹
Lower heating value of H_2 (<i>LHV</i> _{H_2})	242	kJ mol ⁻¹
Lower heating value of CH_4 (LHV_{CH_4})	802.7	$kJ mol^{-1}$
Lower heating value of CO (LHV_{CO})	283	kJ mol ⁻¹

the temperature of 1000 K and S/C of 2. Water and heat balances within the system are managed to improve the system efficiency. The parameters used in the simulation of the HT-PEMFC system are given in Table 2. To reduce the requirement of the external heat, some of the energy required by the reforming process is supplied by the heat recovered from the anode and cathode off gases and the hot reformate gas, whereas water removed from the reformate gas and the fuel cell exhaust gas is sent to the reforming process with the aim to reduce a water fresh feed (see Fig. 3).

4.3.1. System efficiency

The performance of the HT-PEMFC system is evaluated by varying the fuel utilization (U_f) and the reformer temperature (Fig. 10). It is noted that the change in the reformer temperature will affect the fuel composition of the reformate gas fed to the HT-PEMFC as mentioned in the previous section. Although the required energy to sustain the reforming reactions increases with increasing the reforming temperature, the hydrogen produced also increases. From Fig. 10, it is found that the efficiency of the HT-PEMFC system increases with increasing the fuel utilization. This is because the required hydrogen feed at high fuel utilization ratio is less than at low fuel utilization ratio. The operation of the HT-PEMFC at low fuel utilization results in the reduction of the external heat requirement; however, the use of hydrogen to produce electricity via the HT-PEMFC, instead of burning it for a heat recovery, is more efficient. In addition, the system efficiency is enhanced when operated at a higher reforming temperature due to more hydrogen produced.

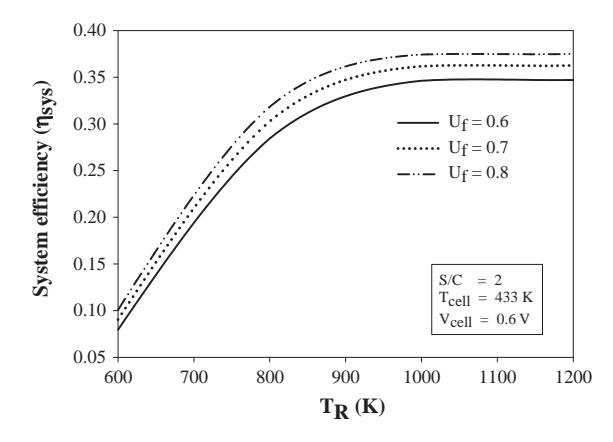


Fig. 10. Effect of reformer temperatures on the efficiency of the HT-PEMFC system at different fuel utilizations.

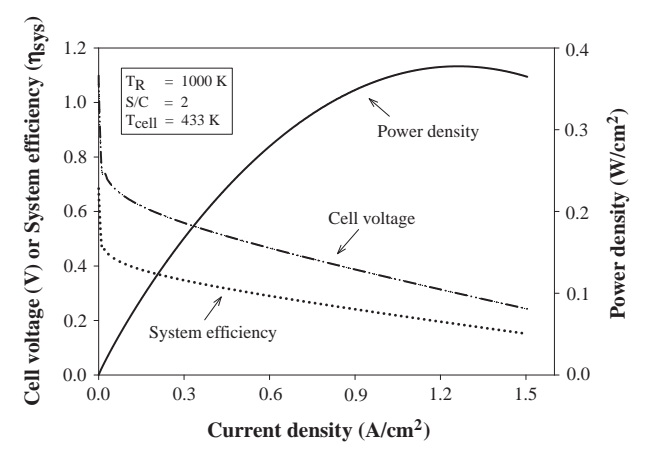


Fig. 11. Electrical characteristics of the HT-PEMFC and efficiency of the HT-PEMFC integrated system.

Fig. 11 shows the electrical characteristics of the HT-PEMFC and the efficiency of the HT-PEMFC system when the HT-PEMFC is operated at different current densities. The cell voltage decreases with increasing the current density due to the voltage losses occurring at the HT-PEMFC. The HT-PEMFC system provides a higher efficiency at a lower current density operation. The efficiency of the HT-PEMFC integrated system is about 30–40% at the cell voltage range of 0.5–0.7 and 20–30% at the maximum power output. Table 3 summarizes the simulation results for the 1 kW HT-PEMFC system.

4.3.2. Heat recovery

The improvement of a thermal management in the HT-PEMFC system is an alternative option for efficient energy usage. A high temperature operation of HT-PEMFC offers the prospect for a combined heat and power system; a waste heat from the fuel cell can be recovered to preheat the fuel or to supply to the reforming process. Here, the remaining heat from the anode and cathode off gases flowing out the HT-PEMFC is utilized to provide heat for glycerol steam reforming process. The anode off gas is combusted in the burner to generate additional heat for the reformer operation. The percentage of the heat recovery from HT-PEMFC for the glycerol processor is defined in the following equation:

$$\% \ heat \ recovery = \frac{heat \ recovered \ from \ HT - PEMFC(Q_3 \ and \ Q_4)}{heat \ required \ for \ fuel \ processor} \\ \times 100 \eqno(18)$$

It is noted that the heat recovered from the HT-PEMFC is the remaining heat from the anode and cathode off gases (Q_3 and Q_4 in Fig. 3). The required heat for the fuel processing is calculated from the difference of the overall heat requirement and the heat recovered from the reformate gas (Q_2) in Fig. 3.

Table 3Summary of the simulation results for a 1 kW HT-PEMFC system operated at voltage of 0.6 V and fuel utilization of 0.8.

Parameters	Value	Unit
Power density	1.2×10^{-1}	${\rm W~cm^{-2}}$
Glycerol flow rate	1.6×10^{-3}	gmole s ⁻¹ gmole s ⁻¹
Reformate gas flow rate (dry basis)	1.5×10^{-2}	gmole s ⁻¹
Q_1	23	W
Q_2	472	W
Q_3	600	W
Q_4	97	W
Electrical efficiency	48	%
System efficiency	37	%

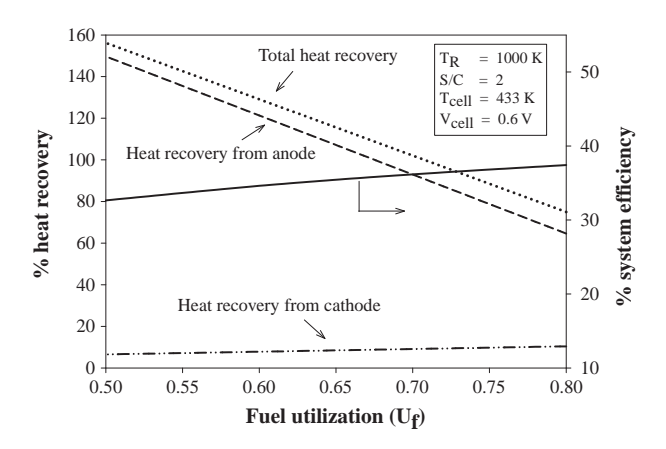


Fig. 12. Heat recovery and system efficiency of the HT-PEMFC integrated system.

Fig. 12 shows that the heat recovered from the cathode off gas is quite constant at around 10%, while for the anode off gas, it varies with the fuel utilization. Furthermore, the total recovered heat from the HT-PEMFC system is higher than 100% at U_f = 0.7. This implies that under these conditions, external heat sources are unnecessary for the integrated system of the glycerol reformer and the HT-PEMFC. However, it is observed that the system efficiency decreases when operated at low fuel utilizations. Considering the efficiency of the HT-PEMFC integrated system, it is suggested that operation at high fuel utilization is a preferable choice and the external heat is needed to supply heat for the steam reformer.

4.3.3. Water recovery

Due to the fact that the fuel processor consumes water to produce hydrogen via a steam reforming reaction with glycerol, while the fuel cell produces water via an electrochemical reaction, the possibility to use water generated by the HT-PEMFC for the fuel processing process without additional water supply is investigated in this study. In such an approach, the unreacted water and the generated water are removed from the fuel processing process and cathode off gases, respectively. The factor used to indicate that the water is sufficiently supplied to the reforming process is the percentage of the water recovery, defined as:

% water recovery =
$$\frac{\text{water recovered from HT} - \text{PEMFC}(W_1 \text{ and } W_2)}{\text{water required for fuel processor}} \times 100$$
(19)

The simulation results show that the % water recovery is higher than 100% in all the studied operating conditions (see Fig. 13). This

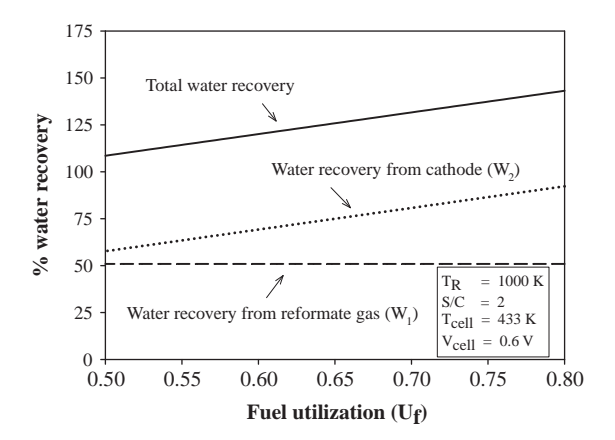


Fig. 13. Water recovery of the HT-PEMFC integrated system.

implies that the water that can be recovered from the HT-PEMFC system is high enough for supplying to the reforming process. Water is mostly derived from the electrochemical reaction at the cathode side. At the specified cell voltage, the produced water from the electrochemical reaction is constant at all the values of fuel utilization but the higher amount of water is required for the reformer to produce more hydrogen at a lower fuel utilization operation. Due to the high water requirement of the fuel processor, the% water recovery at the cathode off gas decreases at a lower fuel utilization. It is note that the %water recovery also depends on the requirement of water at the reforming process. Although the water obtained at the anode is higher when the fuel utilization factor decreases, the % total water recovery decreases because more water is required for the steam reformer.

5. Conclusions

In this study, the integration system of a steam reforming process and high-temperature proton exchange membrane fuel cell (HT-PEMFC) is studied. Glycerol, a renewable fuel from biodiesel production, is used for hydrogen production and its performance is compared with methane in terms of carbon formation, fuel consumption and product distribution. A glycerol reforming process consisting of a steam reformer and a water gas shift unit is investigated with the aim to determine optimal operating conditions. The performance and efficiency of the glycerol reforming process and HT-PEMFC integrated system is analyzed and the important results obtained are summarized as follows:

- Because a glycerol molecule have high oxygen atom, the possibility to carbon formation from the steam reforming of glycerol is less than that of methane. The consumption of glycerol to produce hydrogen is lower than methane at the same hydrogen production rate. When comparing with methane, the reforming of glycerol generates more CO₂ that will decrease the fraction of hydrogen in the reformate gas and requires a higher energy to vaporize and preheat reactants.
- The glycerol reforming process is independent of the steam-to-carbon ratio (S/C) and the reformer temperature (*T*) when operated at S/C > 2 and *T* > 1000 K. The content of CO in all studied operational range satisfies the desired specification of the reformate gas for HT-PEMFC.
- Increases in the fuel utilization and reformer temperature can improve the efficiency of the glycerol reforming process and HT-PEMFC integrated system.
- Water obtained from the HT-PEMFC is sufficient to supply to the steam reformer, whereas external heat is required to maintain the steam reforming to achieve high system efficiency at high fuel utilization.

Acknowledgements

Support from the Thailand Research Fund, Office of the Higher Education Commission and the Higher Education Research Promotion and National Research University Project of Thailand (EN276B) is gratefully acknowledged.

References

- Toonssen R, Woudstra N, Verkooijen AHM. Decentralized generation of electricity from biomass with proton exchange membrane fuel cell. J Power Sources 2009;194:456–66.
- [2] Hedstrom L, Tingelof T, Alvfors P, Lindbergh G. Experimental results from a 5 kW PEM fuel cell stack operated on simulated reformate from highly diluted hydrocarbon fuels: efficiency, dilution, fuel utilisation, CO poisoning and design criteria. Int J Hydrogen Energy 2009;34:1508–14.
- [3] Saebea D, Arpornwichanop A, Patcharavorchot Y, Assabumrungrat S. Adsorption-membrane hybrid system for ethanol steam reforming: thermodynamic analysis. Int J Hydrogen Energy 2012;36:14428-34.
- [4] Zhang J, Xie Z, Zhang J, Tang Y, Song C, Navessin T, et al. High temperature PEM fuel cells. J Power Sources 2006;160:872–91.
- [5] Li Q, He R, Gao JA, Jensen JO, Bjerrum NJ. The CO poisoning effect in PEMFCs operational at temperatures up to 200 °C. J Electrochem Soc 2003;150:A1599–605.
- [6] Das SK, Reis A, Berry KJ. Experimental evaluation of CO poisoning on the performance of a high temperature proton exchange membrane fuel cell. J Power Sources 2009;193:691–8.
- [7] Jannelli E, Minutillo M, Galloni E. Performance of a polymer electrolyte membrane fuel cell system fueled with hydrogen generated by a fuel processor. I Fuel Cell Sci Tech 2007;4:435–40.
- [8] Wu W, Pai C. Control of a heat-integrated proton exchange membrane fuel cell system with methanol reforming. J Power Sources 2009;194:920–30.
- [9] Oliva DG, Francesconi JA, Mussati MC, Aguirre PA. Energy efficiency analysis of an integrated glycerin processor for PEM fuel cells: comparison with an ethanol-based system. Int J Hydrogen Energy 2010;35:709–24.
- [10] Perna A. Hydrogen from ethanol: theoretical optimization of a PEMFC system integrated with a steam reforming processor. Int J Hydrogen Energy 2007;32:1811–9.
- [11] Korsgaard AR, Nielsen MP, Kær SK. Part one: a novel model of HTPEM-based micro-combined heat and power fuel cell system. Int J Hydrogen Energy 2008;33:1909–20.
- [12] Pan C, He R, Li Q, Jensen JO, Bjerrum NJ, Hjulmand HA, et al. Integration of high temperature PEM fuel cells with a methanol reformer. J Power Sources 2005:145:392–8.
- [13] Hyprotech, a subsidiary of Aspen Technology, Inc. HYSYS Plant 3.1 documentation. Cambridge; 2002.
 [14] Profeti LPR, Ticianelli EA, Assaf EM. Production of hydrogen via steam
- [14] Profeti LPR, Ticianelli EA, Assaf EM. Production of hydrogen via steam reforming of biofuels on Ni/CeO₂-Al₂O₃ catalysts promoted by noble metals. Int J Hydrogen Energy 2009;34:5049-60.
- [15] Chen WH, Hsieh TC, Jiang TL. An experimental study on carbon monoxide conversion and hydrogen generation from water gas shift reaction. Energy Convers Manage 2008;49:2801–8.
- [16] Ramousse J, Lottin O, Didierjean S, Maillet D. Heat sources in proton exchange membrane (PEM) fuel cells. J Power Sources 2009;192:435–41.
- [17] Shamardina O, Chertovich A, Kulikovsky AA, Khokhlov AR. A simple model of a high temperature PEM fuel cell. Int J Hydrogen Energy 2010;35:9954–62.
- [18] Cheddie D, Munroe N. Mathematical model of a PEMFC using a PBI membrane. Energy Convers Manage 2006;47:1490–504.

ELSEVIER

Contents lists available at SciVerse ScienceDirect

Energy

journal homepage: www.elsevier.com/locate/energy



Use of different renewable fuels in a steam reformer integrated into a solid oxide fuel cell: Theoretical analysis and performance comparison*

Dang Saebea a , Suthida Authayanun a , Yaneeporn Patcharavorachot b , Woranee Paengjuntuek c , Amornchai Arpornwichanop a,d,*

ARTICLE INFO

Article history: Received 27 August 2012 Received in revised form 7 December 2012 Accepted 17 December 2012 Available online 21 January 2013

Keywords:
Renewable fuels
Steam reformer
Hydrogen production
Solid oxide fuel cell
Integrated system

ABSTRACT

Hydrogen production from renewable energy resources has received significant attention with advances in fuel cell technology. The fuel type and operational reforming conditions directly affect fuel cell electricity generation. This study analyzes the theoretical performance of a solid oxide fuel cell (SOFC) integrated with a steam reforming process using three different renewable fuels: ethanol, glycerol and biogas. The effects of key steam reformer operating parameters on the hydrogen production for SOFCs are investigated. The performances of SOFC systems run on different fuels are compared in terms of electrical and thermal efficiencies. It is found that the biogas-fueled SOFC system requires the most energy, whereas the ethanol-fueled SOFC system achieves the highest electrical and thermal efficiencies.

1. Introduction

Fuel cells can generate electricity via an electrochemical reaction using hydrogen as fuel and oxygen as an oxidant. Thus, hydrogen production technology has developed in parallel with advances in fuel cell technology. Traditionally, hydrogen has been produced by reforming methane derived from natural gas, which mostly comes from fossil resources. As fossil fuel is in limited supply and causes environmental problems, hydrogen production from renewable and environmentally friendly fuels should be explored.

Among such renewable fuels, ethanol, biogas and glycerol have received considerable attention [1–4]. Ethanol is one of the most attractive raw materials for use in fuel cell hydrogen production because of its non-toxicity and liquid form. Many studies have been devoted to hydrogen production from ethanol [5–9]. Sun et al. [10]

E-mail address: Amornchai.A@chula.ac.th (A. Arpornwichanop).

studied hydrogen production from ethanol using steam reforming, autothermal reforming and partial oxidation. They found that ethanol steam reforming provides the highest hydrogen yield. A steam-to-ethanol ratio above 6 and temperatures greater than 900 K produce a high hydrogen yield with low carbon monoxide (CO) and carbon formation in the steam reforming environment.

Biogas is also a promising fuel, especially for developing countries. Biogas can be produced by the anaerobic digestion of animal and human waste, agricultural residues, aquatic weeds and other organic matters and mainly consists of methane (CH₄) and carbon dioxide (CO₂), containing CH₄ up to 60 vol.% [11]. To date, use of biogas for hydrogen production process has been widely studied; however, works on the integration of a biogas-based fuel system and a high-temperature fuel cell, such as molten carbonate fuel cells (MCFCs) and solid oxide fuel cells (SOFCs), are quite limited.

Glycerol is another potential fuel for hydrogen production. It is a byproduct of the production of biodiesel, whose consumption is continually increasing. Generally, crude glycerol always contains impurities; however, the purifying process for crude glycerol has a high operational cost and is uneconomic [12]. The utilization of glycerol for hydrogen production is considered promising [13–20].

^a Department of Chemical Engineering, Faculty of Engineering, Chulalongkorn University, Bangkok 10330, Thailand

^b School of Chemical Engineering, Faculty of Engineering, King Mongkut's Institute of Technology Ladkrabang, Bangkok 10520, Thailand

^c Department of Chemical Engineering, Faculty of Engineering, Thammasat University, Patumthani 12120, Thailand

^d Computational Process Engineering, Chulalongkorn University, Bangkok 10330, Thailand

 $^{^{\}mbox{\tiny{$^{\dot{}}$}}}$ The extended version of the paper presented at ICREPQ 2012.

 $^{^{*}}$ Corresponding author. Department of Chemical Engineering, Faculty of Engineering, Chulalongkorn University, Bangkok 10330, Thailand. Tel.: $+66\ 2\ 218\ 6878$; fax: $+66\ 2\ 218\ 6877$.

Nomenc	lature	R _{ohm}	total internal resistance (Ωm^2)
		\Re	gas constant (kJ $\text{mol}^{-1} \text{ K}^{-1}$)
$a_{\rm c}$	activity coefficient of carbon	T	temperature (K)
a_{ji}	number of atoms of element j in species i	u_{a}	fuel velocity at fuel channel (m s ⁻¹)
$A_{\rm c}$	fuel cell active area (m ²)	u_{f}	fuel velocity at fuel channel $(m s^{-1})$
A_j	total number of atoms of element j	$U_{ m f}$	fuel utilization factor
C_i	molar concentration of component $i \pmod{m^{-3}}$	V	operating cell voltage (V)
$D_{\rm eff,anode}$	effective gaseous diffusivity through anode (m ² s ⁻¹)	W	cell width (m)
$D_{\rm eff,cathod}$	e effective oxygen diffusivity through cathode (m ² s ⁻¹)		
E ^{OCV}	open-circuit voltage (V)	Greek sy	
E^0	open-circuit voltage at the standard pressure (V)	α	transfer coefficient
$E_{\rm act}$	activation energy for reforming reaction (kJ mol ⁻¹)	$\eta_{ m ohmic}$	ohmic losses (V)
$E_{\rm anode}$	activation energy of anode (kJ mol ⁻¹)	η_{act}	activation overpotentials (V)
$E_{\rm cathode}$	activation energy of cathode (kJ mol ⁻¹)	$\eta_{ m conc}$	concentration overpotentials (V)
F	Faraday constant (C mol ⁻¹)	$\eta_{ m el,sofc}$	stack electrical efficiency (%)
Ģ	total Gibbs free energy	$\eta_{ m el}$	system electrical efficiency (%)
h	enthalpy (kJ mol ⁻¹)	λ_{air}	excess air ratio
h_{a}	air channel height (m)	ν_i	stoichiometric coefficient of component i
$h_{ m f}$	fuel channel height (m)	$\sigma_{ m anode}$	electronic conductivity of anode $(\Omega^{-1} \text{m}^{-1})$
ΔH^0	standard heat of reaction (kJ mol ⁻¹)	$\sigma_{ m cathode}$	electronic conductivity of cathode $(\Omega^{-1} m^{-1})$
j	current density (A cm ⁻²)	$\sigma_{ m electrolyt}$	te ionic conductivity of electrolyte (Ω^{-1} m ⁻¹)
$j_{ m avg}$	average current density (A cm ⁻²)	$ au_{ ext{anode}}$	thickness of anode (m)
$j_{0, m anode}$	exchange current density at anode (A m ⁻²)	$ au_{\mathrm{cathode}}$	thickness of cathode (m)
$j_{0, m cathode}$	exchange current density at cathode ($A m^{-2}$)	$ au_{ m electrolyte}$	_e thickness of electrolyte (m)
K	total number of element <i>j</i>		
$k_{\rm act}$	pre-exponential constant for reforming reaction (mol s	Superscr	
	$^{-1} \text{m}^{-2} \text{bar}^{-1})$	0	standard condition
$k_{ m anode}$	pre-exponential factor of the anode (A m ⁻²)	in	feed inlet condition
$k_{ m cathode}$	pre-exponential factor of cathode (A m ⁻²)	out	feed outlet condition
k_{WGSR}	pre-exponential constant for reforming reaction		
k_{shift}	equilibrium constants for water gas shift reaction	Subscrip	
$K_{\rm BR}$	equilibrium constant of the Boudouard reaction	a	air channel
L	cell length (m)	act	activation overpotentials
LHV_i	low heating value (kJ s ⁻¹)	avg	average
n	number of electrons transferred	conc	concentration overpotentials
n_i	number of moles of species <i>i</i> (mol)	f	fuel channel
$\dot{n}_{ m i}$	molar flow rate of component $i \pmod{s^{-1}}$	i	chemical component
$p_{\rm i}$	partial pressures of component <i>i</i> (bar)	k	reaction
P	operating pressure of SOFC (bar)	ohm	ohmic loss
P_{sofc}	electrical power output (W)	r	reformer
P^0	operating pressure at standard condition (bar)	sofc	solid oxide fuel cell
Q	thermal energy $(kJ s^{-1})$	BR	Boudouard reaction
$Q_{\rm rec}$	thermal energy obtained from the SOFC system $(kJ s^{-1})$	TPB	three-phase boundary
$Q_{\rm use}$	total amount of thermal energy used in system (kJ s ⁻¹)		

For environmental and availability reasons, renewable energy resources have become important alternative fuels in the production of hydrogen.

Among the various fuel cell types, the solid oxide fuel cell (SOFC) is the most promising and can be used in a wide range of commercial applications. High-temperature SOFC operation has many advantages. For example, the high-temperature waste heat from SOFCs can be recovered for use in other heat-requiring SOFC components. In addition, SOFCs can utilize a variety of fuels (i.e., methane, methanol and ethanol) [21–23]. The use of an expensive catalyst can be avoided by the use of high temperatures, which promote the electrochemical reaction [24].

Many previous works have studied SOFC systems integrated into hydrogen production processes using different fuels. Pironelekgul et al. [25] found that steam is the most suitable reforming agent when biogas is used as fuel. Douvartzides et al. [26] showed that, in addition to the traditional use of natural gas, ethanol is an attractive fuel for SOFC operation. Tsiakaras et al. [27]

revealed that the ethanol-fueled SOFCs exhibit the highest theoretical efficiency when operated at 800–1200 K and that the ethanol steam reforming is the most attractive fuel processing system. Farhad et al. [28] studied biogas-fueled SOFC systems and observed that the best system thermal and electrical efficiencies can be achieved when the heat generated by an afterburner is used to supply other heat-requiring units in the SOFC system. Because the thermal and electrical efficiencies of SOFC systems depend on the fuel type, the thermal management and performance of SOFC systems using different fuels should be studied in detail to select the best fuel for different SOFC applications.

The aim of this study is to theoretically analyze a SOFC system integrated with a steam reforming process and compare several important renewable resources for hydrogen production: biogas, ethanol and glycerol. The effect of operating conditions on the reformer performance is investigated in terms of hydrogen yield, product distribution and carbon formation. The energy requirements of each unit in the SOFC system fed by different fuels

are also examined. In addition, the electrical efficiency, thermal efficiency and cell-stack efficiency of the SOFC integrated system for power generation is investigated. Finally, the amount of CO_2 released from the SOFC system using different fuels is investigated to address environmental concerns.

2. Fuel processor and SOFC integrated system

Fig. 1 shows the external reformer and SOFC integrated system, which comprises heat exchangers, fuel processor, SOFC and afterburner. Steam and fuel are mixed, then preheated at operating reforming temperatures and sent to the steam reformer, where a synthesis gas (hydrogen-rich gas) is produced. Next, the synthesis gas is preheated at the desired temperature and then fed to the SOFC. Air is also compressed and preheated before being fed to the SOFC. The SOFC produces electrical power and steam via the electrochemical reaction of hydrogen and oxygen in air. In general, SOFCs cannot be operated at complete fuel utilization; thus, the residual fuel is combusted in an afterburner to generate heat for use in other heat-requiring units in the SOFC system, such as a reformer and fuel and air pre-heaters (dash line in Fig. 1).

In this study, biogas, ethanol and glycerol are considered the potential fuels to produce hydrogen for SOFC systems. Biogas is composed of 60 mol% methane and 40 mol% carbon dioxide. To analyze the theoretical performance of the SOFC system, it is assumed that the system is run under steady-state conditions and that all gases behave as ideal gases. Furthermore, heat losses from individual components in the SOFC system are negligible and the operating pressure and temperature of the reformer and the SOFC are constant. The considered SOFC is planar and described by a one-dimensional model, which is operated at a constant cell voltage along the cell coordinate.

2.1. Fuel processor

Hydrocarbon fuels are reformed to produce a synthesis gas via a steam reforming reaction. The final composition of the produced synthesis gas under equilibrium conditions is determined from the minimization of the Gibbs free energy. The main products of each fuel processing system are hydrogen, methane, carbon dioxide, carbon monoxide and water. Their equilibrium compositions depend on the operating temperature and pressure of the steam reformer. Eq. (1) gives the total Gibbs free energy of the system [29]:

$$G = \sum_{i} n_i G_i^0 + \Re T \sum_{i} n_i \ln \frac{y_i \varphi_i P_r}{P^0}$$
 (1)

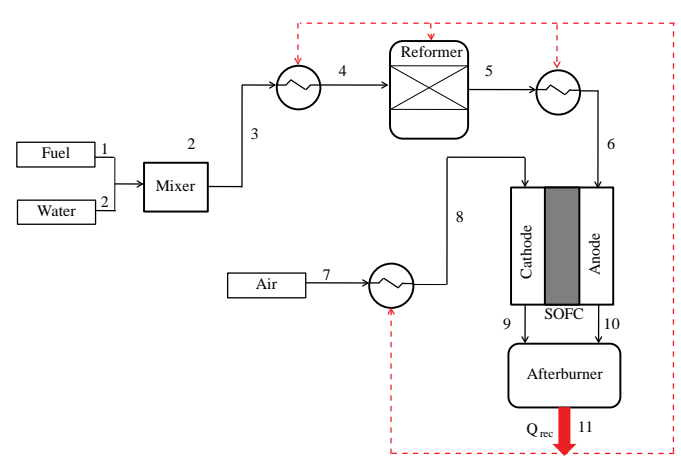


Fig. 1. Schematic of an SOFC system integrated with a fuel processor.

where G is the total Gibbs free energy, n_i is the number of moles of species i, G_i^0 is the standard Gibbs free energy of species i, \Re is the gas constant, T is the reforming temperature, P_T is the operating pressure of the reformer, y_i is the mole fraction of species i and ϕ_i is the fugacity coefficient of a gas mixture ($\phi_i = 1$ for ideal gas).

The equilibrium compositions obtained by minimizing the Gibbs free energy must satisfy the following constraints:

$$\sum_{i} a_{ji} n_{i} = A_{j}; \ j = 1, ..., k$$
 (2)

where a_{ji} is the number of atoms of element j in species i and A_j is the total number of atoms of element j in the feed stream. The Lagrange multiplier method is applied to find the product composition of the reactive system [30].

The overall steam reforming reactions of ethanol, glycerol and biogas are represented by Eqs. (3)–(5), respectively.

$$C_2H_5OH + 3H_2O \leftrightarrow 2CO_2 + 6H_2$$
 (3)

$$C_3H_8O_3 + 3H_2O \leftrightarrow 3CO_2 + 7H_2$$
 (4)

$$CH_4 + 2H_2O \leftrightarrow CO_2 + 4H_2 \tag{5}$$

Regarding carbon formation in the reforming system, a stoichiometric approach is applied to determine the boundary of the carbon formation. The reactions that are most likely to lead to carbon formation in the reforming system with hydrocarbon fuels are as follows:

$$2CO \leftrightarrow CO_2 + C \tag{6}$$

$$CH_4 \leftrightarrow 2H_2 + C$$
 (7)

$$CO + H_2 \leftrightarrow H_2O + C \tag{8}$$

$$CO_2 + 2H_2 \leftrightarrow 2H_2O + C \tag{9}$$

From a thermodynamic viewpoint, the Boudouard reaction (Eq. (6)) is considered the major carbon generation reaction because it has the lowest Gibbs free energy. The possibility of carbon formation can be calculated from the value of carbon activity [31], defined as

$$a_{\rm c} = \frac{K_{\rm BR} x_{\rm CO}^2 P_{\rm r}}{x_{\rm CO_2}} \tag{10}$$

where $a_{\rm C}$ is the activity coefficient of carbon and $K_{\rm BR}$ represents the equilibrium constant of the Boudouard reaction. For carbon activities greater than unity, the system is not in equilibrium and carbon formation occurs. When the carbon activity equals unity, the system is in equilibrium. Finally, for carbon activities less than unity, carbon formation is thermodynamically impossible. Note that the carbon activity is only an indicator of the presence of carbon in a system and does not indicate the quantity of carbon generated.

The heat required for the operation of the steam reformer under isothermal conditions can be computed from the following energy balance equation:

$$Q_{SR} = \left(\sum_{i} \dot{n}_{i,r}^{\text{out}} \dot{h}_{i,r}^{\text{out}}\right) - \left(\sum_{i} \dot{n}_{i,r}^{\text{in}} \dot{h}_{i,r}^{\text{in}}\right)$$
(11)

where $\dot{n}_{i,\mathrm{r}}$ is the molar flow rate of species i and $\dot{h}_{i,\mathrm{r}}$ is the enthalpy of species i

The enthalpy can be calculated by:

$$\dot{h} = h^0 + \int_{298}^{T_{\text{sofc}}} C_{\text{p}} dT \tag{12}$$

where h^0 is the enthalpy at the standard condition [29].

To evaluate the steam reforming performance of the fuel, the hydrogen yield is defined as

$$H_2 \text{ yield (Ethanol)} = \frac{n_{H_2,r}^{\text{out}}}{6(n_{C,H_5\text{OH,r}}^{\text{in}})}$$
 (13)

$$H_2 \text{ yield (Glycerol)} = \frac{n_{H_2,r}^{\text{out}}}{7(n_{C_3H_8O_3,r}^{\text{in}})}$$
 (14)

$$H_2 \text{ yield (Biogas)} = \frac{n_{\text{H}_2,\text{r}}^{\text{out}}}{4\left(n_{\text{CH}_4,\text{r}}^{\text{in}}\right)} \tag{15}$$

The factors in the denominator of Eqs. (13)–(15) depend on the number of moles of hydrogen obtained from the steam reforming reactions of ethanol, glycerol and biogas as shown in Eqs. (3)–(5).

2.2. SOFC

Reformate gas consisting of CH_4 , H_2O , CO, H_2 , and CO_2 is fed into the fuel channel of the SOFC, and air consisting of O_2 and O_2 is fed into the air channel. In general, hydrocarbon fuels can be further converted into hydrogen and carbon dioxide by steam reforming and water gas shift reactions (Eqs. (16) and (17)) within the SOFC because of its high temperatures and the use of an anode catalyst to accelerate these reactions.

Steam reforming reaction:

$$CH_4 + H_2O \leftrightarrow 3H_2 + CO \tag{16}$$

Water gas shift reaction:

$$CO + H_2O \leftrightarrow H_2 + CO_2 \tag{17}$$

In SOFC operation, hydrogen is consumed in an electrochemical reaction to produce electricity, whereas the oxygen in air is reduced into oxygen ions at the cathode side. The electrochemical reactions occurring at the SOFC fuel and air channels are given in Eqs. (18)—(20). The kinetic equations of all reactions occurring within the SOFC are given in Table 1 [32,33].

Hydrogen oxidation reaction:

$$H_2 + O^{2-} \leftrightarrow H_2O + 2e^-$$
 (18)

Oxygen reduction reaction:

$$1/2O_2 + 2e^- \leftrightarrow O^{2-} \tag{19}$$

Overall cell reaction:

$$H_2 + 1/2O_2 \leftrightarrow H_2O \tag{20}$$

Table 1 SOFC reaction kinetics

Steam reforming reaction
$$R_{(I)} = k_{\rm act} p_{\rm CH_4,f,} \exp\left(\frac{-E_{\rm act}}{RT_{\rm f}}\right)$$
 Water gas shift reaction
$$R_{(I)} = k_{\rm WGSR} p_{\rm CO,f} \left(1 - \frac{p_{\rm CO_2,f} p_{\rm H_2,f}}{k_{\rm shift} p_{\rm CO,f} p_{\rm H_2O,f}}\right)$$
 Electrochemical reaction
$$R_{(I)} = \frac{j}{2F}$$

The component concentrations in fuel and air channels along the flow direction can be described by the following equations:

Fuel channel: $(i = CH_4, H_2O, CO, H_2 \text{ and } CO_2)$

$$\frac{dC_{i,f}}{dx} = \frac{1}{u_f} \sum_{k \in \{(i),(ii),(v)\}} \nu_{i,k} R_k \frac{1}{h_f}
C_{i,f} \Big|_{v=0} = C_{i,f}^0$$
(21)

Air channel: $(i = O_2 \text{ and } N_2)$

$$\frac{dC_{i,a}}{dx} = \frac{1}{u_a} \nu_{i,(v)} R_{(v)} \frac{1}{h_a}$$

$$C_{i,a}|_{x=0} = C_{i,a}^0$$
(22)

The theoretical open-circuit potential can be expressed by the Nernst equation:

$$E^{\text{OCV}} = E^{0} - \frac{\Re T}{2F} \ln \left(\frac{p_{\text{H}_{2}\text{O}}}{p_{\text{H}_{2}} p_{\text{O}_{2}}^{0.5}} \right)$$
 (23)

where E^0 , the open-circuit voltage at standard pressure, is a function of the operating temperature:

$$E^0 = 1.253 - 2.4516 \times 10^{-4} T \tag{24}$$

Due to internal voltage losses, the actual voltage (V) is lower than the open-circuit voltage (Eq. (25)).

$$V = E - \eta_{\text{ohmic}} - \eta_{\text{conc}} - \eta_{\text{act}} \tag{25}$$

where $\eta_{\rm ohmic}, \eta_{\rm conc}, \eta_{\rm act}$ are the ohmic, concentration, and activation losses, respectively.

The ohmic losses can be explained by the linear relation between the voltage drop and current density:

$$\eta_{\rm ohm} = jR_{\rm ohm} \tag{26}$$

where R_{ohm} is the internal electrical resistance, which depends on the conductivity and thickness of individual fuel cell layers as follows:

$$R_{\text{Ohm}} = \frac{\tau_{\text{anode}}}{\sigma_{\text{anode}}} + \frac{\tau_{\text{electrolyst}}}{\sigma_{\text{electrolyst}}} + \frac{\tau_{\text{cathode}}}{\sigma_{\text{cathode}}}$$
(27)

where $\tau_{\rm anode}$, $\tau_{\rm cathode}$ and $\tau_{\rm electrolyte}$ are the thickness of the anode, cathode and electrolyte layers, respectively. $\sigma_{\rm anode}$ and $\sigma_{\rm cathode}$ are the electronic conductivity of the anode and cathode, respectively, and $\sigma_{\rm electrolyte}$ is the ionic conductivity of the electrolyte.

The concentration overpotentials are due to insufficient hydrogen at the reaction sites [34,35], as described by Eq. (28):

$$\eta_{\mathrm{conc}} = \eta_{\mathrm{conc,anode}} + \eta_{\mathrm{conc,cathode}}$$

$$= \left(\frac{\Re T}{2F} \ln \left(\frac{p_{\mathrm{H_2O,TPB}} p_{\mathrm{H_2,f}}}{p_{\mathrm{H_2O,f}} p_{\mathrm{H_2,TPB}}}\right)\right)_{\mathrm{anode}} + \left(\frac{\Re T}{4F} \ln \left(\frac{p_{\mathrm{O_2,a}}}{p_{\mathrm{O_2,TPB}}}\right)\right)_{\mathrm{cathode}}$$
(28)

The partial H_2 , H_2O and O_2 pressures at the three-phase boundaries can be determined using a gas transport model in porous media [34], as given by

$$p_{\rm H_2,TPB} = p_{\rm H_2,f} - \frac{\Re T \tau_{\rm anode}}{2F D_{\rm eff,anode}} j$$
 (29)

$$p_{\text{H}_2\text{O,TPB}} = p_{\text{H}_2\text{O,f}} + \frac{\Re T\tau_{\text{anode}}}{2FD_{\text{eff,anode}}} j$$
 (30)

$$p_{O_2,TPB} = P - \left(P - p_{O_2,a}\right) \exp\left(\frac{\Re T \tau_{cathode}}{4FD_{eff,cathode}}P^{j}\right)$$
(31)

where $D_{\rm eff,anode}$ is the effective gaseous diffusivity through the anode (considering a binary gas mixture of H₂ and H₂O) and $D_{\rm eff,-cathode}$ is the effective oxygen diffusivity through the cathode (binary gas mixture of O₂ and N₂).

The activation overpotentials can be determined from the nonlinear Butler—Volmer equation, which relates the current density to the activation overpotential:

$$j = j_{0,\text{anode}} \left[\frac{p_{\text{H}_2,\text{TPB}}}{p_{\text{H}_2,\text{f}}} \exp\left(\frac{\alpha nF}{\Re T} \eta_{\text{act,anode}}\right) - \frac{p_{\text{H}_2\text{O},\text{TPB}}}{p_{\text{H}_2\text{O},\text{f}}} \exp\left(-\frac{(1-\alpha)nF}{\Re T} \eta_{\text{act,anode}}\right) \right]$$
(32)

$$j = j_{0,\text{cathode}} \left[\exp \left(\frac{\alpha nF}{\Re T} \eta_{\text{act,cathode}} \right) - \exp \left(-\frac{(1-\alpha)nF}{\Re T} \eta_{\text{act,cathode}} \right) \right]$$
(33)

where α is the transfer coefficient (=0.5), n is the number of electrons transferred in the single elementary rate-limiting reaction step, and $j_{0,\text{cathode}}$ and $j_{0,\text{anode}}$ are the exchange current densities at the anode and cathode (Eqs. (34) and (35)), respectively.

$$j_{0,\text{cathode}} = \frac{\Re T}{nF} k_{\text{cathode}} \exp\left(-\frac{E_{\text{cathode}}}{\Re T}\right)$$
 (34)

$$j_{0,\text{anode}} = \frac{\Re T}{nF} k_{\text{anode}} \exp\left(-\frac{E_{\text{anode}}}{\Re T}\right)$$
 (35)

where $E_{\rm cathode}$ and $E_{\rm anode}$ represent the activation energies of the cathode and anode exchange current densities and are 137 and 140 kJ mol⁻¹, respectively. $k_{\rm cathode}$ and $k_{\rm anode}$ represent the pre-exponential factors and are 2.35×10^{11} and $6.54 \times 10^{11} \, \Omega^{-1} \, {\rm m}^{-2}$, respectively [35].

The average current density (j_{ave}) can be computed from the current density distribution along the cell length, which is obtained by solving the fuel cell model:

Table 2Kinetic and material property parameters for the planar SOFC.

Anode diffusion coefficient, $D_{\text{eff,anode}}$ (m ² s ⁻¹) Cathode diffusion coefficient, $D_{\text{eff,anode}}$ (m ² s ⁻¹)	3.66×10^{-5} 1.37×10^{-5}
Anode electrical conductivity, $\sigma_{\rm anode}(\Omega^{-1}{\rm m}^{-1})$	$\frac{4.2\times10^7}{T}\exp\left(\frac{-1200}{T}\right)$
Cathode electrical conductivity, $\sigma_{\rm cathode}$ ($\Omega^{-1}{\rm m}^{-1}$)	$\frac{9.5\times10^7}{T}\exp\left(\frac{-1150}{T}\right)$
Electrolyte ionic conductivity, $\sigma_{\rm electrolyte}$ ($\Omega^{-1}{ m m}^{-1}$)	$33.4 \times 10^3 \exp\left(\frac{-10300}{T}\right)$
Pre-exponential factor of anode exchange current density, k_{anode} (A m ⁻²)	6.54×10^{11}
Pre-exponential factor of cathode exchange current density, k_{cathode} (A m ⁻²)	2.35×10^{11}
Activation energy of anode exchange current density, E _{anode} (kJ mol ⁻¹)	140
Activation energy of cathode exchange current density, E_{cathode} (kJ mol ⁻¹)	137

 Table 3

 Value of operating conditions and parameters used for model validation

Cell length, L (m)	0.1
Cell width, W (m)	0.1
Fuel channel height, $h_{\rm f}$ (mm)	1
Air channel height, h_a (mm)	1
Anode thickness, τ_{anode} (μm)	500
Cathode thickness, $\tau_{cathode}$ (μm)	50
Electrolyte thickness, $\tau_{\text{electrolyte}}$ (μm)	20
Inlet fuel and air temperature, T_{sofc} (K)	1023
Operating pressure, P_{sofc} (bar)	1
Air composition	21% O ₂ , 79% N ₂
Fuel composition	33% CH ₄ , 67% H ₂ O
Fuel utilization	0.8
Operating voltage (V)	0.6582

$$j_{\text{avg}} = \frac{1}{L} \int_{L}^{0} j(z) dz \tag{36}$$

To evaluate the performance of the SOFC, the overall fuel utilization (U_f) and the electrical power output (P_{sofc}) are determined by

$$U_{\rm f} = \frac{j_{\rm avg}LW}{2F\left(4\dot{n}_{\rm CH_4}^{\rm in} + \dot{n}_{\rm H_2}^{\rm in} + \dot{n}_{\rm co}^{\rm in}\right)}$$
(37)

$$P_{\rm sofc} = j_{\rm avg} V A_{\rm c} \tag{38}$$

where \dot{n}_i^{in} is the inlet molar flow rate of gas species i and V represents the actual potentials.

As the SOFC operation is operated under isothermal conditions, excess air is fed into the SOFC to maintain the operating temperature at a desired value. The difference in the inlet and outlet fuel cell temperatures is limited to 100 K [36,37]. As a result, the amount of the inlet air can be calculated from the energy balance around a fuel cell control volume as

$$\left(\sum_{i} \dot{n}_{i,an}^{in} \dot{h}_{i,an}^{in}\right) + \left(\sum_{i} \dot{n}_{i,ca}^{in} \dot{h}_{i,ca}^{in}\right) - \left(\sum_{o} \dot{n}_{i,an}^{out} \dot{h}_{i,an}^{out}\right) - \left(\sum_{o} \dot{n}_{i,ca}^{out} \dot{h}_{i,ca}^{out}\right) - P_{sofc} = 0$$
(39)

where \dot{n}_i is the inlet and outlet molar flow rates of species i through the SOFC and \dot{h}_i is the inlet and outlet enthalpies of formation of species i which is a function of temperature.

The performance of the SOFC system is considered in terms of the stack electrical efficiency, the system electrical efficiency (η_{el}) and the thermal efficiency (η_{th}), which are defined as

Table 4 Validation of the SOFC model.

	Kanga et al. [38]	Model	Error (%)
Gas composition at the outlet of the j	fuel channel (mole fra	ction)	
Methane	0.0001	0.0001	0
Water	0.6772	0.6871	1.46
Hydrogen	0.1239	0.1215	1.94
Carbon monoxide	0.0349	0.0336	3.72
Carbon dioxide	0.1639	0.1577	3.78
Gas composition at the outlet of the air channel (mole fraction)			
Oxygen	0.1872	0.1885	0.69
Nitrogen	0.8128	0.8115	0.16
SOFC performance parameters			
Air ratio	7.5	7.5670	0.89
Average current density (A cm ⁻²)	0.5	0.4988	0.24
Power density (W cm ⁻²)	0.3291	0.3283	0.24

Table 5Values of operating conditions for SOFC system under nominal conditions.

Reformer	
Operating temperature (K)	1073
Operating pressure (bar)	1
S/C	1.5
Solid oxide fuel cell	
Cell operating temperature (K)	1173
Cell operating pressure (bar)	1
Net power output (kW)	150
Air composition	21% O ₂ , 79% N ₂
Cell fuel utilization factor (%)	0.7
Fuel cell active area (m ²)	55.2
Anode thickness, τ_{anode} (μm)	500
Cathode thickness, $\tau_{cathode}$ (μm)	50
Electrolyte thickness, f $\tau_{\text{electrolyte}}$ (μm)	20
Fuel channel height, h_a (mm)	1
Air channel height, h_a (mm)	1
DC-AC inverter efficiency	96
Afterburner	
Afterburner combustion efficiency (%)	98

$$\eta_{\text{el,sofc}} = \frac{P_{\text{sofc}}}{\dot{n}_{\text{H}_2} \text{LHV}_{\text{H}_2} + \dot{n}_{\text{CO}} \text{LHV}_{\text{CO}} + \dot{n}_{\text{CH}_4} \text{LHV}_{\text{CH}_4}}$$
(40)

$$\eta_{\rm el} = \frac{P_{\rm sofc}}{\dot{n}_i \rm LHV_i} \tag{41}$$

$$\eta_{\text{th}} = \frac{Q_{\text{rec}} - Q_{\text{use}}}{\dot{n}_i \text{LHV}_i} \tag{42}$$

where \dot{n}_i is the inlet molar flow rate of component i, LHV $_i$ is the lower heating value of component i, $Q_{\rm use}$ is the total thermal energy used in the SOFC system and $Q_{\rm rec}$ is the thermal energy obtained from the afterburner. Note that the reference temperature of 100 °C is given to determine an amount of heat that can be recovered from the afterburner. The thermal efficiency defined as Eq. (42) indicates the maximum theoretical thermal efficiency that the SOFC system can achieve and no heat loss is assumed.

All of the system model equations describing the SOFC system are coded and solved using Matlab. Table 2 shows the material property parameters of the SOFC. To verify the SOFC model used here, the modeling results are compared with the simulation data of Kanga et al. [38] under the same operating conditions, as shown

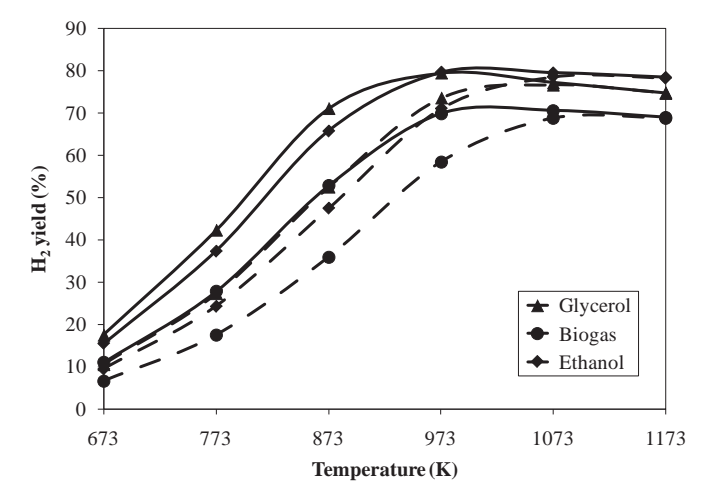


Fig. 2. Effect of reforming temperature on H_2 yield at S/C = 2:1 and pressures of 1 bar (solid line) and 3 bar (dashed line)

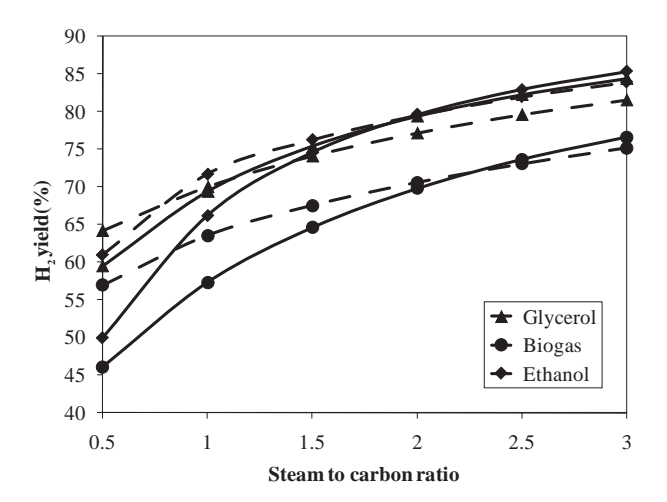


Fig. 3. Effect of S/C ratio on H_2 yield (P = 1 bar): T = 973 K (solid line) and T = 1073 K (dashed line).

in Table 3. The results show that the model prediction agrees very well with the published data (Table 4). The maximum error of around 4% is found for predicting the fractions of CO and CO_2 at the outlet of the fuel channel. The predicted parameters of the SOFC performance, such as average current density and power density, are less than 1% different from the reported values.

The models used for other components of the SOFC system, such as vaporizers, pre-heaters, the mixer and the afterburner, are reported elsewhere [39]. In this study, the SOFC system is designed for a net power output of 150 kW and a fuel utilization of 0.7. The operating conditions for the SOFC system under nominal conditions are given in Table 5.

3. Results and discussion

3.1. Hydrogen production from various fuels

In this section, hydrogen production via steam reforming using ethanol, biogas and glycerol as fuels is investigated. Fig. 2 shows the effect of operating temperature on hydrogen production from the steam reforming of these three fuels. The results show a similar trend for each fuel type; this behavior is also observed for other fuels, such as methane and methanol [40,41]. An increase in the reforming

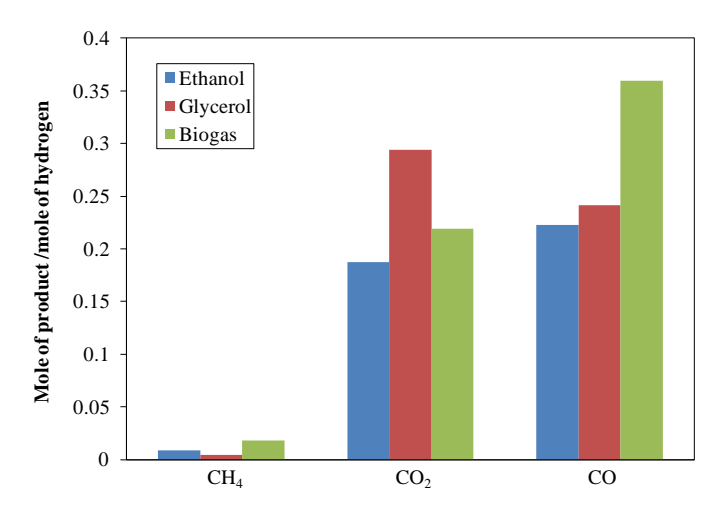


Fig. 4. Product distribution from the steam reforming of glycerol, ethanol and biogas (T = 973 K and S/C = 2).

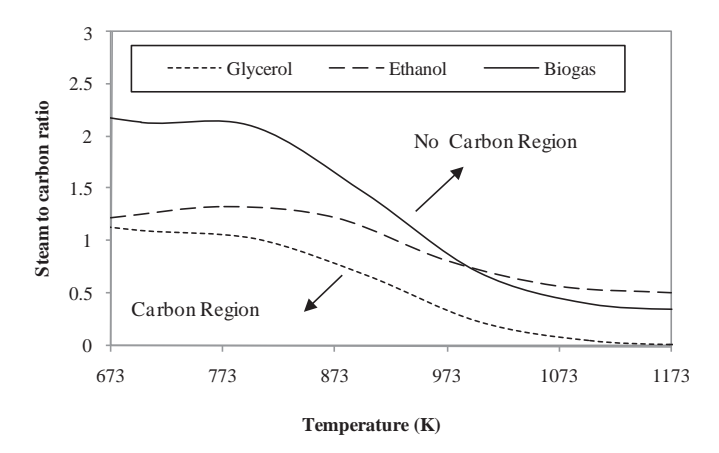


Fig. 5. Carbon boundary of various fuels.

temperature enhances the hydrogen yield due to the endothermicity of the steam reforming reaction. Ethanol and glycerol provide a higher hydrogen yield than biogas does. At atmospheric pressure, glycerol provides a slightly higher hydrogen yield than ethanol at temperatures below 973 K. When the steam reformer is operated at high pressure, glycerol produces more hydrogen than ethanol at temperatures below 1033 K. The operating pressure does not affect the hydrogen yield at temperatures above 1073 K.

Fig. 3 shows the effect of the steam-to-carbon (S/C) ratio on hydrogen yield at a pressure of 1 bar. At a low S/C ratio, glycerol produces more hydrogen than ethanol does. However, ethanol gives the highest hydrogen yield for higher S/C ratios. The use of biogas provides the lowest hydrogen yield throughout the operational range studied. Fig. 4 shows the ratio of the amount of gaseous product to that of hydrogen produced from the steam reforming of glycerol, ethanol and biogas at a temperature of 973 K and an S/C ratio of 2. The glycerol reforming process yields the highest CO_2 concentration because glycerol has a hydrogen-to-carbon ratio lower than other fuels. The results also indicate that when ethanol is used as a fuel, less CO is produced. The presence of CO may cause the formation of carbon in the steam reforming process and the CO

Fig. 5 shows the carbon formation boundary when glycerol, ethanol and biogas are used to produce hydrogen. The carbon

formation tendencies of the different fuels are similar, being lower for high-temperature operation and high S/C ratios. Because the steam reforming of biogas generates more carbon monoxide, shifting the Boudouard reaction towards the products, this process must be performed at a higher temperature and S/C ratio to avoid carbon formation. Although the amount of carbon monoxide generated by the steam reformer fueled by ethanol is lower than that fueled by glycerol, ethanol reforming exhibits a higher carbon formation tendency than glycerol reforming because glycerol has a higher oxygen-to-carbon ratio than ethanol. Thus, glycerol is more likely than ethanol to be reformed to CO and CO_2 rather than carbon.

3.2. SOFC system

Next, the performance of the SOFC fed by the synthesis gas obtained from the steam reforming of ethanol, glycerol and biogas is investigated. The power output of the SOFC system is specified at 150 kW. Fig. 6 presents the fraction of the heat duty required for each unit in the SOFC systems. The air preheater requires the most heat input, 79–81% of the overall heat consumption of the SOFC system, compared to other heat-requiring units. SOFCs are usually operated at high temperatures, and the electrochemical reaction is an exothermic reaction. These factors cause a temperature gradient in the SOFC stack. Therefore, excess air is required to maintain the SOFC temperature at a suitable level. The steam reformer also requires a large amount of energy.

The energy consumptions for each unit of the SOFC system are compared in Fig. 7 for different fuels. The results indicate that the SOFC system run on biogas requires the most external energy, whereas the ethanol-fueled SOFC system requires the least energy. Biogas reforming requires the most energy (77.9 kW) because the high CO₂ content in biogas promotes a reverse water gas shift reaction, which is an endothermic reaction. Although the energy requirement of the glycerol steam reforming is lower, more heat is needed for the evaporator due to the high boiling point of glycerol (561.9 K).

Fig. 8 shows the SOFC stack efficiency and the thermal and electrical efficiencies of the SOFC systems supplied by different fuels. As observed in the figure, the SOFC system fueled by ethanol gives the best performance in terms of the SOFC stack efficiency.

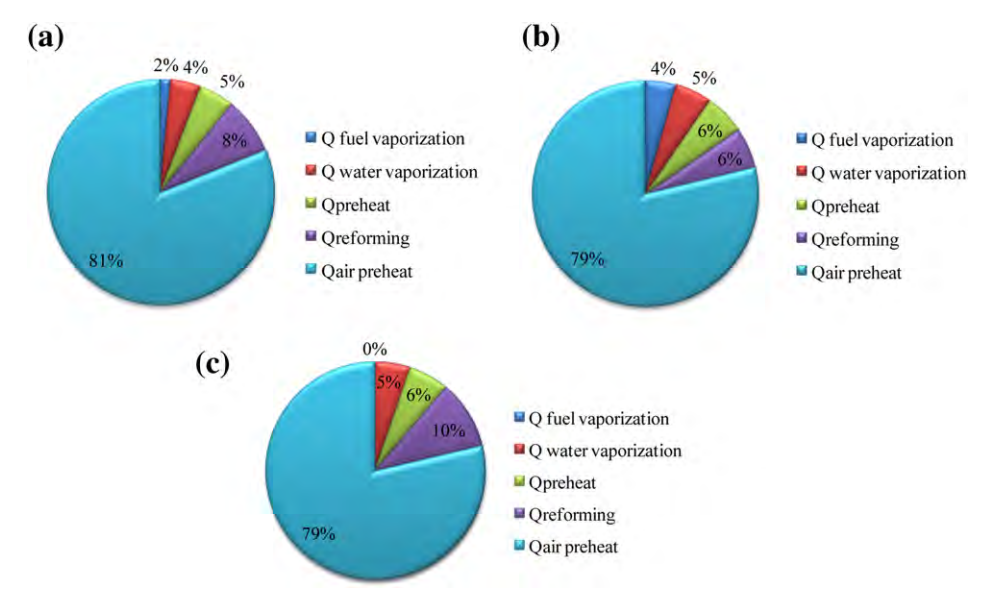


Fig. 6. Distribution of energy consumption in an SOFC system fed by different fuels: (a) ethanol, (b) glycerol and (c) biogas.

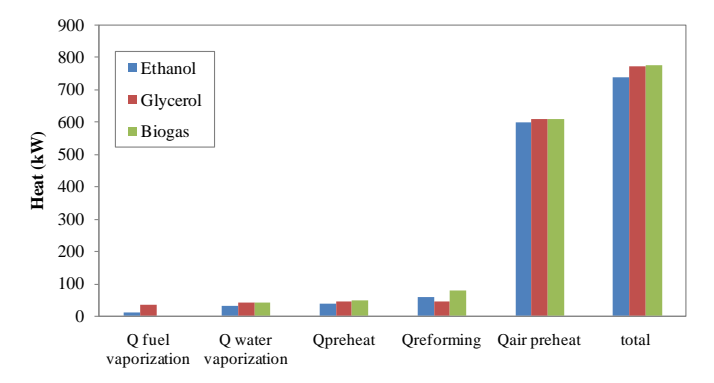
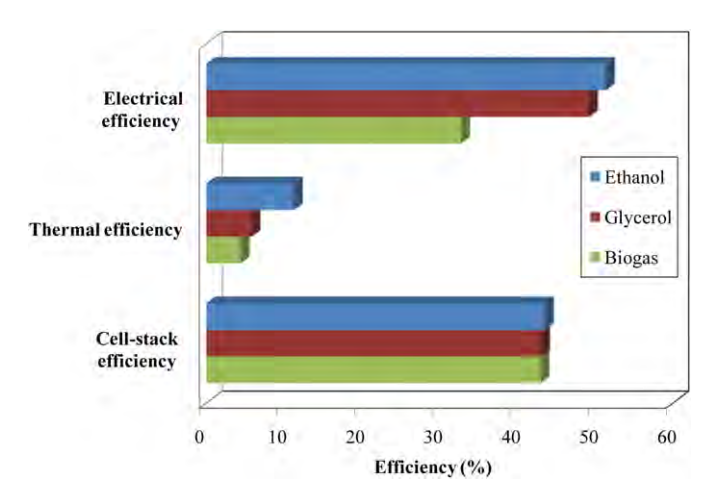


Fig. 7. Energy required by each unit of an SOFC system for different fuel feeds.

the electrical efficiency and the thermal efficiency due to the superior performance of the ethanol steam reformer compared that of other fuels, which translates into the greatest hydrogen production. The ethanol-fueled SOFC system can achieve an electrical efficiency of 51%, whereas the electrical efficiencies of the glyceroland biogas-fueled SOFC systems are 49% and 32%, respectively. The use of biogas as a fuel for the SOFC system provides the worst electrical efficiency because biogas mainly consists of carbon dioxide, which dilutes the hydrogen fuel fed into the SOFC stack. This dilution lowers the reversible cell voltage and increases the concentration and activation overpotentials in the SOFC. The efficiency of the SOFC stack is fairly independent of fuel type (42–43%). The SOFC system fed by biogas shows the lowest thermal efficiency at the desired power output of 150 kW because a large amount of heat is lost to preheat carbon dioxide in the biogas feed.

Fig. 9 presents the amount of carbon dioxide released from the SOFC system at a power output of 150 kW. The SOFC system fed by ethanol minimizes the emission of carbon dioxide, whereas the glycerol-fueled SOFC system produces the most carbon dioxide. The carbon dioxide emission of the ethanol-fed SOFC system is less than that of the other systems by 21.76% (glycerol) and 19.97% (biogas). The simulation study indicates that ethanol is the most suitable of the three renewable fuels studied for use in an SOFC system integrated with an external steam reformer. The use of ethanol as fuel provides the greatest SOFC stack efficiency, system electrical efficiency and thermal efficiency and the least carbon dioxide emission. When biogas is used as a fuel for SOFC, the use of a purification unit is suggested to remove carbon dioxide from the biogas, thereby improving both the thermal and electrical system efficiencies.



 $\textbf{Fig. 8.} \ \, \textbf{Efficiencies of the SOFC systems with different type of fuels.}$

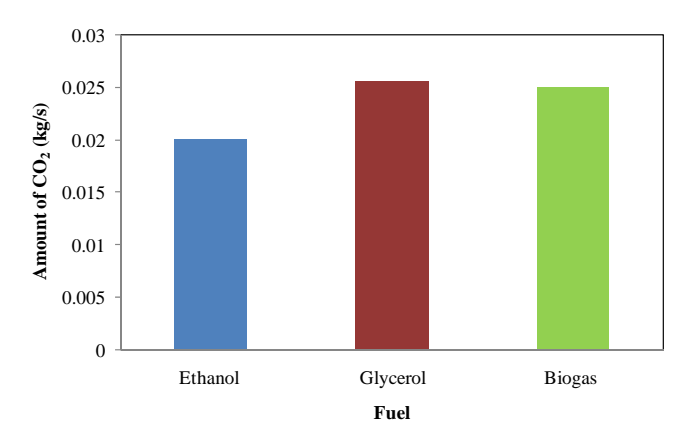


Fig. 9. CO₂ released from SOFC systems with different fuels.

4. Conclusions

The performance and efficiency of a steam reforming process and solid oxide fuel cell (SOFC) integrated system was theoretically analyzed in this study. Different renewable fuels, i.e., glycerol, ethanol and biogas, were applied to generate hydrogen for SOFC. The results showed that ethanol can produce the most hydrogen at an operating temperature of 1073 K. The utilization of glycerol for hydrogen production shows the least tendency toward carbon formation. The SOFC system supplied by biogas requires the most energy and has the lowest electrical and thermal efficiencies. Ethanol is a suitable fuel for the SOFC system; it has the highest electrical and thermal efficiencies of the three fuels, and it has low carbon dioxide emission.

Acknowledgments

Support from the Thailand Research Fund and the Special Task Force for Activating Research (STAR), Chulalongkorn University Centenary Academic Development Project, is gratefully acknowledged.

D. Saebea would like to thank the Office of the Higher Education Commission, Thailand for their grant support under the program "Strategic Scholarships for Frontier Research Network for the Joint Ph.D. Program Thai Doctoral degree" for this research.

References

- Ashrafi M, Proll T, Pfeifer C, Hofbauer H. Experimental study of model biogas catalytic steam reforming: 1. thermodynamic optimization. Energy Fuels 2008:22:4182-9.
- [2] Yu CY, Lee DW, Park SJ, Lee KY, Lee KH. Study on a catalytic membrane reactor for hydrogen production from ethanol steam reforming. Int J Hydrogen Energy 2009;34:2947–54.
- [3] Dou B, Dupont V, Rickett G, Blakeman N, Williams PT, Chen H, et al. Hydrogen production by sorption-enhanced steam reforming of glycerol. Bioresour Technol 2009;100:3540-7.
- [4] Mohseni F, Magnusson M, Görling M, Alvfors P. Biogas from renewable electricity increasing a climate neutral fuel supply. Appl Energy 2012;90:11–6.
- [5] Akande A, Aboudheir A, Idem R, Dalai A. Kinetic modeling of hydrogen production by the catalytic reforming of crude ethanol over a co-precipitated Ni-Al₂O₃ catalyst in a packed bed tubular reactor. Int J Hydrogen Energy 2006;31:1707—15.
- [6] Garcia E, Laborde MA. Hydrogen product by the steam reforming of ethanol: Thermodynamic analysis. Int J Hydrogen Energy 1991;16:307–12.
- [7] Vasudeva K, Mitra N, Umasankar P, Dhingra SC. Steam reforming of ethanol for hydrogen production: thermodynamic analysis. Int J Hydrogen Energy 1996;21:13–8.
- [8] Liguras DK, Kondarides DI, Verykios XE. Production of hydrogen for fuel cells by steam reforming of ethanol over supported noble metal catalysts. Appl Catal B: Environ 2003;43:345–54.
- [9] Kwak BS, Lee JS, Lee JS, Choi BH, Ji MJ, Kang M. Hydrogen-rich gas production from ethanol steam reforming over Ni/Ga/Mg/Zeolite Y catalysts at mild temperature. Appl Energy 2011;88:4366-75.

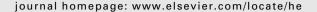
- [10] Sun S, Yan W, Sun P, Chen J. Thermodynamic analysis of ethanol reforming for hydrogen production. Energy 2012;44:911–24.
- [11] Pandya JD, Ghosh KK, Rastogi SK. A phosphoric acid fuel cell coupled with biogas. Energy 1988;13:383–8.
- [12] Demirbas A. Biodiesel from waste cooking oil via base catalytic and supercritical methanol transesterification. Energy Convers Manage 2009;50: 923-7.
- [13] Byrd AJ, Pant KK, Gupta RB. Hydrogen production from glycerol by reforming in supercritical water over Ru/Al₂O₃ catalyst. Fuel 2008;87:2956–60.
- [14] Pompeo F, Santori G, Nichio NN. Hydrogen and/or syngas from steam reforming of glycerol: Study of platinum catalysts. Int J Hydrogen Energy 2010;35:8912–20.
- [15] Chen H, Ding Y, Cong NT, Dou B, Dupont V, Ghadiri M, et al. A comparative study on hydrogen production from steam-glycerol reforming: thermodynamics and experimental. Renew Energy 2011;36:779–88.
- [16] Guo Y, Azmat MU, Liu Z, Wang Y, Lu G. Effect of support's basic properties on hydrogen production in aqueous-phase reforming of glycerol and correlation between WGS and APR. Appl Energy 2012;92:218–23.
- [17] Adhikari S, Fernando S, Gwaltney SR, To SDF, Bricka MR, Steele H, et al. A thermodynamic analysis of hydrogen production by steam reforming of glycerol. Int J Hydrogen Energy 2007;32:2875–80.
- [18] Dauenhauer PJ, Salge JR, Schmidt LD. Renewable hydrogen by autothermal steam reforming of volatile carbohydrates. | Catal 2006;244:238–47.
- [19] Luo N, Zhao X, Cao F, Xiao T, Fang D. Thermodynamic study on hydrogen generation from different glycerol reforming processes. Energy Fuels 2007;21: 3505—12.
- [20] Slinn M, Kendall K, Mallon C, Andrews J. Steam reforming of biodiesel by-product to make renewable hydrogen. Bioresour Technol 2008;99: 5851–8.
- [21] Lai WH, Hsiao CA, Lee CH, Chyou YP, Tsai YC. Experimental simulation on the integration of solid oxide fuel cell and micro-turbine generation system. J Power Sources 2007;171:130–9.
- [22] Liu HC, Lee CH, Shiu YH, Lee RY, Yan WM. Performance simulation for an anode-supported SOFC using Star-CD code. J Power Sources 2007;167: 406–12.
- [23] Cheddie DF. Integration of a solid oxide fuel cell into a 10 MW gas turbine power plant. Energy 2010;3:754–69.
- [24] Cordiner S, Feola M, Mulone V, Romanelli F. Analysis of a SOFC energy generation system fuelled with biomass reformate. Appl Therm Eng 2007;27:738–47.
- [25] Piroonlerkgul P, Assabumrungrat S, Laosiripojana N, Adesina AA. Selection of appropriate fuel processor for biogas-fuelled SOFC system. Chem Eng J 2008; 140:341–51.

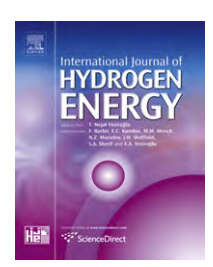
- [26] Douvartzides SL, Coutelieris FA, Tsiakaras PE. On the systematic of ethanol fed SOFC-based electricity generating system in terms of energy and exergy. Power Sources 2004;114:203–12.
- [27] Tsiakaras P, Demin A. Thermodynamic analysis of a solid oxide fuel cell system fuelled by ethanol. I Power Sources 2001;102:210–7.
- [28] Farhad S, Hamdullahpur F, Yoo Y. Performance evaluation of different configurations of biogas-fuelled SOFC micro-CHP systems for residential applications. Int J Hydrogen Energy 2010;35:3758–68.
- [29] Yaws C. Chemical properties handbook. McGraw-HILL; 1998.
- [30] Smith JM, Van Ness HC, Abbott MM. Introduction to chemical engineering thermodynamics. 6th ed. McGraw-HILL; 2005.
- [31] Vasudeva K, Mitra N, Umasankar P, Dhingra SC. Steam reforming of ethanol hydrogen production: Thermodynamic analysis. Int J Hydrogen Energy 1996; 21:13—8
- [32] Achenbach E, Riensche E. Methane/steam reforming kinetics for solid oxide fuel cells. J Power Sources 1994;52:283–8.
- [33] Sobyanin VA, Belyaev VD, Politova TI, Marina OA. Internal steam reforming of methane over Ni-based electrode in solid oxide fuel cells. Appl Catal A: General 1995;133:47—57.
- [34] Aguiar P, Adjiman CS, Brandon NP. Anode-supported intermediatetemperature direct internal reforming solid oxide fuel cell I: model-based steady-state performance. J Power Sources 2004;138:120–36.
- [35] Patcharavorachot Y, Arpornwichanop A, Chuachuensuk A. Electrochemical study of a planar solid oxide fuel cell: Role of support structures. J Power Sources 2008;177:254–61.
- [36] Aguiar P, Adjiman CS, Brandon NP. Anode-supported intermediate-temperature direct internal reforming solid oxide fuel cell II. Model-based dynamic performance and control. J Power Sources 2005;147:136–47.
- [37] Liese EA, Gemmen RS. Performance comparison of internal reforming against external refroming in a solid oxide fuel cell, gas turbine hybrid system. ASME J Eng Gas Turb Power 2005;127:86–90.
- [38] Kanga YW, Li J, Cao GY, Tu HY, Li J, Yang J. A reduced 1D dynamic model of a planar direct internal reforming solid oxide fuel cell for system research. | Power Sources 2009;188:170–6.
- [39] Saebea D, Patcharavorachot Y, Arponwichanop A. Analysis of an ethanol-fuelled solid oxide fuel cell system using partial anode exhaust gas recirculation. J Power Sources 2012;208:120–210.
- [40] Seo YS, Shirley A, Kolaczkowski ST. Evaluation of thermodynamically favourable operating conditions for production of hydrogen in three different reforming technologies. J Power Sources 2002;108:213–25.
- [41] Faungnawakij K, Kikuchi R, Eguchi K. Thermodynamic evaluation of methanol steam reforming for hydrogen production. J Power Sources 2006;161:87–94.



Available online at www.sciencedirect.com

SciVerse ScienceDirect





Analysis of a pressurized solid oxide fuel cell—gas turbine hybrid power system with cathode gas recirculation

Dang Saebea a , Yaneeporn Patcharavorachot b , Suttichai Assabumrungrat a , Amornchai Arpornwichanop a,c,*

- ^a Department of Chemical Engineering, Faculty of Engineering, Chulalongkorn University, Bangkok 10330, Thailand
- ^b School of Chemical Engineering, Faculty of Engineering, King Mongkut's Institute of Technology Ladkrabang, Bangkok 10520, Thailand
- ^c Computational Process Engineering, Chulalongkorn University, Bangkok 10330, Thailand

ARTICLE INFO

Article history:
Received 13 June 2012
Received in revised form
2 November 2012
Accepted 21 January 2013
Available online 28 February 2013

Keywords:
Solid oxide fuel cell
Gas turbine
Ethanol reforming
Hybrid system
Cathode gas recirculation

ABSTRACT

A pressurized solid oxide fuel cell-gas turbine hybrid system (SOFC-GT system) has been received much attention for a distributed power generation due to its high efficiency. When considering an energy management of the system, it is found that a heat input is highly required to preheat air before being fed to the SOFC stack. The recirculation of a hightemperature cathode exhaust gas is probably an interesting option to reduce the requirement of an external heat for the SOFC-GT system. This study aims to analyze the pressurized SOFC-GT hybrid system fed by ethanol with the recycle of a cathode exhaust gas via a simulation study. Effect of important operating parameters on the electrical efficiency and heat management of the system is investigated. The results indicate that an increase in the operating pressure dramatically improves the system electrical efficiency. The suitable pressure is in a range of 4-6 bar, achieving the highest system electrical efficiency and the lowest recuperation energy from the waste heat of the GT exhaust gas. In addition, it is found that the waste heat obtained from the GT is higher than the heat required for the system, leading to a possibility of the SOFC-GT system to be operated at a self-sustainable condition. Under a high pressure operation, the SOFC-GT system requires a high recirculation of the cathode exhaust gas to maintain the system without supplying the external heat; however, the increased recirculation ratio of the cathode exhaust gas reduces the system electrical efficiency.

Copyright © 2013, Hydrogen Energy Publications, LLC. Published by Elsevier Ltd. All rights reserved.

1. Introduction

Decrease in fossil fuels and awareness in environmental issues has stimulated the need to develop power generation technologies that are environmentally friendly and highly efficient to replace a conventional combustion-based power system. A fuel cell is regarded as the promising technology for

power generation which will become increasingly important due to its low emissions, quiet operation, high efficiency and high reliability. Among the various types of fuel cell, solid oxide fuel cell (SOFC) is the most attractive fuel cell technology that can be used in a wide range of commercial applications [1]. SOFC is operated at high temperatures so that the exhaust gas from the SOFC can be used as a heat source for other

^{*} Corresponding author. Department of Chemical Engineering, Faculty of Engineering, Chulalongkorn University, Bangkok 10330, Thailand. Tel.: +66 2 218 6878; fax: +66 2 218 6877.

E-mail address: Amornchai.A@chula.ac.th (A. Arpornwichanop).

heat-requiring units in the SOFC system, resulting in the improvement of the system thermal efficiency. Moreover, SOFC can be integrated with a gas turbine to generate more electricity. At present, the power generation of an SOFC—gas turbine hybrid system (SOFC—GT) has been increasingly received much attention because of its high system efficiency.

A number of researchers have studied and developed the SOFC—GT system running on natural gas with the aim at stationary applications. However, for remote areas where a natural gas pipeline network cannot reach, the use of liquid fuels seems to be suitable, especially for auxiliary power units [2]. In comparison with other liquid fuel feedstocks, ethanol is a very attractive green fuel for use in fuel cells. It has relatively high hydrogen content and is easy to store, handle, and transport in a safe way. Moreover, ethanol can be produced renewably through the fermentation process of agricultural products and thus, a promising alternative fuel for the SOFC—GT system.

In general, an SOFC-GT hybrid system can be run at either atmospheric (non-pressurized system) or high pressure (pressurized system) conditions. In the non-pressurized SOFC-GT hybrid system, a gas turbine operation does not depend directly on the SOFC leading to a simple cycle system. Nevertheless, heat exchangers in the system have to be operated at very high-temperature and pressure differences, thereby requiring a highly effective material [3]. At present, the pressurized SOFC-GT hybrid system has attracted more attention because it can achieve higher system efficiency [4-6]. A number of investigations on the pressurized SOFC-GT system have been carried out in various aspects. Some researchers studied the effect of parameters on the SOFC system performance by performing energy and exergy analyses to determine the optimum parameters for the systems that are operated under full and partial loads [7-10]. In addition, a design of the pressurized SOFC-GT system was proposed in order to improve the system efficiency. Yang et al. [11] considered the effect of operating temperatures on the performance of the pressurized SOFC-GT hybrid system that is designed by supplying the additional air or fuel to a combustor of the gas turbine system. Kuchonthara et al. [12] developed the pressurized SOFC-GT system fuelled by a natural gas. Heat in the exhaust gas of the gas turbine was recuperated and used for steam generation. The generated steam is injected into a GT combustion chamber in order to increase the GT power and the system efficiency. Park et al. [13] analyzed the influence of steam generation by using the gas turbine exhaust gas on the performance of both the nonpressurized and pressurized SOFC-GT hybrid system.

Apart from the electrical efficiency, a heat management of the SOFC system should also be considered [14]. Braun et al. [15] focused on a design of the SOFC system for a residential application taking into account a combined heat and power (CHP). Jia et al. [16] investigated the SOFC power system with cathode gas recycling. The results showed that the efficiency of the SOFC system using a cathode gas recirculation can be improved by a reduction of the energy supplied to the air preheater. The SOFC—GT hybrid system with cathode exhaust gas recycling is an interesting and potential power system that minimizes the system heat requirement and maximizes the system efficiency. However, there are few studies that perform a detailed analysis of such a system. An understanding

of the effect of the cathode gas recirculation on both the SOFC and gas turbine performances would lead to an optimal design of the SOFC—GT system.

The aim of this study is to analyze the performance of a pressurized SOFC—GT hybrid system with and without a cathode gas recirculation. Ethanol is used as a fuel for hydrogen production via a steam reforming process. An energy management of the SOFC—GT system is considered with an aim to achieve the highest electrical generation and thermal energy usage. Effect of the recirculation ratio of cathode exhaust gas on the system efficiency is also investigated.

2. Description of SOFC-GT hybrid system

The schematic diagram of a pressurized SOFC-GT hybrid system is illustrated in Fig. 1(a). The system consists of a pump, evaporator, heat exchanger, fuel processor, SOFC, combustor, gas turbine and compressor. The steam and ethanol are pumped and then vaporized in the evaporator. The mixture of ethanol and steam is preheated to a desired temperature and converted into a synthesis gas in the steam reformer. The synthesis gas is preheated and fed into the SOFC. Hydrogen in the synthesis gas reacts with oxygen in the compressed air to produce electrical power and steam via the electrochemical reaction. In general, SOFC cannot be operated at the full utilization of fuel. As a result, the residue fuel in the SOFC outlet stream is combusted in the combustor and the obtained exhaust gas is then fed into the gas turbine to generate more electricity. Due to its high temperature, the gas turbine outlet can be used as a heat source for other heatrequiring units. The heat management of the SOFC system can reduce the requirement of an external heat. Fig. 1(b) shows the SOFC-GT hybrid system in which a portion of the cathode exhaust gas is recycled to mix with the compressed fresh air via a blower. The retrofitted SOFC-GT hybrid system would minimize the energy requirement of the air pre-heater.

3. Model of SOFC-GT hybrid system

Modeling of the SOFC—GT system is based on the following assumptions: (i) the system is operated at steady state, (ii) heat loss in each unit of the system is negligible, (iii) all gases behave as ideal gases, (iv) the pressure and temperature of each individual unit of the system are constant and (v) the SOFC operating voltage is constant along the cell coordinate.

3.1. Fuel processor

Ethanol is converted into a synthesis gas with high hydrogen content via a steam reforming process. The main reactions of the ethanol steam reforming to produce hydrogen are as follows [17]:

$$C_2H_5OH + H_2O \leftrightarrow 4H_2 + 2CO \tag{1}$$

$$CO + H_2O \leftrightarrow H_2 + CO_2 \tag{2}$$

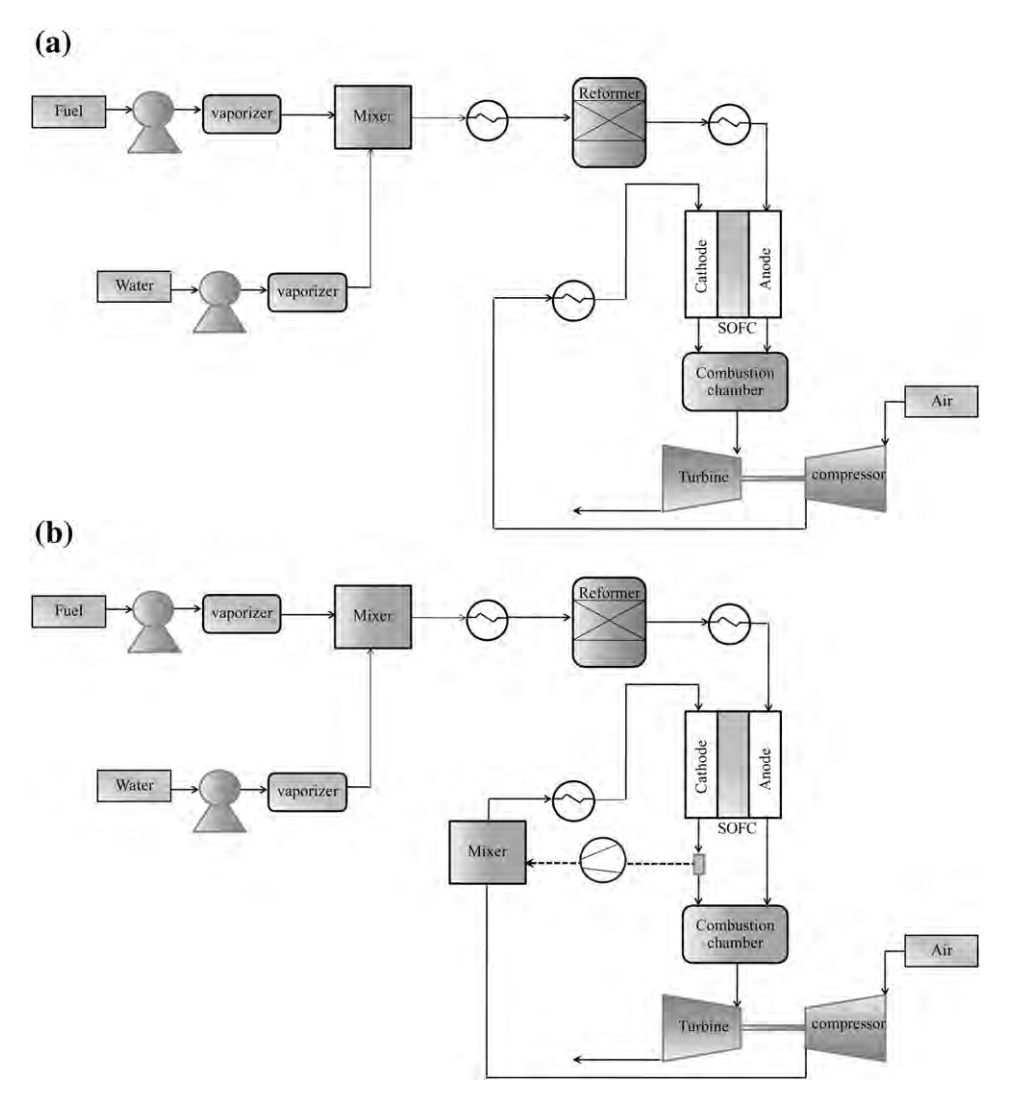


Fig. 1 – Schematic diagram of an ethanol-fuelled SOFC system integrated with gas turbine: (a) a conventional SOFC–GT system and (b) an SOFC–GT system with cathode gas recirculation.

$$CO + 3H_2 \leftrightarrow CH_4 + H_2O \tag{3}$$

The composition of the synthesis gas obtained from the ethanol steam reformer is assumed to be at equilibrium condition. It can be determined based on a thermodynamic analysis using the stoichiometric approach in which the equilibrium constants of all the reactions are computed by the Van't Hoff equation [18]. The heat used to maintain the steam reformer at the constant temperature operation can be calculated from the energy balance around the reformer, given as:

$$Q_{SR,r} = \left(\sum_{o} \dot{n}_{i,r}^{out} \dot{h}_{i,r}^{out}\right) - \left(\sum_{i} \dot{n}_{i,r}^{in} \dot{h}_{i,r}^{in}\right) \tag{4}$$

where $\dot{n}_{i,r}^{in}$ and $\dot{n}_{i,r}^{out}$ are the molar flow rate of species i at the inlet and outlet and $\dot{h}_{i,r}^{in}$ and $\dot{h}_{i,r}^{out}$ are the enthalpy of formation of species i at the inlet and outlet, respectively.

3.2. SOFC model

The synthesis gas obtained from the ethanol steam reformer is fed to the fuel channel of the SOFC and simultaneously, air is fed to the air channel. The SOFC based on oxygen ion conducting electrolyte is considered. Yttria-stabilized zirconia (YSZ), strontium-doped lanthanum manganite (LSM) and nickel/YSZ are used as the electrolyte, cathode and anode, respectively. Hydrogen in the synthesis gas is consumed via the electrochemical reaction to produce electricity; oxygen in air is reduced into oxygen ions at the cathode side, which move through the electrolyte to react with hydrogen to form water and electron at the anode. Since the synthesis gas contains some residual fuels such as methane and carbon monoxide, it can be internally reformed to produce more hydrogen via steam reforming and water shift reactions at the anode. These reactions can be occurred due to the hightemperature operation of SOFC and the presence of SOFC anode catalyst. All the reactions (i.e., electrochemical and reforming reactions) taking place at the anode and cathode sides of the SOFC are summarized in Table 1. The distribution of gas composition within the fuel and air channels along the flow direction can be written as follows [19,20]:

Fuel channel ($i = CH_4$, H_2O , CO, H_2 and CO_2):

$$\frac{dC_{i,f}}{dx} = \frac{1}{u_f} \sum_{j \in \{(i),(ii),(v)\}} \nu_{i,j} R_j \frac{1}{h_f}$$
 (5)

Air channel ($i = O_2$ and N_2):

$$\frac{dC_{i,a}}{dx} = \frac{1}{u_a} \nu_{i,(v)} R_{(v)} \frac{1}{h_a}$$
 (6)

where $C_{i,f}$ and $C_{i,a}$ are the concentrations of species i in the fuel and air channels, h_f and h_a are the height of fuel and air channels and u_f and u_a are the inlet gas velocities of fuel and air, which are defined by Eqs. (7) and (8).

$$u_f = \frac{F_{total,f}^0 RTA_c}{P} \tag{7}$$

$$u_a = \frac{F_{\text{total},a}^0 RTA_c}{P} \tag{8}$$

where $F^0_{total,f}$ and $F^0_{total,a}$ are the total molar flow rates of fuel and air at the inlet of fuel and air channels, T and P are the operating temperature and pressure of SOFC, respectively.

The inlet boundary conditions are defined as:

Fuel channel:

$$C_{i,f}|_{\mathbf{x}=0} = C_{i,f}^{0}$$
 (9)

Air channel:

$$C_{i,a}|_{x=0} = C_{i,a}^0$$
 (10)

where $C_{i,f}^0$ and $C_{i,a}^0$ are the concentrations of species i at the inlet of fuel and air channels. It is noted that the inlet gas concentration at the air channel is determined from that of fresh air mixed with recycled cathode exhaust gas.

The reversible cell voltage or the theoretical open-circuit potentials that occurs from the difference in the thermodynamic potentials of the electrode reactions can be expressed by the Nernst equation:

$$E^{\text{OCV}} = E^{0} - \frac{RT}{2F} \ln \left(\frac{p_{\text{H}_{2}\text{O}}}{p_{\text{H}_{2}} p_{\text{O}_{2}}^{0.5}} \right)$$
 (11)

where *E*⁰ is the open-circuit voltage at the standard pressure, which is a function of the operating temperature, given as:

$$E^{0} = 1.253 - 2.4516 \times 10^{-4} T (K)$$
 (12)

In real fuel cell operation, the actual fuel cell voltage (V) is decreased from its open-circuit voltage due to the internal

voltage losses, that is, ohmic loss (η_{ohmic}), concentration overpotentials (η_{conc}) and activation overpotentials (η_{act}) (Eq. (13)).

$$V = E - \eta_{act} - \eta_{ohmic} - \eta_{conc}$$
 (13)

The activation loss is caused by the sluggishness of the electrochemical reaction at the electrode–electrolyte interfaces and can be computed by solving the non-linear Butler–Volmer equation (Eqs. (14)–(17)). The ohmic loss occurs due to the resistance to the flow of ions in the electrolyte and electrons through the electrode and is given by Eqs. (18) and (19). The concentration loss is caused by a decrease in the substance concentration at the electrode–electrolyte interface due to the resistance to mass transport, as expressed by Eqs. (20)–(25) [21,22].

Activation loss:

$$j = j_{0,anode} \left[\frac{p_{H_2,TPB}}{p_{H_2,f}} exp\left(\frac{\alpha nF}{RT} \eta_{act,anode}\right) - \frac{p_{H_2O,TPB}}{p_{H_2O,f}} exp\left(-\frac{(1-\alpha)nF}{RT} \eta_{act,anode}\right) \right]$$
(14)

$$j = j_{0, cathode} \left[exp \left(\frac{\alpha nF}{RT} \eta_{act, cathode} \right) - exp \left(-\frac{(1-\alpha)nF}{RT} \eta_{act, cathode} \right) \right]$$
(15)

$$j_{0,cathode} = \frac{RT}{nF} k_{cathode} exp\left(-\frac{E_{cathode}}{RT}\right)$$
 (16)

$$j_{0,anode} = \frac{RT}{nF} k_{anode} exp \left(-\frac{E_{anode}}{RT} \right)$$
 (17)

Ohmic loss:

$$\eta_{ohm} = jR_{ohm} \tag{18}$$

$$R_{Ohm} = \frac{\tau_{anode}}{\sigma_{anode}} + \frac{\tau_{electrolyst}}{\sigma_{electrolyst}} + \frac{\tau_{cathode}}{\sigma_{cathode}}$$
(19)

Concentration loss:

$$\eta_{\rm conc} = \eta_{\rm conc,anode} + \eta_{\rm conc,cathode}$$
(20)

$$\eta_{conc,anode} = \frac{RT}{2F} ln \left(\frac{p_{H_2O,TPB}p_{H_2f}}{p_{H_2Of}p_{H_2,TPB}} \right)$$
(21)

$$\eta_{\text{conc,cathode}} = \frac{RT}{4F} \ln \left(\frac{p_{O_2, a}}{p_{O_2, TPB}} \right)$$
 (22)

$$p_{\text{H}_2,\text{TPB}} = p_{\text{H}_2,f} - \frac{RT\tau_{anode}}{2FD_{\text{eff,anode}}} j$$
 (23)

Table 1 $-$ Reactions occurred within the SOFC.				
(i)	Steam reforming reaction	$CH_4 + H_2O \leftrightarrow 3H_2 + CO$	$R_{(I)} = k_{act} p_{CH_4, f} exp\left(\frac{-E_{act}}{RT_f}\right)$	
(ii)	Water gas shift reaction	$CO + H_2O \leftrightarrow H_2 + CO_2$	$R_{(II)} = k_{WGSR} p_{CO,f} \left(1 - \frac{p_{CO_2,f} p_{H_2,f}}{k_{shift} p_{CO,f} p_{H_2O,f}} \right)$	
(iii)	Hydrogen oxidation reaction	$H_2 + O^{2-} \leftrightarrow H_2O + 2e^-$, in the second of the second	
(iv)	Oxygen reduction reaction	$1/2O_2 + 2e^- \leftrightarrow O^{2-}$	i	
(v)	Overall cell reaction	$H_2 + 1/2O_2 \leftrightarrow H_2O$	$R_{(V)} = \frac{J}{2F}$	

$$p_{\rm H_2O,TPB} = p_{\rm H_2O,f} + \frac{RT\tau_{anode}}{2FD_{eff,anode}} j$$
(24)

$$p_{O_{2,TPB}} = P - \left(P - p_{O_{2,a}}\right) \exp\left(\frac{RT\tau_{cathode}}{4FD_{eff,cathode}}\vec{p}\right)$$
(25)

Since the operating cell voltage (V) is pre-specified, the average current density (j_{ave}) can be calculated from a distribution of the current density along the cell length (Eq. (26)), which is obtained from the solution of the fuel cell model mentioned above. The fuel and air compositions vary along the fuel cell channel under a real operation due to fuel and oxygen utilizations by the electrochemical reaction. The overall fuel utilization (U_f) and the electrical power output (P_{sofc}) are defined by Eqs. (27) and (28), respectively.

$$j_{avg} = \frac{1}{L} \int_{1}^{0} j(z) dz$$
 (26)

$$U_{f} = \frac{j_{avg}LW}{2F\left(4\dot{n}_{CH_{4}}^{in} + \dot{n}_{H_{2}}^{in} + \dot{n}_{CO}^{in}\right)} \tag{27}$$

$$P_{sofc,dc} = j_{avg} \times A_c \times V \tag{28}$$

As the SOFC generates a direct current (DC), an electrical inverter is used to convert the DC to the alternating current (AC). The dc—ac inverter efficiency is specified at 94% [7] and thus, the AC power output of the SOFC is as follows:

$$P_{\text{sofc,ac}} = P_{\text{sofc,dc}} \times \eta_{\text{invert}} \tag{29}$$

Because the SOFC is operated under isothermal condition and no heat loss is assumed, heat generation from SOFC is removed by using an excess air, so that the operating SOFC temperature is maintained at a desired value. An amount of the excess air can be calculated from an energy balance around the fuel cell, given as:

$$\left(\sum_{i} \dot{n}_{i,an}^{in} \dot{h}_{i,an}^{in}\right) + \left(\sum_{i} \dot{n}_{i,ca}^{in} \dot{h}_{i,ca}^{in}\right) - \left(\sum_{o} \dot{n}_{i,an}^{out} \dot{h}_{i,an}^{out}\right) - \left(\sum_{o} \dot{n}_{i,an}^{out} \dot{h}_{i,an}^{out}\right) - \left(\sum_{o} \dot{n}_{i,ca}^{out} \dot{h}_{i,ca}^{out}\right) - P_{sofc} = 0$$
(30)

It is noted that as heat of formation is used to determine inlet and outlet enthalpies, the heats of reforming and water gas shift reactions are implicitly included in the energy balance. In this study, the difference in the temperature of the SOFC inlet and outlet streams is limited by 100 °C to avoid a fuel cell degradation problem [23,24].

3.3. Gas turbine and compressor

The exhaust gas from the SOFC stack is fed to the gas turbine in order to generate more power. The power produced by the gas turbine and the power consumed by the air compressor can be computed from the energy balances around the gas turbine and the compressor as follows:

$$P_{t} = \sum_{i} \left(\dot{n}_{i,t}^{in} \dot{h}_{i,t}^{in} \right) - \sum_{i} \left(\dot{n}_{i,t}^{out} \dot{h}_{i,t}^{out} \right) \tag{31}$$

$$P_{c} = \sum_{i} \left(\dot{n}_{i,c}^{in} \dot{h}_{i,c}^{in} \right)_{out} - \sum_{i} \left(\dot{n}_{i,c}^{in} \dot{h}_{i,c}^{in} \right)_{in}$$
 (32)

The net electric power output of the gas turbine section can be expressed as:

$$P_{qt} = (P_t - P_c)\eta_m \eta_a \tag{33}$$

where P_t is the power obtained from the gas turbine, P_c is the power consumed by the compressor and η_m and η_g are the mechanical and generator efficiencies, respectively.

The temperature of the gas turbine and compressor outlet gases can be determined based on the isentropic efficiency (Eqs. (34) and (35)) [7,25].

$$T_t^{\text{out}} = T_t^{\text{in}} \left(1 - \eta_t \left(1 - \left(\frac{p_t^{\text{out}}}{p_t^{\text{in}}} \right)^{\frac{\gamma - 1}{\gamma}} \right) \right) \tag{34}$$

$$T_c^{\text{out}} = T_c^{\text{in}} \left(1 + \frac{1}{\eta_c} \left(\left(\frac{p_c^{\text{out}}}{p_c^{\text{in}}} \right)^{\frac{\gamma - 1}{\gamma}} - 1 \right) \right)$$
 (35)

where γ is the ratio of the specific heat capacities at the constant pressure and volume.

3.4. Other units

3.4.1. Pump

Pump is used to increase the mechanical energy of ethanol and water before being fed to the mixer. The power consumption is estimated based on the Bernoulli equation as follows:

$$W_{i,pum} = \frac{\left(p_{i,pum}^{out} - p_{i,pum}^{in}\right) \times \dot{n}_{i,pum}^{in}}{n_{r}\rho_{i}}$$
(36)

where $p_{i,pum}^{in}$ and $p_{i,pum}^{out}$ are the inlet and desired outlet pressure, $\dot{\eta}_{i,pum}^{in}$ is the inlet molar flow rate of the substance i flowing through the pump and η_p is the pump efficiency, which is specified at 75% in this study [26].

3.4.2. Vaporizer

Ethanol and water are changed from the liquid to the gas phase in the vaporizer. The required heat for the operation of the vaporizer can be expressed as:

$$Q_{C_2H_SOH,vap} = \left(\dot{n}_{C_2H_SOH,vap}^{out}\dot{h}_{C_2H_SOH,vap}^{out}\right) - \left(\dot{n}_{C_2H_SOH,lia}^{in}\dot{h}_{C_2H_SOH,lia}^{in}\right) \quad (37)$$

$$Q_{H_{2O,vap}} = \left(\dot{n}_{H_{2O,vap}}^{out} \dot{h}_{H_{2O,vap}}^{out} \dot{h}_{H_{2O,vap}}^{out} \right) - \left(\dot{n}_{H_{2O,liq}}^{in} \dot{h}_{liq}^{H_{2O}} \right) \tag{38}$$

3.4.3. Pre-heaters

The SOFC system has three pre-heaters that are used to preheat the feed streams of a mixture of ethanol and steam and air. The energy required for running the pre-heaters can be computed by the following equation:

$$Q_{ph} = \sum_{o} (\dot{n}_{i,ph}^{out} \dot{h}_{i,ph}^{out}) - \sum_{i} (\dot{n}_{i,ph}^{in} \dot{h}_{i,ph}^{in})$$
 (39)

3.4.4. Mixer

For the SOFC—GT hybrid system with cathode gas recycling, a portion of the cathode gas stream is recirculated to mix with the fresh air in the mixer. The mixer outlet flow rate can be calculated from the mass balance equation (Eq. (40)), whereas

(42)

the outlet temperature of the mixer is determined by solving the energy balance equation (Eq. (41)).

$$\dot{n}_{i,mix}^{out} = \dot{n}_{i,mix1}^{in} + \dot{n}_{i,mix2}^{in}$$
 (40)

$$\left(\sum_{i}\dot{n}_{i,\text{mix1}}^{in}\dot{h}_{i,\text{mix2}}^{in}\right) + \left(\sum_{i}\dot{n}_{i,\text{mix2}}^{in}\dot{h}_{i,\text{mix2}}^{in}\right) - \left(\sum_{o}\dot{n}_{i,\text{mix}}^{out}\dot{h}_{i,\text{mix}}^{out}\right) = 0 \tag{41}$$

3.4.5. Combustor

 $H_2 + 0.5O_2 \rightarrow H_2O$

The residual gas from the anode outlet and the unused oxidant gas from the cathode outlet are mixed and burnt in the combustor. The combustion reactions occurred are as follows:

$$CO + 0.5O_2 \rightarrow CO_2 \tag{43}$$

The efficiency of the combustion process is set at 98% [7]. The composition of the combustor outlet gas can be computed based on the mass balance equations, given as:

$$n_{H_2,cb}^{out} = n_{H_2,an}^{out} - \dot{k}_{1,cb}$$
 (44)

$$n_{\text{CO},cb}^{\text{out}} = n_{\text{CO},an}^{\text{out}} - \dot{k}_{2,cb} \tag{45}$$

$$n_{\text{CH}_4,\text{cb}}^{\text{out}} = n_{\text{CH}_4,an}^{\text{out}} \tag{46}$$

$$n_{\text{CO}_2,cb}^{\text{out}} = n_{\text{CO}_2,an}^{\text{out}} + \dot{k}_{\text{2,cb}}$$

$$\tag{47}$$

$$n_{H_2O,cb}^{out} = n_{H_2O,an}^{out} + \dot{k}_{1,cb}$$
 (48)

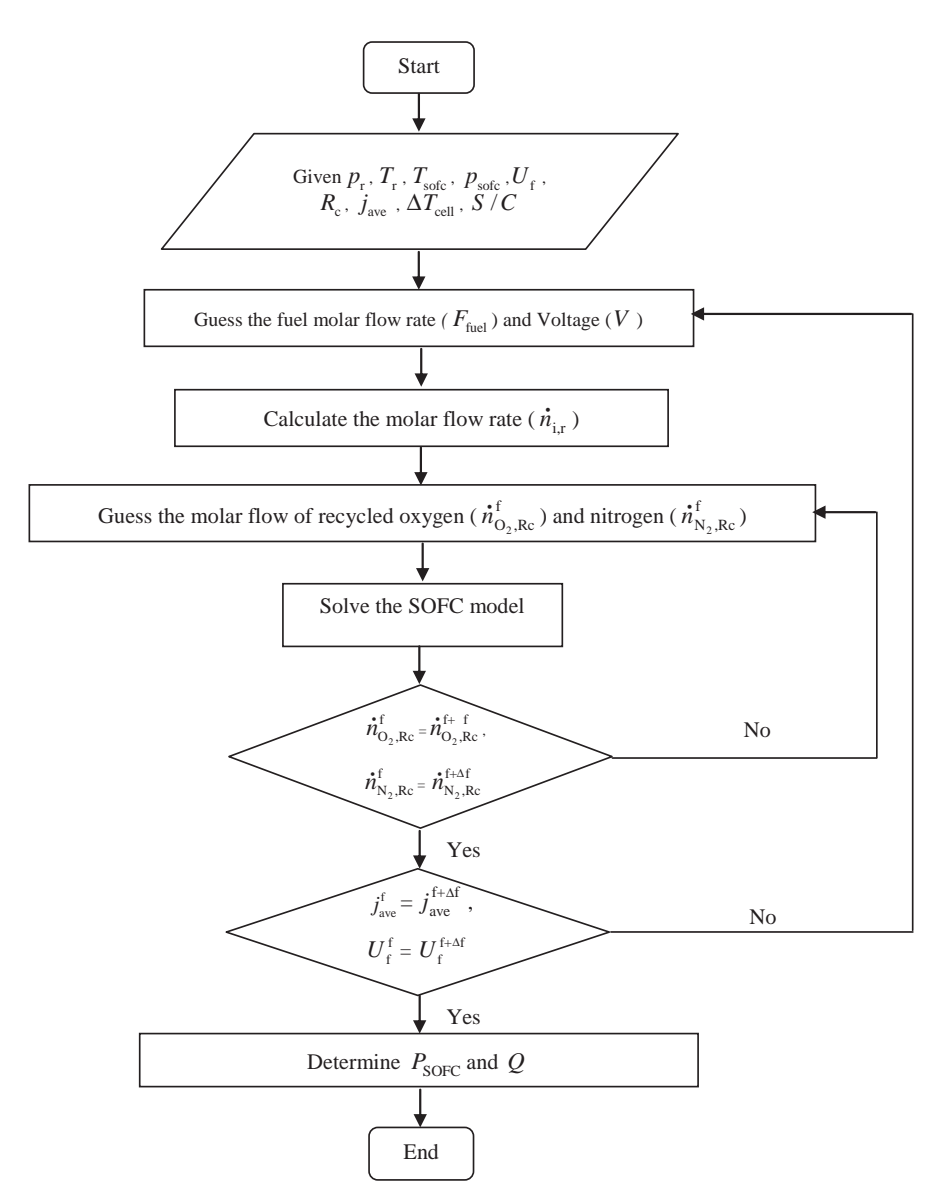


Fig. 2 - A solution algorithm of the SOFC model with a cathode exhaust gas recirculation.

Table 2 $-$ Values of structural and material property parameters for the SOFC.	
Cell length, L (m)	0.4
Cell width, W (m)	0.1
Fuel channel height, h_f (mm)	1
Air channel height, h_a (mm)	1
Anode thickness, $ au_{anode}$ (μ m)	500
Cathode thickness, $ au_{cathode}$ (μ m)	50
Electrolyte thickness, $\tau_{electrolyte}$ (μ m)	20
Pre-exponential factor of anode exchange current density, γ_a (A m $^{-2}$)	6.54×10^{11}
Pre-exponential factor of cathode exchange current density, $\gamma_{\rm c}$ (A m $^{-2}$)	2.35×10^{11}
Activation energy of anode exchange current density, E_{anode} (kJ mol $^{-1}$)	140
Activation energy of cathode exchange current density, $E_{cathode}$ (kJ mol $^{-1}$)	137
Anode diffusion coefficient, $D_{eff,anode}$ (m ² s ⁻¹)	3.66×10^{-5}
Cathode diffusion coefficient, $D_{eff,cathode}$ (m ² s ⁻¹)	1.37×10^{-5}
Anode electrical conductivity, σ_{anode} (Ω^{-1} m $^{-1}$)	$\frac{4.2\times10^7}{T} exp\left(\frac{-1200}{T}\right)$
Cathode electrical conductivity, $\sigma_{cathode}$ (Ω^{-1} m $^{-1}$)	$\frac{9.5\times10^7}{T} exp\left(\frac{-1150}{T}\right)$
Electrolyte ionic conductivity, $\sigma_{electrolyte}$ (Ω^{-1} m ⁻¹)	$33.4\times10^3\exp\left(\frac{-10,300}{T}\right)$

$$n_{O_2,cb}^{out} = n_{O_2,ca}^{out} - 0.5\dot{k}_{1,cb} - 0.5\dot{k}_{2,cb}$$
(49)

$$n_{N_0,ch}^{out} = n_{N_0,ca}^{out} \tag{50}$$

where $\dot{k}_{1,cb}$ and $\dot{k}_{2,cb}$ are the extent of the hydrogen and carbon monoxide combustion reactions, respectively.

The exit temperature of the combustor outlet gas can be calculated from the energy balance as follows:

$$\left(\sum_{i}\dot{n}_{i,an}^{in}\dot{h}_{i,an}^{in}\right) + \left(\sum_{i}\dot{n}_{i,rca}^{in}\dot{h}_{i,rca}^{in}\right) - \left(\sum_{o}\dot{n}_{i,cb}^{out}\dot{h}_{i,cb}^{out}\right) = 0 \tag{51}$$

The pressurized SOFC—GT system is analyzed based on the SOFC system model mentioned above, which consists of a system of differential and algebraic equations. The model equations are implemented and solved by Matlab. To evaluate

Table 3 — Values of operating conditions used for simulation of the SOFC—GT system under nominal conditions.

Pre-reformer unit	
Operating temperature (K)	973
Steam to ethanol ratio	3
Solid oxide fuel cell unit	
Operating temperature (K)	1073
Average current density (A/cm²)	0.4
Air composition	21% O ₂ , 79% N ₂
Fuel utilization	0.7
SOFC pressure loss (%)	2
dc-ac inverter efficiency (%)	94
Combustor pressure loss (%)	3
Combustor efficiency (%)	98
Gas turbine	
Turbine isentropic efficiency (%)	82
Compressor isentropic efficiency (%)	78
Generator mechanical efficiency (%)	94
Pump efficiency (%)	80
Blower efficiency (%)	70

the SOFC system performance, the SOFC electrical efficiency and the net electrical efficiency of the system are defined as:

SOFC electrical efficiency =
$$\frac{P_{sofc,ac}}{\dot{n}_{C_{2}H_{c}OH}^{in}LHV_{C_{2}H_{5}OH}}$$
 (52)

$$System \ electrical \ efficiency = \frac{P_{SOFC,ac} + P_{GT} - P_{H_2O,pump} - P_{C_2H_5OH,pump}}{\dot{n}_{C_2H_5OH}^{in} LHV_{C_2H_5OH}}$$
 (53)

For the SOFC–GT system with cathode exhaust gas recycling, the numerical solution of the SOFC system model is quite complicated due to the interaction among the units in the SOFC system. A solution algorithm of the SOFC model with cathode exhaust gas recirculation is shown in Fig. 2. This study employs the iterative procedure in which the gas compositions of the cathode exhaust gas assumed to be unknown variables and the SOFC system model is solved until the assumed variables are recalculated. This procedure is iterative until the difference in the values of the assumed and calculated variables satisfies a desired accuracy (10^{-4}). Tables 2 and 3 show the values of material properties, cell geometry and operating conditions used for simulation of the SOFC system under nominal conditions.

4. Results and discussion

4.1. A pressurized SOFC-GT system

Firstly, the performance of a pressurized SOFC—GT hybrid system is analyzed. Fig. 3(a) shows the effect of the operating pressure on the electrical efficiency of the SOFC—GT system, whereas its effect on the SOFC electrical efficiency and the power ratio of gas turbine to SOFC (PGT/PSOFC) is given in Fig. 3(b). It can be seen that the system efficiency is considerably improved when increasing the operating pressure from 2 to 4 bar. This is because the SOFC and GT can generate more electrical power; the PGT/PSOFC ratio increases with increasing

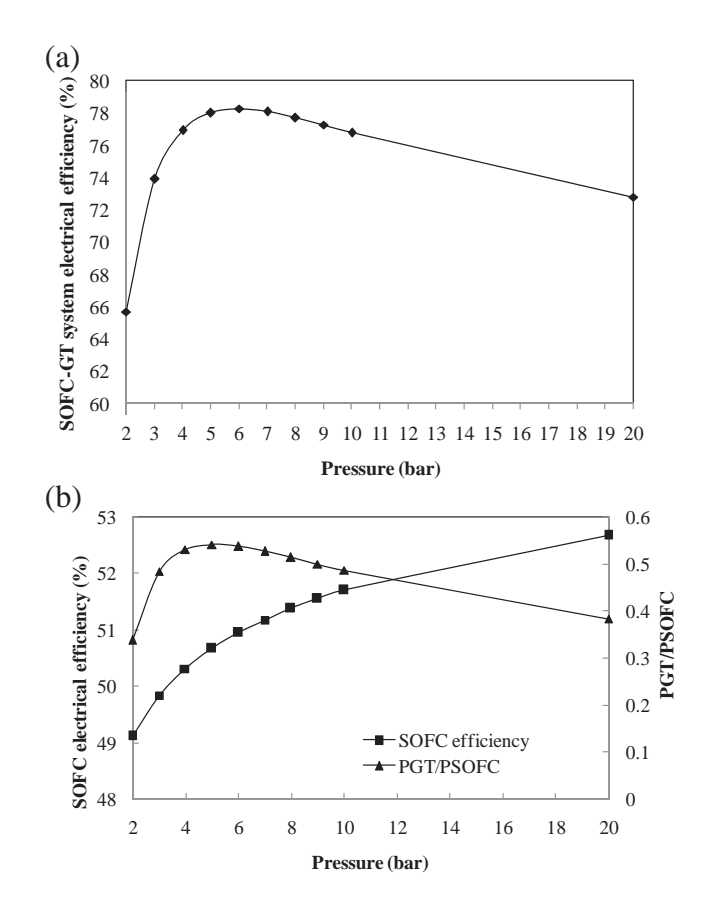


Fig. 3 – Effect of operating pressure on the conventional SOFC—GT hybrid system: (a) system electrical efficiency and (b) SOFC electrical efficiency and power ratio of GT to SOFC.

the operating pressure (Fig. 3(b)). The increased pressure increases the partial pressure of H₂ in the fuel channel and O₂ in the air channel. In addition, the transport of gases to the electrolyte-electrode interfaces is improved, thereby reducing the concentration losses. These factors lead to the improvement of fuel cell performance. However, it is found that the system efficiency decreases when the operating pressure is higher than 6 bar. This is caused by that the compressor consumes more power at the high pressure operation, while the power produced by the GT slightly increases. As a result, the pressurized SOFC-GT hybrid system should not be operated at a higher pressure. Moreover, the high pressure operation of the SOFC system causes a faster fuel cell degradation and higher capital cost. From Fig. 3(a), the SOFC-GT system gives the maximum electrical efficiency of 78.27% when operated at the pressure of 6 bar. The SOFC generates the power output at 60-75% of the overall power produced by the SOFC-GT system.

When considering the GT operation, although the temperature of the GT outlet gas decrease, it is still high enough and is considered a useful heat source for supplying to other heat-requiring units within the SOFC system. Fig. 4(a) shows the effect of the operating pressure of the SOFC system on the thermal energy of the GT outlet gas, which is calculated based on the reference temperature of 100 $^{\circ}$ C. It is found that the thermal

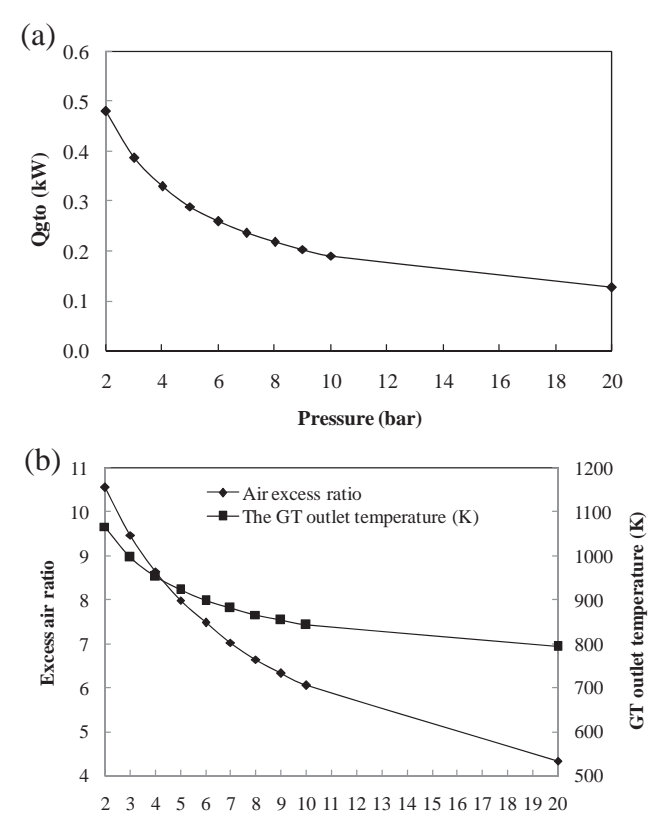


Fig. 4 – Effect of operating pressure on (a) thermal energy of the GT outlet gas (Qgto) and (b) excess air ratio and GT outlet temperature (the conventional SOFC–GT hybrid system).

Pressure (bar)

energy of the GT outlet gas reduces when the SOFC system is operated at a higher pressure. This thermal energy depends on the inlet gas flow to the GT, the GT inlet temperature and the operating pressure of the GT. Fig. 4(b) shows the relation of the operating pressure to the GT outlet temperature and the excess air ratio. The results indicate that the temperature of the GT

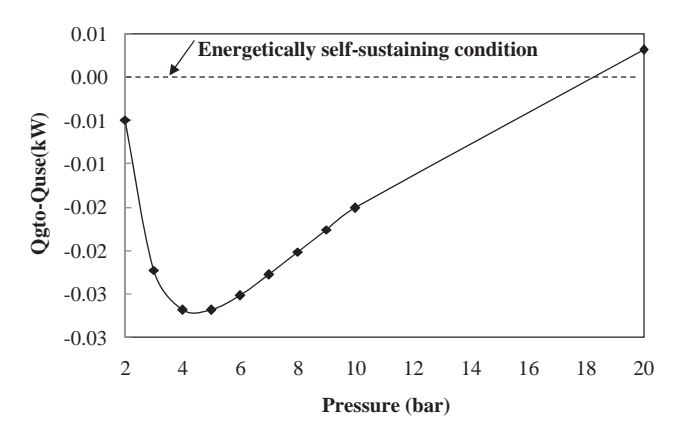


Fig. 5 – Effect of operating pressure on the remaining energy of the GT exhaust gas (the conventional SOFC–GT hybrid system).

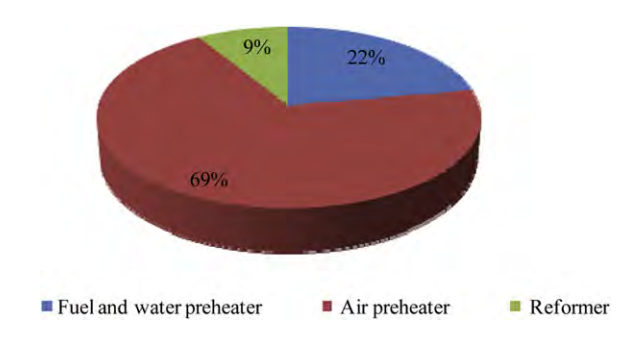


Fig. 6 – Distribution of heat used in the conventional SOFC-GT hybrid system (P = 6 bar).

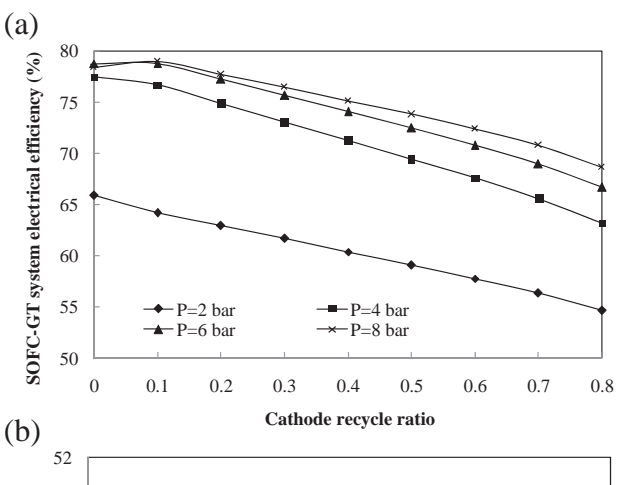
outlet decreases with increasing the operating pressure. Furthermore, the excess air needed for supplying to the SOFC is lower when the SOFC system is run at a higher pressure, leading to a decrease in the flow rate of gas fed into the GT.

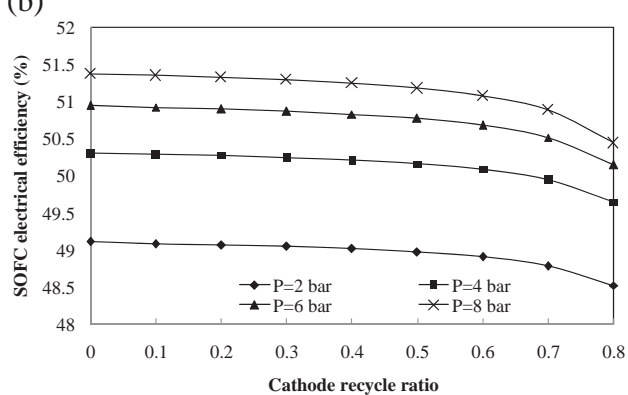
Regarding the energy management of the SOFC-GT hybrid system, the thermal energy in the turbine exhaust gas is generally utilized for pre-heating air fed to the SOFC. However, this study focuses on the use of this remaining thermal energy for supplying to all other heat-requiring units in order to reduce the requirement of the external heat. Fig. 5 shows the impact of the operating pressure on the residual energy calculated from the thermal energy of the GT exhaust gas subtracted by the system heat requirement. The negative value of the residual energy indicates that the thermal energy from the GT outlet gas is insufficient to supply the SOFC system and thus the external heat is needed. It is found that an increase in the operating pressure reduces the external heat requirement because the ethanol steam reformer needs less energy. It is noted that when operated at the pressure of 20 bar, the SOFC-GT system can be operated at a self-sustainable condition where the external heat is unnecessary; however, at high pressure operation, a low system electrical efficiency is obtained.

Fig. 6 shows the energy requirement in each part of the pressurized SOFC—GT hybrid system. It can be divided into three parts, namely the energy used for pre-heating air, pre-heating fuel and water and ethanol steam reformer. The air pre-heating unit consumes the highest energy; it takes about 65—74% of the overall energy consumption of the SOFC—GT system. Therefore, if the energy used for the air pre-heater operation can be reduced, the requirement of the external heat for supplying to the SOFC system would be minimized and the energy management of the system would be probably better.

4.2. A pressurized SOFC/GT system with cathode gas recirculation

In the previous section, it was found that most thermal energy consumption in the SOFC system is caused by the air preheater. To improve the system performance, a portion of the cathode exhaust gas is recycled and then mixed with a fresh air feed to reduce a heat duty of the air pre-heater. Regarding the system electrical efficiency, the pressurized SOFC—GT hybrid system is studied under a pressure range of 2—8 bar. The influence of a recirculation ratio of the cathode exhaust





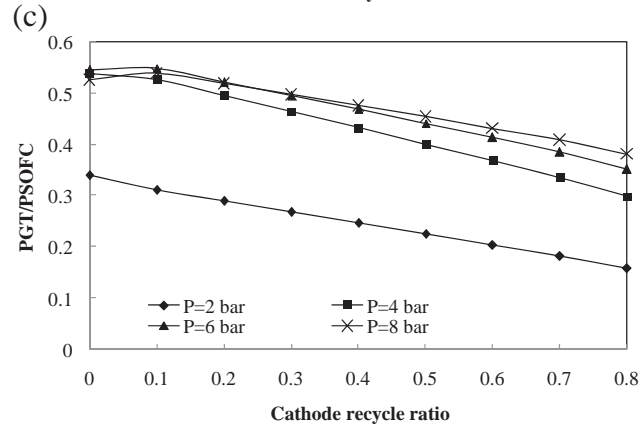
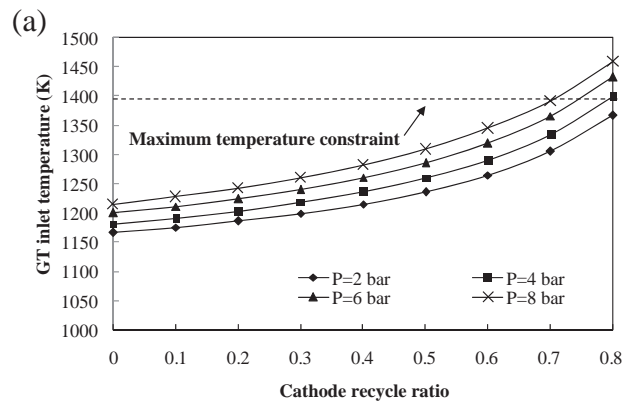


Fig. 7 — Effect of recirculation ratio of cathode gas on the SOFC—GT hybrid system with cathode gas recirculation at different operating pressure: (a) system electrical efficiency, (b) SOFC electrical efficiency and (c) power ratio of GT to SOFC.

gas at different operating pressures on the system electrical efficiency, SOFC electrical efficiency and the PGT/PSOFC ratio is illustrated in Fig. 7(a-c), respectively. The system electrical efficiency decreases with increasing the recirculation ratio of the cathode exhaust gas at all the operating pressure considered, and the SOFC efficiency and the PGT/PSOFC ratio show similar trends. The results also indicate that the recirculation ratio has impact on the performance of the GT more than the SOFC. The electrical efficiency of the SOFC slightly declines with increasing the recirculation ratio of the cathode exhaust gas (0.1-0.7); however, the decrement of the SOFC efficiency is



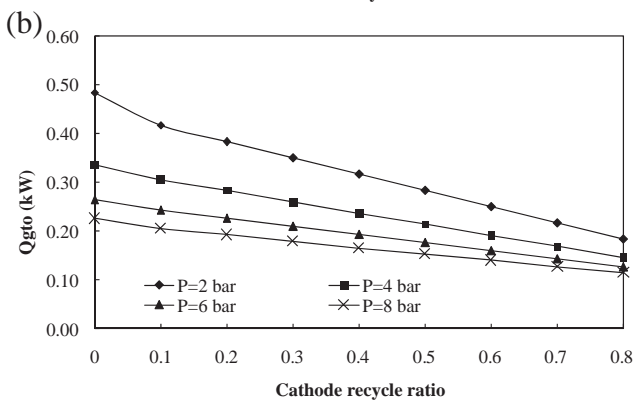


Fig. 8 – Effect of recirculation ratio of cathode gas on (a) the GT inlet temperature and (b) the thermal energy of the GT outlet gas (the SOFC–GT hybrid system with cathode gas recirculation).

obviously observed at the recirculation ratio of higher than 0.7. This is because the oxygen feed is diluted when increasing the recirculation ratio and consequently, a larger concentration loss in the SOFC appears. An increase in the cathode gas recycle also decreases the PGT/PSOFC ratio as the gas inlet flow to the GT drop and thus the GT power is less generated.

Fig. 8 shows the variations in the GT inlet temperature and the thermal energy of the GT outlet gas as a function of the recirculation ratio of the cathode gases at different operating pressures. An increase in the cathode gas recycle results in the elevated temperature of the GT inlet because the air stream fed to the combustor decreases while the fuel in the anode exhaust gas is still constant. It is noted that the fuel utilization of the SOFC is kept constant at 70% in all case studies. Although the increased temperature of the GT inlet enhances the performance of the GT, the GT inlet temperature should not exceed the endurance limit of GT materials. In general, the maximum GT inlet temperature is 1400 K [27]. Taking this constraint into consideration, the cathode recirculation ratio should not be higher than 0.7-0.8, depending on the operating pressure (Fig. 8(a)). When considering the thermal energy of the GT exhaust gas (Fig. 8(b)), it decreases with the increased recirculation ratio because a decrease in the GT inlet feed flow has more effect on the thermal energy of the GT outlet gas than an increase in the GT inlet temperature.

Fig. 9 shows the effect of the cathode gas recirculation on the residual thermal energy of the SOFC—GT system. When

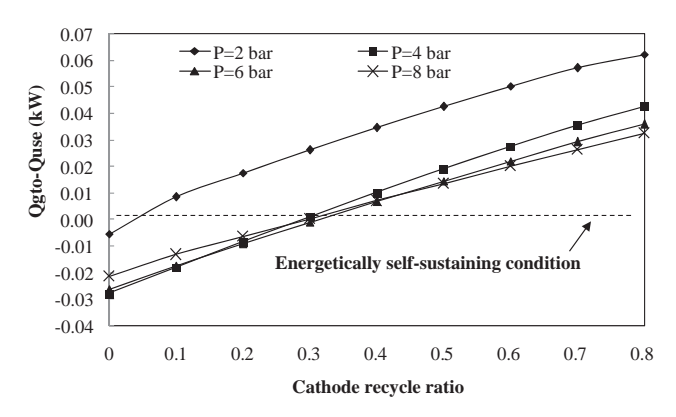


Fig. 9 – Effect of recirculation ratio of cathode-off gas on the residual energy from the outlet GT energy (the SOFC-GT hybrid system with cathode gas recirculation).

the system is operated at a higher recirculation of the cathode gas, it is found that the SOFC system generates the thermal energy higher than its consumption. This result indicates a possibility of the SOFC-GT system with cathode gas recirculation to be operated at the self-sustainable condition. At high recirculation ratio of the cathode exhaust gas, the requirement of the fresh air fed to the SOFC reduces, resulting in the decreased heat duty of the air pre-heater. Because the recirculation of the cathode gas has a positive effect on the thermal management of the pressurized SOFC-GT hybrid system but decreases the system electrical efficiency. Therefore, the recirculation ratio of the cathode exhaust gas should be carefully selected. In this study, it is found that the pressurized SOFC-GT hybrid system should be operated at pressure of 6 bar because the highest electrical efficiency can be achieved and the cathode gas recirculation ratio of 0.3 is selected. At this condition, the SOFC system can be selfsustainable and the system electrical efficiency slightly decreases (3%).

5. Conclusions

A pressurized solid oxide fuel cell and gas turbine hybrid system (SOFC-GT) fed by ethanol is studied. The performance of the SOFC system in terms of the electrical efficiency and thermal management is analyzed with respect to the operating pressure and recycle ratio of a cathode exhaust gas. The simulation results show that the optimal operating pressure of the pressurized SOFC system is in a range of 4-6 bar. Under this condition, the system can achieve the highest electrical efficiency, whereas the recuperation of the waste heat from the GT exhaust gas is minimized. The recirculation of the cathode exhaust gas in the SOFC system can reduce the external heat requirement of an air preheater. However, the electrical efficiency of the SOFC system with cathode gas recycling is lower than the conventional SOFC system. In addition, it is found that the SOFC system with cathode gas recycling can be operated at a selfsustainable condition.

 η_q

Acknowledgements

Support from the Thailand Research Fund and the Special Task Force for Activating Research (STAR), Chulalongkorn University Centenary Academic Development Project is gratefully acknowledged.

Nomenclature

 A_c cell active area, m² molar concentration of component i, mol m⁻³ C_i $D_{eff,anode}$ effective gaseous diffusivity through the anode, D_{eff,cathode} effective oxygen diffusivity through the cathode, $m^2 \, s^{-1}$ E_{OCV} open-circuit voltage, V EO open-circuit voltage at the standard pressure, V activation energy for reforming reaction, kJ mol-1 E_{act} activation energies of the anode, kJ mol-1 Eanode activation energies of the cathode, kJ mol⁻¹ Ecathode F Faraday constant, C mol⁻¹ h enthalpy, kJ mol⁻¹ h_a air channel height, m fuel channel height, m h_f current density, A m⁻² exchange current density at the anode, A m⁻² jo,anode exchange current density at the cathode, A m⁻² Jo.cathode pre-exponential constant for reforming reaction, k_{act} ${
m mol}\ {
m s}^{-1}\ {
m m}^{-2}\ {
m bar}^{-1}$ k_{anode} pre-exponential factor of the anode, A m⁻² $k_{cathode}$ pre-exponential factor of the cathode, A m⁻² k_{WGSR} pre-exponential constant for reforming reaction, -L cell length, m $LHV_{C_2H_5OH}$ low heating value of ethanol, mol s^{-1} number of electrons transferred n 'n molar flow rate, mol s^{-1} partial pressures of the component i, bar p_i P electrical power, W thermal energy, kJ s⁻¹ Q amount of thermal energy from the SOFC system, Q_{rec} $kJ s^{-1}$ total amount of thermal energy used in system, Quse $kJ s^{-1}$ Gas constant, $kJ \text{ mol}^{-1} K^{-1}$ R rate of reaction j, mol m⁻²s⁻¹ R_i R_{ohm} total internal resistance, Ω^{-1} m² T temperature, K u_{α} air velocity, m s⁻¹ fuel velocity, m s⁻¹ u_f V operating cell voltage, V W cell width, m U_f fuel utilization factor, -

Greek symbols

lpha transfer coefficient, — γ pre-exponential factor η_{act} activation overpotentials, V concentration overpotentials, V

mechanical efficiency, % η_m ohmic loss, V η_{ohmic} pump efficiency, % η_p dc-ac inverter efficiency, % η_{invert} excess air ratio, - λ_{air} stoichiometric coefficient of component i, - ν_i density of component i, kg m⁻³ ρ_i electronic conductivity of the anode, Ω^{-1} m⁻¹ σ_{anode} electronic conductivity of cathode, Ω^{-1} m⁻¹ ionic conductivity of the electrolyte, Ω^{-1} m⁻¹ $\sigma_{\rm electrolyte}$ thickness of anode, m τ_{anode} thickness of cathode, m $\tau_{cathode}$ thickness of electrolyte, m $\tau_{electrolyte}$ Superscript in inlet out outlet Subscripts air channel а anode side an average avg alternating current ас compressor cathode side ca combustor cb concentration overpotentials conc dc direct current electrochemical reaction elec fuel channel gt gas turbine chemical component i reaction lia liauid mix mixer ohm ohmic loss ph pre-heater pum pump reformer sofc solid oxide fuel cell SR steam reforming reaction turbine three-phase boundary TPB vaporizer vap

generator efficiency, %

REFERENCES

WGS

- [1] Zhu X, Sun K, Le S, Zhang N, Fu Q, Chen X, et al. Electrochim Acta 2008;54:862-7.
- [2] Santin M, Traverso A, Magistri L. Appl Energy 2009;86: 2204–12.

water gas shift reaction

- [3] Burbank W, Witmer DD, Holcomb F. J Power Sources 2009; 193:656–64.
- [4] Park SK, Oh KS, Kim TS. J Power Sources 2007;170:130-9.
- [5] Zhou L, Cheng M, Yi B, Dong Y, Cong Y, Yang W. Electrochim Acta 2008;53:5195–8.
- [6] Henkea M, Willicha C, Westnera C, Leuchta F, Leibingera R, Kalloa J, et al. Electrochim Acta 2012;66:158–63.

- [7] Akkaya AV, Sahin B, Erdem HH. Int J Hydrogen Energy 2008; 33:2566-77.
- [8] Calise F, Palombo A, Vanoli L. J Power Sources 2006;158: 225–44.
- [9] Haseli Y, Dincer I, Naterer GF. Theor Chim Acta 2008;480:1-9.
- [10] Motahar S, Alemrajabi AA. Int J Hydrogen Energy 2009;34: 2396–407.
- [11] Yang WJ, Park SK, Kim TS, Kim JH, Sohn JL, Ro ST. J Power Sources 2006;160:462–73.
- [12] Kuchonthara P, Bhattacharya S, Tsutsumi A. J Power Sources 2003;117:7–13.
- [13] Park SK, Kim TS, Sohn JL. J Mech Sci Technol 2009;23:550-8.
- [14] Lisbona P, Corradetti A, Bove R, Lunghi P. Electrochim Acta 2007;53:1920–30.
- [15] Braun RJ, Klein SA, Reindl DT. J Power Sources 2006;158: 1290–305.
- [16] Jia J, Li Q, Luo M, Wei L, Abudul A. Energy 2011;36:1068-75.
- [17] Freni S, Maggio G, Cavallaro S. J Power Sources 1996;62: 67–73

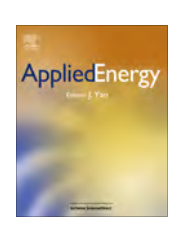
- [18] Saebea D, Patcharavorachot Y, Arpornwichanop A. J Power Sources 2012;208:120–30.
- [19] Arpornwichanop A, Chalermpanchai N, Patcharavorachot Y, Assabumrungrat S, Tade M. Int J Hydrogen Energy 2009;34: 7780–8
- [20] Patcharavorachot Y, Paengjuntuek W, Assabumrungrat S, Arpornwichanop A. Int J Hydrogen Energy 2010;35:4301–10.
- [21] Suwanwarangkul R, Croiset E, Flower MW, Douglas PL, Entchev E, Douglas MA. J Power Sources 2003;122:9–18.
- [22] Pramuanjaroenkij A, Kakac S, Zhou XY. Int J Hydrogen Energy 2008;33:2547–65.
- [23] Aguiar P, Adjiman CS, Brandon NP. J Power Sources 2005;147: 136–47
- [24] Liese EA, Gemmen RS. ASME 2005;127:86-90.
- [25] Wu XJ, Huang Q, Zhu XJ. Int J Hydrogen Energy 2011;36: 885–92.
- [26] Calise F, Accadia MD, Palombo A, Vonolim L. Energy 2006;31: 3278–99.
- [27] Cheddie DF. Energy 2010;3:754-69.

ELSEVIER

Contents lists available at SciVerse ScienceDirect

Applied Energy

journal homepage: www.elsevier.com/locate/apenergy



Comparison of high-temperature and low-temperature polymer electrolyte membrane fuel cell systems with glycerol reforming process for stationary applications



Suthida Authayanun^a, Mohamed Mamlouk^b, Keith Scott^b, Amornchai Arpornwichanop^{a,c,*}

- ^a Department of Chemical Engineering, Faculty of Engineering, Chulalongkorn University, Bangkok 10330, Thailand
- ^b School of Chemical Engineering and Advanced Materials (CEAM), Newcastle University, Newcastle upon Tyne NE17RU, UK
- ^c Computational Process Engineering, Chulalongkorn University, Bangkok 10330, Thailand

HIGHLIGHTS

- PEMFC systems with a glycerol steam reformer for stationary application are studied.
- Performance of HT-PEMFC and LT-PEMFC systems is compared.
- HT-PEMFC system shows good performance over LT-PEMFC system at a high current density.
- HT-PEMFC system with water gas shift reactor shows the highest system efficiency.
- Heat integration can improve the efficiency of HT-PEMFC system.

ARTICLE INFO

Article history: Received 26 August 2012 Received in revised form 2 April 2013 Accepted 3 April 2013

Keywords:
High-temperature polymer electrolyte
membrane fuel cell
Glycerol reforming
Hydrogen production
Fuel cell system
Stationary application

ABSTRACT

A high-temperature polymer electrolyte membrane fuel cell (HT-PEMFC) has a major advantage over a low-temperature polymer electrolyte fuel cell (LT-PEMFC) demonstrated by a tolerance to a higher CO content in the hydrogen feed and thus a simpler fuel processing. In this study, a direct comparison between the performance of HT-PEMFC and LT-PEMFC systems integrated with a glycerol steam reformer with and without a water gas shift reactor is shown. Under pure hydrogen operation, the LT-PEMFC performance is superior to the HT-PEMFC. However, the HT-PEMFC system shows good performance over the LT-PEMFC system when operated under high current density and high pressure (3 atm) and using the reformate gas derived from the glycerol processor as fuel. At high current density, the high concentration of CO is the major limitation for the operation of HT-PEMFC system without water gas shift reactor, whereas the LT-PEMFC suffers from CO poisoning and restricted oxygen mass transport. Considering the system efficiency with co-heat and power generation, the HT-PEMFC system with water gas shift reactor shows the highest overall system efficiency (approximately 60%) and therefore one of the most suitable technologies for stationary applications.

© 2013 Elsevier Ltd. All rights reserved.

1. Introduction

Due to the need for clean energy and efficiency technology, great efforts have focused on fuel cells' research for electricity generation. The high current density, low operating temperature and rapid start up of a polymer electrolyte membrane fuel cell (PEMFC) make it a promising candidate for transportation and stationary power generation [1–4]. In general, a conventional PEMFC, operated at temperatures below 373.15 K, has a serious water manage-

E-mail address: Amornchai.A@chula.ac.th (A. Arpornwichanop).

ment challenge and requires pure hydrogen fuel with no CO to avoid catalyst poisoning. To overcome some limitations of the low-temperature PEMFC (LT-PEMFC), a high-temperature PEMFC (HT-PEMFC) has been developed using a phosphoric acid doped polybenzimidazole membrane. CO poisoning (adsorption) on the surface of a platinum catalyst decreases by increasing the operating temperature. The higher temperatures allow the use of reformate gas directly from a fuel processor to feed HT-PEMFCs with simple purification processes [5]. In the case of LT-PEMFC based on Nafion membranes, the reformate gas must be treated by water gas shift and preferential oxidation processes in order to reduce CO content below 10 ppm [6,7]. These treatments will cause hydrogen and parasitic losses. Another advantage of HT-PEMFC is that it does not rely on water for proton transport and can be operated at dry

^{*} Corresponding author at: Department of Chemical Engineering, Faculty of Engineering, Chulalongkorn University, Bangkok 10330, Thailand. Tel.: +66 2 218 6878; fax: +66 2 218 6877.

Nomenclatures E_c activation energy, I mole⁻¹ K⁻¹ transfer coefficient α $E_{\rm cell}$ cell voltage, V transfer coefficient α reversible cell potential, V E_r reaction order F faraday constant, 96,485 C mol⁻¹ water content enthalpy, J mol⁻¹ Н θ_{CO} CO coverage proton conductivity of LT-PEMFC, S cm⁻¹ K_m H₂ coverage θ_{H} proton conductivity, S cm⁻¹ catalyst loading, mg cm⁻² σ_m lower heating value, kJ mol⁻¹ LHV ohmic loss, V $\eta_{\rm ohmic}$ molar flow rate, mol s activation loss. V m η_{act} pressure, atm system efficiency $\eta_{\rm sys}$ P_{FC} power output of fuel cell, W cogeneration system efficiency $\eta_{\text{sys,co}}$ $P_{\text{parasitic}}$ power used in auxiliary unit, W target power output, W Subscripts and superscripts heat flow, $J s^{-1}$ 0 anode gas constant (=8.314), J $\text{mol}^{-1} \text{ K}^{-1}$ R С cathode T cell temperature, K membrane m current density, A m⁻² i components "i" and "i" i, j exchange current density, A m⁻² i_0 in inlet stream l_m membrane thickness, m out outlet stream Greek letters

condition [8], allowing for a further simplification with the removal of humidifiers. However, the complexity of the integrated system depends on the fuel used and the requirement of each application as well [9].

Until a suitable hydrogen infrastructure and storage are readily available, reformate gas from fuel processors is a promising alternative hydrogen source for PEMFC. Among the various types of fuel, glycerol is considered a potential feedstock for producing hydrogen and one of the most attractive fuels for sustainable development of hydrogen production [10–13]. It is a by-product of biodiesel process via the transesterification of vegetable oil and alcohol. The use of glycerol to produce high-value added products can also reduce the biodiesel production cost. In addition, it is a liquid phase at room temperature and thus can easily be stored and transported. A carbon formation from the reforming of glycerol is lower than that of non-oxygen-containing hydrocarbon fuels [10].

In general, fuel cell systems' design depends greatly on their applications and desired efficiency. For automotive applications, weight and size of the overall system are critical. The fast starting up is also preferred and thus the autothermal reforming is suitable for this application more than steam reforming [14]. On the other hand, stationary applications require high overall efficiency without specific weight or size restrictions [15]. Heat and power cogeneration is favourably suited for stationary application as an effective way to improve the overall system efficiency combined with the highly efficient steam reforming [16]. For low-temperature fuel cells, high system efficiency can be achieved when low quality heat released from fuel cell is applied to household usage [17]. The PEMFC cogeneration system is considered an effective system, which meets both electrical and thermal demands of residential applications [18].

This study focuses on the performance analysis and design of a HT-PEMFC system for a stationary power generation. The efficiency of the HT-PEMFC system with different fuel processors is investigated and compared with a LT-PEMFC system. The HT-PEMFC system considered here can be divided into two cases. The first one involves the HT-PEMFC and a glycerol reformer without a CO removal process; whereas in the second one, a water gas shift reactor is included to improve further its overall system efficiency. The CO impact, performance and overall system efficiency of LT-PEMFC

and HT-PEMFC systems are compared under pure hydrogen and reformate gas from glycerol fuel processor. The integrated system is studied as a combined heat and power (CHP) for stationary application, where the waste heat generated during fuel cell operation is utilized in producing hot water for household use.

2. PEMFC systems for stationary applications

A fuel steam reforming (SR) is regarded as a suitable process to produce hydrogen for stationary application of fuel cells because of its high hydrogen yield [19]. The heat integration of a fuel processor and a fuel cell is preferred to enhance the overall efficiency. As shown in Fig. 1a–c, the excess un-reacted hydrogen and oxygen from the fuel cell are sent to a burner to supply heat for the glycerol steam reforming. In addition, water is recovered from hot reformate gas and flue gas and used in the steam reformer and humidifier.

Due to a high CO tolerance of HT-PEMFCs, it is possible to use the reformate gas obtained directly from the glycerol reformer without further CO removal. This system is presented in Fig. 1a. Generally, to increase hydrogen yield in endothermic steam reforming processes, high reforming temperature and excess steam feed are required. However, this will also result in the undesired increase of CO content. With the aim at direct use of the reformate gas, the operating temperature of the steam reformer needs to be reduced to satisfy the operational constraint of the HT-PEMFC. Similarly, excess steam is necessary to enhance the hydrogen yield at the low-temperature operation of the reformer shifting the equilibrium of the steam reforming reaction toward the product side (hydrogen production). However, this will lead to a higher energy requirement to preheat excess steam, sacrificing the overall system efficiency. To improve the HT-PEMFC performance, the fuel processing subsystem, i.e., a water gas shift reactor (WGS), is added to the steam reformer (Fig. 1b) to maximize the hydrogen content and reduce CO fraction. It should be noted that the large size of the water gas shift reactor is the main restriction in the use of PEMFC systems for automotive applications, but not for stationary applications [20].

For LT-PEMFCs, they are operated at low temperatures and require reformate fuel with less CO to avoid catalyst poisoning. The

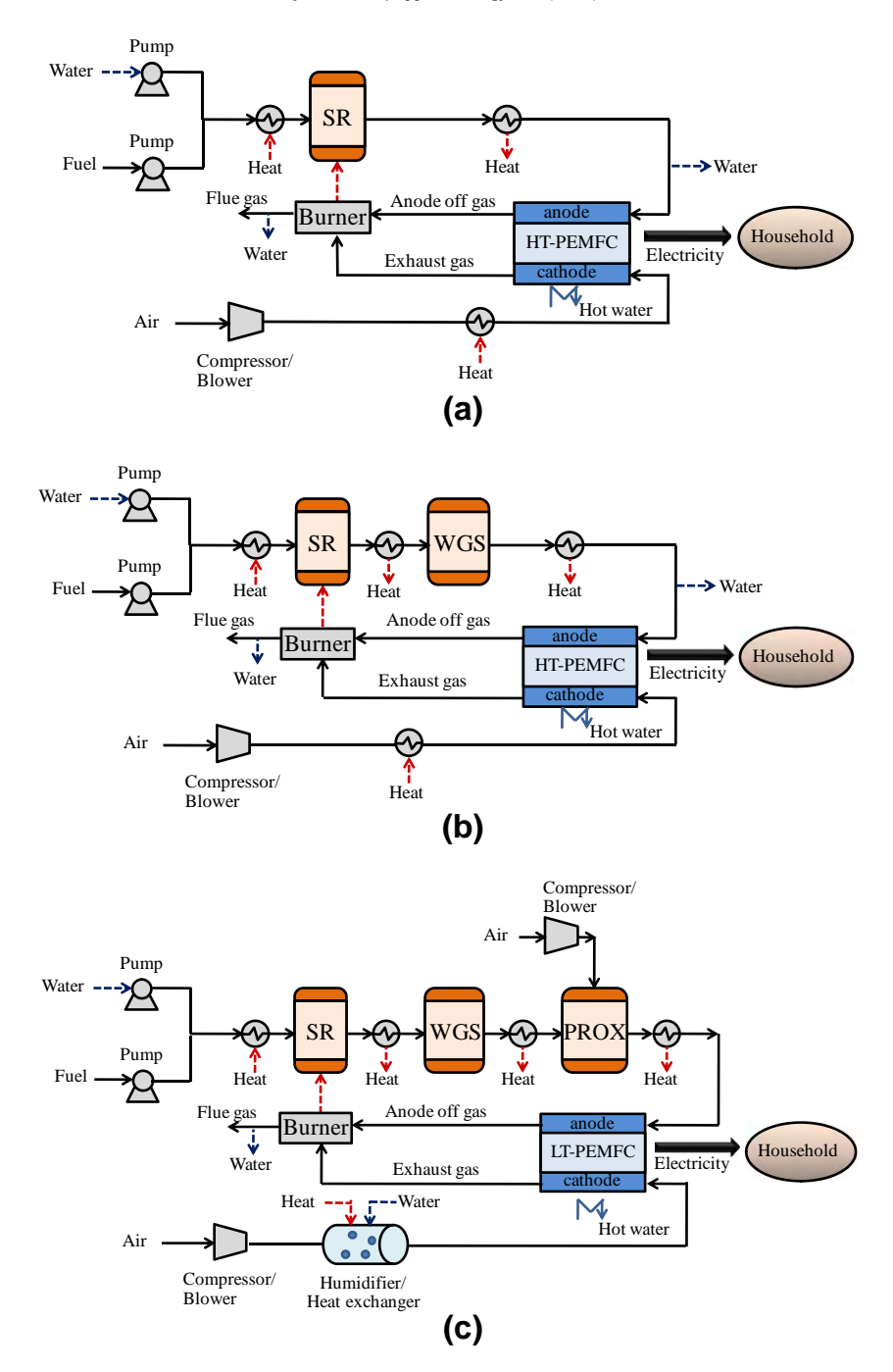


Fig. 1. PEMFC system integrated with a fuel processing process for stationary application: (a) HT-PEMFC with only a steam reformer (case 1), (b) HT-PEMFC with a steam reformer and a water gas shift reactor (case 2) and (c) LT-PEMFC with a steam reformer, a water gas shift reactor and a preferential oxidation reactor (case 3).

content of CO in a hydrogen feed for LT-PEMFC is limited to be less than 10 ppm. Therefore, both water gas shift and preferential oxidation (PROX) processes are added to the fuel reforming process for the LT-PEMFC system. Typical fuel processing system for LT-PEMFCs is demonstrated in Fig. 1c. In the WGS reactor, CO is reduced and at the same time, more hydrogen is generated. Nonetheless, the reformate gas obtained from this process still has CO exceeding the acceptable level of LT-PEMFC. Therefore, the reformate gas should be further treated by the PROX reactor to reduce the concentration of CO to a satisfactory level. The oxidation reactions occurring in this process cause loss of hydrogen and parasitic loss from a compressor (for feeding air to the reactor).

Apart from the CO purification process, the main difference between the LT-PEMFC and HT-PEMFC systems involves the use of a humidifier unit. Due to the fact that HT-PEMFC can be operated at dry condition, the humidification is unnecessary for this type of PEMFC, contrast to LT-PEMFC where humidification is essential to prevent drying out of a Nafion membrane. However, when operated using the reformate gas, LT-PEMFC does not require further anode humidification, as the reformate gas is already saturated with water (from the reforming process).

A designed configuration of the PEMFC systems investigated in this study is shown in Table 1. The target power output of both the HT-PEMFC and LT-PEMFC systems for a stationary application is

Table 1Designed configuration of the PEMFC systems.

	Stationary application (household)
Power output	3 kW
Heat integration between fuel cell and fuel processing	Included
Water recovery	Included
Type of reforming process	Steam reformer
Cogeneration system	Included

3 kW, which is sufficient for small household. The released heat from the fuel cell will be used to generate hot water for a boiler heating system.

3. Modeling of PEMFC systems

3.1. Fuel processing

The equilibrium composition of a reformate gas obtained from the steam reforming of glycerol is calculated from the direct minimization of Gibbs free energy. The external heat used to maintain the glycerol reformer at isothermal condition is determined by considering the enthalpy change between reactants and products of the reformer when inlet and outlet temperatures are equal to the reforming temperature. The WGS reactor is also modeled as an equilibrium reactor and its operating temperature is specified at 473.15 K [20]. The reaction occurring in the WGS reactor involves a water gas shift reaction. For PROX process, the conversion reactor model is chosen. It is operated at oxygen to CO ratio of 1.5 and temperature of 423.15 K. The CO conversion is fixed at 95% [21] and the remaining oxygen will react with hydrogen. In addition, the sequentially two stages of the PROX reactor are applied to reduce the CO concentration lower than 10 ppm (in case of the LT-PEMFC system).

3.2. PEMFC

The basic relation of voltage and current density for PEMFC is described in Eq. (1). The cell voltage ($E_{\rm cell}$) can be calculated by subtracting the reversible cell potential (E_r), the maximum voltage that can be achieved by a fuel cell at specific operating condition, by various voltage losses.

$$E_{\text{cell}} = E_r - \eta_{\text{act},a} - \eta_{\text{act},c} - \eta_{\text{ohmic}} \tag{1}$$

where $\eta_{\text{act},a}$ is the activation loss at the anode, $\eta_{\text{act},c}$ is the activation loss at the cathode and η_{ohmic} is the ohmic loss. Detail of the model describing the voltage losses of the HT-PEMFC based on a phosphoric acid doped polybenzimidazole membrane and the LT-PEMFC using a Nafion membrane is given in Table 2. It is noted that since the concentrations of hydrogen and oxygen at the catalyst surface

are used to determine the reversible cell potential and activation loss, concentration losses do not appear in Eq. (1).

The reversible cell potential is described by Nernst equation:

$$E_{r} = -\left(\frac{\Delta H_{T}}{nF} - \frac{T\Delta S_{T}}{nF}\right) + \frac{RT}{nF} \ln \left[\frac{(RT)^{1.5}C_{H_{2}-Pt}C_{O_{2}-Pt}^{0.5}}{a_{H_{2}O}}\right]$$
(2)

where $a_{\rm H_2O}$ is the water activity defined by the ratio of water partial pressure to its saturation pressure.

Table 3 shows the parameters used for calculating the activation loss at the cathodes of HT-PEMFC and LT-PEMFC. The model parameters of the LT-PEMFC are estimated from experimental data [25] and the validation of the LT-PEMFC model with the experimental data [25,26] is shown in Fig. 2. For HT-PEMFC, its model parameters reported by Mamlouk et al. [22] are employed in this work and the validation of the HT-PEMFC model can be seen in our previous work [27]. Due to the fact that the fuel used at the anode is a reformate gas from the fuel processor section, the effect of CO poisoning is included in the anode activation loss model of both the HT-PEMFC and LT-PEMFC. The CO poisoning model of LT-PEMFC, which is proposed by Bhatia and Wang [23], is used in this work. For HT-PEMFC, the exchange current density of hydrogen oxidation in the presence of CO is $i_0^{\rm CO}$ instead of i_0 (for pure hydrogen). The $i_0^{\rm CO}$ can be calculated from CO coverage ($\theta_{\rm CO}$) assuming the bridge model of CO adsorption on Pt as follows:

$$i_0^{\text{CO}} = i_0 (1 - \theta_{\text{CO}})^2 \tag{3}$$

The CO coverage of the HT-PEMFC is described as follows [27]:

$$\theta_{\text{CO}} = a * \ln \frac{[\text{CO}]}{[\text{H}_2]} + b * \ln(i) * \ln \frac{[\text{CO}]}{[\text{H}_2]} + c$$
 (4)

$$a = -0.00012784 * T^2 + 0.11717499 * T - 26.62908873$$

 $b = 0.0001416 * T^2 - 0.12813608 * T + 28.852463626$
 $c = -0.00034886 * T^2 + 0.31596903 * T - 70.11693333$

The concentration of hydrogen and oxygen at catalyst surface is determined from the Stefan Maxwell equation and the Fick's law which represent the diffusion model of the reactant in the gas diffusion layer and film electrolyte [22]. It is noted that the concentrations of all components along the gas flow channels are assumed to be constant and determined from the average concentrations of the feed and outlet gas composition. The outlet gas compositions are calculated from a fuel utilization.

Diffusion of multi-component gas streams through the porous carbon electrode can be described by using the Stefan-Maxwell equation in:

$$\frac{dX_i}{dz} = \frac{RT}{P} \sum \frac{X_i N_j - X_j N_i}{D_{ii}^{eff}}$$
 (5)

where N is the molar flux of each component at the anode and cathode sides of HT-PEMFC and LT-PEMFC, X is the mole fraction of each component, D_{ij}^{eff} is the diffusion coefficient calculated by using the

 Table 2

 Voltage loss models used in simulation of HT-PEMFC and LT-PEMFC.

Voltage loss	HT-PEMFC	Ref.	LT-PEMFC	Ref.
Anode activation	$ \eta_{act,a} = \frac{RT}{2F} \sinh^{-1} \left(\frac{i}{2i_0 (1 - \theta_{CO})^2} \right) $	[22]	$\eta_{act,a} = \frac{RT}{\alpha t} \sinh^{-1} \left(\frac{i}{2K_{ch}\theta_{H}} \right)$	[23]
Cathode activation	$ \eta_{act,c} = \frac{RT}{2F} \sinh^{-1} \left(\frac{i}{2i_0} \right) $	[22]	$\eta_{act,c} = \frac{RT}{\alpha t} \sinh^{-1} \left(\frac{i}{2l_0} \right)$	This work
	$i_0 = i_{0,c}^{ref} a_{c,c} L_{c,c} \left(\frac{C_{Pt}}{C_{ref,c}} \right)^{\gamma} \exp \left[-\frac{E_{c,c}}{RT} \left(1 - \frac{T}{T_{ref,c}} \right) \right]$		$i_0 = i_{0,c}^{\text{ref}} a_{c,c} L_{c,c} \left(\frac{C_{PL}}{C_{\text{ref,c}}}\right)^{\gamma} \exp \left[-\frac{E_{c,c}}{RT} \left(1 - \frac{T}{T_{\text{ref,c}}}\right)\right]$	
Ohmic loss	$oldsymbol{\eta}_{ ext{ohmic}} = \left(rac{\sigma_m}{l_m} ight) oldsymbol{i}$	[22]	$\eta_{ m ohmic} = \left(rac{K_{ m mem}}{l_m} ight)$ i	[24]
	$\sigma_m = rac{A}{T} \exp\left(rac{-B}{R(T)} ight)$		$K_{\text{mem}} = (0.5139\lambda - 0.326) \exp\left[1268\left(\frac{1}{303} - \frac{1}{7}\right)\right] \times 100$	

Table 3Value of the parameters used to compute the cathode activation loss.

Parameters	HT- PEMFC	LT-PEMFC
Cell operating pressure at anode, P (atm) Cathode reference exchange current density, $i_{0,c}^{\text{ref}}$ (A m ⁻²)	3 0.0004	$\begin{array}{c} 3 \\ 4.2 \times 10^{-4} \end{array}$
Cathode catalyst surface area, $a_{c,c}$ (m² g ⁻¹) Cathode catalyst loading, $L_{c,c}$ (mg cm ⁻²) Transfer coefficient at the cathode, α_c (–) Reaction order, γ (–) Cathode reference concentration, $c_{\text{ref,c}}$ (mol cm ⁻³) Cathode activation energy, $E_{c,c}$ (J mol ⁻¹ K ⁻¹) Cathode reference cell temperature, $T_{\text{ref,c}}$ (K)	64 0.4 0.75 1.375 0.0004 72,400 373.15	54 0.4 0.45 1.3 2.03×10^{-7} $66,000$ 298.15

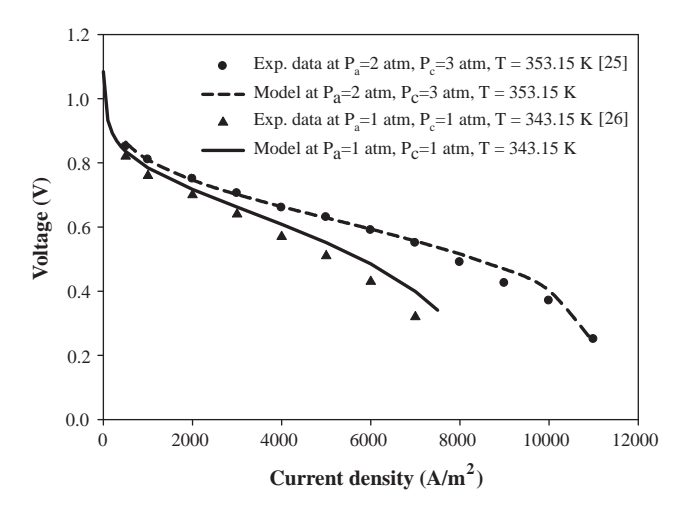


Fig. 2. Validation of the LT-PEMFC model and experimental data [25,26].

Slattery–Bird correlation [28] and corrected to account for the porosity/tortuosity effects using the Bruggeman correlation [8].

$$D_{ij}^{eff} = \frac{a}{P} \left(\frac{T}{\sqrt{T_{c,i}T_{c,j}}} \right)^b (P_{c,i}P_{c,j})^{1/3} (T_{c,i}T_{c,j})^{5/12} \left(\frac{1}{M_i} + \frac{1}{M_j} \right)^{1/2} \varepsilon^{\tau}$$
 (6)

where T_c and P_c are the gas critical temperature and pressure, respectively, M is the molecular weight, ε and τ are the porosity and the tortuosity. It is noted that a equals to 0.0002745 for diatomic gases and 0.000364 for water vapor and b equals to 1.832 for di-atomic gases and 2.334 for water vapor.

To find H_2 and O_2 concentrations at the catalyst surface, Fick's law is applied (Eqs. (7) and (8)). Gaseous reactants need to diffuse through the electrolyte film layer before arriving at the catalyst active surface [22].

$$\frac{N_{O_2}}{S_{Pt-cathode}} = \frac{-D_{O_2} \left(C_{O_2-pt} - C_{O_2(dissolve)}\right)}{\delta_{cathode}} \tag{7}$$

$$\frac{N_{\text{H}_2}}{S_{\text{Pt-anode}}} = \frac{-D_{\text{H}_2} \left(C_{\text{H}_2-\text{pt}} - C_{\text{H}_2(\text{dissolve})} \right)}{\delta_{\text{anode}}} \tag{8}$$

where N is the molar flux, C_{Pt} is the reactant concentration on the catalyst surface, C_{dissolve} is the equilibrium reactant concentration in the electrolyte film at the studied temperature, S_{Pt} is the real platinum surface area and δ is the film thickness.

The concentration of H_2 and O_2 dissolving at the film electrolyte layer boundary can be calculated from their solubility ($C_i^{\text{dissolved}}$) as follows:

$$C_{H_2(dissolve)} = C_{H_2}^{dissolved} \cdot X_{H_2} \cdot P \tag{9}$$

$$C_{O_2(dissolve)} = C_{O_2}^{dissolved} \cdot X_{O_2} \cdot P \tag{10}$$

where $X_{\rm H_2}$ and $X_{\rm O_2}$ are the mole fraction of H₂ and O₂ at the GDL/electrolyte film interface.

It is noted that the solubility ($C_i^{\rm dissolved}$) and diffusion coefficient (D_i) of HT-PEMFC can be calculated from the correlation reported by Mamlouk et al. [22], whereas the solubility ($C_i^{\rm dissolved}$ (mol dm⁻³)) and diffusion coefficient (D_i (m² s)) of LT-PEMFC at the cathode side can be calculated as follows:

$$ln C_i^{dissolved} = \frac{662.50}{T} - 7.2805 \tag{11}$$

$$\ln D_i = \frac{-2983.6}{T} - 12.442 \tag{12}$$

This correlation is obtained from experimental data of oxygen solubility and diffusion at different temperatures using Nafion membrane [29]. The gas diffusion via film electrolyte at the anode is neglected in this work.

The power output of fuel cell (P_{FC}) and target power output (P_T) can be calculated from current density (i), E_{cell} and parasitic loss ($P_{parasitic}$) as follows:

$$P_{\text{FC}} = i \cdot A \cdot n \cdot E_{\text{cell}} \tag{13}$$

$$P_T = P_{FC} - P_{\text{parasitic}} \tag{14}$$

where *A* is the cell active area and *n* is the number of cell.

3.3. Auxiliary units

To supply fuel for the fuel processor and PEMFC, a pump and a compressor are used as auxiliary units. Therefore, the required power of pump and compressor is taken into account for calculating the system efficiency. Here, the efficiencies of the pump and compressor are specified at 0.7. Furthermore, the heat management in the integrated systems is carried out by using a heat exchanger and a burner. The heat from the product streams of the reformer and the anode and cathode off gases are recovered via heat exchangers. The recovered heat will be utilized to preheat and vaporize water for the glycerol reformer. The amount of energy recovered from the heat exchanger is calculated from the enthalpy change between the inlet and outlet of hot and cold streams. To keep the fuel cell temperature at a desired level, water is used as a cooling medium to remove the excess heat from PEMFC. The hot water obtained can be used in a boiler heating process for the cogeneration system. The heat recovery from the fuel cell can be calculated by

$$Q_{\text{thermal}} = m_{a,\text{in}} H_{a,\text{in}} + m_{c,\text{in}} H_{c,\text{in}} - m_{a,\text{out}} H_{a,\text{out}} - m_{c,\text{out}} H_{c,\text{out}} - P_{\text{FC}}$$

$$(15)$$

For the LT-PEMFC system, a humidifier is needed to produce a humidified air for the cathode and the amount of heat required for this unit is determined by:

$$Q_{hum} = m_{air,out} H_{air,out} - m_{air,in} H_{air,in} - m_{H_2O,in} H_{H_2O,in}$$
 (16)

3.4. System efficiency

Considering the heat integration of PEMFC and reforming processes, the required energy for the reforming process is partially supplied by the heat recovered from the anode and cathode exhaust gases. The system efficiency is calculated by

$$\eta_{\rm sys} = \frac{P_{\rm FC} - P_{\rm parasitic}}{m_{\rm glycerol} \cdot LHV_{\rm glycerol} + Q_{\rm ref} - Q_{\rm rec}} \tag{17}$$

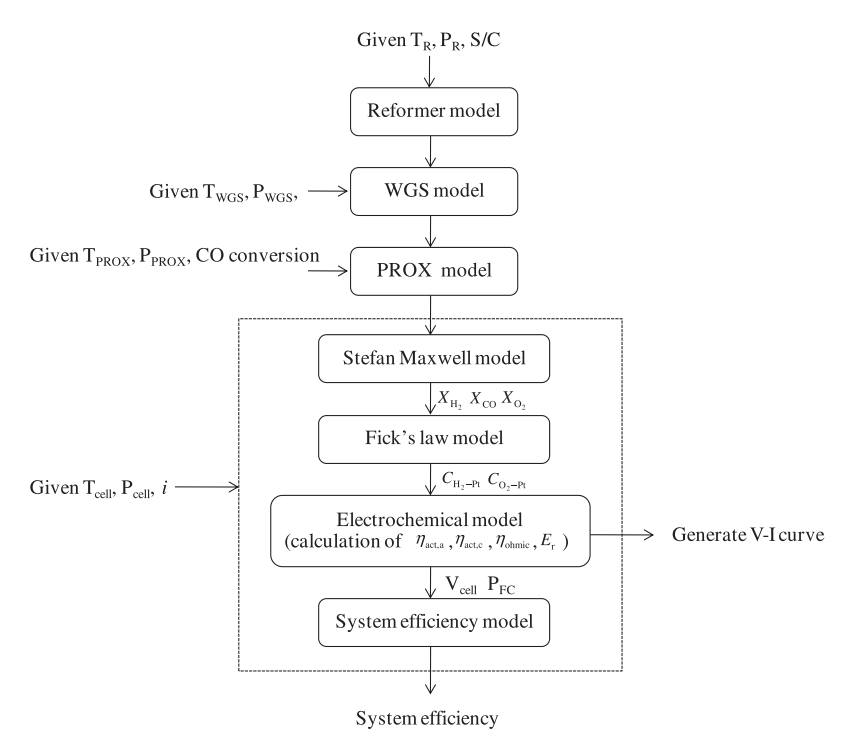


Fig. 3. Flow diagram of the numerical solution of PEMFC system models.

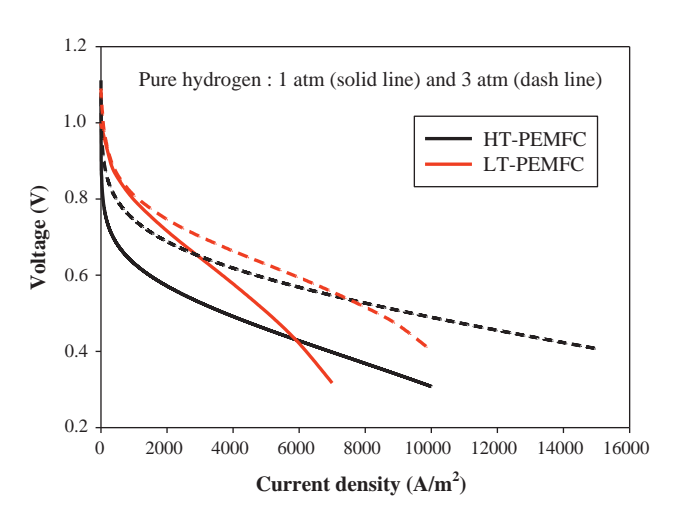


Fig. 4. Polarization curves of HT-PEMFC and LT-PEMFC at pure hydrogen operation.

where $m_{\rm glycerol}$ is the molar flow rate of glycerol used for producing hydrogen for PEMFC (the molar flow rate of glycerol depends on the cell operating current). LHV_{glycerol} is the lower heating value of glycerol. Q_{ref} is the energy required for the humidifier (in case of the LT-PEMFC system) and steam reforming process accounting for the heat of vaporization, specific heat to heat up the reactants to the desired temperature and the heat needed for maintaining the reformer at an isothermal operation level. Q_{rec} is the recovered heat from the anode and cathode exhaust gases as well as from the high temperature product gas of the glycerol reformer. $P_{\text{parasitic}}$ is the required power used in auxiliary units, namely compressor and pump. When the heat integration is not considered, the recovered heat (Q_{rec}) accounts for only the heat that recovered from the high temperature product gas of the reformer. It is also noted that the recovered heat from WGS and PROX units are included in the determination of the system efficiency when these units involve the PEMFC system.

For the power and heat cogeneration of the PEMFC system, both the electrical and thermal output are included in the calculation of the cogeneration system efficiency, as defined by Eq. (18). The thermal output ($Q_{\rm thermal}$) is the heat recovery from the fuel cell, which can be used to produce hot water for household usage via a boiler heating system.

$$\eta_{\text{sys,co}} = \frac{P_{\text{FC}} - P_{\text{parasitic}} + Q_{\text{thermal}}}{m_{\text{glycerol}} \cdot LHV_{\text{glycerol}} + Q_{\text{ref}} - Q_{\text{rec}}}$$
(18)

Furthermore, since the fuel processor consumes steam and at the same time, the fuel cell produces some steam, the steam balance between the steam recovered from the fuel cell exhaust gas and that required for the reforming process is considered in this study.

3.5. Numerical solution

In this work, the mathematical models of LT-PEMFC and HT-PEMFC systems integrated with a glycerol fuel processor process are solved by Matlab. A flow diagram of the numerical solution is shown in Fig. 3. At design conditions, the composition of the reformate gas fed to PEMFC can be calculated from the reformer model for HT-PEMFC (case 1), the reformer and WGS models for HT-PEMFC (case 2) and the reformer, WGS and PROX models for LT-PEMFC (case 3). The cell performance (*V-I* curve) is then determined from the Stefan Maxwell, Fick's law and electrochemical model. The CO poisoning model is included in computing the anode activation loss. Finally, the system efficiency is calculated by considering the heat recovery and parasitic loss from auxiliary units.

4. Results and discussion

4.1. HT-PEMFC and LT-PEMFC performances

4.1.1. Pure hydrogen operation

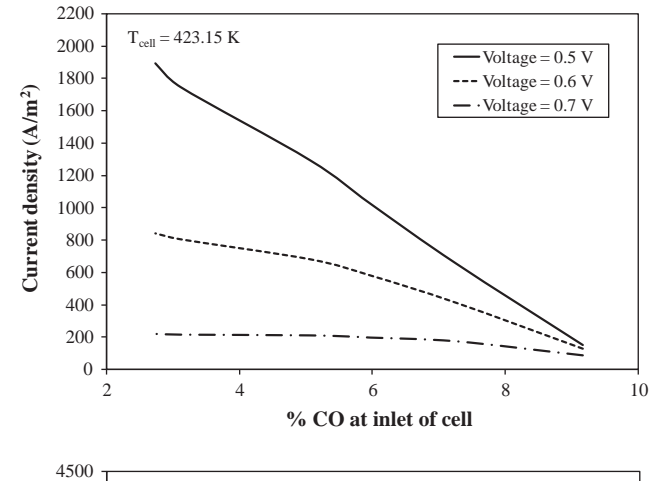
Fig. 4 shows the performance of HT-PEMFC and LT-PEMFC running on pure hydrogen and air when the inlet temperature of water, fuel and air is specified at the fuel cell temperature. Under the atmospheric pressure operation, the simulation results show

Table 4Mole fraction of hydrogen at each unit of the HT-PEMFC and LT-PEMFC systems operated at pressure of 3 atm.

System	S/	Reformer temperature (K)	Fuel cell temperature (K)	Hydrogen (mole fraction)				
		Glycerol steam reforming (wet basis)	WGS (wet basis)	PROX (wet basis)	Humidifier/heat exchanger			
HT-PEMFC: case 1	4	900	448.15	0.3014	-	-	0.6513 (RH = 0)	
HT-PEMFC: case 2	2	1000	448.15	0.4135	0.5164	-	0.6882 (RH = 0)	
LT-PEMFC	2	1000	353.15	0.4135	0.5164	0.5076	0.5704 (RH = 1)	

Table 5Composition (dry basis) of other gaseous products containing in hydrogen feed stream for HT-PEMFC and LT-PEMFC systems.

System	СО	CO_2	CH ₄	N ₂
HT-PEMFC: case 1 HT-PEMFC: case 2 LT-PEMFC	0.0663 0.0023 6 ppm	0.2584 0.3003 0.2999	0.0240 0.0093 0.0092	- - 0.0101
LI-I LIVII C	o ppiii	0.2333	0.0032	0.0101



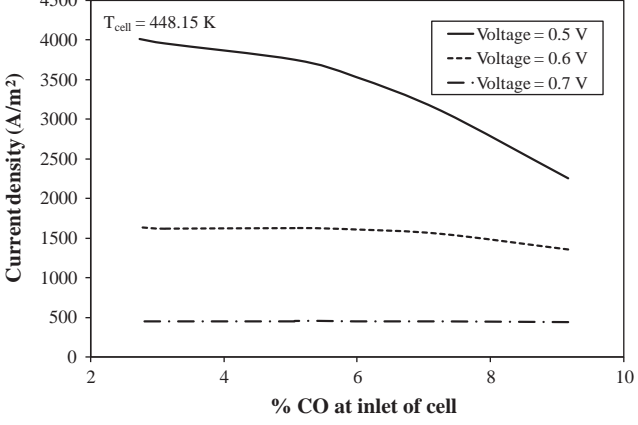


Fig. 5. Effect of CO on HT-PEMFC performance.

that the LT-PEMFC has a higher performance, compared with the HT-PEMFC at current densities lower than 6000 A m⁻². Although the exchange current density at Nafion/Pt interface is higher than that of H₃PO₄/Pt, low oxygen permeability and strong phosphate adsorption (phosphoric acid is required for HT-PEMFCs operation) are the main reasons for the observed slower oxygen reduction kinetics in HT-PEMFCs cathodes even at the higher operating temperature [30].

However, the performance of the HT-PEMFC improves significantly and becomes comparable to that of LT-PEMFC when the fuel cell pressure is increased to 3 atm. Increasing the operating pressure causes a higher hydrogen and oxygen partial pressures, resulting in enhanced kinetics and mass transport. The increase in pressure has larger impact on the HT-PEMFCs in comparison to the LT-PEMFCs due to the lower permeability of oxygen in phosphoric acid in comparison to that in Nafion. Nevertheless, in comparison with the HT-PEMFC, the LT-PEMFC seems to have a superior performance under a practically operational range (voltage of 0.5–0.7) when pure hydrogen is used as a fuel feed.

4.1.2. Reformate operation

A reformate gas that is derived from the glycerol steam reforming process contains H₂, CO, CO₂, CH₄, H₂O and some trace of N₂ (in case of applying a PROX unit in the glycerol processor). The operating condition of the glycerol processor is chosen by considering the operational constraints (i.e., CO contamination) of HT-PEMFCs and LT-PEMFCs (see Table 4). The corresponding hydrogen fraction from the glycerol processor is given in Table 4 for different PEMFC systems, whereas the fraction of other gaseous components containing in the reformate gas is reported in Table 5. The CO fraction coming from PROX in the glycerol processor at a desired condition is lower than 10 ppm in case of LT-PEMFC system. The performance of HT-PEMFC running on the reformate gas with different %CO is shown in Fig. 5. It is found that at cell temperature of 448.15 K, the current density generated insignificantly changes under the studied voltage range when the reformate gas contains CO less than 5% because of the high CO tolerance of HT-PEMFC, which is operated under high temperatures. However, when cell temperature is reduced to 423.15 K, a drop in the current density is observed if the HT-PEMFC is run at the voltage less than 0.6.

Considering the HT-PEMFC system without the WGS reactor (case 1), the optimal condition of the reformer providing the highest system efficiency is used in this study when CO fraction is about 7% [24]. It is noted that although the steam reformer operated at the conditions providing low CO content will show a better performance in term of hydrogen yield, but the reformer efficiency is lower due to a high energy requirement for producing more steam for the reformer. For the HT-PEMFC system including the WGS reactor (case 2), the CO fraction in the synthesis gas obtained from the WGS reactor operated under the defined reformer and WGS reactor conditions is lower than 0.25% [31]. The simulation results (Table 4) show that the hydrogen fraction in the anode feed is in order: HT-PEMFC (case 2) > HT-PEMFC (case 1) > LT-PEMFC.

From the simulation result in Fig. 6, it can be seen that when operated at 1 atm, the HT-PEMFC system without a WGS reactor (case 1) has the same performance as that with the WGS reactor (case 2) at a low current density operation. However, the performance of the HT-PEMFC without a WGS reactor decreases sharply at high current densities because of poisoning effect of the increased CO concentration in reformate gas towards the end of the anode channels at high current densities (hydrogen is

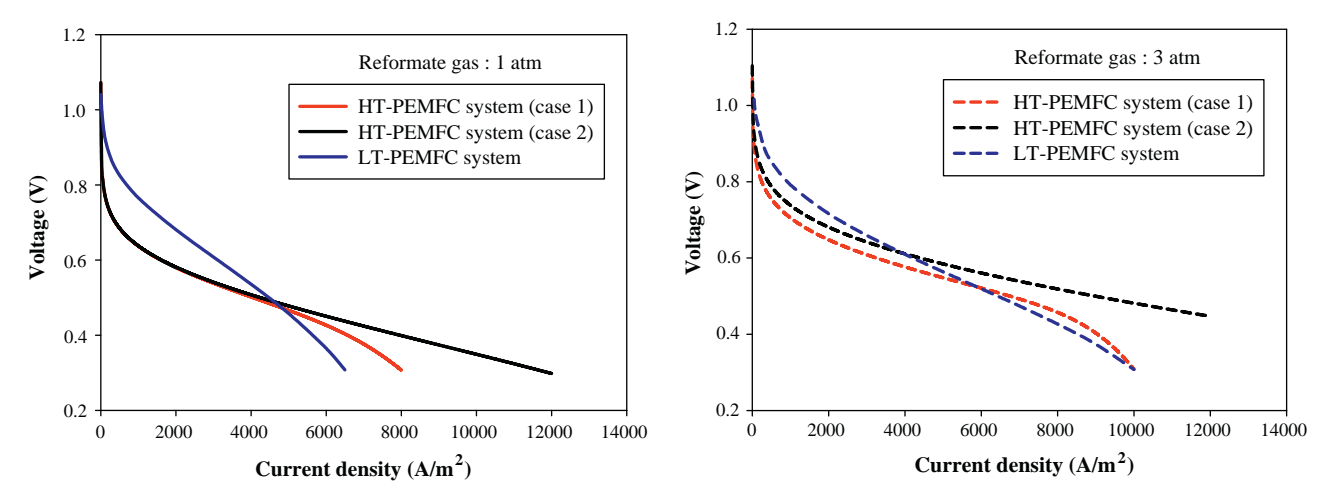


Fig. 6. Polarization curves of HT-PEMFC and LT-PEMFC at reformate operation.

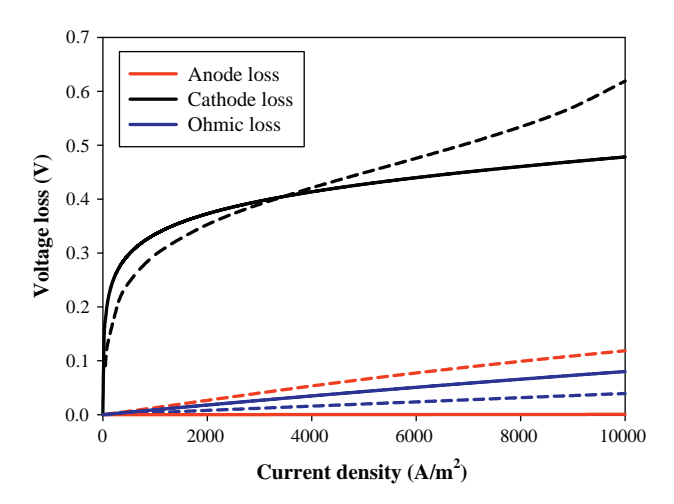


Fig. 7. Voltage loss of PEMFC systems at reformate operation and cell pressure of 3 atm: HT-PEMFC system (case 2) (solid line) and LT-PEMFC (dash line).

Table 6Value of the parameters used for the efficiency analysis of HT-PEMFC and LT-PEMFC.

Parameters	Value	Unit
System pressure Active area	3 250	atm cm²
Number of cell • HT-PEMFC (case 1) • HT-PEMFC (case 2) • LT-PEMFC	115 81 71	- - -
Cell temperature • HT-PEMFC • LT-PEMFC Anode stoichiometry Cathode stoichiometry	448.15 353.15 1.25 2	K K -

consumed). For LT-PEMFC system, superior performance is obtained at current densities up to $5000 \, \text{A m}^{-2}$ beyond which the cell performance drops sharply. At high pressure (3 atm) operation, the HT-PEMFC with a WGS reactor shows the highest performance among the studied systems at high current density above $4000 \, \text{A m}^{-2}$, whereas LT-PEMFC system shows superior performance at lower current densities known as the kinetic region (see Fig. 6). The limited performance of LT-PEMFC system operated on reformate gas at high current densities results from the CO poi-

soning effect on anode and oxygen starvation at the cathode caused by flooding and low oxygen partial pressure (humidified air). However, the LT-PEMFC performance at high current density can be improved by using air bleeding technique to suppress CO poisoning effect. Fig. 7 shows the individual voltage loss in HT-PEMFC and LT-PEMFC operated on the reformate gas. As expected the CO poisoning problem is more pronounced in LT-PEMFC than HT-PEMFC resulting in larger anode over-potentials of LT-PEMFC in comparison to that of HT-PEMFC. The ohmic loss in HT-PEMFC, on the other hand, is marginally greater than that in LT-PEMFCs as Nafion exhibits higher ionic conductivities at fully humidified conditions. The cathode activation loss in LT-PEMFCs is smaller than that of HT-PEMFCs. This is due to the higher exchange current density at Nafion/Pt interface in comparison to that of H₃PO₄/Pt. As cathode current density increases, mass transport limitation in LT-PEMFCs becomes pronounced at current densities as low as 4000 A m⁻² when operated with air. The decrease of oxygen partial pressure due to cathode steam humidification, cathode flooding and slower oxygen diffusion in the gaseous phase in comparison to HT-PEMFCs (higher operating temperature) is the main reason for the observed limitation. These behaviors explain why the performance of HT-PEMFC surpasses that of LT-PEMFC at high current density (>4000 A m⁻²).

4.2. Comparison of HT-PEMFC and LT-PEMFC system efficiencies

To compare the efficiency of HT-PEMFC and LT-PEMFC systems for small stationary application, the power output target is specified at 3 kW and the PEMFC systems is operated at pressure of 3 atm. The efficiency of LT-PEMFC and HT-PEMFC system is investigated at the same power output (3 kW) and voltage (0.65 V). The parameters used for efficiency analysis in this work are shown in Table 6. The main purpose of examining LT-PEMFC and HT-PEMFC for small household electricity generation is to determine the system that will achieve the maximum possible overall efficiency. In order to improve the system efficiency, the cogeneration system of heat and power is also considered.

The system efficiency of individual integrated PEMFC system at full (3 kW) and partial loads (50%, 1.5 kW) is shown in Table 7. It is found that the highest system efficiency is obtained when using HT-PEMFC system with WGS reactor (case 2) followed closely by LT-PEMFCs. While the HT-PEMFC system without the WGS reactor (case 1) provides the lowest system efficiency among the studied systems. Without WGS, a higher steam to carbon ratio is required to reduce the fraction of CO in the reformate gas and thus, high

Table 7System efficiency and water balance of the designed PEMFC systems.

Parameters	Full load	Partial load
Net power (kW)	3	1.5
Voltage (V) • HT-PEMFC system (case 1) • HT-PEMFC system (case 2) • LT-PEMFC system	0.65 0.65 0.65	0.716 0.723 0.766
Current (A) • HT-PEMFC system (case 1) • HT-PEMFC system (case 2) • LT-PEMFC system	5621 5619 5639	2487 2458 2300
Parasitic loss (W) • HT-PEMFC system (case 1) • HT-PEMFC system (case 2) • LT-PEMFC system	665 653 652	261 281 278
Glycerol flow rate (mol/s) • HT-PEMFC system (case 1) • HT-PEMFC system (case 2) • LT-PEMFC system	0.0065 0.0055 0.0056	0.0029 0.0024 0.0023
System efficiency (%) • HT-PEMFC system (case 1) • HT-PEMFC system (case 2) • LT-PEMFC system	27.55 32.98 29.03	30.96 37.48 35.30
Water balance (mole/s) • HT-PEMFC system (case 1) • HT-PEMFC system (case 2) • LT-PEMFC system	0.0074 0.0076 0.0097	0.0033 0.0033 0.0040

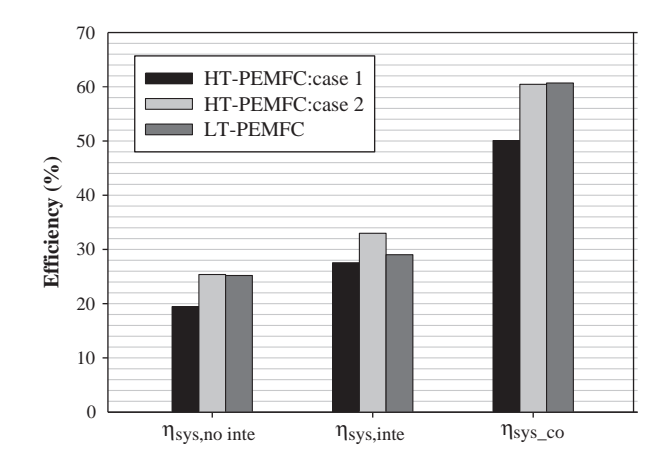


Fig. 8. PEMFC System efficiencies with and without heat integration between PEMFC and reforming process ($\eta_{\text{sys,int}}$ and $\eta_{\text{sys,noint}}$) as well as cogeneration system efficiency ($\eta_{\text{sys,co}}$).

Table 8The released heat from fuel cell and the flow rate of produced hot water (323.15 K) in each system.

System	Released heat from fuel cell (W)	Molar flow rate of hot water (L/min)
HT-PEMFC system (case 1)	3126	1.816
HT-PEMFC system (case 2)	3080	1.790
LT-PEMFC system	3297	1.916

energy is required to generate steam for this system. In addition, in the HT-PEMFC system (case 1), the reformate gas obtained from the glycerol processor contains a lower hydrogen fraction and a higher CO fraction, compared to the HT-PEMFC system with WGS (case 2). Additionally, the high CO fraction results in a large anode activation loss (case 1). When the system is operated at partial load

condition (1.5 kW), a higher efficiency is achieved (from 33% to 37.5% for HT-PEMFC case 2) on the expense of lower power output (50%). In addition, the water balance of all the systems shows a positive value even at the half load condition. This means water recovered from the PEMFC system is sufficient and exceeds the required amount for reformer and humidifier operation (for LT-PEMFC system).

The system efficiency with and without heat integration between PEMFC and reforming process ($\eta_{\rm sys,int}$ and $\eta_{\rm sys,noint}$) as well as cogeneration system efficiency ($\eta_{\rm sys,co}$) of individual integrated system are shown in Fig. 8. It is found that the PEMFC system without heat integration between PEMFC and the reforming process provides low overall efficiency around 20-25%. However, the system efficiency increases to 28-33% when heat recovered from anode and cathode exhaust gas is used to maintain the endothermic reforming process. The results show that this integrated system provides higher efficiency than a conventional electrical generator like a gas turbine. The efficiency (based on a lower heating value) of a glycerol combustion engine is around 19-29% depending on operation conditions of gas turbine. It is noted that the predicted system efficiency is in the same range of the achieved efficiency reported in other works: HT-PEMFC system [32] and LT-PEMFC system [33]. In addition, it is found that the system efficiency increases further to 50–60% (cogeneration system efficiency) when the released heat from the electrochemical reaction is utilized to heat up water for household usage. The LT-PEMFC shows higher cogeneration system efficiency than HT-PEMFC system (case 1) and has a similar efficiency to the HT-PEMFC system (case 2). This is because at a given operating voltage (0.65), the current density of LT-PEMFC and HT-PEMFC system (case 2) is higher than HT-PEMFC system (case 1). Therefore, the heat released from the electrochemical reaction and cogeneration efficiency (see Eq. (17)) of LT-PEMFC and HT-PEMFC systems (case 2) are higher. In addition, the released heat from fuel cell and the molar flow of produced hot water (323.15 K) are shown in Table 8.

5. Conclusions

The system efficiency of HT-PEMFC systems with different fuel processors for a small 3 kW stationary application is investigated and compared with a LT-PEMFC system. The HT-PEMFC system integrates a glycerol reformer with and without a CO removal process using a water gas shift reactor. For pure hydrogen operation, LT-PEMFC shows higher performance than HT-PEMFC at a practical operation (cell voltage of 0.5-0.7). However, for reformate gas operation, the HT-PEMFC system with the water gas shift reactor provides higher performance than the LT-PEMFC system when the system operating pressure is 3 atm and the fuel cell is operated at current density higher 4000 A m⁻² (cell voltage less than 0.6 V). Considering the system efficiency, it is found that HT-PEMFC system with water gas shift reactor shows the highest value, followed by the LT-PEMFC system and the HT-PEMFC system without the water gas shift reactor. The highest efficiency obtained from HT-PEMFC system is approximately 33% and 37.5% at full load and partial load conditions, respectively. Furthermore, the efficiency can be increased up to 60% in case of HT-PEMFC system with the water gas shift reactor and LT-PEMFC system when the heat generated in the fuel cell is used to produce hot water for cogeneration system (household usage).

Acknowledgements

This work was supported by the Higher Education Research Promotion and National Research University Project of Thailand, Office of the Higher Education Commission (EN280A) and Ratchadaphiseksomphot Endowment Fund (CU-CLUSTER-FUND). The authors also gratefully acknowledge the support of the Thailand Research Fund (TRF).

References

- Corbo P, Migliardini F, Veneri O. Experimental analysis of a 20 kW_e PEM fuel cell system in dynamic conditions representative of automotive applications. Energy Convers Manage 2008;49:2688–97.
- [2] Wang Y, Chen KS, Mishler J, Cho SC, Adroher XC. A review of polymer electrolyte membrane fuel cells: technology, applications, and needs on fundamental research. Appl Energy 2011;88:981–1007.
- [3] Hou Y, Wang B, Yang Z. A method for evaluating the efficiency of PEM fuel cell engine. Appl Energy 2011;88:1181–6.
- [4] Arsalis A, Nielsen MP, Kær SK. Modeling and off-design performance of a 1 kW_e HT-PEMFC (high temperature-proton exchange membrane fuel cell)-based residential micro-CHP (combined-heat-and-power) system for Danish single-family households. Energy 2011;36:993–1002.
- [5] Das SK, Reis A, Berry KJ. Experimental evaluation of CO poisoning on the performance of a high temperature proton exchange membrane fuel cell. J Power Sources 2009;193:691–8.
- [6] Cipiti F, Pino L, Vita A, Lagan M, Recupero V. Model-based investigation of a CO preferential oxidation reactor for polymer electrolyte fuel cell systems. Int J Hydrogen Energy 2007;32:4040–51.
- [7] Song S, Douvartzides S, Tsiakaras P. Exergy analysis of an ethanol fuelled proton exchange membrane (PEM) fuel cell system for automobile applications. J Power Sources 2005;145:502–14.
- [8] Scott K, Pilditch S, Mamlouk M. Modelling and experimental validation of a high temperature polymer electrolyte fuel cell. J Appl Electrochem 2007;37:1245–59
- [9] Lindstrom B, Karlsson JAJ, Ekdunge P, De Verdier L, Haggendal B, Dawody J, et al. Diesel fuel reformer for automotive fuel cell applications. Int J Hydrogen Energy 2009;34:3367–81.
- [10] Slinn M, Kendall K, Mallon C, Andrews J. Steam reforming of biodiesel byproduct to make renewable hydrogen. Bioresour Technol 2008;99:5851–8.
- [11] Byrd AJ, Pant KK, Gupta RB. Hydrogen production from glycerol by reforming in supercritical water over Ru/Al₂O₃ catalyst. Fuel 2008;87:2956–60.
- [12] Pompeo F, Santori G, Nichio NN. Hydrogen and/or syngas from steam reforming of glycerol. Study of platinum catalysts. Int J Hydrogen Energy 2010:35:8912–20.
- [13] Chen H, Ding Y, Cong NT, Dou B, Dupont V, Ghadiri M, et al. A comparative study on hydrogen production from steam-glycerol reforming: thermodynamics and experimental. Renew Energy 2011;36:779–88.
- [14] Sopena D, Melgara A, Briceno Y, Navarrob RM, Alvarez-Galvan MC, Rosa F. Diesel fuel processor for hydrogen production for 5 kW fuel cell application. Int J Hydrogen Energy 2007;32:1429-36.
- [15] Barbir F. PEM fuel cells: theory and practice. In: Sammes N, editor. Fuel cell technology reaching towards commercialization. Germany: Springer Academic Press; 2006. p. 27–52.

- [16] Hubert CE, Achard P, Metkemeijer R. Study of a small heat and power PEM fuel cell system generator. J Power Sources 2006;156:64–70.
- [17] Oh SD, Kim KY, Oh SB, Kwak HY. Optimal operation of a 1-kW PEMFC-based CHP system for residential applications. Appl Energy 2012;95:93–101.
- [18] Barelli L, Bidini G, Gallorini F, Ottaviano A. An energetic-exergetic analysis of a residential CHP system based on PEM fuel cell. Appl Energy 2011;88:4334-42.
- [19] Zalc JM, Loffler DG. Fuel processing for PEM fuel cells: transport and kinetic issues of system design. J Power Sources 2002;111:58–64.
- [20] Chen WH, Hsieh TC, Jiang TL. An experimental study on carbon monoxide conversion and hydrogen generation from water gas shift reaction. Energy Convers Manage 2008;49:2801–8.
- [21] Hu JE, Pearlman JB, Jackson GS, Tesluk CJ. Evaluating the impact of enhanced anode CO tolerance on performance of proton-exchange-membrane fuel cell systems fueled by liquid hydrocarbons. J Power Sources 2010;195:1926–35.
- [22] Mamlouk M, Sousa T, Scott K. A high temperature polymer electrolyte membrane fuel cell model for reformate gas. Int J Electrochem 2011;2011:1–18.
- [23] Bhatia KK, Wang CY. Transient carbon monoxide poisoning of a polymer electrolyte fuel cell operating on diluted hydrogen feed. Electrochim Acta 2004;34:2333-41.
- [24] Springer TE, Zawodzinski TA, Gottesfeld S. Polymer electrolyte fuel cell model. J Electrochem Soc 1991;138:2334–42.
- [25] Yan Q. Toghiani H, Causey H. Steady state and dynamic performance of proton exchange membrane fuel cells (PEMFCs) under various operating conditions and load changes. J Power Sources 2006;161:492–502.
- [26] Ziogou C, Voutetakis S, Papadopoulou S, Georgiadis MC. Modeling, simulation and experimental validation of a PEM fuel cell system. Comput Chem Eng 2011:35:1886–900.
- [27] Authayanun S, Mamlouk M, Arpornwichanop A. Maximizing the efficiency of a HT-PEMFC system integrated with glycerol reformer. Int J Hydrogen Energy 2012;37:6808–17.
- [28] Slattery JC, Bird RB. Calculation of the diffusion coefficient of dilute gases and of the self-diffusion coefficient of dense gases. AIChE J 1958;4:137–42.
- [29] Parthasarathy A, Srinivasan S, Appleby AJ, Martin CR. Temperature dependence of the electrode kinetics of oxygen reduction at the platinum/ Nafion interface – a microelectrode investigation. J Electrochem Soc 1992:139:2530-7.
- [30] Mamlouk M, Scott K. The effect of electrode parameters on performance of a phosphoric acid-doped PBI membrane fuel cell. Int J Hydrogen Energy 2010;35:784–93.
- [31] Authayanun S, Wiyaratn W, Assabumrungrat S, Arpornwichanop A. Theoretical analysis of a glycerol reforming and high-temperature PEMFC integrated system: hydrogen production and system efficiency. Fuel 2013;105:345–52.
- [32] Martin S, Worner A. On-board reforming of biodiesel and bioethanol for high temperature PEM fuel cells: comparison of autothermal reforming and steam reforming. J Power Sources 2011;196:3163–71.
- [33] De Melo Furtado JG, Gatti GC, Serra ET, Anibal de Almeida SC. Performance analysis of a 5 kW PEMFC with a natural gas reformer. Int J Hydrogen Energy 2010;35(18):9990–5.



Contents lists available at SciVerse ScienceDirect

Energy

journal homepage: www.elsevier.com/locate/energy



Performance analysis of an integrated biomass gasification and PEMFC (proton exchange membrane fuel cell) system: Hydrogen and power generation



Bhawasut Chutichai ^a, Suthida Authayanun ^b, Suttichai Assabumrungrat ^a, Amornchai Arpornwichanop ^{a, c, *}

- ^a Department of Chemical Engineering, Faculty of Engineering, Chulalongkorn University, Bangkok 10330, Thailand
- ^b Department of Chemical Engineering, Faculty of Engineering, Srinakharinwirot University, Nakhon Nayok 26120, Thailand
- ^c Computational Process Engineering, Department of Chemical Engineering, Faculty of Engineering, Chulalongkorn University, Bangkok 10330, Thailand

ARTICLE INFO

Article history: Received 17 November 2012 Received in revised form 29 March 2013 Accepted 30 March 2013 Available online 29 April 2013

Keywords:
Biomass gasification
PEMFC
Hydrogen
Integrated system
Performance analysis

ABSTRACT

The PEMFC (proton exchange membrane fuel cell) is expected to play a significant role in next-generation energy systems. Because most hydrogen that is used as a fuel for PEMFCs is derived from the reforming of natural gas, the use of renewable energy sources such as biomass to produce this hydrogen offers a promising alternative. This study is focused on the performance analysis of an integrated biomass gasification and PEMFC system. The combined heat and power generation output of this integrated system is designed for residential applications, taking into account thermal and electrical demands. A flowsheet model of the integrated PEMFC system is developed and employed to analyze its performance with respect to various key operating parameters. A purification process consisting of a water—gas shift reactor and a preferential oxidation reactor is also necessary in order to reduce the concentration of CO in the synthesis gas to below 10 ppm for subsequent use in the PEMFC. The effect of load level on the performance of the PEMFC system is investigated. Based on an electrical load of 5 kW, it is found that the electrical efficiency of the PEMFC integrated system is 22%, and, when waste heat recovery is considered, the total efficiency of the PEMFC system is 51%.

© 2013 Elsevier Ltd. All rights reserved.

1. Introduction

The PEMFC (proton exchange membrane fuel cell) has received growing attention as an efficient power generation device due to its low emissions, potentially high energy density, compactness, modularity, light weight, fast start-up and fast response to load changes. For residential applications, PEMFCs can be employed as either primary or backup energy sources; a PEMFC can produce about 5 kW of power or 120 kWh of energy per day as a cogeneration system [1].

Pure hydrogen is an ideal fuel for PEMFCs; however, it is not available in nature and must be extracted from various fuels via reforming technologies. Most fuels considered to be hydrogen sources are based on hydrocarbon compounds [2]. These include

E-mail address: Amornchai.A@chula.ac.th (A. Arpornwichanop).

coal [3], natural gas [4] and methanol [5], all of which contain carbon, hydrogen and oxygen. Since hydrocarbon fuels are derived from petroleum, which is an inherently limited source of energy, the use of renewable fuels such as biomass to produce hydrogen has been widely explored [6]. Several types of biomass are considered to be valuable feedstocks for hydrogen production processes [7]. Among the various fuel production processes available, gasification is accepted as an efficient technology for the conversion of biomass to synthesis gas [8]. Using steam as a major gasifying agent seems to be an effective method for producing hydrogen-rich gas [9]; however, in practice, air is generally fed into the gasifier in order to enhance the combustion reaction [10] and to enable self-sustainable operation of the system [11]. Because synthesis gas obtained from gasification contains a high CO fraction that can deteriorate PEMFC performance, a purification process is necessary to decrease the content of CO to an acceptable of 10 ppm or less to avoid catalyst poisoning [12,13].

PEMFC-based cogeneration systems have higher efficiencies than traditional power generation systems because heat and electricity are generated and utilized closer to the user. Various studies

 $^{^{*}}$ Corresponding author. Department of Chemical Engineering, Faculty of Engineering, Chulalongkorn University, Bangkok 10330, Thailand. Tel.: $+66\ 2\ 218\ 6878$; fax: $+66\ 2\ 218\ 6877$.

on PEMFC systems have been performed over the past several decades. The chemical and thermodynamic aspects of the electrical characteristics of a PEMFC were studied by Yan et al. [14] and Asl et al. [15]. Although the design and analysis of fuel cell-based CHP (combined heat and power) systems are subjects of interest [1,16], only limited information is available regarding PEMFC systems integrated with biomass gasification. Toonssen et al. [17] studied the integration of PEMFC and biomass gasification. The results of this study indicated that the efficiency of such an integrated system is around 30%. The effect of the purity level of hydrogen on the efficiency of the cogeneration system was investigated without considering the effect of the operating parameters on the gasification process and the fuel cell.

It is known that the performance of heat and power cogeneration systems depends on their operating conditions. Thus, a comprehensive understanding of a biomass gasification system coupled with PEMFC is essential for achieving efficient system operation. The goal of this study is to analyze the performance of an integrated biomass gasification and PEMFC system. The simulation of this integrated system is carried out using a process flowsheet simulator to investigate system performance with respect to key operating parameters, including air and steam feed rate, gasification temperature, biomass composition and load change. The PEMFC integrated system studied in this work is designed to supply an electrical load of 5 kW to cover a power demand for residential applications. The efficiency of the PEMFC system including heat recovery is also considered.

2. Integrated biomass gasification and PEMFC system

Fig. 1 shows a schematic diagram for the integrated biomass gasification and PEMFC system. It consists of two main sections: (1) the hydrogen production and purification system, in which biomass is converted into an H₂-rich gas via a fluidized bed gasifier; and (2) the PEMFC stack, in which electricity is generated from the electrochemical reaction of hydrogen and oxygen. This goal of this study is to design and analyze this integrated PEMFC system. A systematic model-based procedure is shown in Fig. 2. First, models of the hydrogen production process and PEMFC are developed and the reliability of the developed models is verified by comparing the modeling results against data reported in the literature. The next

step involves parametric analysis. For the biomass gasification process, the effect of the operating conditions is investigated to find optimal conditions at which a maximum quantity of H_2 is produced. Finally, performance of the PEMFC integrated system is analyzed to determine the electrical, thermal and overall efficiencies. In this study, the PEMFC system is designed with a power generation of 5 kW.

2.1. Hydrogen production from biomass gasification

This section describes the hydrogen production system for the integrated PEMFC system, which is based on a biomass gasification process. The goal of this system is to produce H₂-rich gas with the required quality and in the required quantity to satisfy the demands of the PEMFC. This system plays a key role in the PEMFC integrated system because of the complexity of the biomass conversion processes, including the biomass gasification and hydrogen purification processes. The hydrogen production system consists of three major units: (1) a biomass gasifier, which converts biomass into H₂-rich gas; (2) high- and low-temperature water—gas shift reactors (HTS and LTS), which remove CO via reaction with steam to produce CO₂ and additional H₂; and (3) a PROX (preferential oxidation reactor) in which the remaining CO in the H₂ feed is reduced to an acceptable level for PEMFC applications (less than 10 ppm).

The reactions that take place in the hydrogen production system are summarized in Table 1. In this study, all gaseous products obtained from each unit are at chemical equilibrium. All gasifier and purification reactors are operated at steady-state, isothermal and isobaric conditions. The compositions of the gaseous streams associated with the gasifier, water—gas shift reactors and preferential oxidation reactor, which contain H₂, CO, CO₂, CH₄, N₂, and H₂O, are determined by minimizing the Gibbs free energy using a flowsheet simulator (Aspen Plus). Various types of biomass feedstock have been used as a carbon source in gasification process such as sewage sludge [18], crop residues [19] and wooden waste [16]. Wooden waste like sawdust, which is widely available in Thailand, is selected as a model biomass feedstock.

Fig. 3 shows the flowsheet for the hydrogen production process based on biomass gasification. The stream BIOMASS is specified as a nonconventional stream. Biomass is fed to DECOMP (RYield), where thermal decomposition occurs and volatile matter, such as H₂, N₂,

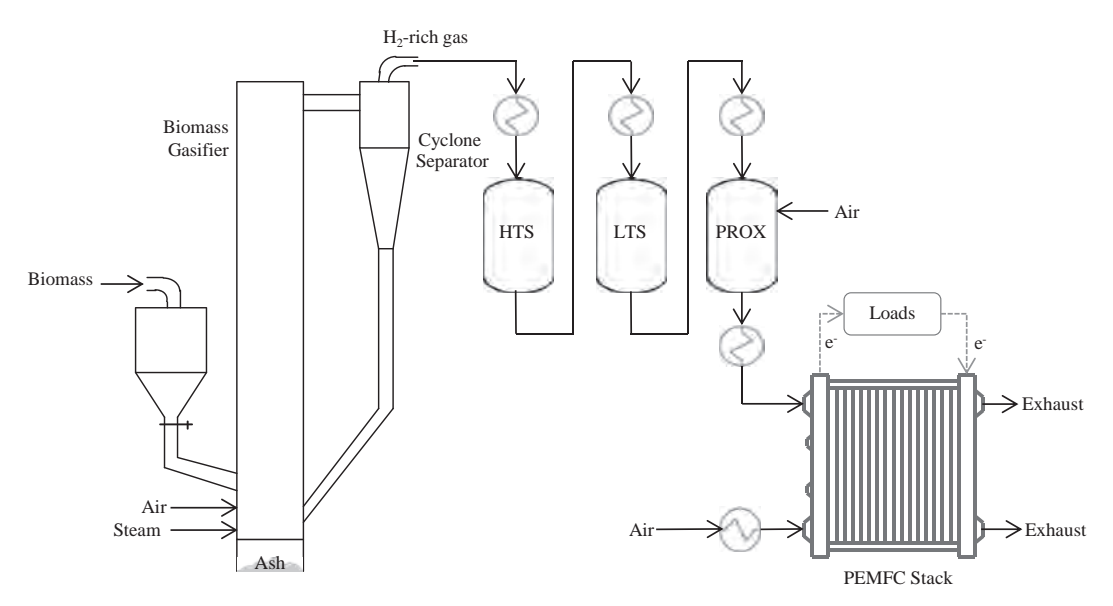


Fig. 1. Schematic diagram of the air—steam biomass gasification and PEMFC integrated system.

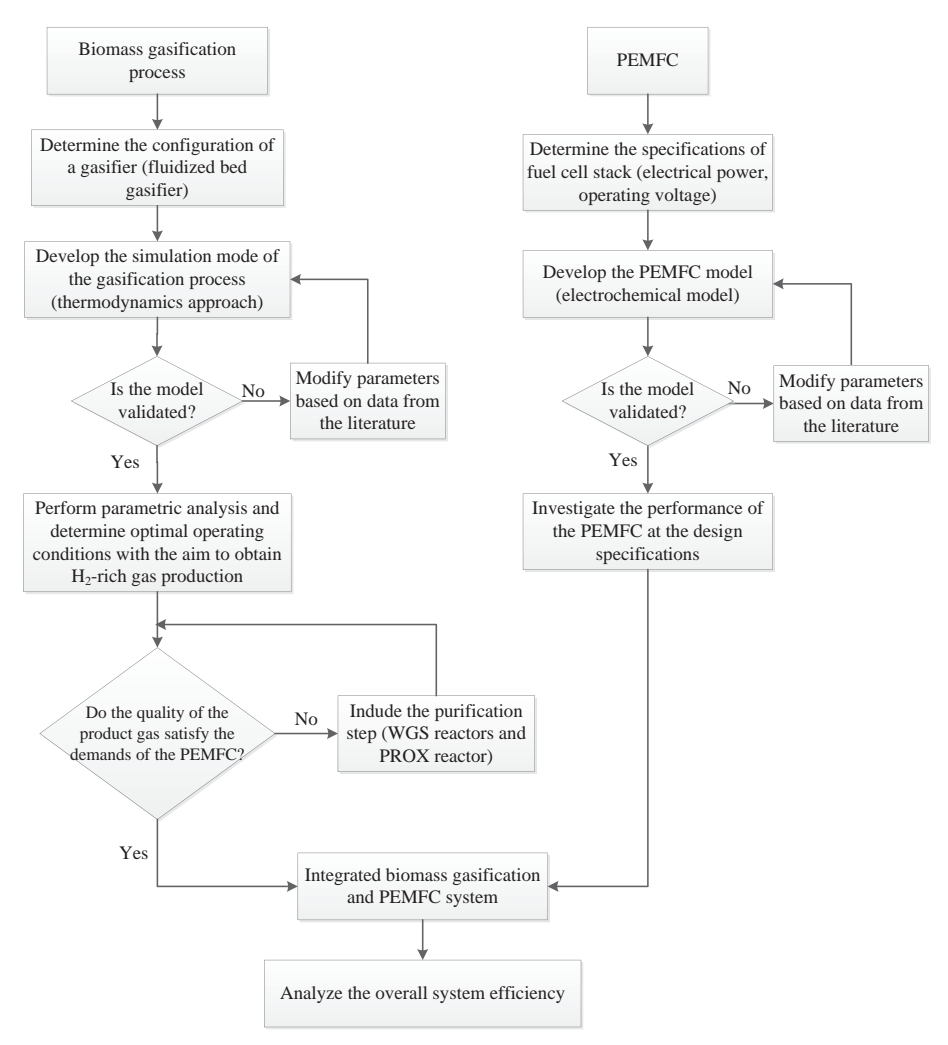


Fig. 2. A systematic model-based analysis of the PEMFC integrated system.

O₂ and S (sulfur), solid particles (carbon) and ash, are generated. This unit is modeled by specifying the distribution of the product yields based on the ultimate analysis of the biomass feedstock. The enthalpy of the product steam is balanced by inserting the heat stream Q-DECOMP. Gasifying agent streams representing steam and air are fed into the GASIF1 reactor (RGibbs). The product gas the GASIF2 reactor (RGibbs) is then sent to ASHSEP (SEP) to remove ash. The unit CYCLONE (SEP) represents a cyclone separator. The residual solid carbon (SOLID) is removed and subsequently fed to the

Table 1Reactions involved in the hydrogen production process.

Biomass gasification Heterogeneous reactions		
Char partial combustion	C + 0.50 ₂ ↔ CO	$\Delta H_{\text{near}}^0 = -111 \text{ kJ/mol}$
Boudouard	$C + CO_2 \leftrightarrow CO$	$\Delta H_{298}^0 = -111 \text{ kJ/mol} \ \Delta H_{298}^0 = +172 \text{ kJ/mol} \$
Water–gas	$C + B_2O \leftrightarrow CO + H_2$	$\Delta H_{298}^{0} = +131 \text{ kJ/mol}$
Methanation	$C + 2H_2 \leftrightarrow CH_4$	$\Delta H_{208}^0 = -75 \text{ kJ/mol}$
Homogeneous reactions	2 3	250
CO partial combustion	$CO + 0.5O_2 \leftrightarrow CO_2$	$\Delta H_{298}^0 = -283 \text{ kJ/mol}$ $\Delta H_{298}^0 = -242 \text{ kJ/mol}$
H ₂ partial combustion	$H_2 + 0.5O_2 \leftrightarrow H_2O$	$\Delta H_{298}^{030} = -242 \text{ kJ/mol}$
Water-gas shift	$CO + H_2O \leftrightarrow CO_2 + H_2$	$\Delta H_{298}^{\circ} = -41 \text{ kJ/mol}$
Steam-methane reforming	$CH_4 + H_2O \leftrightarrow CO + 3H_2$	$\Delta H_{298}^0 = +206 \text{ kJ/mol}$
Water—gas shift reactor (H	TS, LTS)	
Water-gas shift	$CO + H_2O \leftrightarrow CO_2 + H_2$	$\Delta H_{298}^0 = -41 \text{ kJ/mol}$
Preferential oxidation reac	tor (PROX)	
CO oxidation	$CO \ + \ 0.5O_2 \leftrightarrow CO_2$	$\Delta H_{298}^0 = -283 \text{ kJ/mol}$

unit CSEP (SEP), from which the solid carbon is circulated back to the gasification process. The stream CWASTE carries 2% of the total solid carbon obtained from the biomass. This stream is mixed with ash in a mixing unit (forming the stream ASH-C).

The operating parameters of the gasification process are obtained from Li et al. [20]. It is assumed that the residual carbon loss to ash in the gasifier is 2% and that the heat loss from the gasifier is equal to 3% of the heat input. The efficiency of the cyclone separation is 85% [21]. In the HTS and LTS reactors (HTS and LTS), the water—gas shift reaction between CO and steam occurs. The HTS (high-temperature water—gas shift reactor) is operated at 400 °C and the LTS (low temperature water—gas shift reactor) is operated at 200 °C [22]. The CO-selective oxidation reaction takes place in the preferential oxidation reactor, represented by the unit PROX in Fig. 3. This reactor is operated at 150 °C [22].

2.2. PEMFC stack

The PEMFC represents one of the most promising power generation technologies for converting the chemical energy contained in hydrogen into electrical power in a single step. A PEMFC system consists of a polymer electrolyte membrane sandwiched between two electrodes: an anode and a cathode. The electrochemical reactions that take place in the fuel cell stack are as follows:

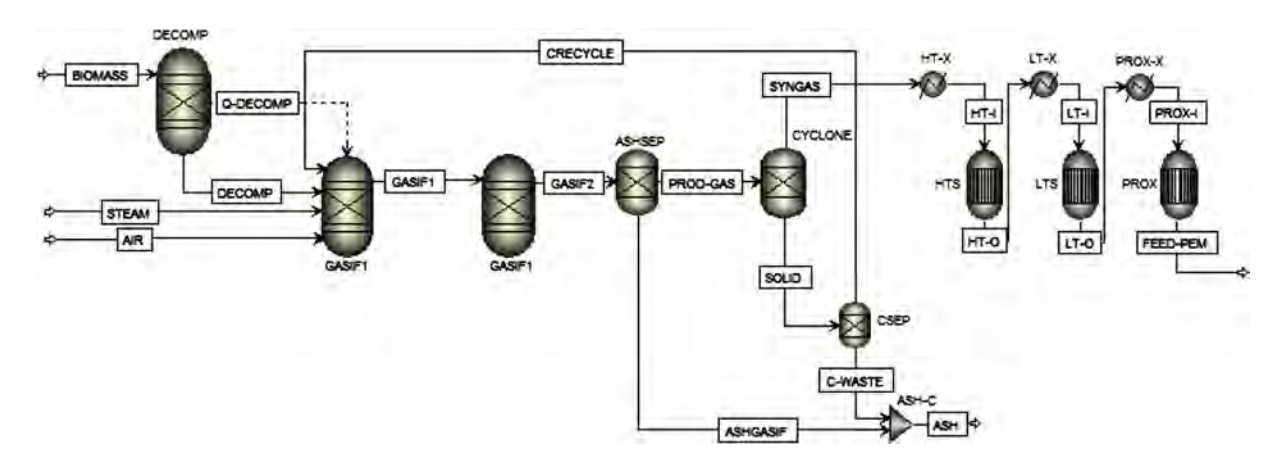


Fig. 3. Flowsheet of the hydrogen production system based on the gasification process.

 $\begin{array}{ll} \text{Anode}: & \text{H}_2 \! \to \! \text{H}^+ + 2e^- \\ \text{Cathode}: & 0.5O_2 + \text{H}^+ + 2e^- \! \to \! \text{H}_2O \\ \text{Overall}: & \text{H}_2 + 0.5O_2 \! \to \! \text{H}_2O \end{array}$

In this study, the electrochemical model used to describe the electrical characteristics of the PEMFC is derived from Springer et al. [23] under the following assumptions: steady-state and isothermal conditions, ideal gas behavior, and no membrane swelling. Anode losses in the fuel cell are not considered due to the fast kinetics of the hydrogen oxidation reaction [24]. The overall cell voltage is obtained by determining the reversible cell potential and then subtracting the voltage losses, such as the kinetic voltage losses at the cathode and the Ohmic resistances of membrane and electrodes. This relationship is described in Eq. (1),

$$E_{\text{cell}} = E_{\text{rev}} - \eta_{\text{c}} - iR, \tag{1}$$

where $E_{\rm cell}$ represents the overall cell voltage, $E_{\rm rev}$ is the reversible cell potential or thermodynamic voltage, η_c is the cathode potential loss and iR is the Ohmic resistance loss.

The reversible voltage can be estimated by using the Nernst equation (Eq. (2)),

$$E_{\text{rev}} = E_{\text{rev}}^0 + \frac{RT}{nF} \ln \left[\frac{P_{\text{H}_2}(P_{\text{O}_2})^{0.5}}{\alpha_{\text{H}_2\text{O}}} \right],$$
 (2)

where $E_{\rm rev}^0$ is the reversible voltage at standard temperature and pressure, T is the operating temperature, R is the ideal gas constant (=8.314 J mol⁻¹ K⁻¹), n is the number of moles of electrons transferred (=2), F is the Faraday constant, $P_{\rm H_2}$ is the partial pressure of H_2 , $P_{\rm O_2}$ is the partial pressure of O_2 and O_2 is the water activity.

In order to calculate the cathode potential losses, the Butler–Volmer equation (Eq. (3)) is employed:

$$i = i_0 \left[\exp\left(\frac{-\alpha_c F}{RT} \eta_c\right) - \exp\left(\frac{\alpha_a F}{RT} \eta_c\right) \right], \tag{3}$$

where i is the current density, i_0 is the exchange current density, α_c is the transfer coefficient of the cathodic reaction (=0.5) and α_a is the transfer coefficient of the anodic reaction (=0.5).

The Ohmic resistance loss depends on the proton conductivity through the membrane (Nafion[®]) and electrodes. In this study, values for the proton conductivity of Nafion[®] and the membrane resistance (R) are taken from the work of Springer et al. [23].

At steady-state conditions, the quantity of H_2 (N_{H_2}) that is consumed by the electrochemical reactions can be derived from the following equation:

$$N_{\rm H_2} = \frac{i}{nE} \tag{4}$$

In general, the operating voltage of a PEMFC has a direct impact on the current and power generation. Typically, a PEMFC is operated at 0.6–0.8 V, compromising its power output [25,26]. In this study, it is assumed that the nominal cell voltage for a single cell of a PEMFC is 0.7 V at full load [27]. Table 2 shows the specifications and operating conditions of a PEMFC stack designed for 5 kW of electrical power. To determine the performance of the PEMFC, the fuel cell stack efficiency is defined as shown in Eq. (5):

Stack efficiency(%) =
$$\frac{P_{e}(W)}{m_{H_2} \times HHV_{H_2}} \times 100,$$
 (5)

where $P_{\rm e}$ is the electrical power that is generated from the fuel cell stack, $m_{\rm H_2}$ is the flow rate of H₂ that is actually supplied to the fuel cell and HHV_{H₂} is the higher heating value of H₂.

2.3. Model validation

The models of the biomass gasification and PEMFC systems described in the previous section are validated to confirm their reliability before they are used to investigate the performance of the integrated PEMFC system for power generation. Fig. 4 shows the model prediction for the product gas composition obtained from the gasification process compared with experimental results obtained under the same conditions reported by Karatas et al. [28]. In the study of Karatas et al. [28], a fluidized-bed gasifier was used to gasify tire waste with different gasifying agents: CO₂, air and steam. Considering the air—steam gasification using commercial tire scraps as an input fuel, these authors reported various experimental results. Experiment number 2 (T#2) from their work [28] was chosen for the model validation. The input data for T#2 are as follows: the gasifying agent consists of air and steam, the gasification agent temperature is 230 °C and the steam-to-air ratio is

Table 2Design specifications and operating conditions for the PEMFC.

Number of cells	50	cells
Active area	0.072	m²/cell
Electrical power	5	kW
Operating voltage	0.7	V/cell
Operating temperature	80	°C
Operating pressure	1	atm
Fuel utilization [30]	80	%
Oxygen utilization [18,30]	50	%

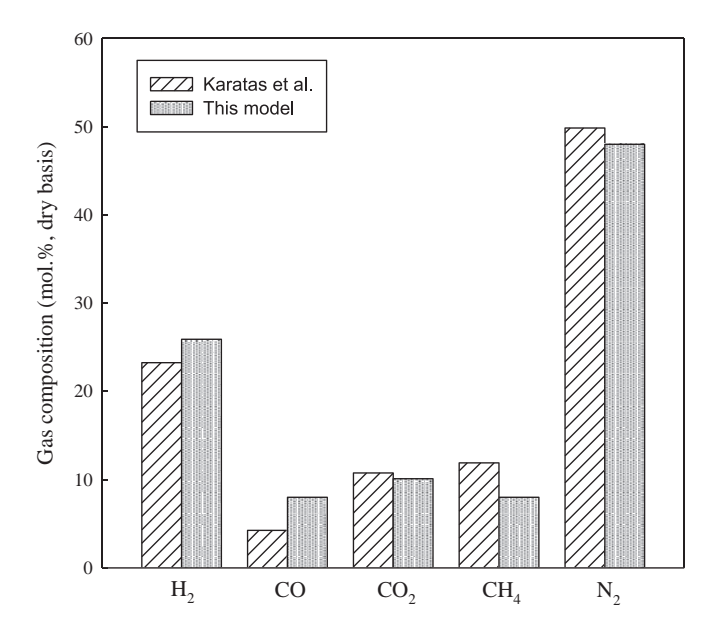


Fig. 4. Comparison of the product gas composition obtained from the model predictions and from data reported in the literature by Karatas et al. [28].

0.239. Fig. 4 shows that the model predictions are found to be in good agreement with the experimental results.

The PEMFC model is validated against the experimental data of Yan et al. [14], who investigated the performance of a PEMFC stack at both steady-state and transient conditions. Yan et al. [14] reported five experimental runs at steady-state to investigate the effect of operating temperature. For model validation, experimental data for a PEMFC stack with an operating temperature of 80 $^{\circ}$ C, an H₂ stoichiometry of 1.2, an air stoichiometry of 2, an anode humidity of 100% and a cathode humidity of 100% were selected. The results indicate that the model predictions and experimental results for the polarization curve are in good agreement (Fig. 5).

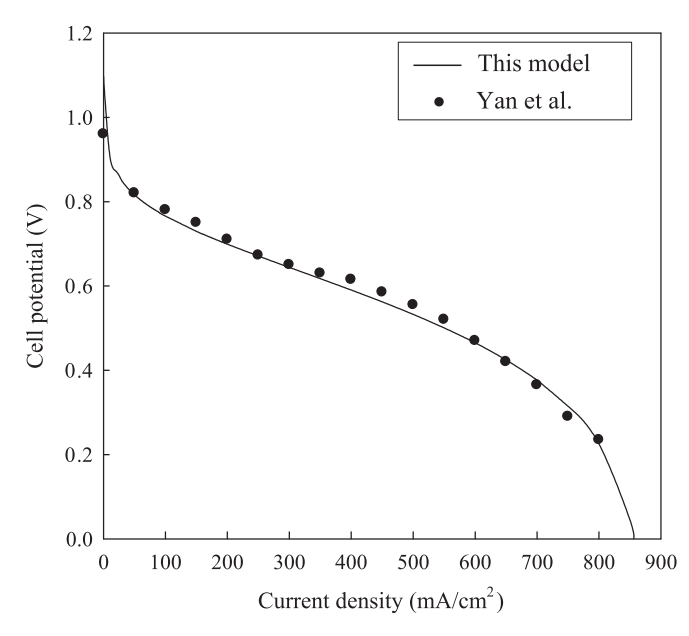


Fig. 5. Comparison of the cell potential obtained from the model predictions and from data reported in the literature by Yan et al. [14].

3. Results and discussion

In this section, the performances of the biomass gasification system for hydrogen production and the PEMFC system for power generation are investigated. Synthesis gas from the gasification process is treated to reduce the quantity of CO it contains to an acceptable level for PEMFC operation. Key operating parameters of the biomass gasifier studied here include the biomass source, the oxygen ER (equivalence ratio), the gasification temperature, and the steam-to-biomass ratio. The performance of the PEMFC is examined by considering the polarization curve. Electrical and thermal efficiencies of the integrated system are also considered. The ER is defined as the ratio of air fed into the gasifier to the stoichiometric amount of air required for complete combustion.

3.1. Effect of biomass source

The effect of biomass composition on the gas produced by the gasification process is studied. The biomass feedstocks considered in this study are wood waste (sawdust), sugarcane bagasse, corn straw, rice husks and rice straw. Table 3 shows the proximate and ultimate analyses and the heating value for each biomass source. The results shown in Fig. 6 indicate that, at the same operating condition, all product gases from the gasification, regardless of the biomass source, contain primarily H₂ and CO₂. The quantities of these major gasification products present in the synthesis gas do not differ significantly among different feedstocks. This results from the similar compositions of all feedstocks, as observed in the results of the ultimate analysis. However, it is expected that the content of H₂ in the synthesis gas could increase if biomass with a high carbon fraction and low ash fraction were used.

3.2. Effect of oxygen equivalence ratio

Since steam gasification is a highly endothermic reaction, air is introduced into the gasifier in order to enhance the combustion of oxygen and solid carbon in the biomass, thereby utilizing the combustion heat to maintain the steam gasification reaction. The amount of air fed into the gasifier is represented by the oxygen equivalence ratio (ER). Fig. 7 shows that when the gasifier is operated at a higher ER, less H_2 is generated. This is because a large quantity of solid carbon is lost as a result of the partial combustion with O_2 . Additionally, the partial combustion of CO and H_2 is more pronounced, decreasing the fractions of H_2 , CO and CH_4 . It is also observed that the fraction of N_2 in the synthesis gas product increases. This is the major drawback of introducing air into the gasifier. The N_2 dilution effect lowers the heating value of the product gas, as shown in Fig. 8. Furthermore, reductions in the H_2

Table 3 Biomass compositions.

Material	Proximate analysis (wt.%)						HHV (MJ/kg)		
	VM	FC	Ash	С	Н	N	0	S	
Sawdust ^a	79.50	16.80	3.70	44.13	6.50	-	45.73	0.08	18.47 ^c
Sugarcane bagasse ^b	83.66	13.15	3.20	45.48	5.96	45.21	0.15	-	18.73
Corn straw ^b	73.15	19.19	7.65	44.73	5.87	0.60	40.44	0.70	17.68
Rice husks ^b	61.81	16.95	21.24	38.50	5.20	_	34.61	_	14.69
Rice straw ^b	65.47	15.86	18.67	38.24	5.20	0.87	36.26	0.18	15.09

VM = volatile matter and FC = fixed carbon.

^a Tan and Zhong [31].

^b Yin [32].

^c Calculated by modified Dulong's equation [33].

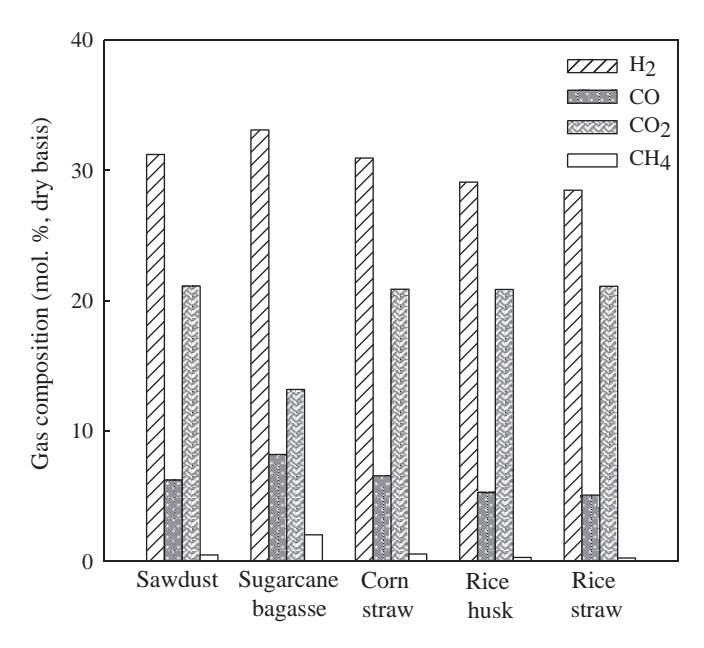


Fig. 6. Effect of biomass source on the composition of the product gas from gasification (temperature = 650 $^{\circ}$ C, ER = 0.28, S/B = 1.0, moisture content = 10%).

and CO yields with increasing ER reduce the heating value of the synthesis gas; a low-quality product gas is therefore obtained.

As mentioned previously, in the air—steam gasification process, the heat of the combustion reaction is used for the endothermic gasification reaction. As a result, it is possible to balance the combustion and gasification reactions by adjusting the air supply such that a self-sustaining energy condition is reached at which an external heat input is unnecessary. The simulation results show that the gasifier can be operated at self-sustaining conditions when air is fed at an ER of 0.28. It should be noted that the demand for air can be reduced when useful heat in the high-temperature product gas is recovered to preheat the air before it is fed to the gasifier.

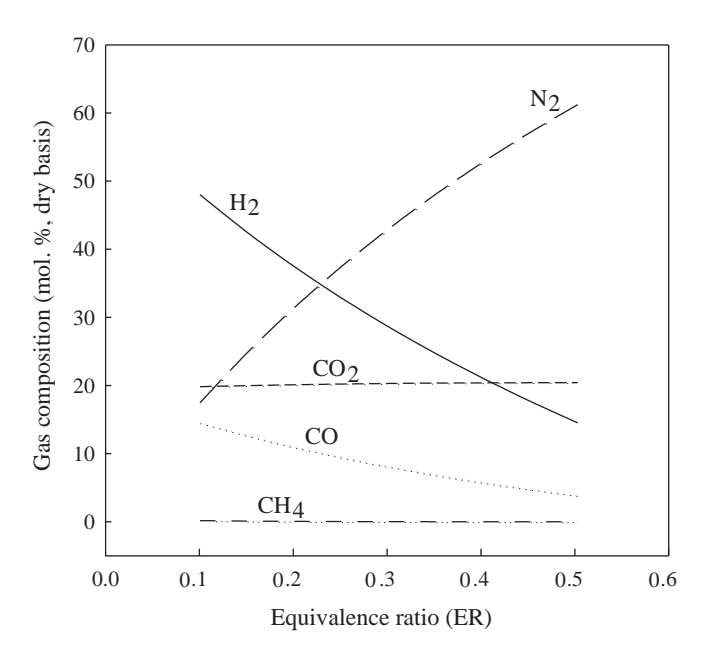


Fig. 7. Effect of oxygen equivalence ratio on the composition of the product gas from gasification (temperature =650 °C, S/B =1.0).

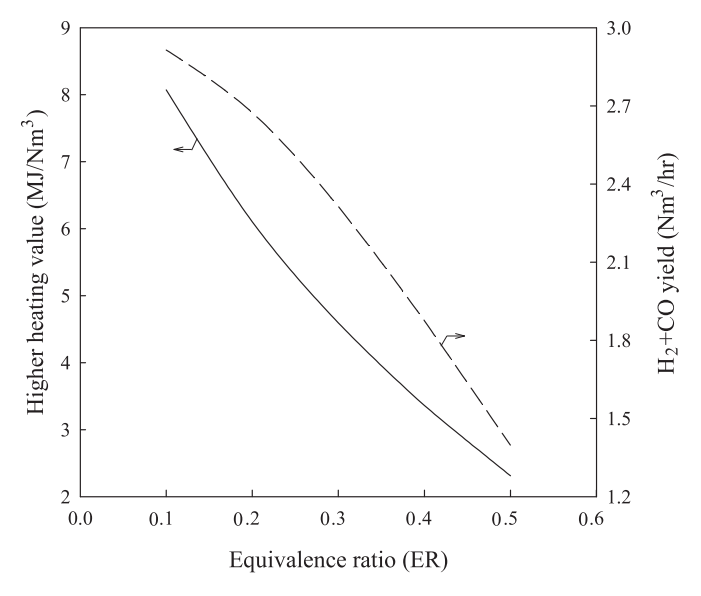


Fig. 8. Effect of oxygen equivalence ratio on the higher heating value and the H_2 and CO yield of the product gas (temperature = 650 °C, S/B = 1.0).

3.3. Effect of gasification temperature

Gasification temperature is one of the most important parameters affecting the H_2 yield. Fig. 9 presents the H_2 yield as a function of the gasification temperature for different values of ER. At ER = 0.28, the H_2 yield initially increases with increased gasification temperature, reaches a maximum at a temperature around 650 °C, and then slightly decreases. When the gasification temperature is increased, the extents of the Boudouard, water—gas shift and reforming reactions are all increased, resulting in an increase in the quantity of H_2 generated. However, at temperatures higher than 650 °C, the H_2 yield is reduced as a result of the reverse water—gas shift reaction.

3.4. Effect of steam-to-biomass ratio

Steam plays a key role in the production of hydrogen-rich gas from the gasification process, because it affects the water—gas shift,

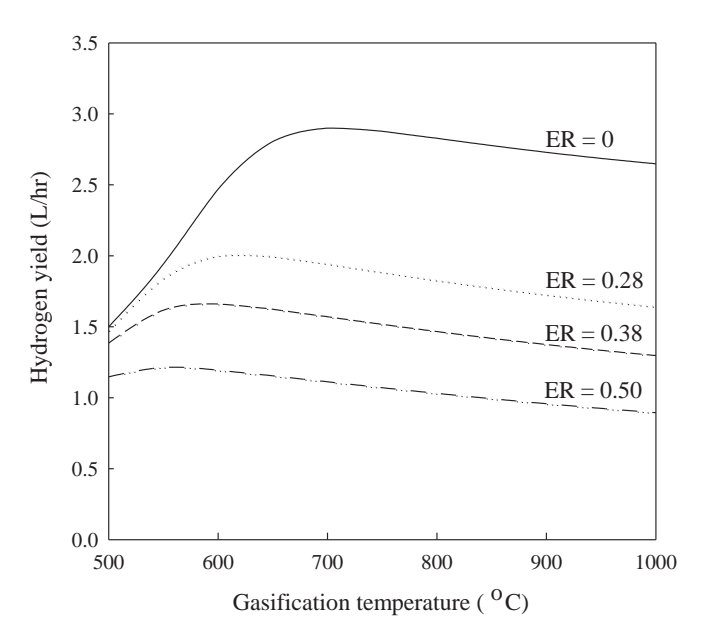


Fig. 9. Effect of gasification temperature on the $\rm H_2$ yield for different values of equivalence ratio.

water—gas and reforming reactions. Fig. 10 shows the effect of the S/B ratio (steam-to-biomass) on the composition of the product gas. When a larger fraction of steam is added to the gasifier, the concentrations of H_2 and CO_2 increase, but those of CO and CH_4 decrease. However, when the gasifier is operated at a higher S/B, a higher energy input is needed for increased steam production. Under the conditions studied, the optimal value for the S/B is in the range of 0.8-1.2. Within this range, synthesis gas with an H_2 fraction of 30 mol.% is generated.

3.5. Hydrogen purification process

Since the product gas from the biomass gasifier contains a CO fraction in excess of the maximum specification for PEMFC operation, the product gas is passed through high- and low-temperature water—gas shift reactors (HTS and LTS) and a preferential oxidation reactor (PROX). The product gas compositions at the outlets of the gasifier, HTS reactor, LTS reactor and PROX reactor are shown in Fig. 11. The final product gas used as a fuel for the PEMFC stack is composed of 33 mol.% H₂ with a CO concentration less than 10 ppm. The efficiency of the hydrogen-production system for converting the energy in biomass into H₂-rich gas is 57.50%.

3.6. PEMFC performance

The performance of the PEMFC is evaluated using a polarization curve showing the relationship between current density, cell potential and power. Fig. 12 shows that the cell potential decreases with increasing current density because larger voltage losses are observed at higher current densities. The maximum power that the PEMFC can generate is around 10 kW at 0.45 V. At this condition, the stack efficiency of the PEMFC is quite low; it is not suitable to operate the PEMFC at its maximum power. Typically, a cell potential of around 0.7 V is chosen as an operating point [30]. Under the design conditions for which the PEMFC is operated at 0.7 V, the generated current density is equal to 198 mA/cm² and 5 kW of electrical power is produced.

In general, the fuel cell stack efficiency is directly related to the fuel cell potential. An increase in the load level results in a decrease in both the fuel cell potential and stack efficiency, as shown in

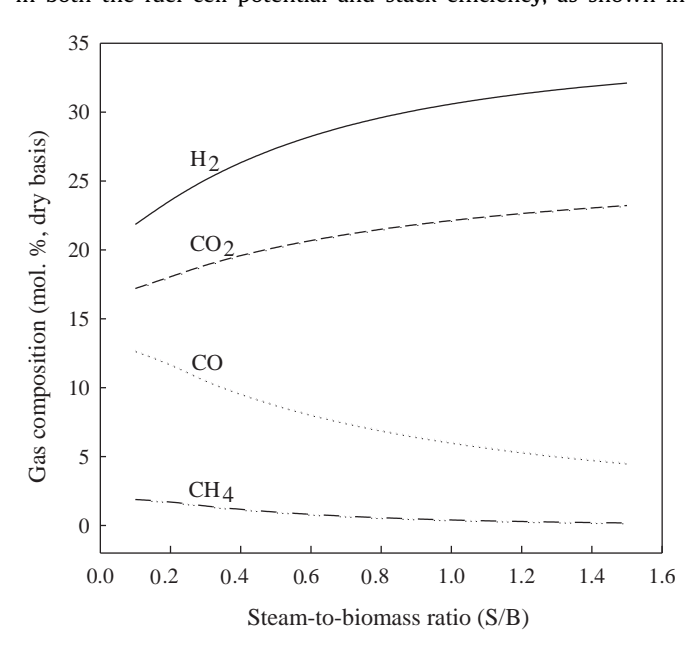


Fig. 10. Effect of steam-to-biomass ratio on the product gas composition (temperature = 650 °C, ER = 0.28).

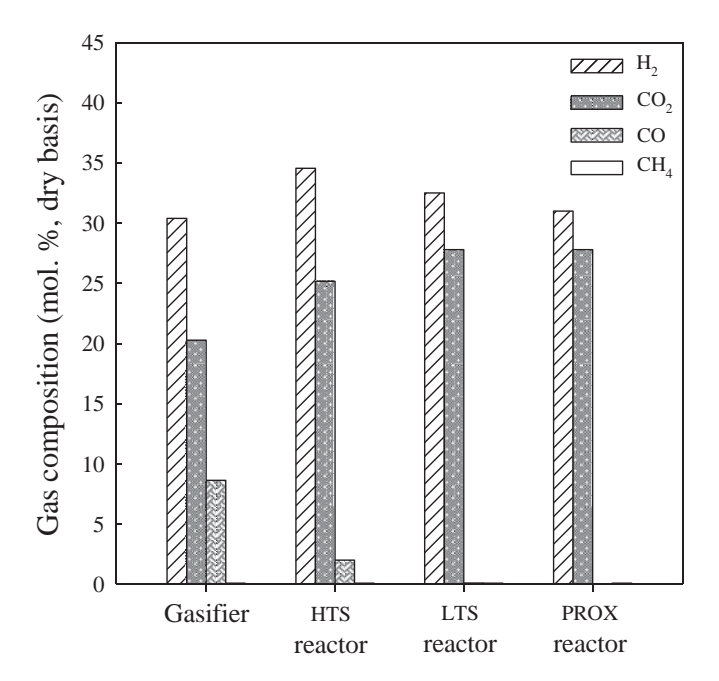


Fig. 11. Product gas compositions at the outlets of the gasifier, HTS reactor, LTS reactor and PROX reactor.

Fig. 13. This implies that, for the required load level, the PEMFC may be operated at a higher efficiency but at a significantly lower power output. At the chosen design condition (5 kW of power generation), the stack efficiency is 47.23% based on the energy content of the hydrogen fed to the stack. By examining the energy contained in the exhaust gas leaving the PEMFC stack, it is found that the thermal energy obtained from the PEMFC stack is around 7.7 kW. This value is computed from the enthalpy of the exhaust gas using the reference temperature of 25 °C. This thermal energy can be utilized for space heating or water heating.

3.7. Performance of the PEMFC integrated system

The biomass gasification and PEMFC integrated system is designed based on a combined heat and power generation

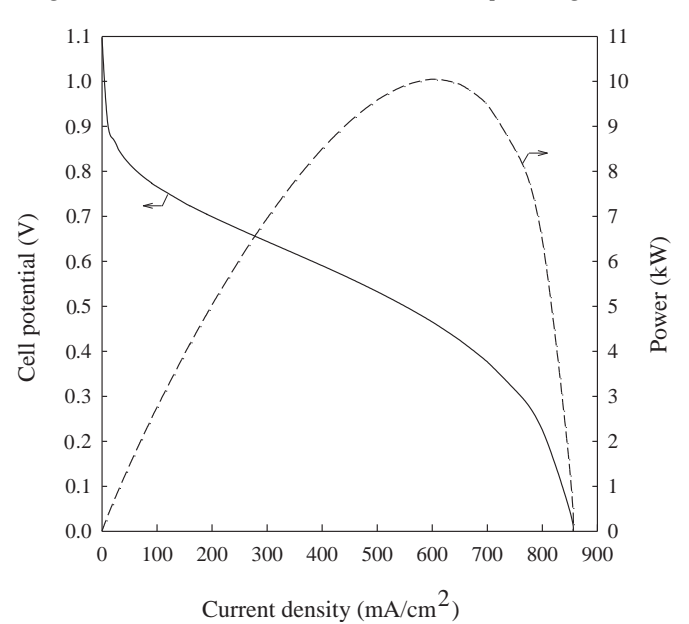


Fig. 12. Polarization curve for the PEMFC.

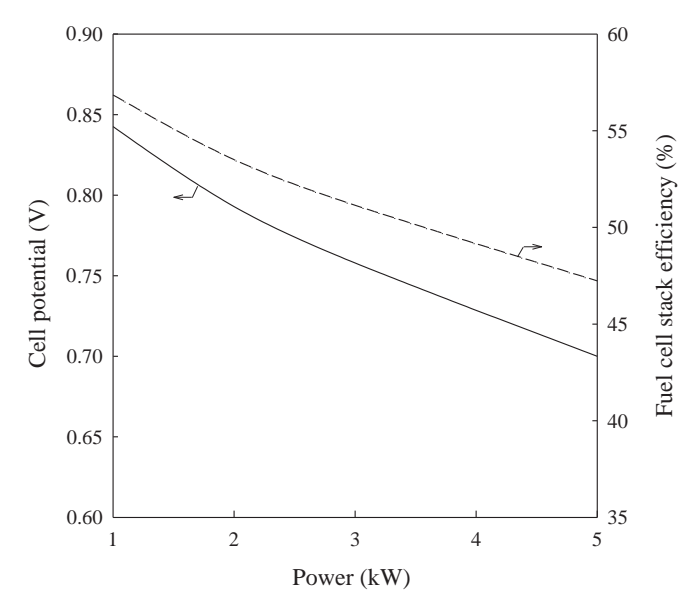


Fig. 13. Effect of load levels on the cell potential and the fuel cell stack efficiency.

approach. This system involves the recovery of waste thermal energy back into the system as a useful thermal power. The performance of this integrated system is defined by its ability to convert the chemical energy contained in biomass into electrical and thermal power. The electrical and thermal efficiencies of the PEMFC integrated system are defined by Eqs. (6) and (7) [29,30]:

System electrical efficiency(%) =
$$\frac{P_{e}(W)}{m_{\text{biomass}} \times \text{HHV}_{\text{biomass}}} \times 100$$
, (6)

System thermal efficiency(%) =
$$\frac{P_h}{m_{\text{biomass}} \times \text{HHV}_{\text{biomass}}} \times 100$$
, (7)

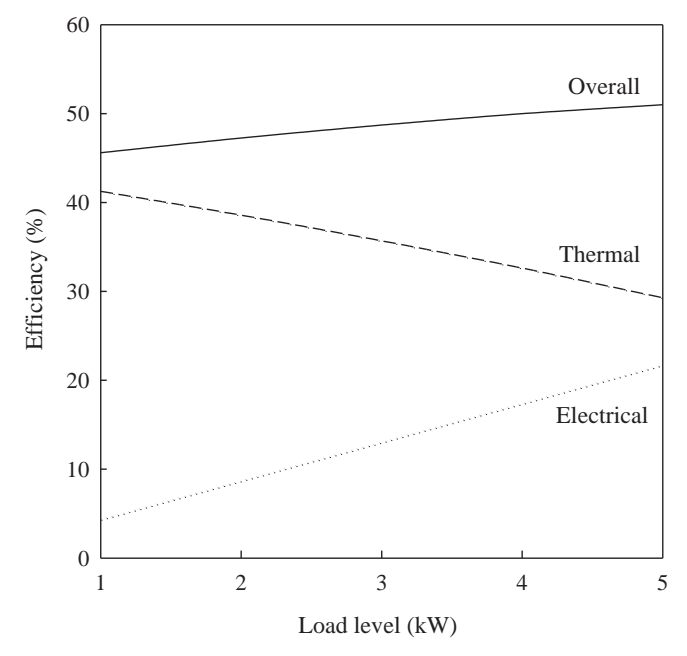


Fig. 14. Efficiency of the PEMFC integrated system.

where m_{biomass} is the mass flow rate of the biomass and HHV_{biomass} is the higher heating value of the biomass.

The overall efficiency of the system is determined from Eq. (8), which represents the ratio of usable energy (electricity and heat) to the energy input [29]:

Overall efficiency(%) =
$$\frac{P_{\rm e} + P_{\rm h}(W)}{m_{\rm biomass} \times {\rm HHV_{biomass}}} \times 100.$$
 (8)

In this study, it is found that changes in the load levels have an impact on the system performance, as shown in Fig. 14. The electrical efficiency is increased with increasing load level because a higher fraction of the energy in the biomass is converted into electricity to meet the power demand. When the system is operated at a higher load level, more hydrogen is consumed and the quality of the exhaust gas from the PEMFC stack is therefore reduced, resulting in a reduction in thermal efficiency. Under the optimal operating conditions described earlier, the PEMFC integrated system has an electrical efficiency of 22% and a thermal efficiency of 29%. Thus, when the waste thermal energy is recovered within the system, the overall efficiency of this integrated system is increased to 51%.

4. Conclusions

In this study, an integrated biomass gasification and PEMFC system was proposed for combined heat and power cogeneration. Simulations of the integrated PEMFC system using sawdust as the major feedstock were performed to analyze the effect of the operating parameters on its performance. Biomass gasification was coupled with a water—gas shift reactor and a preferential oxidation reactor to purify the synthesis gas obtained from the gasifier. It was found that when the gasifier is operated at an optimal operating temperature in the range of 600—650 °C, a steam-to-biomass ratio of 0.8—1.2 and an oxygen equivalence ratio of 0.28, the synthesis gas obtained contains approximately 33 mol.% H₂ and the efficiency of the gasifier in converting biomass is around 57%. The PEMFC stack generates electricity and low-grade heat with an efficiency of 47—60%. The total efficiency of the PEMFC integrated system operated at the design condition is around 51%.

Acknowledgments

Support from the Thailand Research Fund, Thailand's Higher Education Commission and Ratchadaphiseksomphot Endowment Fund (CU-CLUSTER-FUND) is gratefully acknowledged.

B. Chutichai would like to thank the Dutsadiphiphat Scholarship, Ratchadaphiseksomphot Endowment Fund, Chulalongkorn University.

References

- [1] Gencoglu M, Ural Z. Design of a PEM fuel cell system for residential application. International Journal of Hydrogen Energy 2009;34:5242-8.
- [2] Ersoz A. Investigation of hydrocarbon reforming processes for micro-cogeneration systems. International Journal of Hydrogen Energy 2008;33:7084–94.
- [3] Liszka M, Malik T, Manfrida G. Energy and exergy analysis of hydrogenoriented coal gasification with CO₂ capture. Energy 2012;45:142–50.
- [4] Welaya Y, Gohary M, Ammar N. Steam and partial oxidation reforming options for hydrogen production from fossil fuels for PEM fuel cells. Alexandria Engineering Journal 2012;51:69-75.
- [5] Chrenko D, Gao F, Blunier B, Bouquain D, Miraoui A. Methanol fuel processor and PEM fuel cell modeling for mobile application. International Journal of Hydrogen Energy 2010;35:6863-71.
- [6] Kalinci Y, Hepbasil A, Dincer I. Biomass-based hydrogen production: a review and analysis. International Journal of Hydrogen Energy 2009;34:8799–817.
- [7] Ni M, Leung D, Leung M, Sumathy K. An overview of hydrogen production from biomass. Fuel Processing Technology 2006;87:461–72.
- [8] Panepinto D, Genon G. Solid waste and biomass gasification: fundamental processes and numerical simulation. Chemical Engineering Transactions 2011;24:25–30.

- [9] Umeki K, Yamamoto K, Namioka T, Yoshikawa K. High temperature steam only gasification of woody biomass. Applied Energy 2010;87:79–98.
- [10] Doherty W, Reynolds A, Kenedy D. The effect of air preheating in a biomass CFB gasifier using ASPEN Plus simulation. Biomass and Bioenergy 2009;33:1158–67.
- [11] Mathieu P, Dubuisson R. Performance analysis of a biomass gasifier. Energy Conversion and Management 2002;43:1291–9.
- [12] Bhatia K, Wang C. Transient carbon monoxide poisoning of a polymer electrolyte fuel cell operating on diluted hydrogen feed. Electrochimica Acta 2004;49:2333—41.
- [13] Zamel N, Li X. Effect of contaminants on polymer electrolyte membrane fuel cells. Progress in Energy and Combustion Science 2011;37:292–329.
- [14] Yan Q, Toghiani H, Causey H. Steady state and dynamic performance of proton exchange membrane fuel cells (PEMFCs) under various operating conditions and load changes. Journal of Power Sources 2006:161:492–502.
- [15] Asl S, Rowshanzamir S, Eikani M. Modelling and simulation of the steady-state and dynamic behavior of a PEM fuel cell. Energy 2010;35:1633—46.
- [16] Francois J, Abdelouahed L, Mauviel G, Feidt M, Rogaume C, Mirgaux O, et al. Estimation of the energy efficiency of a wood gasification CHP plant using Aspen Plus. Chemical Engineering Transactions 2012;29:769–74.
- [17] Toonssen R, Woudstra N, Verkooijen A. decentralized generation of electricity from biomass with proton exchange membrane fuel cell. Journal of Power Sources 2004:194:456–66.
- [18] Werle S, Wilk R. Experimental investigation of the sewage sludge gasification process in the fixed bed gasifier. Chemical Engineering Transactions 2012;29: 715–70
- [19] Azlina W, Ghani W. Modelling and optimization of gasification for palm kernel shell (PKS) in a fluidized bed gasifier. In: The 20th international congress of chemical and process engineering (CHISA 2012); Aug. 25–29, 2012, Prague, Czech Republic
- [20] Li XT, Grace JR, Lim CJ, Watkinson AP, Chen HP, Kim JR. Biomass gasification in a circulating fluidized bed. Biomass and Bioenergy 2004;26:171–93.

- [21] Zhang R, Basu P. A simple model for prediction of solid collection efficiency of a gas-solid separator. Powder Technology 2004;147:86–93.
- [22] Sammes N. Fuel cell technology reaching toward commercialization. Germany: Springer; 2006.
- [23] Springer T, Zawodzinski T, Gottesfeld S. Polymer electrolyte fuel cell model. Journal of the Electrochemical Society 1991;138:2234–42.
- [24] Liu RS, Zhang L, Sun X, Lui H, Zhang J. Electrochemical technologies for energy storage and conversion. Singapore: Wiley; 2012.
- [25] Grujicic M, Chittajallu KM. Design and optimization of polymer electrolyte membrane (PEM) fuel cells. Applied Surface Science 2004;227:56-72.
- [26] Pearlman JB, Bhargav A, Shields EB, Jackson GS, Hearn PL. Modeling efficiency and water balance in PEM fuel cell systems with liquid fuel processing and hydrogen membranes, Journal of Power Sources 2008;185:1056—65.
- [27] Barbir F. PEM fuel cell theory and practice. 1st ed. US: Academic Press: Elsevier Inc.; 2005.
- [28] Karatas H, Olgun H, Akgun F. Experimental results of gasification of waste tire with air&CO₂, air&steam and steam in a bubbling fluidized bed gasifier. Fuel Processing Technology 2012;102:166–74.
- [29] Ertesvag I. Exergetic comparison of efficiency indicators for combined heat and power (CHP). Energy 2007;33:2038–50.
- [30] Corre O, Rahmouni C, Saikaly K, Dincer I. Effect of H₂ produced through steam methane reforming on CHP plant efficiency. International Journal of Hydrogen Energy 2011;36:11457–66.
- [31] Tan W, Zhong Q. Simulation of hydrogen production in biomass gasifier by ASPEN PLUS. Proceeding of Power and Energy Engineering Conference 2010: 1–4.
- [32] Yin CY. Prediction of higher heating values of biomass from proximate and ultimate analyses. Fuel 2011;90:1128—32.
- [33] Tchobanoglous G, Theisen H, Vigil SA. Integrated solid waste management: engineering principles and management issues. International editions, Civil Engineering series. US: McGraw Hill; 1993.



Contents lists available at SciVerse ScienceDirect

Chemical Engineering Research and Design



journal homepage: www.elsevier.com/locate/cherd

Investigation of a proton-conducting SOFC with internal autothermal reforming of methane

Amornchai Arpornwichanopa, Yaneeporn Patcharavorachotb,*

- ^a Computational Process Engineering, Department of Chemical Engineering, Faculty of Engineering, Chulalongkorn University, Bangkok 10330, Thailand
- ^b School of Chemical Engineering, Faculty of Engineering, King Mongkut's Institute of Technology Ladkrabang, Bangkok 10520, Thailand

ABSTRACT

This study presents a performance analysis of a proton-conducting SOFC (SOFC-H⁺) with internal reforming of methane. The autothermal reforming within the SOFC-H⁺ stack is considered to be a potential solution of the carbon formation problem facing in operation of internal steam reforming SOFC-H⁺. A one-dimensional, steady-state model of the SOFC-H⁺ coupled with a detailed electrochemical model is employed to investigate its performance in terms of power density and fuel cell efficiency. The simulation results show that when SOFC-H⁺ is operated under an autothermal reforming environment, the presence of carbon monoxide, which is a major cause of carbon formation, in the fuel cell stack decreases. Effect of key operating parameters, such as temperature, steam-to-carbon and oxygen-to-carbon feed ratios, current density and fuel utilization, on the SOFC-H⁺ performance in terms of electrical efficiencies and energy demand is also investigated. The results indicate that operating temperatures have strong influence on SOFC-H⁺ performance, carbon monoxide production and heat generation.

© 2013 The Institution of Chemical Engineers. Published by Elsevier B.V. All rights reserved.

Keywords: Proton-conducting SOFC; Direct internal reforming; Autothermal reforming; Theoretical analysis

1. Introduction

A solid oxide fuel cell (SOFC) has attracted considerable interest for distributed power sources due to its higher efficiency, compared with other types of fuel cell. Typically, SOFC is operated under high temperatures (800–1000 °C) and thus, a waste gas released from SOFC stack at high temperatures can be used as a heat source for cogeneration applications and bottoming cycles to further enhance the overall efficiency of a power system (Akkaya et al., 2008; Santin et al., 2010). In addition, various hydrocarbon fuels, e.g., methane, ethanol, methanol, ammonia and biogas, can be directly fed to the SOFC anode side where hydrogen is generated through reforming reactions and used for power generation (Arpornwichanop et al., 2009, 2010; Shiratori et al., 2010; Vakouftsi et al., 2011; Hajimolana et al., 2012; Leone et al., 2012). This operation is referred to as a direct internal reforming SOFC (DIR-SOFC). The benefits of DIR-SOFC are that no external reformer is needed and the overall system efficiency is higher as well as the operating cost can be reduced (Arpornwichanop et al., 2010).

In general, there are two types of electrolyte (i.e., oxygenion and proton-conducting electrolytes) possible for use in SOFCs. For a conventional SOFC based on an oxygen-ion conductor (SOFC-O²⁻), oxygen ions migrate through the electrolyte from the cathode to the anode and react with hydrogen at the anode side to produce water and electrons. Water generated at the anode always dilutes the concentration of hydrogen, and thereby decreasing fuel cell efficiency. In case of an SOFC based on a proton conductor (SOFC-H+), protons are formed at the anode side, move to the cathode side and react with oxygen to produce electrons and water. As a result, the performance of SOFC-H+ is not influenced by a dilution effect. In addition, because SOFC-H+ exhibits a high proton conductivity at intermediate temperature operations (300-700 °C) (D'Epifanio et al., 2008), it is possible to use SOFC-H+ for vehicular applications with an acceptable start-up time (Zamfirescu

^{*} Corresponding author. Tel.: +66 2 3298360; fax: +66 2 3298360x4. E-mail address: kpyaneep@kmitl.ac.th (Y. Patcharavorachot).

Nomenclature cross section area of reactor (m²) heat capacity of component i (J/mol K) $C_{p,i}$ C_i molar concentration of component i (mol m^{-3}) D_{an,eff} effective gas diffusion coefficient in the anode side ($m^2 s^{-1}$) $D_{\text{ca,eff}} \\$ effective gas diffusion coefficient in the cathode side ($m^2 s^{-1}$) activation energy (kJ/mol) E_a $E_{a,j}$ E^{OCV} activation energy of reaction j (J/mol) open-circuit voltage (OCV) (V) E^0 OCV at standard temperature and pressure (V) F Faraday's constant ($C \text{ mol}^{-1}$) molar flow rate of air (mol s^{-1}) F_{air} molar flow rate of the fuel (mol s^{-1}) F_{fuel} h_a air channel height (m) h_{f} fuel channel height (m) $\Delta H_{\text{ads,i}}$ adsorption heat of components i heat of reactions j (J/mol) H_i j_{ave,j} average and local current density (A m^{-2}) $j_{0,\text{electrode}}$ exchange current density (A m⁻²) equilibrium constant for water gas shift reac- K_{eq} tion k_0 pre-exponential constant for reforming reaction (mol s⁻¹ m⁻² bar⁻¹) k_i rate constant of reactions j (mol/kgs) k_{oj} pre-exponential factor of rate constant for reactions j (mol/kgs) $K_{eq,j}$ equilibrium constant of reactions j adsorption coefficient of component i K_i K_i^0 adsorption coefficient of component i for oxidation reaction van't Hoff parameters of component i Koi pre-exponential factor for water gas shift reac k_{WGSR} tion (mol s⁻¹ m⁻³ Pa⁻²) cell length (m) LHV lower heating value (kJ/mol) number of electrons participating in the electrochemical reaction P absolute pressure (kPa) partial pressure of component i (kPa) p_i P_{SOFC} power density (W m^{-2}) ohmic resistance (Ω m²) R_{ohm} R gas constant (kJ $mol^{-1} K^{-1}$) rate of reaction j (mol m⁻² s⁻¹) R_i Т temperature (K) fuel utilization U_{fuel} air velocity ($m s^{-1}$) u_a fuel velocity ($m s^{-1}$) Иf V operating cell voltage (V)

W

٧i

 ε_{SOFC}

 η_{act}

 η_{con}

 $\eta_{\rm ohm}$

Greek symbols

cell width (m)

transfer coefficient

porosity of catalyst

fuel cell efficiency (%)

ohmic overpotential (V)

activation overpotential (V)

concentration overpotential (V)

mole fraction of component i

```
conductivity of electrolyte (\Omega^{-1} m<sup>-1</sup>)
\sigma_{\rm ele}
           anode thickness (m)
\tau_{an}
           cathode thickness (m)
\tau_{ca}
           electrolyte thickness (m)
\tau_{\rm ele}
           effectiveness factor of reactions j
\eta_i
           density of catalyst (kg/m<sup>3</sup>)
\rho_{cat}
           stoichiometric coefficient of component i in
           reaction j
Superscripts
           electrode|electrolyte interface
in
           feed inlet condition
Subscripts
           air channel
а
           anode
an
           cathode
ca
cat
           catalyst
ele
           electrolyte
           fuel channel
f
           component
i
           reaction
j
           channel
k
```

and Dincer, 2009). Due to the advantages of SOFC-H⁺, many researchers have concentrated on development of a proton-conducting electrolyte for SOFC-H⁺ (Taherparvar et al., 2003; Jamsak et al., 2009; Ni et al., 2008; Zamfirescu and Dincer, 2009; Arpornwichanop et al., 2010; Patcharavorachot et al., 2010; Ding et al., 2011; Bavarian and Soroush, 2012); however, works on design and analysis of SOFC-H⁺ in either stack or system levels are quite limited, especially on the SOFC-H⁺ with DIR operation (Jamsak et al., 2009; Ni et al., 2008; Arpornwichanop et al., 2010).

Theoretically, the reforming process for the DIR operation of SOFCs involves an endothermic steam reforming reaction to which the heat released from electrochemical reactions in fuel cell can supply. However, the high endothermicity of steam reforming reaction and the unbalance of reaction heats may cause a large temperature gradient across the SOFC stack. This factor leads to high internal stresses in the cell component and consequently, a mechanical failure (Aguiar et al., 2004; Vijay et al., 2012). In addition, a complete internal reforming of fuel may lead to a carbon deposition at the anode side, resulting in loss of the SOFC performance (Chen et al., 2011). It is also reported that when the SOFC-H⁺ is operated under the internal steam reforming of methane, high content of carbon monoxide (25 mol.%) exists in the fuel channel and would cause a carbon formation, according to the Boudouard reaction (2CO \rightarrow C+CO₂), thereby hindering the SOFC-H⁺ performance (Arpornwichanop et al., 2010). To overcome such a difficulty, oxygen or air is fed to the SOFC-H+ coupled with methane and steam feed streams. The combination of steam reforming and partial oxidation, also known as an autothermal reforming operation, provides efficient heat balance and can decrease the requirement of an external heat for the reaction (Hiei et al., 1996; Authayanun et al., 2010; Dokmaingam et al., 2008). Furthermore, it was reported in the literature that the addition of air to the steam reforming reaction suppresses the carbon formation (Laosiripojana et al., 2007; Halabi et al., 2008). To improve its performance and achieve its

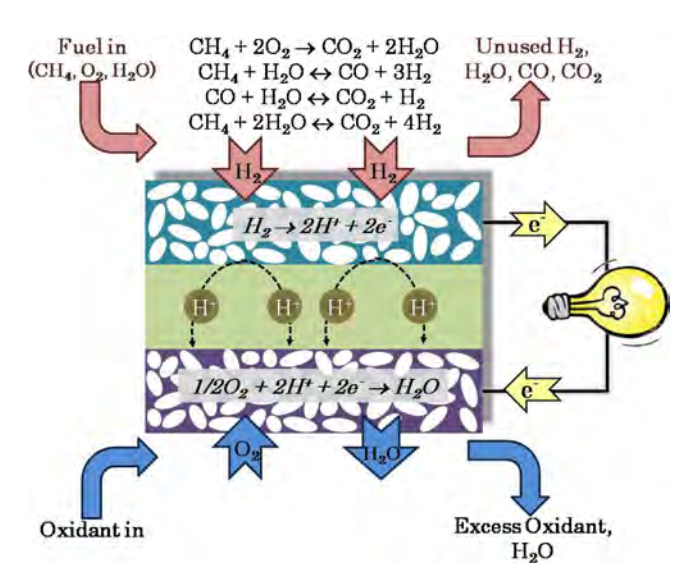


Fig. 1 – Schematic diagram of the SOFC-H⁺ with internal autothermal reforming of methane.

optimal design, the SOFC-H⁺ with internal autothermal reforming should be further studied and analyzed. Operating conditions should also be carefully determined to compromise the SOFC-H⁺ performance and operation.

This study aims to perform a detailed analysis of a DIR-SOFC-H⁺ in which the autothermal reforming of methane is carried out. A DIR-SOFC-H⁺ stack model coupled with a detailed electrochemical model taking into account all voltage losses is employed for steady state simulations. Effect of key operating parameters, e.g., temperature, steam-to-carbon and oxygen-to-carbon feed ratios and fuel utilization on the DIR-SOFC-H⁺ performance in terms of power density, cell efficiency and carbon formation is investigated. In addition, the net heat produced from the DIR-SOFC-H⁺ is also considered.

SOFC-H⁺ with internal autothermal reforming of methane

A single planar anode-supported SOFC-H⁺ has three main parts: the fuel channel, the air channel and the solid part that consists of anode, proton-conducting electrolyte and cathode, as shown in Fig. 1. The most common materials used for the electrodes and electrolyte of the SOFC-H⁺ are Pt and $SrCe_{0.95}Yb_{0.05}O_{3-\alpha}$ (SCY), respectively. The SCY electrolyte is established as a proton-conducting material with relatively high proton conductivity and has been used in several studies (Taherparvar et al., 2003; Potter and Baker, 2006; Pekridis et al., 2007).

2.1. SOFC-H+ operation

When SOFC-H⁺ is operated under the internal autothermal reforming of methane, a gas mixture of methane, steam and oxygen is fed into a fuel channel. There are main four reactions occurred within the SOFC-H⁺: the oxidation (Eq. (1)), the methane steam reforming (Eq. (2)), the water gas-shift (Eq. (3)) and the reverse methanation (Eq. (4)).

$$CH_4 + 2O_2 \rightarrow CO_2 + 2H_2O$$
 $\Delta H_{298K} = -802.7 \text{ kJ/mol}$ (1)

$$CH_4 + H_2O \leftrightarrow CO + 3H_2$$
 $\Delta H_{298K} = 206.2 \text{ kJ/mol}$ (2)

$$CO + H_2O \leftrightarrow CO_2 + H_2$$
 $\Delta H_{298K} = -41.1 \text{ kJ/mol}$ (3)

$$CH_4 + 2H_2O \leftrightarrow CO_2 + 4H_2$$
 $\Delta H_{298K} = 164.9 \text{ kJ/mol}$ (4)

Hydrogen produced from these reactions is oxidized to produce protons and electrons at the anode side. The electrons flow from the anode to the cathode through the external circuit while the protons move through the electrolyte to the interface where they react with oxygen molecules in the oxidant fed to the cathode side and here the water is produced. The overall electrochemical reaction in the SOFC-H⁺ is shown below:

$$H_2 + 0.5O_2 \rightarrow H_2O$$
 (5)

2.2. SOFC-H+ model

A mathematical model of SOFC-H+ consists of two mass balances around the fuel and air channels and an electrochemical model that relates the fuel and air compositions and temperature to the fuel cell voltage, current density and voltage losses. The assumptions used to develop the model of the DIR-SOFC-H+ are as follows: (1) steady state operation, (2) one-dimensional variation in a gas flow direction, (3) uniform operating temperature and pressure over the fuel cell geometry, (4) all gas components have ideal gas behavior, (5) hydrogen is only electrochemically oxidized and (6) constant fluid properties. Although the temperature profiles developed along the gas channel can be different, it is rational to assume that the SOFC can be operated under the isothermal condition as a single cell with an efficient heat management system was considered in this study. However, the predicted performance of the SOFC operated under the isothermal condition would be higher than the non-isothermal operation (Vakouftsi et al., 2011). In addition, the velocities of fuel and air are assumed to be constant along the channels. Arpornwichanop et al. (2010) investigated the effect of changing fuel velocity on the SOFC-H+ performance and showed that although simulations with the isochoric assumption cause the error in the prediction of the SOFC-H⁺ performance, it is in the acceptable range.

2.2.1. Mass balances

By performing mass balances, the differential equations describing the changes in the concentration of gas in fuel and air channels along the axial direction can be written as:

Fuel channel

$$\begin{split} \frac{dC_{i,f}}{dx} &= \frac{1}{u_f} \sum_{j \in \{(1)-(5)\}} \nu_{i,j} R_j \frac{1}{h_f} \\ i &\in \left\{ \text{CH}_4, \text{H}_2\text{O}_{(\text{an})}, \text{O}_{2(\text{an})}, \text{CO}, \text{H}_2, \text{CO}_2 \right\} \end{split} \tag{6}$$

Air channel

$$\frac{dC_{i,a}}{dx} = \frac{1}{u_a} \sum_{j \in \{(5)\}} v_{i,j} R_j \frac{1}{h_a}
i \in \{H_2O_{(ca)}, O_{2(ca)}, N_2\}$$
(7)

where "an" and "ca" stand for the anode and cathode sides, respectively, $C_{i,j}$ and $C_{i,a}$ represent the molar concentration of component i in fuel and air channels, respectively, $v_{i,j}$ is the stoichiometric coefficient of component i in reaction j, R_j is the rate of reaction j, u_f and u_a are the fuel and air velocities, and h_f and h_a are the height of fuel and air channels, respectively.

Table 1 – Reaction equilibrium constants and Arrhenius kinetic parameters.							
1	k _{1,a} k _{1,b}	$8.11 \times 10^5 \text{bar}^{-2}$ $6.82 \times 10^5 \text{bar}^{-2}$	86.00 86.00				
2 3 4	k_2 k_3 k_4	$1.17 \times 10^{15} \mathrm{bar^{0.5}}$ $5.43 \times 10^{5} \mathrm{bar^{-1}}$ $2.83 \times 10^{14} \mathrm{bar^{0.5}}$	240.10 67.13 243.90	5.7×10^{12} 1.2×10^{-2} 7.24×10^{10}	11,476 -4639 21,646		

2.2.2. Kinetic model

The kinetic rate equations for the oxidation, steam reforming, water gas-shift reactions and reverse methanation reactions are obtained from Halabi et al. (2008) as follows:

$$r_{1} = \frac{k_{1a}p_{CH_{4}}p_{O_{2}}}{\left(1 + K_{CH_{4}}^{ox}p_{CH_{4}} + K_{O_{2}}^{ox}p_{O_{2}}\right)^{2}} + \frac{k_{1b}p_{CH_{4}}p_{O_{2}}}{1 + K_{CH_{4}}^{ox}p_{CH_{4}} + K_{O_{2}}^{ox}p_{O_{2}}}$$
(8)

$$r_{2} = \frac{k_{2}/p_{\rm H_{2}}^{2.5}(p_{\rm CH_{4}}p_{\rm H_{2}O} - p_{\rm H_{2}}^{3}p_{\rm CO}/K_{\rm eq,2})}{(1 + K_{\rm CO}p_{\rm CO} + K_{\rm H_{2}}p_{\rm H_{2}} + K_{\rm CH_{4}}p_{\rm CH_{4}} + K_{\rm H_{2}O}p_{\rm H_{2}O}/p_{\rm H_{2}})^{2}}$$
(9)

$$r_3 = \frac{k_3/p_{\rm H_2}(p_{\rm CO}p_{\rm H_2O} - p_{\rm H_2}p_{\rm CO_2}/K_{\rm eq,3})}{(1 + K_{\rm CO}p_{\rm CO} + K_{\rm H_2}p_{\rm H_2} + K_{\rm CH_4}p_{\rm CH_4} + K_{\rm H_2O}p_{\rm H_2O}/p_{\rm H_2})^2}$$
 (10)

$$r_4 = \frac{k_4/p_{\rm H_2}^{3.5}(p_{\rm CH_4}p_{\rm H_2O}^2 - p_{\rm H_2}^4p_{\rm CO_2}/K_{\rm eq,4})}{(1 + K_{\rm CO}p_{\rm CO} + K_{\rm H_2}p_{\rm H_2} + K_{\rm CH_4}p_{\rm CH_4} + K_{\rm H_2O}p_{\rm H_2O}/p_{\rm H_2})^2} \eqno(11)$$

where r_j is the rate of reaction j (Eqs. (1)–(4)), k_j is the kinetic rate constant of reactions j, $K_{\rm eq,j}$ is the equilibrium constant of reaction j, K_i^C is the adsorption constant of component i (i= CH₄ and O₂) in the oxidation reaction. The reaction equilibrium constants and Arrhenius kinetic parameters are listed in Table 1. The Van't Hoff parameters for species adsorption are given in Table 2.

To account for the intraparticle transport limitation, average reaction rates are determined by multiplying the reaction rates (Eqs. (8)–(11)) with the effectiveness factor (η) that are $\eta_1 = 0.05$, $\eta_2 = 0.07$, $\eta_3 = 0.7$, and $\eta_4 = 0.06$, respectively (Halabi et al. (2008)).

Table 2 – Van't Hoff parameters for species adsorption.			
Component	k _{oj}	$\Delta H_{ads,i}$ (J/mol)	
CH ₄ (combustion)	$1.26 \times 10^{-1} bar^{-1}$	-27.23	
O ₂ (combustion)	$7.87 \times 10^{-7} bar^{-1}$	-92.80	
CH ₄	$6.65 \times 10^{-4} bar^{-1}$	-38.28	
CO	$8.23 \times 10^{-5} \ bar^{-1}$	-70.65	
H_2	$6.12 \times 10^{-9} \ bar^{-1}$	-82.90	
H ₂ O	1.77×10^{5}	88.68	

The rate expression of the electrochemical reaction based on the amount of H_2 and O_2 consumed and H_2O produced is related to the electric current density (j) as:

$$R_5 = \frac{j}{2F} \tag{12}$$

2.2.3. Electrochemical equations

The electrochemical equations describing the mechanism of fuel conversion to electricity are employed to predict the performance of SOFC by correlating current density with cell voltage and voltage losses found in the fuel cell. Under an ideal condition, the SOFC can achieve the maximum voltage, referred to as an open circuit voltage ($E^{\rm OCV}$). However, in real operation, the cell voltage at the closed-circuit condition (V) is always lower than $E^{\rm OCV}$ due to the presence of various voltage losses. In general, there are main five loss mechanisms at a given current density. They are: (1) activation loss at the anode ($\eta_{\rm act,an}$), which is the voltage loss caused by the hydrogen oxidation at the anode side, (2) concentration loss at the anode ($\eta_{\rm conc,an}$), which is caused by the transport of gaseous fuel through porous anode, (3) ohmic loss ($\eta_{\rm ohm}$), which is due

Table 3 – Electrochemical model of SOFC-H ⁺ .	
Open-circuit voltage (E ^{OCV}):	
$E^{OCV} = E^{0} + \frac{\Re T}{2F} \ln \left(\frac{p_{H_{2}(an)}p_{O_{2}(ca)}^{0.5}}{p_{H_{2}O(ca)}} \right)$	(13)
Operating voltage (V):	
$V = E^{OCV} - \eta_{act,an} - \eta_{conc,an} - \eta_{ohm} - \eta_{act,ca} - \eta_{conc,ca}$	(14)
Ohmic loss (η_{ohm}) :	
$\eta_{\rm ohm} = j R_{\rm ohm} \ {\rm where} R_{\rm ohm} = \tau_{\rm ele} / \sigma_{\rm ele}$	(15)
Activation overpotential (η_{act}):	
$j = j_{0,\text{electrode}} \left[\exp \left(\frac{\alpha nF}{\Re T} \eta_{\text{act,electrode}} \right) - \exp \left(-\frac{(1-\alpha)nF}{\Re T} \eta_{\text{act,electrode}} \right) \right]$	(16)
Concentration overpotential (η_{conc}):	
$\eta_{\text{conc,an}} = rac{\mathfrak{R}T}{2F} \ln \left(rac{p_{ ext{H}_2(ext{an})}}{p_{ ext{H}_2(ext{an})}^{ ext{I}}} ight)$	(17)
$\eta_{\text{conc,ca}} = \frac{\Re T}{2F} \ln \left(\left(\frac{p_{\text{O}_2(\text{ca})}}{p_{\text{O}_2(\text{ca})}^I} \right)^{0.5} \frac{p_{\text{H}_2\text{O}(\text{ca})}^I}{p_{\text{H}_2\text{O}(\text{ca})}} \right)$	(18)
where $p_{\text{H}_2(\text{an})}^{\text{I}} = P - (P - p_{\text{H}_2(\text{an})}) \exp\left(\frac{\Re T \tau_{\text{an}}}{2FD_{\text{an,eff}}P}j\right)$	(19)
$p_{O_2(ca)}^I = p_{O_2(ca)} - \frac{\Re T \tau_{ca}}{2FD_{ca,eff}} j$	(20)
$p_{\mathrm{H}_{2}\mathrm{O(ca)}}^{\mathrm{I}} = p_{\mathrm{H}_{2}\mathrm{O(ca)}} + \frac{\Re \mathrm{Tr}_{\mathrm{ca}}}{4\mathrm{FD}_{\mathrm{ca,eff}}} \mathbf{j}$	(21)

Table 4 – Electrochemical	parameters for simulating the
SOFC-H ⁺ performance.	

Electrolyte	225.92 exp(- 6.3 \times 10 ³ /T) Ω^{-1} m ⁻¹
protonic	
conductivity, $\sigma_{\rm ele}$	
Electrode	$800 \mathrm{A}\mathrm{m}^{-2}$
exchange current	
density, $j_{0,\text{electrode}}$	
Effective gas	$8.98 \times 10^{-5} \text{m}^2 \text{s}^{-1}$
diffusion	
coefficient in the	
anode side, D _{an,eff}	
Effective gas	$6.31 \times 10^{-6} m^2 s^{-1}$
diffusion	
coefficient in the	
cathode side,	
$D_{ca,eff}$	

to the resistance to the flow of protons in the electrolyte, (4) activation loss at the cathode ($\eta_{\rm act,can}$), which is the voltage loss caused by the oxygen reduction at the cathode side and (5) concentration loss at the cathode side ($\eta_{\rm conc,ca}$), which is caused by the transport of gaseous oxidant through porous cathode. The electrochemical equations of the SOFG-H⁺ (Eqs. (13)–(21)) used in this study were reported in our previous work (Patcharavorachot et al., 2010), as summarized in Table 3.

For SOFC-H+, the protonic conductivity of the SCY electrolyte as a function of temperature is extracted from the experimental results of Potter and Baker (2006). In this study, the electrode exchange current density $(j_{0.\text{electrode}})$ is assumed to be constant since the rate expression is not available. The effective gas diffusivity coefficients used in the calculation of partial pressure of substances at the interface depend on a microstructure of the porous electrodes (porosity, pore size and tortuosity) and the operating conditions (temperature and pressure), as described in our previous work (Patcharavorachot et al., 2010). It is noted that the effective gas diffusivity coefficient in the anode (Dan,eff) is calculated from the effective diffusivity coefficient of H2, whereas that in the cathode (D_{ca.eff}) is calculated from the effective diffusivity coefficient of O2 and H2O averaged by its mole fraction. Table 4 presents the electrochemical parameters for the SOFC-H+. The values of $D_{an,eff}$ and $D_{ca,eff}$ in Table 4 is calculated based on the following conditions and parameters: $T = 750 \,^{\circ}\text{C}$, $P = 1 \,\text{bar}$, $\varepsilon = 0.4$, $r = 0.5 \,\mu\text{m}$ and $\tau = 5$.

2.2.4. SOFC performance

In order to evaluate the steady-state fuel cell performance, the model equations of the SOFC-H+ consisting of mass balances and electrochemical equations as well as the kinetic reaction equations are simultaneously solved by using MATLAB. The average current density (j_{ave}), the fuel utilization factor (U_f) and the air ratio (λ_a) have to be pre-specified to determine the molar flow rate of fuel (F_f) and air (F_a) supplied to the fuel cell. The output parameters showing the SOFC performance are the power density (P_{SOFC}) and the fuel cell efficiency (ε_{SOFC}) as:

$$U_f = \frac{j_{\text{ave}}LW}{2F(4y_{\text{CH}_a}^{\text{in}})F_f}$$
 (22)

$$\lambda_a = \frac{2F(y_{O_2}^{\text{in}})F_a}{j_{\text{aveLW}}} \tag{23}$$

$$P_{SOFC} = j_{ave}V \tag{24}$$

Table 5 – Comparison of the maximum power density of SOFC-H⁺ obtained from model prediction and experimental data (Taherparvar et al., 2003).

T (°C)	Maximum power densit P _{SOFC,max} (mW/cm ⁻²)	y,	Error (%)
	Taherparvar et al. (2003)	Model	
600	2.14	2.27	6.07
700	3.56	4.04	12.92
800	7.70	7.95	3.25

$$\varepsilon_{\text{SOFC}} = \frac{P_{\text{SOFC}}LW}{(y_{\text{CH}_{a}}^{\text{in}}LHV_{\text{CH}_{4}})F_{f}} \times 100\%$$
 (25)

It is noted that in this study, SOFC-H $^+$ is assumed to be operated under isothermal condition; therefore, the heat duty of the fuel cell (Q_{SOFC}) can be calculated based on the energy balance around the fuel cell stack as:

$$Q_{SOFC} = \left(\sum_{\text{in,anode}} n_i H_i - \sum_{\text{out,anode}} n_i H_i\right) + \left(\sum_{\text{in,cathode}} n_i H_i - \sum_{\text{out,cathode}} n_i H_i\right) - P_{SOFC}$$
(26)

where n_i and H_i denote the molar flow rate (mol s⁻¹) and the enthalpy (kJ/mol) of component i, respectively.

2.2.5. Model validation

To verify the SOFC-H+ model used in this study, the modeling results are compared with experimental data of Taherparvar et al. (2003) who investigated the electrochemical characteristics of SOFC-H+ fueled by hydrogen—oxygen. The experiment was carried out at temperatures of 600–800 °C using proton-conducting Yb-doped SrCeO3 as electrolyte and platinum as electrode. The fuel and oxidation used in the experiment were 10% H2 (~3% H2O) and dry air (<0.1% H2O), respectively. The comparison of the model prediction and experimental data in terms of the maximum power density at different operating temperatures is shown in Table 5. The results show that the maximum power density obtained from the model prediction is higher than that from the experiment. The maximum error of ~10% is found when the SOFC-H+ was operated at 700 °C.

3. Results and discussion

Table 6 shows the values of operating condition, cell geometry and material property for simulation of the SOFC-H+ with internal autothermal reforming of methane. Under the standard conditions, the DIR-SOFC-H+ is fed by methane, steam and air at the steam-to-carbon ratio (S/C) of 2 and oxygen-to-carbon ratio (O/C) of 0.2 at the fuel channel while the dry air (\sim 0.1% H₂O) is fed at the air channel. The proposed models as described in the previous section are employed to predict the distribution of gas composition along the fuel and air channels and all the electrochemical-related variables (e.g., open-circuit voltage, activation, ohmic, and concentration overpotential and cell voltage) as well as the fuel cell efficiency and power density.

Fig. 2(a) and (b) shows the molar flow rate profiles of all components in the fuel and air channels along the cell length. As seen in Fig. 2(a), CH_4 , O_2 and H_2O are consumed suddenly at the inlet of the fuel channel while the generation of H_2 , CO and

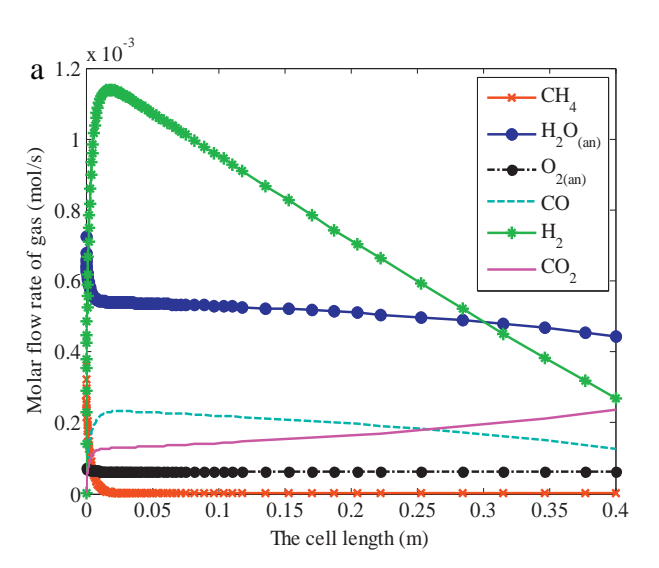
Table 6 – Input model parameters used for simulation of SOFC-H $^{\scriptsize +}$.

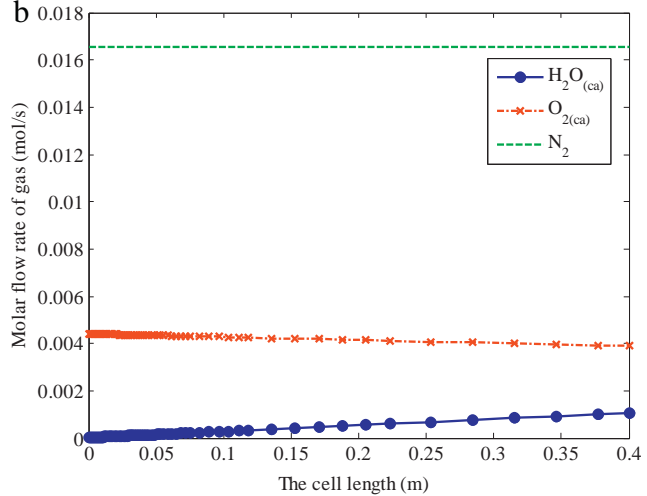
Operating conditions Operating temperature, T 750°C Operating pressure 1.0 bar Air feed 0.1% H₂O, 20% O₂, 79% N₂ S/C = 2, O/C = 0.2Fuel composition $5000 \, A \, m^{-2}$ Average current density Fuel utilization 0.75 Air ratio 8.5 Dimensions of fuel cell elements Cell length I. 0.4 m Cell width, W 0.1 m Fuel channel height, hf 1 mm Air channel height, ha 1 mm Anode thickness, τ_{an} 500 μm Cathode thickness, τ_{ca} 50 µm Electrolyte thickness, $\tau_{\rm ele}$ $20 \, \mu m$ Material properties $1870 \, kg/m^3$ Catalyst density, $\rho_{\rm cat}$

CO2 can be observed. This is because the oxidation and steam reforming reactions are much faster reactions. When most CH4 is completely consumed, H2 decreases along the length of fuel cell because the electrochemical reaction becomes important. Regarding the SOFC-H+ operation, H2O is produced at the cathode side as shown in Fig. 2(b), thereby the amount of H2O in the fuel channel is relatively constant. At the exit of the SOFC-H+, the compositions of the fuel stream are 38.89% H₂O, 5.52% O₂, 11.04% CO, 23.7% H₂ and 20.84% CO₂, whereas the oxidant stream consists of 4.91% H₂O, 18.07% O₂ and 77.02% N2. From the simulation result, it is obvious that the DIR-SOFC-H+ with autothermal reforming of methane can reduce the content of CO compared to that with steam reforming operation (Arpornwichanop et al., 2010). For the DIR-SOFC-H+ with steam reforming, H2O is required to shift the steam reforming toward and convert CO to H2. However, due to the generation of H2O at the cathode side, there are less amount of H₂O appeared at the anode side and thus, the high content of CO is observed. Unlike the DIR-SOFC-H+ with steam reforming operation, use of the autothermal reforming can suppress the CO formation. The addition of oxygen in the fuel channel increases the methane conversion and more H2 and H2O are generated by the oxidation (Eq. (1)) and steam reforming (Eq. (2)). H₂O produced from these reactions is sufficient to convert CO and thus, the amount of CO in the exit fuel stream of the DIR-SOFC-H+ with autothermal reforming is lower.

In this study, the average current density (j_{ave}) , corresponding to the fuel utilization factor (U_f) and the air ratio (λ_a) , was pre-specified to determine the molar flow rate of fuel (F_f) and air (F_a) supplied to the fuel cell. Fig. 2(c) shows the distribution of current density along the cell length. It can be seen that the current density sharply increases at the inlet and continuously decreases toward the fuel cell outlet. This is related to the local H_2 concentration in the fuel channel and the local H_2 and H_2 in the air channel.

Under the standard conditions, the cell voltage, power density and fuel cell efficiency predicted are 0.53 V, 0.26 W cm $^{-2}$ and 37.95%, respectively. When considering individual voltage losses, it is found that the activation losses ($\eta_{\rm act,an}$ and $\eta_{\rm act,ca}$ = 0.3274 V) represent a major loss in the SOFC-H+, followed by the ohmic loss ($\eta_{\rm ohm}$ = 0.207 V), cathode concentration loss ($\eta_{\rm conc,ca}$ = 0.10052 V) and anode concentration loss ($\eta_{\rm conc,an}$ = 0.0008 V). It is noted that the anode activation loss





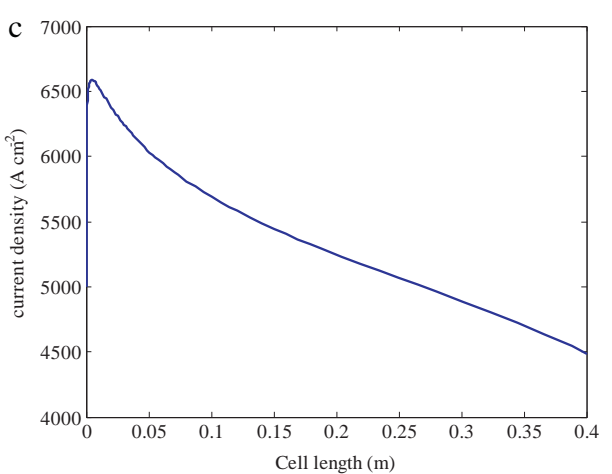


Fig. 2 – (a) Profiles of gas compositions at fuel channel, (b) Profiles of gas compositions at air channel and (c) distribution of current density.

is equal to the cathode activation loss because the exchange current densities of the anode and cathode are assumed to be the same (Table 4). The results also indicate that the anode concentration loss can be negligible, compared to the cathode concentration loss. This is due to the fact that there is only H_2 at the anode side, thereby it is easily to transport to the reaction site, leading to a lower concentration loss. Unlike the anode side, there are the reactant O_2 and the product H_2O in the cathode side, the H_2O molecules hinder the transport of O_2 , resulting in a higher concentration loss. In addition, the

Table 7 – The range of operating conditions considered in the performance analysis of SOFC-H ⁺ .						
Parameter	Unit	Level				
		1	2	3	4	5
T	°C	600	650	700	750	800
S/C	-	2	3	4	5	6
O/C	-	0.05	0.10	0.15	0.20	0.25
jave	Acm^{-2}	0.3	-	0.5	-	0.7
$U_{ m fuel}$	-	0.65	-	0.75	-	0.85

simulation result reveals that under the isothermal condition, the SOFC-H $^+$ generates the net heat of 0.16 kJ/s.

In the next subsection, the effect of key operating conditions, e.g., operating temperature (T), steam-to-carbon ratio (S/C), oxygen-to-carbon ratio (O/C), average current density (j_{ave}) and fuel utilization (U_{fuel}) on the DIR-SOFC-H⁺ performance is examined. Table 7 summarizes a range of operating conditions studied here. Fig. 3 presents the influences of operating temperature, S/C and O/C on the power density, cell efficiency, CO content as well as the net heat produced by the SOFC. Furthermore, the results of changing in the average current density and fuel utilization are shown in Fig. 4.

3.1. Effect of operating temperature

In order to study the effect of operating temperatures on SOFC-H⁺ performance, CO content and net heat generation as shown in Fig. 3(a)–(d), the operating temperature are varied from 600 to 800 °C, according to the level of operating conditions (1–5) given in Table 7, whereas the other parameters reported in Table 6 are kept constant. The DIR-SOFC-H⁺ performance is improved when operating temperatures increase. A raise in the operating temperature strongly increase the

rate of chemical reactions; more hydrogen produced from the reforming reactions (Eqs. (1)–(4)) is highly consumed by the electrochemical reaction (Eq. (5)) and thus, the cell voltage is higher. Moreover, a higher temperature operation causes a reduction of the ohmic loss and consequently, the power density (Fig. 3(a)) and the cell efficiency (Fig. 3(b)) are enhanced. However, the increment of the operating temperature results in a higher content of CO in the fuel stream, as illustrated in Fig. 3(c). This is mainly because the water gas-shift reaction (Eq. (3)) is favored at a lower temperature operation.

In general, the DIR-SOFC-H+ with autothermal reforming operation, which is a mildly exothermic reaction, should generate more heat when operating at higher temperatures. However, the simulation result shows a decrease in the net heat produced by the DIR-SOFC-H+ (Fig. 3(d)). This can be explained that when oxygen is completely reacted with methane via the oxidation reaction, the steam reforming reaction is more pronounced and its reaction rate increases with the increased operating temperature. Thus, the reaction heat released by the electrochemical reaction is more consumed to accomplish the reforming reaction. It is noted that the amount of oxygen fed to the DIR-SOFC-H+ is generally limited for a safety reason. From the simulation results, it can be further observed that the CO generation can be reduced when the

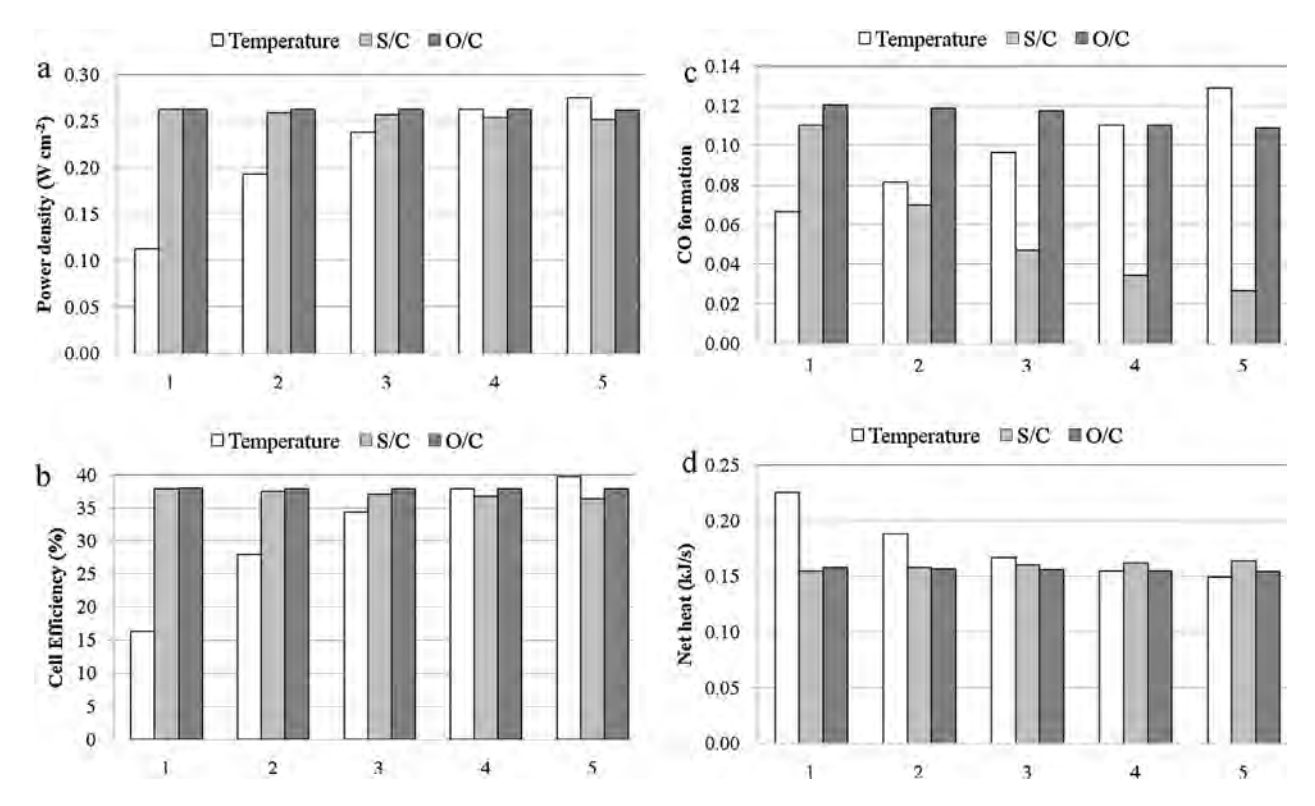


Fig. 3 – Effect of operating temperatures, S/C and O/C feed ratios on: (a) power density, (b) cell efficiency, (c) CO content and (d) net heat generation (the number showing on the x-axis is referred to the level of operating conditions as given in Table 7).

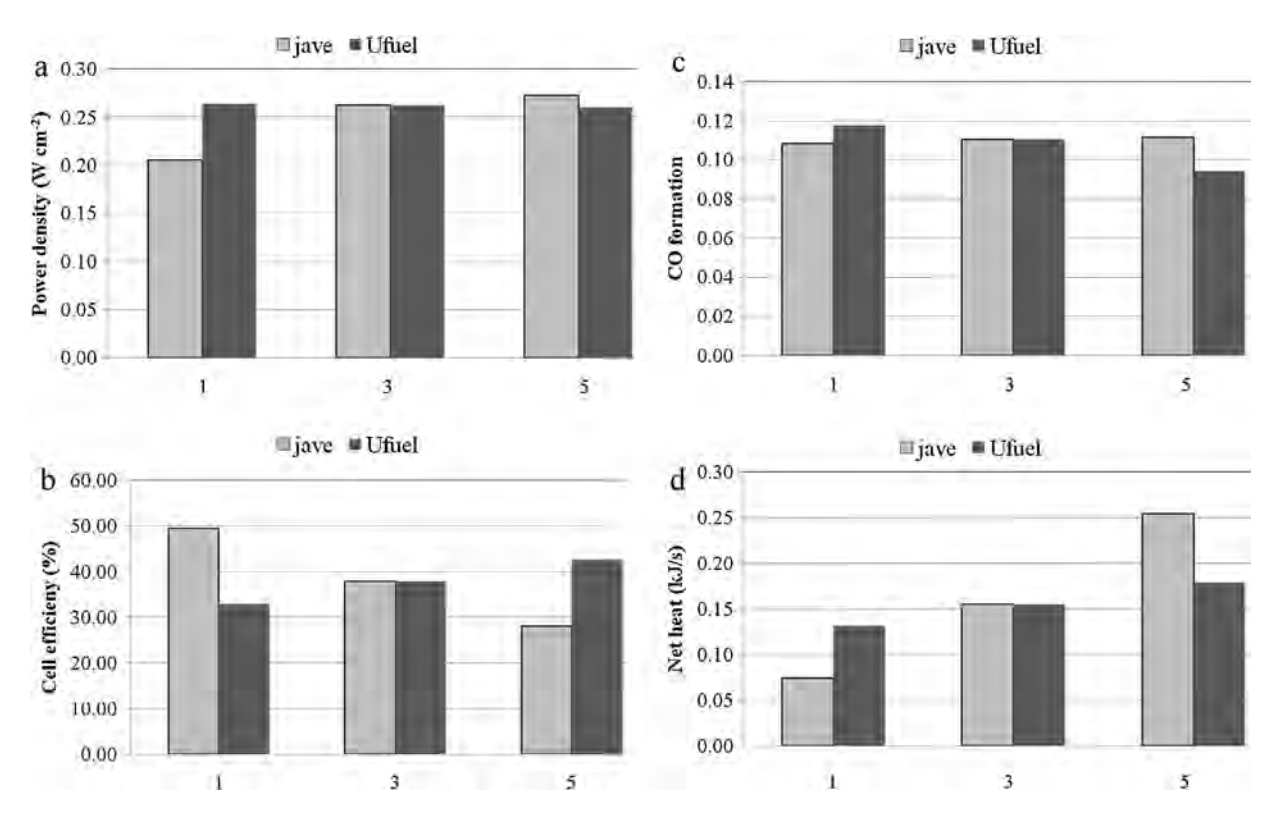


Fig. 4 – Effect of operating current density and fuel utilization on: (a) power density, (b) cell efficiency, (c) CO content and (d) net heat generation (the number showing on the x-axis is referred to the level of operating conditions as given in Table 7).

operating temperature is lower. However, under this operation, the SOFC-H⁺ performance in terms of the power density and cell efficiency is also greatly decreased. As a consequence, the operating temperature should be carefully selected to be a good compromise between the cell performance and the CO formation.

3.2. Effect of steam-to-carbon and oxygen-to-carbon feed ratios

In this section, the effect of S/C and O/C feed ratios on the power density, cell efficiency, CO production and net generated heat is investigated. As seen in Fig. 3(a) and (b), the increases of S/C and O/C have insignificant effect on the fuel cell performance. Increasing S/C (at constant O/C = 0.2) causes a slight decrease in the power density and cell efficiency due to the dilution effect of H_2 . However, the use of excess H_2 O is beneficial to the decrease of CO, as demonstrated in Fig. 3(c), because an addition of H_2 O can promote the water gas-shift reaction.

Likewise, the DIR-SOFC-H $^+$ operated at a higher O/C ratio (at constant S/C = 2) can reduce the generation of CO. Adding O $_2$ strongly affects the methane conversion through the oxidation reaction and a significant increase in H $_2$ O generation is observed instead of H $_2$. As a consequence of the H $_2$ O production, the presence of CO in the fuel channel reduces (Fig. 3(c)). The addition of O $_2$ along with CH $_4$ and H $_2$ O, however, should be carefully determined. It is also found that the increases of S/C and O/C feed ratios have less influence on the net heat obtained from the SOFC-H $^+$ (Fig. 3(d)).

3.3. Effect of average current density

In this study, the average current density and fuel utilization factor, which are used to determine the molar flow rate of fuel and air supplied to the fuel cell, are key parameters having an effect on the SOFC operation. It is found from the results that an increase in average current density results in the increased power density even the voltage losses increase (Fig. 4(a)). Unlike the power density, the cell efficiency is hindered when the SOFC-H⁺ is operated at a higher operating current density (Fig. 4(b)). Under this operating condition, the molar flow rate of fuel fed to the fuel cell is much higher and thus, the cell efficiency is strongly reduced. Fig. 4(c) shows that the increment of average current density hardly affects the CO formation. Since an increase in the average current density cause a higher electrochemical reaction rate, the DIR-SOFC-H⁺ generates more heat to the surrounding (Fig. 4(d)).

3.4. Effect of fuel utilization

As mentioned above, the fuel utilization is a key parameter to indicate the performance of SOFC. For operation of the SOFC-H+ under high fuel utilization, a concentration loss becomes the dominant loss due to the large reduction of H_2 fuel at the fuel channel, resulting in the reduced power density (Fig. 4(a)). However, at high fuel utilization, the chemical energy of the fuel can be converted into electricity, leading to the improved fuel cell efficiency (Fig. 4(b)). Furthermore, it is noticed that the content of CO reduces when the SOFC-H+ is operated at higher fuel utilization. Due to a higher consumption of H_2 , water gasshift reaction is shifted toward the product side and thus, a lower amount of CO is present. (Fig. 4(c)). In addition, the net heat obtained from the SOFC-H+ can be raised by increasing the fuel utilization (Fig. 4(d)) as can be explained in a similar way with the effect of the average current density.

4. Conclusions

In this study, a performance of a SOFC-H+ with internal autothermal reforming of methane is analyzed based on a

one-dimensional, steady-state model of the SOFC-H+ coupled with a detailed electrochemical model. The results show that the DIR-SOFC-H+ operated at 750 $^{\circ}\text{C}$ and 1 bar with the average current density of 0.5 A cm⁻², fuel utilization of 0.75 and air ratio of 8.5 gives the power density of 0.26 W cm⁻² and fuel cell efficiency of 38%. Interestingly, the introduction of oxygen to a steam reforming environment, known as an autothermal reforming is beneficial to the SOFC-H+ operation; the presence of CO, which is related to the possibility of carbon formation, in the fuel cell is reduced. The simulation results show that CO generation can be significantly reduced by increasing the S/C and O/C feed ratios as well as decreasing the operating temperature. Furthermore, the SOFC-H+ with internal autothermal reforming release heat, which can be used for other energy-demanding units in the SOFC system. From the simulation results, it can be concluded that operating temperature, S/C and O/C feed ratios, current density and fuel utilization have greatly effect on the cell performance, CO formation and net heat generation. The operating conditions of the SOFC-H+ should be carefully determined by considering both the cell performance and the CO formation.

Acknowledgements

This work was supported by the Faculty of Engineering, King Mongkut's Institute of Technology Ladkrabang and the Higher Education Research Promotion and National Research University Project of Thailand, Office of the Higher Education Commission (EN280A). The authors also gratefully acknowledge the support of the Thailand Research Fund (TRF).

References

- Aguiar, P., Chadwick, D., Kershenbaum, L., 2004. Dynamic effects in autothermal systems: application to a coated-wall internally reformed solid oxide fuel cell. Chem. Eng. Res. Des. 82, 259–266.
- Akkaya, A.V., Sahin, B., Erdem, H.H., 2008. An analysis of SOFC/GT CHP system based on exergetic performance criteria. Int. J. Hydrogen Energy 33, 2566–2577.
- Arpornwichanop, A., Chalermpanchai, N., Patcharavorachot, Y., Assabumrungrat, S., Tade, M., 2009. Performance of an anode-supported solid oxide fuel cell with direct-internal reforming of ethanol. Int. J. Hydrogen Energy 34, 7780–7788.
- Arpornwichanop, A., Patcharavorachot, Y., Assabumrungrat, S., 2010. Analysis of a proton-conducting SOFC with direct internal reforming. Chem. Eng. Sci. 65, 581–589.
- Authayanun, S., Arpornwichanop, A., Paengjuntuek, W., Assabumrungrat, S., 2010. Thermodynamic study of hydrogen production from crude glycerol autothermal reforming for fuel cell applications. Int. J. Hydrogen Energy 35, 6617–6623.
- Bavarian, M., Soroush, M., 2012. Mathematical modeling and steady-state analysis of a proton-conducting solid oxide fuel cell. J. Bavarian Process Control 22, 1521–1530.
- Chen, T., Guo, W., Miao, W.H., Li, T., Xu, C., 2011. Evaluation of carbon deposition behavior on the nickel/yttrium-stabilized zirconia anode-supported fuel cell fueled with simulated syngas. J. Power Sources 196, 2461–2468.
- D'Epifanio, A., Fabbri, E., Di Bartolomeo, E., Licoccia, S., Traversa, E., 2008. Design of $BaZr_{0.8}Y_{0.2}O_{3-\delta}$ protonic conductor to improve the electrochemical performance in intermediate temperature solid oxide fuel cells (IT-SOFCs). Fuel Cells 8, 69–76.

- Ding, H., Xie, Y., Xue, X., 2011. Electrochemical performance of $BaZr_{0.1}Ce_{0.7}Y_{0.1}Yb_{0.1}O_{3-\delta}$ electrolyte based proton-conducting SOFC solid oxide fuel cell with layered perovskite $PrBaCo_2O_{5+\delta}$ cathode. J. Power Sources 196, 2602–2607.
- Dokmaingam, P., Irvine, J.T.S., Assabumrungrat, S., Charojrochkul, S., Laosiripojana, N., 2008. Modeling of IT-SOFC with indirect internal reforming operation fueled by methane: effect of oxygen adding as autothermal reforming. Int. J. Hydrogen Energy 35, 13271–13279.
- Halabi, M.H., Croon, J.M., Schaaf, J., Cobden, P.D., Schouten, J.C., 2008. Modeling and analysis of autothermal reforming of methane to hydrogen in a fixed bed reformer. Chem. Eng. J. 137, 568–578.
- Hajimolana, S.A., Hussain, M.A., Wan Daud, W.M.A., Chakrabarti, M.H., 2012. Dynamic modelling and sensitivity analysis of a tubular SOFC fuelled with NH_3 as a possible replacement for H_2 . Chem. Eng. Res. Des., http://dx.doi.org/10.1016/j.cherd.2012.03.004 (in press, Corrected Proof, Available online 12.03.12).
- Hiei, Y., Ishihara, T., Takita, Y., 1996. Partial oxidation of methane for internally reformed solid oxide fuel cell. Solid State Ionics 86–88, 1267–1272.
- Jamsak, W., Assabumrungrat, S., Douglas, P.L., Laosiripojana, N., Suwanwarangkul, R., Charojrochkul, S., Croiset, E., 2009. Performance of ethanol-fuelled solid oxide fuel cells: proton and oxygen ion conductors. Chem. Eng. J. 133, 187– 194.
- Laosiripojana, N., Assabumrungrat, S., Charojrochkul, S., 2007. Steam reforming of ethanol with co-fed oxygen and hydrogen over Ni on high surface area ceria support. Appl. Catal. A 327, 180–188.
- Leone, P., Lanzini, A., Ortigoza-Villalba, G.A., Borchiellini, R., 2012. Operation of a solid oxide fuel cell under direct internal reforming of liquid fuels. Chem. Eng. J. 191, 349–355.
- Ni, M., Leung, D.Y.C., Leung, M.K.H., 2008. Modeling of methane fed solid oxide fuel cells: comparison between proton conducting electrolyte and oxygen ion conducting electrolyte. J. Power Sources 183, 133–142.
- Patcharavorachot, Y., Brandon, N.P., Paengjuntuek, W., Assabumrungrat, S., Arpornwichanop, A., 2010. Analysis of planar solid oxide fuel cells based on proton-conducting electrolyte. Solid State Ionics 181, 1568–1576.
- Pekridis, G., Kalimeri, K., Kaklidis, N., Athanasiou, C., Marnellos, G., 2007. Electrode polarization measurements in the Fe|SrCe_{0.95}Yb_{0.05}O_{2.975}|Au proton conducting solid electrolyte cell. Solid State Ionics 178, 649–656.
- Potter, A.R., Baker, R.T., 2006. Impedance studies on $Pt|SrCe_{0.95}Yb_{0.05}O_3|Pt$ under dried and humidified air argon and hydrogen. Solid State Ionics 177, 1917–1924.
- Santin, M., Traverso, A., Magistri, L., Massardo, A., 2010. Thermoeconomic analysis of SOFC-GT hybrid systems fed by liquid fuels. Energy 35, 1077–1083.
- Shiratori, Y., Ijichi, T., Oshima, T., Sasaki, K., 2010. Internal reforming SOFC running on biogas. Int. J. Hydrogen Energy 35, 7905–7912.
- Taherparvar, H., Kilner, J.A., Baker, R.T., Sahibzada, M., 2003. Effect of humidification at anode and cathode in proton-conducting SOFCs. Solid State Ionics 162–163, 297–303.
- Vakouftsi, E., Marnellos, G., Athanasiou, C., Coutelieris, F.A., 2011. A detailed model for transport processes in a methane fed planar SOFC. Chem. Eng. Res. Des. 89, 224–229.
- Vijay, P., Hosseini, S., Tadé, M., 2012. A novel concept for improved thermal management of the planar SOFC. Chem. Eng. Res. Des., http://dx.doi.org/10.1016/j.cherd.2012.09.004 (in press, Corrected Proof, Available online 15.09.12).
- Zamfirescu, C., Dincer, I., 2009. Thermodynamic performance analysis and optimization of a SOFC-H⁺ system. Thermochim. Acta, 32–40.

ELSEVIER

Contents lists available at ScienceDirect

Bioresource Technology

journal homepage: www.elsevier.com/locate/biortech



Energy and exergy analysis of an ethanol reforming process for solid oxide fuel cell applications



Phanicha Tippawan, Amornchai Arpornwichanop*

Computational Process Engineering Research Unit, Department of Chemical Engineering, Faculty of Engineering, Chulalongkorn University, Bangkok 10330, Thailand

HIGHLIGHTS

- Energy and exergy analysis of ethanol reforming processes for SOFC are preformed.
- Steam reforming, partial oxidation and autothermal reforming are considered.
- The possibility of carbon formation in different ethanol reformings are examined.
- Use of ethanol reforming for fuel cell applications is discussed.
- The best ethanol reforming process for SOFC applications is identified.

ARTICLE INFO

Article history: Received 5 December 2013 Received in revised form 25 January 2014 Accepted 27 January 2014 Available online 5 February 2014

Keywords: Ethanol reforming Solid oxide fuel cell System performance Energy analysis Exergy analysis

ABSTRACT

The fuel processor in which hydrogen is produced from fuels is an important unit in a fuel cell system. The aim of this study is to apply a thermodynamic concept to identify a suitable reforming process for an ethanol-fueled solid oxide fuel cell (SOFC). Three different reforming technologies, i.e., steam reforming, partial oxidation and autothermal reforming, are considered. The first and second laws of thermodynamics are employed to determine an energy demand and to describe how efficiently the energy is supplied to the reforming process. Effect of key operating parameters on the distribution of reforming products, such as H₂, CO, CO₂ and CH₄, and the possibility of carbon formation in different ethanol reformings are examined as a function of steam-to-ethanol ratio, oxygen-to-ethanol ratio and temperatures at atmospheric pressure. Energy and exergy analysis are performed to identify the best ethanol reforming process for SOFC applications.

© 2014 Elsevier Ltd. All rights reserved.

1. Introduction

A solid oxide fuel cell (SOFC) is considered the most promising technology for power generation for residential and stationary applications. Presently, hydrogen is a primary fuel for SOFC stacks. It can be produced from a wide range of fossil and renewable fuels via thermal-chemical and biological processes (Lin et al., 2013). Among the various renewable fuels, ethanol is a very attractive green fuel as it is produced by fermentation of agricultural products and easy to handle as a liquid fuel (Cardona and Sánchez, 2007). There are several methods to produce hydrogen rich gas from ethanol. A steam reforming is among the widely used processes due to its high hydrogen yield; however, this process involves a highly endothermic reaction and requires high energy supply. To minimize the external heat input, partial oxidation and autothermal reforming are alternative routes for hydrogen

production (Rabenstein and Hacker, 2008). Because SOFC is operated at high temperatures and a waste heat recovery is generally included in the SOFC system to enhance its performance, a selection of appropriate fuel processing technology should also take an efficient energy usage into account.

Regarding the first law of thermodynamics, an energy balance can be used to determine the energy requirement in the forms of matter streams, heat and work, but fails to provide accurate information on how efficiently the supplied energy is used in a system. This is due to the fact that such an energy analysis cannot identify the real thermodynamic inefficiencies associated with the energy conversion system. On the other hand, an entropy balance determines entropy generation within the system, which is the indicator of its inefficient energy usage. However, since the entropy still fails to account for the quality of energy, the true thermodynamic value (quality) of an energy carrier is characterized by its exergy. Exergy destruction which is one of the exergy-based variables represents the exergy destroyed by an irreversibility (entropy generation) process within the system (El-Emam and Dincer,

^{*} Corresponding author. Tel.: +66 2 218 6878; fax: +66 2 218 6877. E-mail address: Amornchai.A@chula.ac.th (A. Arpornwichanop).

2011). The irreversibility is caused by chemical reaction, heat transfer through a finite temperature difference, mixing of matter and unrestrained expansion and friction. In the past, there are few studies concerning about a comparison of hydrogen production from ethanol using different reforming processes. The investigation of the ethanol processing, i.e., steam reforming, partial oxidation and autothermal reforming, and the range of optimal operating conditions for each process was given. However, based on their results, it is difficult to determine exactly the suitable operational policy of the reforming processes. Furthermore, the process performance in terms of the energy demand was only focused (Rabenstein and Hacker, 2008). The thermodynamic analysis of different ethanol reforming processes was also studied (Sun et al., 2012). The optimal conditions for operating the ethanol reformer were proposed. It was found that the partial oxidation of ethanol provides the lowest H₂ yield with high possibility of coke formation, so it is not a suitable process for hydrogen production. However, the benefit of the partial oxidation process is to give useful heat, which can improve the system thermal management.

It is known that the first law of thermodynamics gives information about the conservation of energy within the process, whereas the second law of thermodynamics can be used to assess and improve the process, leading to a better understanding of the process energy usage. This meaningful information of the process operation cannot be attained by an energy analysis alone (Rosen et al., 2008). Even though, some researchers focused on an exergy analysis of the hydrogen production from ethanol (Douvartzides et al., 2004; Song et al., 2005; Casas et al., 2010), only the steam reforming process was chosen without comparing to other reforming processes. To date, exergatic information of each ethanol reforming process has not been clearly reported. The effect of the reforming factor on the exergetic efficiency of the solid oxide fuel cell (SOFC) power plant based on an external ethanol steam reforming was analyzed (Douvartzides et al., 2004). It indicated that the maximum exergy destruction rate is found in a combustion process. The study of the ethanol-fueled proton exchange membrane fuel cell for automobile applications can be concluded that the utilization of excess steam results in an increase of the overall exergy destruction and lowers the plant efficiency (Song et al., 2005). Recently, the model based energy-exergy analysis of the SOFC power plant was performed (Casas et al., 2010). The study suggested that the efficient use of waste heat in the SOFC combined cycle can reduce the irreversibility of the system, resulting in increases in the energy and exergy efficiencies.

In this study, the first and second laws of thermodynamics are applied to analysis of an ethanol reforming process to produce hydrogen fuel. Three different reforming methods, i.e., steam reforming, partial oxidation and autothermal reforming, are considered. Effects of key operating parameters, such as reactant feed ratio and operating reforming temperatures, on the equilibrium composition of reforming products are also presented. The performance assessment of each ethanol reforming process in terms of product yield, carbon-free operational region and energy usage is carried out in detail with the aim to optimize the process operation. Based on the second law of thermodynamics, the comprehensive analysis of an exergy destruction in different ethanol reforming processes is also discussed. Finally, the application of the ethanol reforming to produce hydrogen for SOFC is commented.

2. Methods

2.1. Ethanol reforming processes

Ethanol is regarded as a promising renewable resource for hydrogen production. Today, a fuel-to-hydrogen rich gas conversion technology has been received considerable interest according to the advancement of a fuel cell technology for power generation. In general, ethanol can be converted to hydrogen through different reforming processes: (i) steam reforming (SR), (ii) partial oxidation (POX) and (iii) autothermal reforming (ATR) (Rabenstein and Hacker, 2008). Each reforming process has its own operational method; thereby the composition and quality of the produced synthesis gas and the energy demand vary. Thus, finding the most suitable ethanol reforming process is important for commercialization. At present, ethanol steam reforming is the most widely used process because it provides a higher hydrogen yield and a lower rate of side reactions. This process, however, has some limitations, e.g., slow start-up time, high energy consumption and severe catalyst deactivation. Ethanol steam reforming is an endothermic process that combines ethanol and steam over catalysts at high temperatures as (Benito et al., 2005):

$$C_2H_5OH + H_2O \leftrightarrow 2CO + 4H_2 \tag{1}$$

However, there are several reaction pathways that could occur in the ethanol/water system, depending on types of catalyst used. Various kinds of intermediate by-products, such as acetaldehyde and ethylene, are usually formed (Vaidya and Rodrigues, 2006). In general, the feasible reactions of the ethanol/water system are ethanol dehydrogenation, acetaldehyde decomposition, ethanol dehydration, methane steam reforming and water gas shift reaction as shown in Eqs. (2)–(6), respectively.

$$C_2H_5OH \leftrightarrow CH_3CHO + H_2 \tag{2}$$

$$CH_3CHO \leftrightarrow CH_4 + CO$$
 (3)

$$C_2H_5OH \to C_2H_4 + H_2O$$
 (4)

$$CH_4 + H_2O \leftrightarrow CO + 3H_2 \tag{5}$$

$$CO + H_2O \leftrightarrow CO_2 + H_2 \tag{6}$$

The steam reforming reaction, which gives the maximum hydrogen yield, is given by the following reaction:

$$C_2H_5OH + 3H_2O \leftrightarrow 2CO_2 + 6H_2$$
 (7)

The partial oxidation of ethanol is an exothermic process in which ethanol and oxygen are reacted in proportions to partially combust ethanol into a gaseous mixture of H₂ and CO. The advantages of the ethanol partial oxidation are fast start-up and less system complexity because it does not need an external heat source and a water balance. However, this process provides low hydrogen yield (Wang and Wang, 2008; Pereira et al., 2011). The ethanol oxidation reaction is shown in Eq. (8)

$$C_2H_5OH + \frac{3}{2}O_2 \leftrightarrow 2CO_2 + 3H_2 \eqno(8)$$

The autothermal reforming of ethanol, also known as an oxidative steam reforming, is almost a thermoneutral process. This type of the reforming method combines the steam reforming and the partial oxidation reactions in a single process. The autothermal reforming reaction is shown in Eq. (9), which 0.61 mole of oxygen is needed to react with one mole of ethanol (Graschinsky et al., 2012).

$$C_2H_5OH + 1.78H_2O + 0.61O_2 \leftrightarrow 2CO_2 + 4.78H_2$$
 (9)

It is noted that in addition to the reforming products, carbon may be occurred under ethanol reforming environmental conditions, as shown in Eqs. (10)–(14). The formation of carbon causes catalyst deactivation, lowering hydrogen production efficiency.

$$2CO \leftrightarrow CO_2 + C \tag{10}$$

$$CH_4 \leftrightarrow 2H_2 + C \tag{11} \\$$

$$CO + H_2 \leftrightarrow H_2O + C \tag{12}$$

$$CO_2 + 2H_2 \leftrightarrow 2H_2O + C \tag{13}$$

$$C_2H_4 \rightarrow polymer \rightarrow 2H_2 + 2C \tag{14} \label{eq:14}$$

2.2. Thermodynamic analysis

Thermodynamic analysis of ethanol reforming processes is performed based on steady-state simulation data (e.g., mass, energy, entropy, and exergy) obtained from a process flowsheet simulator (Aspen Plus). The equilibrium composition of the reforming products is determined by the minimization of a total Gibbs free energy (a non-stoichiometric approach). It is assumed that the reformer is run at atmospheric pressure and a pressure drop is neglected; heat required for the reforming process is supplied by an external source and there are no heat losses to the surrounding; Peng-Robinson equation of state is employed to compute the thermodynamic properties of substances in the process. The primary components involved the ethanol reforming processes are C2H5OH, H2O, O2, CH₃CHO, C₂H₄, H₂, CH₄, CO₂, CO, and C (Lima da Silva et al., 2009). To analyze the carbon formation from thermodynamic point of view, it is assumed that pure carbon is present in the graphitic form. Changes in kinetic and potential exergies are neglected to perform the exergy analysis.

2.2.1. Energy and exergy analysis

Under the steady-state condition, a conservation balance equation around each unit operation in the reforming process can be written as follows (Cohce et al., 2011):

Mass balance:

$$\sum_{i=1}^{N} m_{i,in} = \sum_{i=1}^{N} m_{i,out}$$
 (15)

Energy balance:

$$\sum_{i=1}^{N} n_{i,in} \overline{h}_{i,in} + \dot{Q}_{system} = \sum_{i=1}^{N} n_{i,out} \overline{h}_{i,out}$$
(16)

Entropy balance:

$$\sum_{i=1}^{N} n_{i,in} \overline{s}_{i,in} + \left(\frac{\dot{Q}}{T}\right)_{\text{cyctom}} + \dot{S}_{\text{gen}} = \sum_{i=1}^{N} n_{i,\text{out}} \overline{s}_{i,\text{out}}$$
 (17)

where \dot{S}_{gen} is the entropy generation associated with process irreversibility (\dot{S}_{gen} = 0 for a reversible process and \dot{S}_{gen} > 0 for an irreversible process). A change in the system entropy is due to an entropy generation from internal irreversibility. Although the entropy change of the system and its surroundings may individually increase, decrease or remain constant, the total entropy change or the total entropy generation cannot be less than zero for any process as:

$$\dot{S}_{gen} = \sum_{i=1}^{N} n_{i,out} \overline{s}_{i,out} - \sum_{i=1}^{N} n_{i,in} \overline{s}_{i,in} - \Delta \dot{S}_{system} \geqslant 0$$
 (18)

Exergy balance:

$$\sum_{i=1}^{N} n_{i,in} \overline{Ex}_{i,in} - \sum_{i=1}^{N} n_{i,out} \overline{Ex}_{i,out} = \dot{E}x_{dest}$$
 (19)

where $\overline{Ex}_{i,in}$ and $\overline{Ex}_{i,out}$ are the total exergy flows of stream i entering and leaving the system, respectively. In general, the exergy destroyed depends on a nature of the process and it accounts for the inherent process irreversibility. The exergy destruction demonstrates an important main difference between energy and exergy;

energy is conserved while exergy, a measure of energy quality, can be consumed.

The exergy analysis focuses on the exergy transfer in three forms; exergy of heat (Ex_Q) , physical (Ex_{phys}) and chemical exergy (Ex_{chem}) . The exergy associated with the heat transfer is governed by the Carnot efficiency:

$$Ex_{Q} = Q \cdot \left(1 - \frac{T_{0}}{T}\right) \tag{20}$$

The specific physical exergy can be defined as:

$$Ex_{phys} = (h - h_0) - T_0(s - s_0)$$
(21)

The standard chemical exergy of relevant substances is reported in Table 1 (Szargut et al., 1988) and the specific chemical exergy contribution can be calculated as follows:

$$Ex_{chem} = \sum_{i} x_i (Ex_{chem,i} - RT_0 \ln x_i)$$
 (22)

Energy and exergy efficiencies are evaluated as a ratio of products to inputs. For the overall electrical efficiency, the energy efficiency η is evaluated as:

$$\eta = \frac{\text{net energy output with electricity}}{\text{energy input}}$$
 (23)

and the exergy efficiency ψ as:

$$\psi = \frac{\text{net exergy output with electricity}}{\text{exergy input}}$$
 (24)

2.2.2. SOFC model

The simulation of a SOFC unit is separated into two parts; the first one is anode in which the reactions occur inside the cell and the second one is cathode which supplies oxygen as an oxidant to the anode side. The anode and cathode are represented by an equilibrium reactor module and a separator module, respectively. Because SOFC is operated at high temperatures (1073 K), the direct oxidation of CO and CH₄ contained in the reformate gas is feasible in the SOFC without a catalyst. However, this reaction is less favored than the water gas shift of CO to H₂ and the reforming of CH₄ to H₂. In this study, it was assumed that only the electrochemical reaction of hydrogen is present because the driving force for the anodic oxidation of CO and CH₄ is lower than that for the oxidation of hydrogen, as shown by the higher open circuit voltage of the hydrogen oxidation. Moreover, the kinetic of hydrogen oxidation on the anode is faster than that of CO and CH₄ oxidations.

A generalized steady state model is considered in order to investigate the performance of a SOFC system integrated with reforming process (Aguiar et al., 2004). The theoretical open-circuit cell voltage, which is the maximum voltage under specific operating conditions, can be calculated from the following equations:

Table 1The standard molar chemical exergy of selected substances at reference states (T° = 298.15 K, P° = 101.325 kPa) (Szargut et al., 1988).

•	, , •	
Substance	State	Exergy [kJ/kmol]
C ₂ H ₆ O	g	1363900
	1	1357700
CH ₄	g	831650
CO	g	275100
CO_2	g	19870
H ₂	g	236100
H_2O	g	9500
	1	900
O_2	g	3970
N_2	g	720
C	s, graphite	410260

$$E = E^{0} + \frac{RT}{2F} \ln \left(\frac{P_{H_{2}} P_{O_{2}}^{0.5}}{P_{H_{2}O}} \right)$$
 (25)

where E^0 is the reversible open-circuit potential at standard pressure and is a function of the operating temperature (Ni et al., 2007) as:

$$E^0 = 1.253 - 2.4516 \times 10^{-4} T \tag{26}$$

The actual voltage is determined from the theoretical open-circuit voltage subtracted by the various voltage losses as:

$$V = E - (\eta_{\text{act}} + \eta_{\text{ohmic}} + \eta_{\text{conc}})$$
 (27)

The activation loss at the electrodes (i.e., anode and cathode) ($\eta_{\rm act}$) is caused by the electrochemical reaction and can be explained by the Butler–Volmer equation:

$$i = i_{0, \text{electrode}} \left\{ exp \left[\frac{\alpha nF}{RT} (\eta_{\text{act, electrode}}) \right] - exp \left[-\frac{(1-\alpha)nF}{RT} (\eta_{\text{act, electrode}}) \right] \right\}$$
(28)

$$i_{0,\text{electrode}} = \frac{RT}{nF} k_{\text{electrode}} \exp\left(-\frac{E_{\text{electrode}}}{RT}\right)$$
 (29)

where i is the current density (A/m²), α is the transfer coefficient and i_0 is the exchange current density (A/m²). The pre-exponential factor and the activation energy of the anode and the cathode used for the calculation of $i_{0,\text{electrode}}$ are shown in Table 2 (Aguiar et al., 2004).

The concentration voltage loss ($\eta_{\rm conc}$) occurs when reactants are rapidly consumed at the electrode via the electrochemical reaction so that the concentration gradients are established. Eq. (30) is used to compute this type of voltage loss.

$$\eta_{\text{conc}} = \frac{RT}{2F} \ln \left(\frac{p_{\text{H}_2\text{O},\text{TPB}} p_{\text{H}_2}}{p_{\text{H}_2\text{O}} p_{\text{H}_2,\text{TPB}}} \right) + \frac{RT}{4F} \ln \left(\frac{p_{\text{O}_2}}{p_{\text{O}_2,\text{TPB}}} \right)$$
(30)

where $p_{\rm H_2.TPB}$, $p_{\rm H_2.0,TPB}$, and $p_{\rm O_2,TPB}$ represent the partial pressures of hydrogen, water, and oxygen at the electrode and electrolyte interface, respectively. Their diffusion transport in a porous electrode can be described by Fick's model as given by:

$$p_{\rm H_2,TPB} = p_{\rm H_2} - \frac{RT\tau_{\rm anode}}{2FD_{\rm eff,anode}}i$$
 (31)

$$p_{\rm H_2O,TPB} = p_{\rm H_2O} + \frac{RT\tau_{\rm anode}}{2F\overline{D}_{\rm eff,anode}}i$$
 (32)

$$p_{O_2,TPB} = P - (P - p_{O_2}) \exp\left(\frac{RT\tau_{cathode}}{4FD_{eff,cathode}P}i\right)$$
 (33)

The diffusion coefficients of anode ($D_{\rm eff,anode}$) and cathode ($D_{\rm eff,cathode}$) are 33.4×10^{-5} and 1.37×10^{-5} m²s⁻¹, respectively. It is noted that the first term on the right-hand side of Eq. (30) refers to the anodic concentration overpotential ($\eta_{\rm conc,a}$) and the second one refers to the cathodic concentration overpotential ($\eta_{\rm conc,c}$).

The ohmic loss ($\eta_{\rm ohmic}$) is due to resistances to the flow of ions in the electrolyte and the flow of electrons through the conductive fuel cell components. This loss can be expressed by Ohm's law:

Table 2Pre-exponential factor and activation energy for computing the activation loss in SOFC (Aguiar et al., 2004).

Anode		Cathode	
$k_{ m anode} \ E_{ m anode}$	$6.54 \times 10^{11}\Omega^{-1}m^{-2}$ 140 kJ mol $^{-1}$	$k_{ m cathode} \ E_{ m cathode}$	$\begin{array}{c} 2.35 \times 10^{11} \Omega^{-1} m^{-2} \\ 137 \; kJ \; mol^{-1} \end{array}$

$$\eta_{\rm ohm} = iR_{\rm ohm} \tag{34}$$

where R_{ohm} is total cell internal resistance ($\Omega \text{ cm}^2$), which is calculated from the conductivity of individual layers as given by:

$$R_{Ohm} = \frac{\tau_{anode}}{\sigma_{anode}} + \frac{\tau_{electrolyst}}{\sigma_{electrolyst}} + \frac{\tau_{cathode}}{\sigma_{cathode}}$$
(35)

where $\tau_{\rm anode}$, $\tau_{\rm electrolyte}$ and $\tau_{\rm cathode}$ represent the thickness of the anode, electrolyte, and cathode layers of 500, 20, and 50 µm, respectively, $\sigma_{\rm anode}$ and $\sigma_{\rm cathode}$ are the electronic conductivity of the anode and cathode of 80×10^3 and $8.4\times 10^3~\Omega^{-1}{\rm m}^{-1}$, respectively, and $\sigma_{\rm electrolyst}$ is the ionic conductivity of the electrolyte, which depends on the cell operating temperature as $33.4\times 10^3~{\rm exp}(-10,300/T)~\Omega^{-1}{\rm m}^{-1}$. It is noted that the SOFC electrolyte, anode and cathode are based on yttria-stabilized zirconia (YSZ), nickel-YSZ cermet and strontium-doped lanthanum manganite (LSM), respectively (Arpornwichanop et al., 2009; Petruzzi et al., 2003).

The SOFC efficiency ($\eta_{\rm SOFC}$) is evaluated by the ratio of fuel cell power to the total energy that could be produced if hydrogen entering into the cell is completely burned:

$$\eta_{SOFC} = \frac{Power_{SOFC}}{n_{ETOH,in} \times LHV_{ETOH}} \times 100$$
 (36)

where Power_{SOFC} is the power output of the SOFC and $n_{\text{ETOH,in}}$ and LHV_{ETOH} are the inlet molar flow rate and the lower heating value of ethanol.

The SOFC model mentioned above is included in the flowsheet simulation using a calculation block option.

2.2.3. Model validation

Here, the simulation model used to predict the equilibrium composition of ethanol reforming processes is validated with experimental and simulation data reported in literatures. Fig. 1(a) shows the model prediction of H₂ yield from the steam reforming compared with experimental data (Biswas and Kunzru, 2007). In their experiment, the reforming of ethanol was carried out using Ni/ZrO2. It is observed from Fig. 1(a) that the model can reliably predict the H₂ product under different operating temperatures. Fig. 1(b) compared the H₂ yield of the ethanol partial oxidation process obtained from the simulation and the studies by Sun et al. (2012) and Wang and Wang (2008). The model prediction agrees very well with the reported data. Comparison of the modeling result and experimental data of the ethanol autothermal reforming based on RhPt/ZrO₂ catalyst (Gutierrez et al., 2011) is shown Fig. 1(c) and a good agreement of the model prediction and experimental data of the H₂ yield is observed. Fig. 2 shows a comparison of the SOFC model prediction and experimental data (Zhao and Virkar, 2005) in term of the cell voltage at different current densities and operating temperatures. In their experiment, the inlet fuel consists of 97% H₂ and 3% H₂O and inlet oxidant comprises of 21% O₂. The thickness of anode, cathode, and electrolyte were 1000, 20, and 8 µm, respectively. It indicates that the model prediction shows good agreement with experimental data reported in literature.

3. Results and discussion

3.1. Product distribution

In order to find the optimal operating conditions of the ethanol reforming, providing the highest SOFC performance without facing a carbon formation problem, an analysis of the effect of key design parameters on the reformer performance is first performed. Table 3 shows a range of operating conditions under consideration in this study (Rabenstein and Hacker, 2008; Sun et al., 2012). Effects of reforming temperatures, steam-to-ethanol (S/E) ratio and

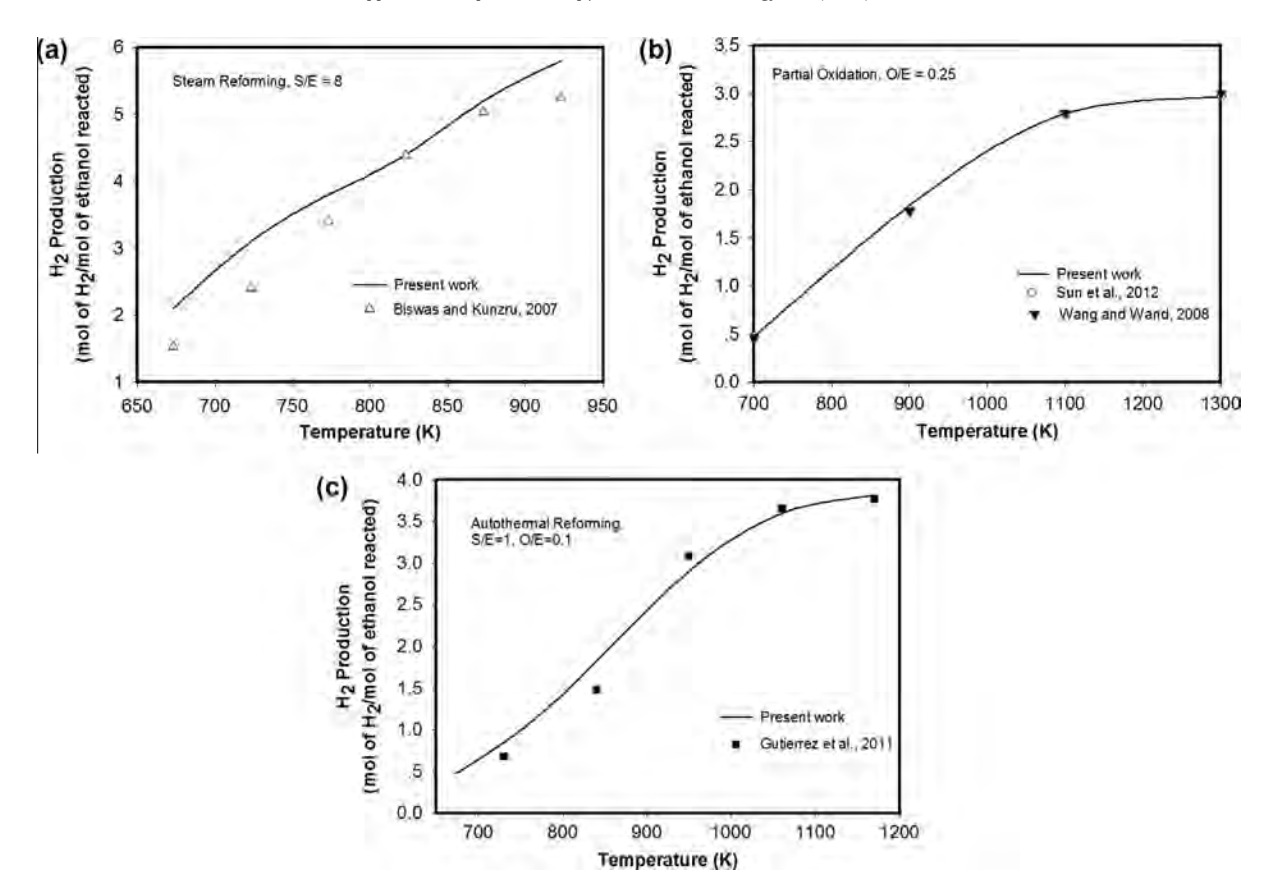


Fig. 1. Comparison of hydrogen yield obtained from the model prediction and reported data in literatures: (a) steam reforming, (b) partial oxidation and (c) autothermal reforming.

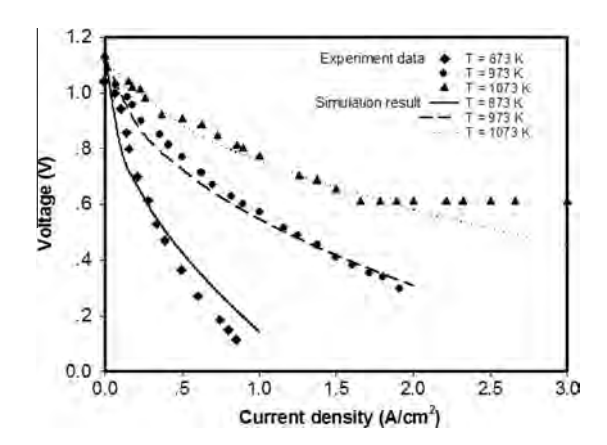


Fig. 2. V-I curve obtained from the SOFC model and experimental data.

oxygen-to-ethanol (O/E) ratio on the product yields of the ethanol reforming processes, i.e., steam reforming, partial oxidation and autothermal reforming, are given in Fig. 3(a)–(c), respectively. A carbon free region of reformer operation is also presented in the figure, so that it will be easy to choose the reforming operational conditions without the formation of carbon. The results clearly indicate that the carbon formation is prone to be occurred when the reformer is operated at low ratio of the reforming reagents for all operating temperatures. It is noted that the intermediate by-products, such as acetaldehyde and ethylene, appears to be a very low content compared with other reforming products.

For the ethanol steam reforming process, H_2 yield increases with the increased temperature and S/E ratio. Severe operating conditions are required to avoid the carbon formation. At temper-

Table 3Range of operating conditions for different ethanol reforming processes.

Ethanol reforming processes	Temperature (K)	S/E	O/E
Steam reforming	700–1200	0-10	-
Partial oxidation	700–1400	-	0-3
Autothermal reforming	700–1200	0-10	0-3

atures higher than 800 K, CH₄ is nearly converted to other reforming products, whereas CO, one of the carbon promoters, is not present in the reforming products at low-temperature operation as a result of the exothermicity of the water gas shift reaction. In order to maximize the SOFC performance, the optimal operating conditions for the reformer is chosen to give high hydrogen fraction without the formation of carbon. When considering the partial oxidation of ethanol, the maximum H₂ and CO yields are found at high operating temperatures (T = 1200-1400 K) and low oxygento-ethanol ratio operation (O/E < 0.5); however, the formation of carbon is unavoidable under these conditions. Thus, it seems that the partial oxidation of ethanol is not a suitable process for hydrogen production. In case of the ethanol autothermal reforming process, oxygen is introduced to the reformer at the oxygento-ethanol ratio of 0.61, according to the stoichiometric ratio of the reaction (Eq. (9)). Fig. 3(c) shows that the product distribution of the autothermal reforming process is similar to that of the steam reforming process and the maximum H2 yield is obtained under the operating temperature above 900 K and the S/E higher than 6; however, high CO₂ is observed under these conditions. A promising advantage of this process is a lower carbon formation activity. When the operating temperature is higher than 1100 K, there is no carbon formation.

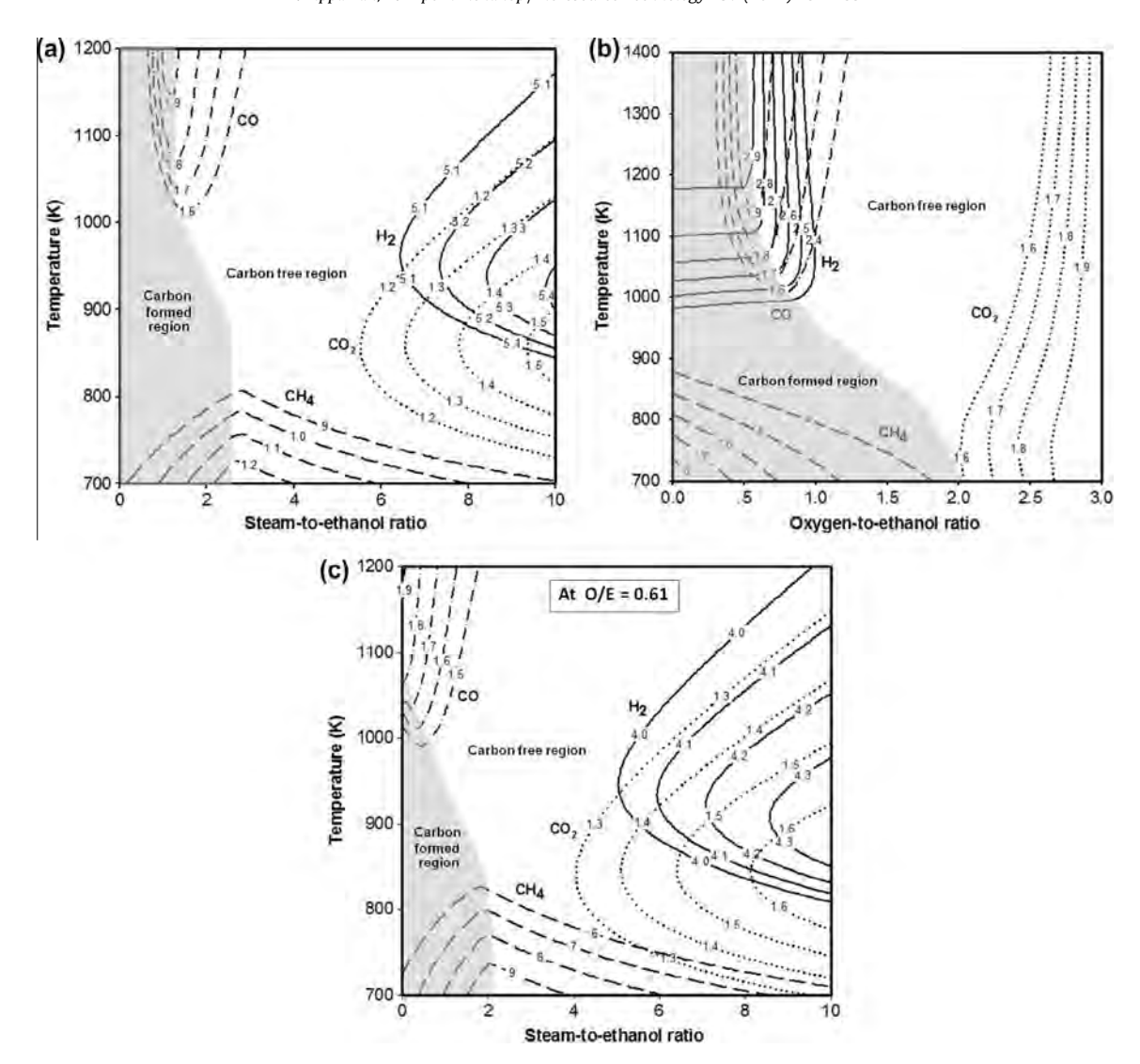


Fig. 3. Effect of temperatures and feed ratio on the product yields: (a) steam reforming, (b) partial oxidation and (c) autothermal reforming (grey area is the carbon formed region and a number on the line is the amount of gaseous products (mole/mole of ethanol feed)).

3.2. SOFC efficiency and reformer heat duty

Fig. 4 shows the effects of feed ratio of ethanol to reforming reagents and operating temperatures on the SOFC efficiency and heat duty required by the reformer. It shows that an increase in the reforming reagents (i.e., H₂O and/or O₂) degrades the efficiency of SOFC because the excess of water causes a fuel dilution effect and the presence of more oxygen enhances the CO oxidation, leading to a decrease in hydrogen fuel. The steam reforming process operated at high temperatures requires more heat duty (Fig. 4(a)). To achieve the maximum SOFC efficiency (≈67.5%), the steam reformer should be operated at temperatures higher than 1000 K and S/E ratio of 1.5; however, under these conditions, the system needs the high level of energy input and faces the carbon formation problem. Thus, the reformer is suggested to be run at a lower temperature (T = 980 K) and more steam input is required (S/E = 1.8) to move the operating point to a carbon free region (star symbol in Fig. 4(a)). Regarding the partial oxidation process as shown in Fig. 4(b), the reformer heat duty depends on the quantity of O_2 feed. If the oxygen-to-ethanol ratio increases, high heat will be released due to the exothermicity of the partial oxidation reaction. However, the SOFC fed by the synthesis gas from the partial oxidation reactor generates less electricity power than that from other reforming processes. When considering the performance of SOFC and the avoidance of carbon formation in the reactor, the partial oxidation reformer is selected to be operated at the temperature of 1150 K and the O/E ratio of 0.6. Fig. 4(c) shows effect of the amount of reforming agents, i.e., steam and oxygen, on the heat duty of the autothermal reformer (operated at 1000 K) and the efficiency of SOFC. The SOFC efficiency is enhanced when less oxygen is introduced to the autothermal reformer. In general, a heat duty of the autothermal reforming is a key operational factor for this process. The results indicate that the endothermic steam reforming and the exothermic partial oxidation can be balanced by adjusting oxygen feed to reach a thermal-neutral operation, which an external heat input is unnecessary. To achieve the maximum efficiency while minimizing the energy demand, the autothermal reformer should be operated at temperature of 1000, S/E ratio of 1.5 and O/E ratio of 0.5 and thus, the SOFC efficiency of 56% is obtained. The selected operating conditions of different ethanol reforming processes are summarized in Table 4.

3.3. Energy and exergy analysis

A comparison of the energy demand for the ethanol reforming processes operated at their optimal conditions is shown in

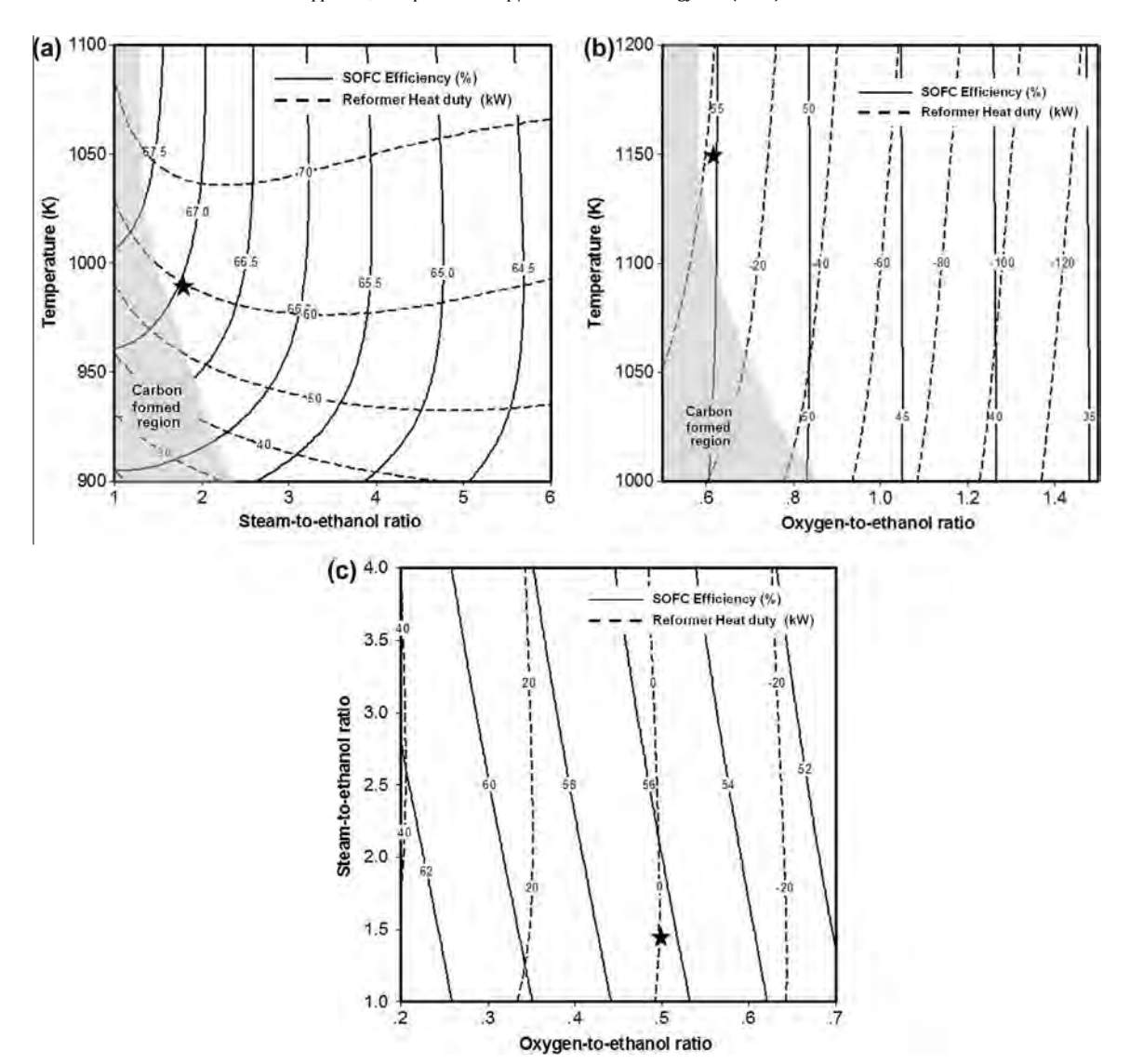


Fig. 4. Effect of temperatures and feed ratio on SOFC efficiency and reformer heat duty: (a) steam reforming, (b) partial oxidation and (c) autothermal reforming.

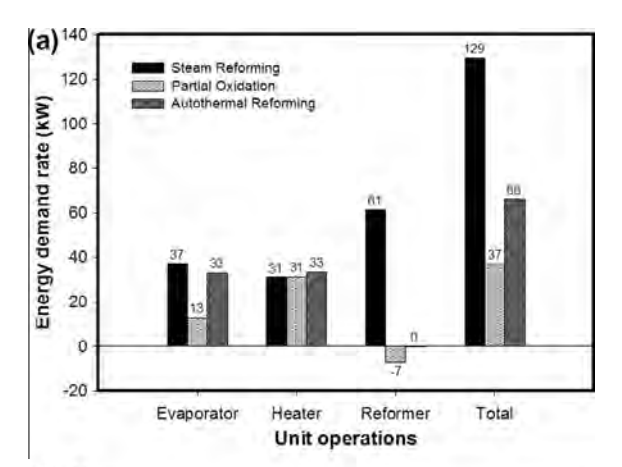
Fig. 5(a). It is found that the steam reforming of ethanol requires the highest energy consumption process because of extremely endothermic operation, whereas the partial oxidation process needs the lowest one. In the partial oxidation process, the heater is a unit that needs the highest energy because preheating air requires high amount of energy. However, the heat requirement in the evaporator is lower than the other two reforming processes because only liquid ethanol is evaporated. When considering the total energy demand of the fuel processor including the evaporator, heater and reformer, the partial oxidation process seems to be operated at a thermoneutral condition. A steam requirement of the steam reforming and autothermal reforming processes causes a higher heat load in the evaporator.

Fig. 5(b) shows the exergy destruction in each unit of the ethanol reforming processes. In general, a process unit involved

chemical reactions affects the overall process irreversibility because chemical reactions are related to the motion of electrons during forming and breaking chemical bonds between atoms. High frequency of molecular collisions causes an increase in entropy within the system, resulting in high exergy destruction. For the reforming processes to produce hydrogen, the ethanol reformer dominates the total rate of exergy destruction. The partial oxidation reactor is the unit that causes the highest exergy destruction because its flow of exergy is associated with a large difference in heat transfer between reactant feed (input) and synthesis gas product (output). In other words, exothermic or combustion processes lose more the exergy of heat. In addition, the partial oxidation is operated at higher temperature than other processes. For this reason, reactant and product gases will spread quickly and collide with each other frequently, so the entropy is more

Table 4Optimal conditions for each ethanol reforming process.

Ethanol reforming processes	T (K)	S/E	O/E	SOFC efficiency (%)	Reformerheat duty (kW)
Steam reforming (SR)	980	1.8	_	66.89	61.20
Partial oxidation (POX)	1150	-	0.6	55.60	-7.22
Autothermal reforming (ATR)	1000	1.5	0.5	56.36	-0.32



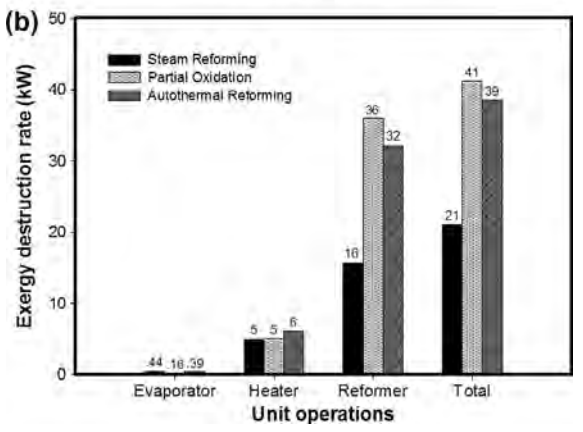


Fig. 5. Comparison of (a) energy demand and (b) exergy destruction in different ethanol reforming processes at the optimal operating conditions.

generated and then destroys some exergy. On the other hand, the steam reformer can maintain the quality of energy as shown in a reformer part of the steam reforming process (Fig. 5(b)). The results also indicate that in the evaporator, high value of the energy demand turns into an excellent exergetic performance. The total exergy destruction in the ethanol reforming processes follows in order: partial oxidation > autothermal reforming > steam reforming.

3.4. Ethanol reforming process for solid oxide fuel cell applications

Based on the thermodynamic analysis, an implementation of the ethanol reforming processes for SOFC applications is addressed from a practical point of view. It is found that the ethanol steam

Table 5Energy and exergy efficiencies of ethanol reforming processes and their exergy destruction in the SOFC system.

Ethanol reforming processes	Efficiency (%)		Exergy destruction	
	Energy	Exergy	(kW)	
Steam reforming (SR)	66.89	60.60	21.11	
Partial oxidation (POX) Autothermal reforming (ATR)	55.60 56.36	50.37 51.06	41.24 38.58	

reforming process requires high energy consumption and thus its integration with the SOFC is preferable as the high quality of an exhaust gas from the anode and afterburner can be employed in the steam reforming process, e.g., evaporation and heating units, as shown in Fig. 6. The SOFC system consists of three main parts: (1) fuel processor where ethanol is converted into hydrogen-rich gases, (2) SOFC where electricity is generated from the electrochemical reaction of hydrogen and oxygen and (3) afterburner where the residual fuel from the SOFC is combusted in order to generate useful heat for other heat requiring parts of the SOFC system. The autothermal reforming process can be managed without the need for external heat sources, leading to a simpler design and higher reforming efficiency. Therefore, it would be more suitable for automobile, residential and portable applications (Lin et al., 2007; Dawes et al., 2009). From the thermodynamic viewpoint, the partial oxidation of ethanol is not a good option for hydrogen production. Although, this process requires less energy demand, its exergetic efficient is low due to the high-temperature operation. In addition, it generates the reformate gas with high CO content and thus, needs a purification process to give more pure hydrogen. It is noted that the autothermal reforming and the partial oxidation of ethanol have lower energy and exergy efficiencies, even though exhaust gases from the anode and afterburner are used in evaporation and heating units. Table 5 summarizes the energy and exergy efficiencies of the ethanol reforming processes and their exergy destruction in the SOFC system.

4. Conclusion

Thermodynamic analysis of different ethanol reforming processes was performed. The optimal operating conditions of each reforming process to maximize the SOFC efficiency were identified. Energy and exergy analysis were also carried out to find the best ethanol reforming process. Although the steam reforming process provides the highest hydrogen yield, it is the highest energy requiring process. The exergy analysis showed that the highest exergy destruction is found in the partial oxidation process. The integration

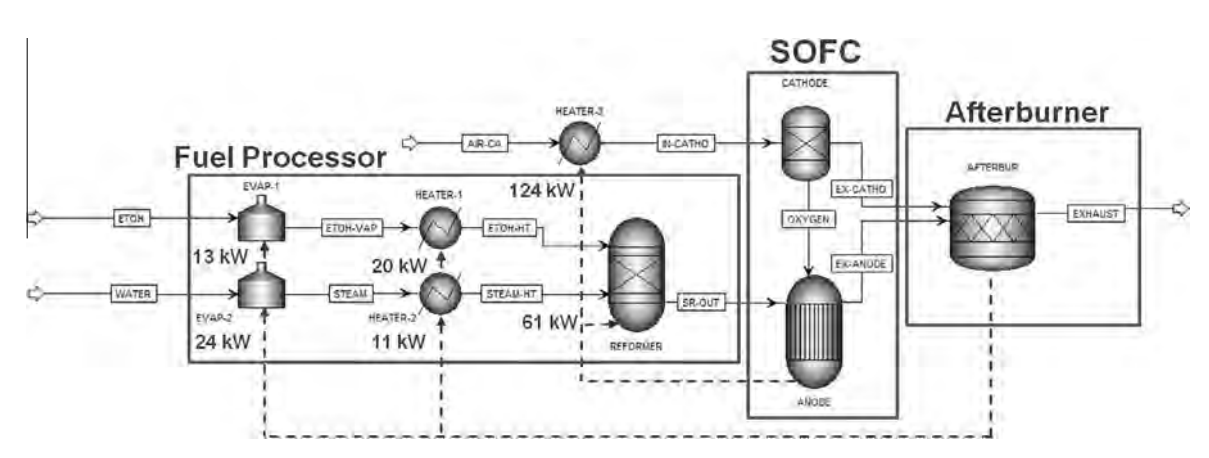


Fig. 6. Ethanol steam reforming integrated with solid oxide fuel cell system.

of ethanol steam reformer operated at temperature of 980 K and steam-to-ethanol ratio of 1.6 and solid oxide fuel cell provides the best energetic and exergetic performances.

Acknowledgements

Support from the Ratchadaphiseksomphot Endowment Fund of Chulalongkorn University (RES560530067-EN) and the Thailand Research Fund is gratefully acknowledged.

P. Tippawan would like to thank the Dutsadiphiphat Scholarship, Ratchadaphiseksomphot Endowment Fund, Chulalongkorn University.

References

- Aguiar, P., Adjiman, C.S., Brandon, N.P., 2004. Anode-supported intermediate temperature direct internal reforming solid oxide fuel cell. I: model-based steady-state performance. J. Power Sources 138, 120–136.
- Arpornwichanop, A., Chalermpanchai, N., Patcharavorachot, Y., Assabumrungrat, S., Tade, M., 2009. Performance of an anode-supported solid oxide fuel cell with direct-internal reforming of ethanol. Int. J. Hydrogen Energy 34, 7780–7788.
- Benito, M., Sanz, J.L., Isabel, R., Padilla, R., Arjona, R., Daza, L., 2005. Bio-ethanol steam reforming: Insights on the mechanism for hydrogen production. J. Power Sources 151, 11–17.
- Biswas, P., Kunzru, D., 2007. Steam reforming of ethanol for production of hydrogen over Ni/CeO₂–ZrO₂ catalyst: effect of support and metal loading. Int. J. Hydrogen Energy 32, 969–980.
- Cardona, C.A., Sánchez, O.J., 2007. Review fuel ethanol production: process design trends and integration opportunities. Bioresour. Technol. 98, 2415–2457.
- Casas, Y., Arteaga, L.E., Morales, M., Rosa, E., Peralta, L.M., Dewulf, J., 2010. Energy and exergy analysis of an ethanol fueled solid oxide fuel cell power plant. Chem. Eng. J. 162, 1057–1066.
- Cohce, M.K., Dincer, I., Rosen, M.A., 2011. Energy and exergy analyses of a biomass-based hydrogen production system. Bioresour. Technol. 102, 8466–8474.
- Dawes, J.E., Hanspal, N.S., Family, O.A., Turan, A., 2009. Three dimensional CFD modelling of PEM fuel cells: an investigation into the effects of water flooding. Chem. Eng. Sci. 64, 2781–2794.
- Douvartzides, S., Coutelieris, F., Tsiakaras, P., 2004. Exergy analysis of a solid oxide fuel cell power plant fed by either ethanol or methane. J. Power Sources 131, 224–230.

- El-Emam, R.S., Dincer, I., 2011. Energy and exergy analyses of a combined molten carbonate fuel cell gas turbine system. Int. J. Hydrogen Energy 36, 8927–8935.
- Graschinsky, C., Giunta, P., Amadeo, N., Laborde, M., 2012. Thermodynamic analysis of hydrogen production by autothermal reforming of ethanol. Int. J. Hydrogen Energy 37, 10118–10124.
- Gutierrez, A., Karinen, R., Airaksinen, S., Kaila, R., Krause, A.O.I., 2011. Autothermal reforming of ethanol on noble metal catalysts. Int. J. Hydrogen Energy 36, 8967–8977.
- Lima da Silva, A., Malfatti, C.F., Müller, I.L., 2009. Thermodynamic analysis of ethanol steam reforming using Gibbs energy minimization method: a detailed study of the conditions of carbon deposition. Int. J. Hydrogen Energy 34, 4321– 4330.
- Lin, Y., Lin, C., Chen, Y., Yin, K., Yang, C., 2007. An analytical study of the PEM fuel cell with axial convection in the gas channel. Int. J. Hydrogen Energy 32, 4477–4488
- Lin, J., Babbitt, C.W., Trabold, T.A., 2013. Life cycle assessment integrated with thermodynamics analysis of bio-fuel options for solid oxide fuel cells. Bioresour. Technol. 128, 495–504.
- Ni, M., Leung, M.K.H., Leung, D.Y.C., 2007. Parametric study of solid oxide fuel cell performance. Energy Convers. Manage 48, 1525–1535.
- Pereira, E.B., Ramírez de la Piscina, P., Homs, N., 2011. Efficient hydrogen production from ethanol and glycerol by vapor-phase reforming processes with new cobalt-based catalysts. Bioresour. Technol. 102, 3419–3423.
- Petruzzi, L., Cocchi, S., Fineschi, F., 2003. A global thermo-electrochemical model for SOFC systems design and engineering. J. Power Sources 118, 96–107.
- Rabenstein, G., Hacker, V., 2008. Hydrogen for fuel cells from ethanol by steam-reforming, partial-oxidation and combined auto-thermal reforming: a thermodynamic analysis. J. Power Sources 185, 1293–1304.
- Rosen, M.A., Dincer, I., Kanoglu, M., 2008. Role of exergy in increasing efficiency and sustainability and reducing environmental impact. Energy Policy 36, 128–137.
- Song, S., Douvartzides, S., Tsiakaras, P., 2005. Exergy analysis of an ethanol fuelled proton exchange membrane (PEM) fuel cell system for automobile applications. J. Power Sources 145, 502–514.
- Sun, S., Yan, W., Sun, P., Chen, J., 2012. Thermodynamic analysis of ethanol reforming for hydrogen production. Energy 44, 911–924.
- Szargut, J., Morris, D.R., Steward, F.R., 1988. Exergy Analysis of Thermal, Chemical, and Metallurgical Processes. Springer.
- Vaidya, P.D., Rodrigues, A.E., 2006. Review insight into steam reforming of ethanol to produce hydrogen for fuel cells. Chem. Eng. J. 117, 39–49.
- Wang, W., Wang, Y., 2008. Thermodynamic analysis of hydrogen production via partial oxidation of ethanol. Int. J. Hydrogen Energy 33, 5035–5044.
- Zhao, F., Virkar, A., 2005. Dependence of polarization in anode-supported solid oxide fuel cells on various cell parameters. J. Power Sources 141, 79–95.



Contents lists available at ScienceDirect

Energy

journal homepage: www.elsevier.com/locate/energy



Effect of different fuel options on performance of high-temperature PEMFC (proton exchange membrane fuel cell) systems



Suthida Authayanun ^a, Dang Saebea ^b, Yaneeporn Patcharavorachot ^c, Amornchai Arpornwichanop ^d,*

- ^a Department of Chemical Engineering, Faculty of Engineering, Srinakharinwirot University, Nakhon Nayok 26120, Thailand
- ^b Department of Chemical Engineering, Faculty of Engineering, Burapha University, Chonburi 20131, Thailand
- ^c School of Chemical Engineering, Faculty of Engineering, King Mongkut's Institute of Technology Ladkrabang, Bangkok 10520, Thailand
- d Computational Process Engineering, Department of Chemical Engineering, Faculty of Engineering, Chulalongkorn University, Bangkok 10330, Thailand

ARTICLE INFO

Article history: Received 13 January 2014 Received in revised form 19 February 2014 Accepted 27 February 2014 Available online 21 March 2014

Keywords: High-temperature PEMFC CO poisoning Reforming Hydrogen Performance analysis

ABSTRACT

High-temperature proton exchange membrane fuel cells (HT-PEMFCs) have received substantial attention due to their high CO (carbon monoxide) tolerance and simplified water management. The hydrogen and CO fractions affect the HT-PEMFC performance and different fuel sources for hydrogen production result in different product gas compositions. Therefore, the aim of this study is to investigate the theoretical performance of HT-PEMFCs fueled by the reformate gas derived from various fuel options (i.e., methane, methanol, ethanol, and glycerol). Effects of fuel types and CO poisoning on the HT-PEMFC performance are analyzed. Furthermore, the necessity of a water-gas shift (WGS) reactor as a CO removal unit for pretreating the reformate gas is investigated for each fuel type. The methane steam reforming shows the highest possibility of CO formation, whereas the methanol steam reforming produces the lowest quantity of CO in the reformate gas. The methane fuel processing gives the maximum fraction of hydrogen (\approx 0.79) when the WGS reactor is included. The most suitable fuel is the one with the lowest CO poisoning effect and the maximum fuel cell performance. It is found that the HT-PEMFC system fueled by methanol without the WGS reactor and methane with WGS reactor shows the highest system efficiency (\approx 50%).

© 2014 Elsevier Ltd. All rights reserved.

1. Introduction

Traditionally, a combustion process of petroleum-derived fuel, which is a limited resource, is used for power generation. However, this process has low efficiency and releases greenhouse gases, which are the major cause of global warming. Because of the need for clean energy and an efficient method for clean energy production, substantial effort has been directed toward the development of fuel cell technology for electricity generation. Fuel cells have been continuously developed to supply considerable energy demand. In addition to electricity, fuel cells generate only water and heat as by-products and are thus environmentally friendly and sustainable [1].

Among the several types of fuel cells, polymer electrolyte membrane or proton exchange membrane fuel cells (PEMFCs) are very attractive for automobile, residential and portable applications because they are operated at low temperatures of approximately 333–353 K, which allows them to start up very quickly. In addition, they exhibit a good response to changes in power demand and high current density [2]. However, there are some difficulties in the operation of PEMFCs that need to be solved for real applications. In general, high-purity hydrogen with few contaminants, especially carbon monoxide (CO), is required for PEMFC. The presence of CO in the hydrogen feed will poison the Pt catalysts at the anode of the PEMFC, reducing the active sites available for electrochemical reactions. Therefore, a complex CO removal process of the hydrogen feedstock is needed to reduce the CO concentration to less than 10 ppm [3]. Another important problem influencing PEMFC operation is water management because of the low operating temperatures and the specific characteristics of the membrane used in the PEMFC [4,5]. The fuel must be saturated with water to avoid the dry-out condition of the polymer membrane. Nevertheless, the excess water may condense into the liquid phase and cause a flooding problem in the cathode gas diffusion layer, which would block oxygen to transport to the catalyst layer, resulting in fuel cell voltage and performance losses.

^{*} Corresponding author. Tel.: +66 2 218 6878; fax: +66 2 218 6877. E-mail address: Amornchai.A@chula.ac.th (A. Arpornwichanop).

To solve the problem mentioned above, a high-temperature proton exchange membrane fuel cell (HT-PEMFC) operating at temperatures of approximately 373-473 K has recently been developed. As a result of the high-temperature operation of the PEMFC, the transport of water within the PEMFC is simplified and electrochemical reaction rates at the anode and cathode are increased. The flooding problem is eliminated because water is present in the vapor phase only at temperatures above 373 K. However, such conditions can lead to the dehydration of the membrane and the loss of membrane ionic conductivity. The efficiency of conventional PEMFCs relies on water content in the membrane; thus, its performance is depressed when the water content is low. To overcome this difficulty, a polybenzimidazole (PBI) has been developed for use in HT-PEMFCs that can be operated at low relative humidity. In addition, it is usually doped with phosphoric acid or other dopants to increase the proton conductivity [6,7].

The enhancement of CO tolerance is an important benefit of operating PEMFCs at high temperatures. From a thermodynamic point of view, the adsorption of CO on the Pt surface is reduced by increasing the temperature and/or decreasing the CO concentration [8]. The possibility of hydrogen adsorption, which is less exothermic than CO adsorption, would increase at higher operating temperatures. Moreover, the CO purification process of the HT-PEMFC system is simpler than that of the conventional PEMFC. The preferential oxidation, pressure swing adsorption or membrane separation is unnecessary for the HT-PEMFC system. Thus, the hydrogen-rich gas from the fuel reforming processes can be fed to the HT-PEMFC directly without the need for the sophisticated CO removal process; instead, only a water-gas shift (WGS) reactor, which functions as a simple CO removal unit, is needed.

Recently, the fuel cell integrated with a fuel processor, which allows hydrogen generation from hydrocarbon fuels, and the combined heat and power (CHP)-based PEMFC system are continuously developing to avoid the issue of hydrogen infrastructure and increase the system efficiency [9,10]. In addition, the performance of conventional PEMFC and HT-PEMFC systems for various applications has been studied [9,11,12]. At present, natural gas is the most common fuel for hydrogen production because of its cost effectiveness for industrial applications. However, natural gas is limited and insufficient for the increased energy demand. Methanol has also received much more attention as a hydrogen-production feedstock for PEMFCs because it is a small molecule and is thus easily converted into hydrogen. The high hydrogen-to-carbon ratio and the absence of carbon-carbon bonds in methanol allow it to be reformed into hydrogen at low operating temperatures [13]. These conditions favor the water-gas shift reaction in the reformer, which reduces the CO content in the reformate gas.

Because of the increased power demand and environmental concerns, the development of a new, sustainable feedstock for hydrogen production is necessary. Ethanol and glycerol as renewable resources will become the most important fuel sources [14–17]. Ethanol appears to be an appropriate fuel for the production of hydrogen for PEMFCs because it can be reformed at low temperatures, similar to methanol. Because the use of biodiesel for diesel engines is growing, the by-product glycerol that is generated from the conventional biodiesel production process is also a potential fuel for use in the production of hydrogen [18–21]. Because hydrogen and CO have an effect on the HT-PEMFC performance and different fuel sources used for hydrogen production result in different product gas compositions, the most suitable fuel for the HT-PEMFC system should be investigated.

The aim of this work is to theoretically study the performance of HT-PEMFCs fueled by various fuel options. The model of HT-PEMFC, which considers the effect of CO poisoning, is used to analyze HT-

PEMFC performance. Methane and other oxygenated hydrocarbons, such as methanol, ethanol and glycerol, are used to produce hydrogen-rich gas (reformate gas) for the HT-PEMFC. In addition, the necessity of a water-gas shift reactor to function as a CO removal unit for pretreating the reformate gas before it is fed to the HT-PEMFC is investigated for each fuel type. The most suitable fuel and optimal conditions, which are those resulting in the lowest CO poisoning effect and the maximum fuel cell performance, are examined.

2. Description of the HT-PEMFC system

The HT-PEMFC system considered here consists of two main parts, which are fuel-processing process and HT-PEMFC. The mathematical models of the HT-PEMFC system are developed and coded in Matlab.

2.1. Fuel-processing process

Considering the fuel-processing process for HT-PEMFC, the steam reforming process with and without water-gas shift reactor is considered in this work. A thermodynamic approach is used to analyze the reforming process with different fuels, i.e., glycerol, ethanol, methanol and methane. For a given set of substances involved in the reforming reactions, the equilibrium composition of the reformate gas from steam reformers is directly determined by solving the minimization problem of the Gibbs free energy (Eq. (1)) [22].

$$\min_{n_i} \left(G^t \right)_{T,P} = \sum_{i=1}^C n_i \overline{G}_i = \sum_{i=1}^C n_i \left(G_i^0 + RT \ln \frac{\overline{f}_i}{f_i^0} \right) \tag{1}$$

where C is the total number of components in the reaction system and n_i is the number of moles of each gaseous component. Regarding the conservation of atomic species, n_i must satisfy the element balance in Eq. (2).

$$\sum_{i} n_{i} a_{ik} - A_{k} = 0 \quad (k = 1, 2, ..., w)$$
 (2)

where a_{ik} is the number of atoms of element k in component i, A_k is the total number of atoms of element k in the reaction mixture, and w is the total number of elements.

The optimization problem mentioned above is finding the set of n_i that minimizes G_t for the specified T and P and that satisfies the element balances. To solve such an optimization problem, Lagrange multipliers method is applied [22]. Table 1 shows the set of substances involved the reforming process of each type of fuel. Based on experimental data of the low-temperature methanol steam reforming, methane is not included in the set of substances in the methanol reforming process [23]. However, methane is a key component of the steam reforming of several fuels, such as natural gas, glycerol, and ethanol [24–26]. For WGS reactor, it is modeled as an equilibrium reactor and only the water gas shift reaction is occurred in this reactor [27].

Table 1Sets of substances resulting from the steam reforming process.

Fuel	Set of substances
Glycerol (C ₃ H ₈ O ₃)	C ₃ H ₈ O ₃ , CH ₄ , CO ₂ , CO, H ₂ O, H ₂
Ethanol (C ₂ H ₅ OH)	C ₂ H ₅ OH, CH ₄ , CO ₂ , CO, H ₂ O, H ₂
Methanol (CH ₃ OH)	CH ₃ OH, CO ₂ , CO, H ₂ O, H ₂
Methane (CH ₄)	CH ₄ , CO ₇ , CO, H ₂ O, H ₇

2.2. HT-PEMFC

The HT-PEMFC is a promising PEMFC technology that has been developed to address the CO poisoning problem. Because the hydrogen and CO fractions of the reformate gas depend on the raw materials used for hydrogen production, HT-PEMFC systems running on different fuels produce different power outputs. In this study, various fuel options for producing the reformate gas from the steam reforming process for HT-PEMFC operation are considered with the aim of finding a suitable fuel and an appropriate fuel processing method for each fuel for this HT-PEMFC system.

An electrochemical model is used to evaluate the cell performance. The relation of voltage and current density for HT-PEMFC is shown in Eq. (3). The cell voltage ($E_{\rm cell}$) is calculated from the reversible cell potential ($E_{\rm r}$) and various voltage losses, which are activation loss at the anode ($\eta_{\rm act,c}$), the activation loss at the cathode ($\eta_{\rm act,c}$) and the ohmic loss ($\eta_{\rm ohmic}$).

$$E_{\text{cell}} = E_{\text{r}} - \eta_{\text{act,a}} - \eta_{\text{act,c}} - \eta_{\text{ohmic}}$$
 (3)

Detail of the model describing the reversible cell potential and voltage losses of the HT-PEMFC based on a phosphoric acid doped polybenzimidazole membrane is summarized in Table 2. The activation loss at the anode and cathode can be calculated from the Butler—Volmer equation. Because the reformate gas from the steam reforming process is used as a fuel, the CO poisoning effect is taken into account by using $i_0^{\rm CO}$ (the exchange current density of hydrogen oxidation in the presence of CO) instead of i_0 at the anode. The Ohmic loss, which is caused by the resistance of ions in the electrolyte through the membrane, can be calculated from the current density, the membrane thickness ($l_{\rm m}$) and the proton conductivity ($\sigma_{\rm m}$), as shown in Table 2.

The concentrations of hydrogen and oxygen at the catalyst surface are determined using the Stefan—Maxwell equation and Fick's law, which represent the diffusion model of the reactant in the gas diffusion layer and film electrolyte, respectively [28]. The Stefan—Maxwell equation (Eq. (4)) is used to describe diffusion of multi-component gaseous streams and find the mole fraction of the components at the gas diffusion layer/electrolyte film interface when the mole fraction of the component at the initial boundary of the gas diffusion layer is calculated from the average value of the component mole fractions at the inlet and outlet of the flow channel.

Table 2 Electrochemical model of the HT-PEMFC [28,29].

Reversible cell potential
$$E_{\Gamma} = -\left(\frac{\Delta H_{\Gamma}}{nF} - \frac{T\Delta S_{\Gamma}}{nF}\right) + \frac{RT}{nF} \ln \left[\frac{(RT)^{1.5}C_{H_2-Pt}C_{0_2-Pt}^{0.5}}{a_{H_2}o}\right]$$
Anode activation loss
$$\eta_{\text{act},a} = \frac{RT}{aF} \sinh^{-1}\left(\frac{i}{2i_0(1-\theta_{\text{co}})^2}\right)$$

$$i_0 = i_{0,a}^{\text{ref}} a_{\text{c},a} L_{\text{c},a} \left(\frac{C_{\text{Pc}}}{C_{\text{ref},a}}\right)^{\gamma} \exp \left[-\frac{E_{c,a}}{RT} \left(1 - \frac{T}{T_{\text{ref},a}}\right)\right]$$

$$\theta_{\text{CO}} = a^* \ln \frac{|C0|}{|C0|} + b^* \ln (i)^* \ln \frac{|C0|}{|E0|} + c$$

$$a = -0.00012784 * T^2 + 0.11717499 * T - 26.62908873$$

$$b = 0.0001416 * T^2 - 0.12813608 * T + 28.852463626$$

$$c = -0.00034886 * T^2 + 0.31596903 * T - 70.11693333$$
Cathode activation
$$loss$$

$$\eta_{\text{act},c} = \frac{RT}{aF} \sinh^{-1}\left(\frac{i}{2l_0}\right)$$

$$i_0 = i_{0,c}^{\text{ref}} a_{\text{cc}} L_{\text{cc}}\left(\frac{C_{\text{N}}}{C_{\text{ref},c}}\right)^{\gamma} \exp \left[-\frac{E_{cc}}{RT} \left(1 - \frac{T}{T_{\text{ref},c}}\right)\right]$$
Ohmic loss
$$\eta_{\text{ohmic}} = \left(\frac{\sigma_m}{I_m}\right) i$$

$$\sigma_m = \frac{A}{T} \exp \left(\frac{-B}{R(T)}\right)$$

$$A = \exp((k_1^n RH^3) + (k_2^n RH^2) + (k_3^n RH) + k_0^n)$$

$$B = (k_1^h RH^3) + (k_2^h RH^2) + (k_3^h RH) + k_0^n$$

$$\frac{\mathrm{d}X_i}{\mathrm{d}z} = \frac{RT}{P} \sum \frac{X_i N_j - X_j N_i}{D_{ii}^{\mathrm{eff}}} \tag{4}$$

In this work, the catalyst layer is assumed to be an average of the solid electrode and the electrolyte. Fick's law is applied to explain a transport of gaseous reactants from the gas diffusion layer through an electrolyte film covering the catalyst agglomerates to reach the catalyst active surface and determine the H₂ and O₂ concentrations at the catalyst active surface covered by the thin polymer/acid film (Eqs. (5) and (6)).

$$\frac{N_{\rm O_2}}{S_{\rm Pt-cathode}} = \frac{-D_{\rm O_2} \left(C_{\rm O_2-Pt} - C_{\rm O_2(dissolve)} \right)}{\delta_{\rm cathode}} \tag{5}$$

$$\frac{N_{\rm H_2}}{S_{\rm Pt-anode}} = \frac{-D_{\rm H_2} \left(C_{\rm H_2-Pt} - C_{\rm H_2(dissolve)} \right)}{\delta_{\rm anode}} \tag{6}$$

The concentrations of H_2 and O_2 dissolving at the film electrolyte layer boundary $(C_{H_2(dissolve)}$ and $C_{O_2(dissolve)})$ can be calculated from their solubility values $(C_i^{dissolved})$ and the mole fractions of H_2 and O_2 at the GDL/electrolyte film interface $(X_{H_2}$ and $X_{O_2})$ as follows:

$$C_{\text{H}_2(\text{dissolve})} = C_{\text{H}_2}^{\text{dissolved}} \cdot X_{\text{H}_2} \cdot P$$
 (7)

$$C_{O_2(dissolve)} = C_{O_2}^{dissolved} \cdot X_{O_2} \cdot P$$
 (8)

To evaluate the performance of the HT-PEMFC, the power density (P_{FC}) is given in Eq. (9).

$$P_{\rm FC} = iE_{\rm cell} \tag{9}$$

The system efficiency of the PEMFC integrated with the reforming process is estimated by Eq. (10). The energy required for the reforming process is partially supplied by the heat recovery $(Q_{\rm rec})$ from the anode and cathode exhaust gases as well as from the high-temperature product gas of the reforming process.

$$\eta_{\rm sys} = \frac{P_{\rm FC}}{m_{\rm fuel} \cdot \rm LHV_{\rm fuel} + Q_{\rm ref} - Q_{\rm rec}}$$
 (10)

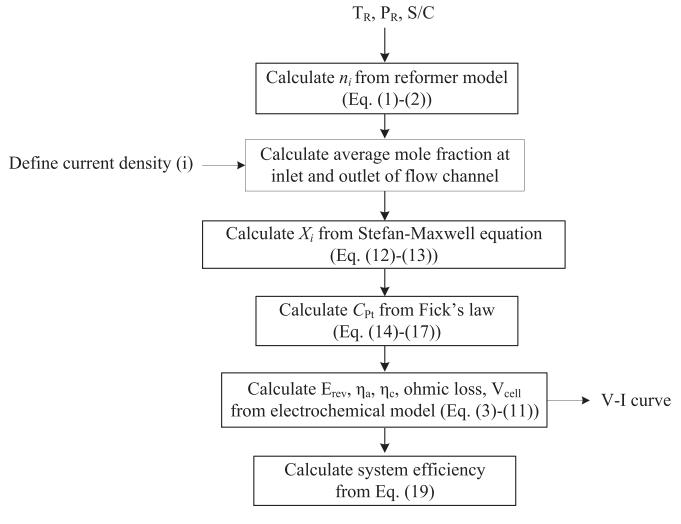


Fig. 1. Model solution of the integrated reforming process and HT-PEMFC system.

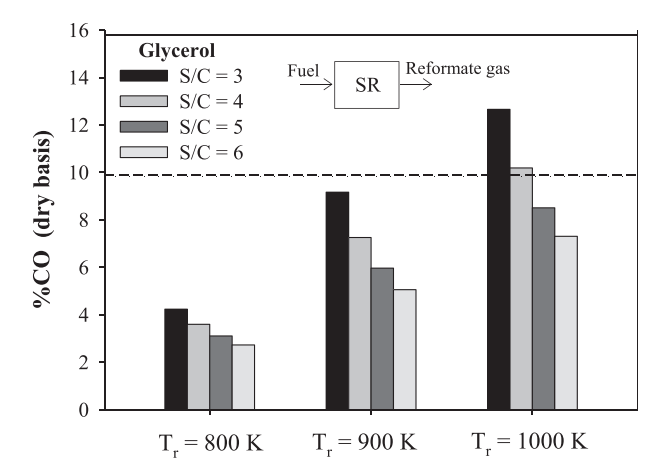


Fig. 2. %CO in the reformate gas from glycerol steam reforming at different operating conditions.

3. Simulation approach

In this work, the mathematical models describing the fuel processor and the HT-PEMFC are programmed using Matlab. The model solution approach to the reforming process and HT-PEMFC integrated system is shown in Fig. 1. The reformer temperature, reformer pressure and steam-to-carbon (S/C) ratio are prespecified. The molar flow rate and composition of the reformate gas are calculated from the direct minimization of Gibbs free energy using the Lagrange multipliers method. The fsolve function in Matlab is employed to solve a set of non-linear thermodynamic equations. Subsequently, the product gases are fed to the flow channel of the HT-PEMFC. All the model parameters in the HT-PEMFC model can be found in our previous work [29]. The outlet gas compositions are calculated from the fuel utilization and current density. The Stefan–Maxwell equation is used to find the mole fraction of the reactant gases at the gas diffusion layer/film electrolyte interface. In general, gaseous reactants diffuse through the electrolyte film layer before reaching the catalyst active area, and Fick's law is applied to explain this phenomenon. Then, the electrochemical model is applied to calculate the activation loss, ohmic loss and cell voltage, and the *V*–*I* curve of the HT-PEMFC is plotted. Finally, the system efficiency is calculated by considering the heat recovery. Heat from hot reformate gases and the anode and cathode off gases are recovered and used to preheat and vaporize the

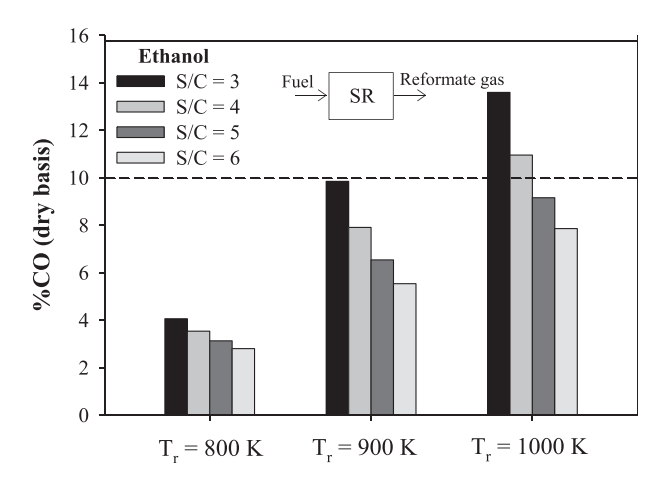


Fig. 3. %CO in the reformate gas from ethanol steam reforming at different operating conditions.

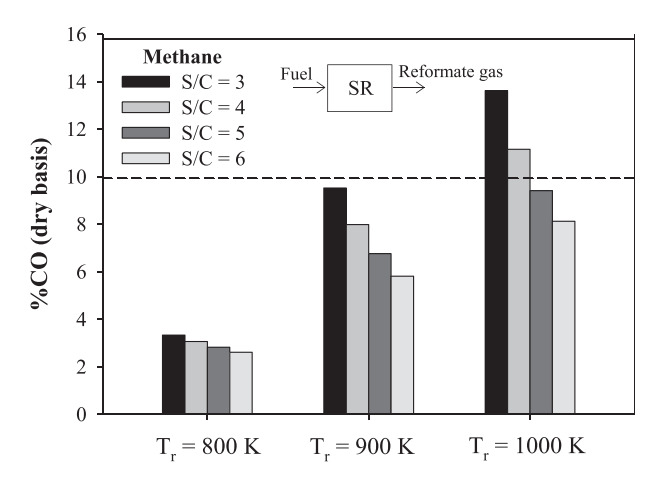


Fig. 4. %CO in the reformate gas from methane steam reforming at different operating conditions

reformer feeds (i.e., fuel and water). The amount of the recovered heat is calculated from enthalpy changes.

4. Results and discussion

A comparison of the different fuels, i.e., glycerol, methanol, ethanol and methane, used for the steam reforming process to produce hydrogen-rich gas for the HT-PEMFC is investigated in this work. The integrated steam reforming and HT-PEMFC systems with and without a water-gas shift reactor are considered. The suitable operating conditions of the steam reformer are first determined by considering the quantity of CO in the obtained reformate gas. Subsequently, the performance of the HT-PEMFCs using different fuel feedstock is analyzed.

The presence of CO (dry basis) in the reformate gas derived from the reforming of glycerol, ethanol, methane and methanol is shown in Figs. 2–5, respectively. A similar %CO trend is observed for all of the fuel types; the %CO increases as the temperature increases but decreases as the steam-to-carbon feed ratio (S/C) increases. This implies that high S/C and low temperature are the favorable operating conditions for producing reformate gas for HT-PEMFCs. Considering the steam reforming of glycerol and ethanol (Figs. 2 and 3), %CO is lower than 10%, the highest CO tolerance value of the HT-PEMFC [30,31], when the reformer is operated at low

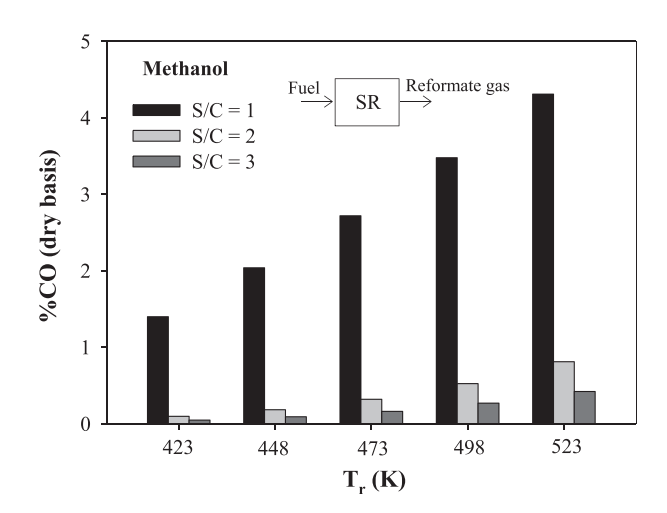


Fig. 5. %CO in the reformate gas from methanol steam reforming at different operating conditions.

temperatures (800–900 K) for all of the studied S/C ratio conditions. However, at the reformer temperature of 1000 K, %CO is higher than 10% when the reformer is operated at an S/C ratio of less than 5. Therefore, to keep the %CO in the reformate gas lower than 10%, the glycerol and ethanol reformers should not be operated at a temperature of 1000 K and an S/C of less than 5. For the methane steam reforming (Fig. 4), a considerable CO content is generated by this process. The operation of the methane reformer at a temperature of 1000 K is unacceptable for HT-PEMFCs at all S/C ratios. However, the steam reforming of methanol, which favors mild conditions, produces an acceptable CO fraction in the reformate gas; the presence of CO in the reformate gas is less than 5% at all of the studied operational ranges (see Fig. 5).

From the simulation results, it can be concluded that to keep the CO concentration at an acceptable level, the glycerol and ethanol reformers can be operated at high temperatures (1000 K) and that the operating S/C ratio should be higher than 5. However, the methane reformer should be operated at a temperature lower than 1000 K for all of the studied S/C ratios to avoid the presence of CO in the reformate gas over the limit. Otherwise, a CO purification unit must be included in the fuel processor. That being so, methanol is an attractive fuel for HT-PEMFCs because the reformate gas produced from the steam reforming of methanol at all studied operating conditions can be used directly in HT-PEMFC. Moreover, the optimal conditions that result in a high hydrogen level (high S/C and temperature) can be applied to control the reformer with no concern about the amount of CO in the reformate gas. In contrast, the reformer operations of glycerol, ethanol and methane are limited by the CO problem. In this work, the reforming conditions that result in %CO values lower than 10% are used to further investigate the performance and efficiency of the integrated HT-PEMFC system. Under such a constraint, although the selection of the reforming operating conditions for glycerol, ethanol and methane used to produce hydrogen-rich gas for HT-PEMFCs is not based on the conditions that produce high hydrogen yield, these conditions constitute the operational boundary of the steam reformer for the HT-PEMFC. In general, the performance and efficiency of the HT-PEMFC system do not depend on only the CO concentration but also rely on the hydrogen fraction and energy consumption in the system. The operating conditions of the steam reformer that give the lowest CO fraction may not present the highest efficiency.

When a water-gas shift reactor is included in the fuel processor to treat the reformate gas from the steam reformer before it is fed into the HT-PEMFC (Figs. 6—9), the CO fraction in the reformate gas

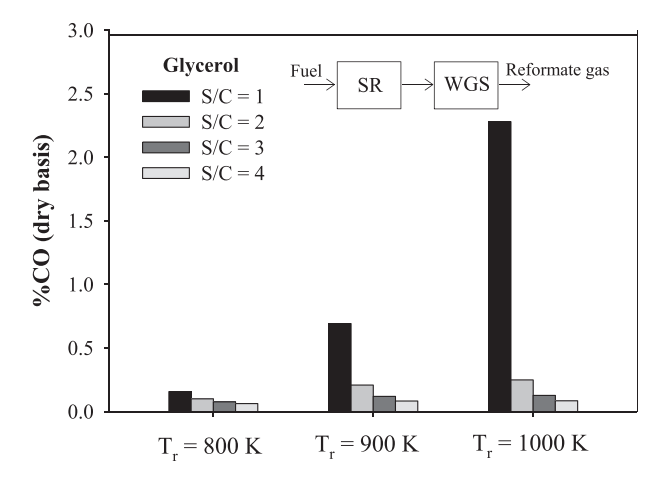


Fig. 6. %CO in the reformate gas from glycerol steam reforming with a water-gas shift reactor at different operating conditions.

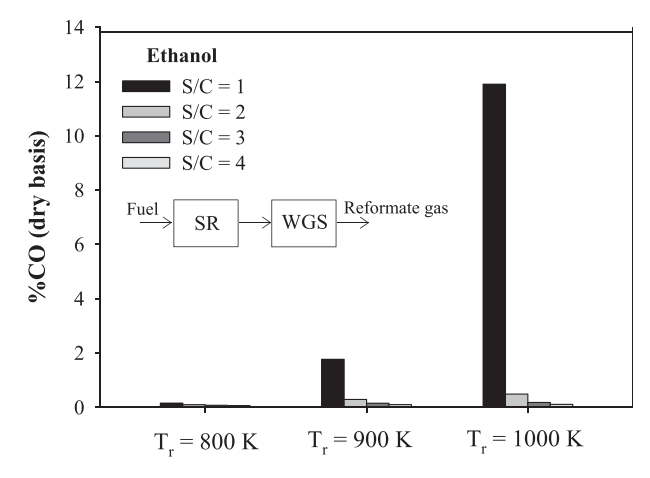


Fig. 7. %CO in the reformate gas from ethanol steam reforming with a water-gas shift reactor at different operating conditions.

of the glycerol and methanol steam reforming is reduced under 2.5% in all of the studied operational ranges. However, the ethanol and methane reformers integrated with the water-gas shift reactor produce reformate gas with high CO content when operating at a temperature of 1000 K and an S/C of one, and thus, these conditions are not selected for further study of the performance of the HT-PEMFC system. In addition, based on the steam reforming processes with and without the water-gas shift, it can be concluded that methane steam reforming has the highest possibility of CO formation, whereas the methanol steam reforming produces the lowest quantity of CO in the reformate gas. However, the presence of CO is not the only factor affecting the HT-PEMFC performance and system efficiency. The content of hydrogen, its purity, and the energy consumption of the system are also key factors.

Fig. 10 shows the electrical characteristics of the HT-PEMFC running on the reformate gas from the steam reformer when different fuels are used. A similar trend of HT-PEMFC performance is observed when glycerol, ethanol and methane are used as fuels. At high current densities, the fuel cell performance decreases when the reformer temperature increases and the S/C ratio decreases. As mentioned above, the CO formation in the reformer favors high temperatures and low S/C values. In addition, the CO content has no effect on the fuel cell performance when operated at low current density. In the case of methanol reforming, a change in the reformer operating conditions also does not affect the fuel cell performance

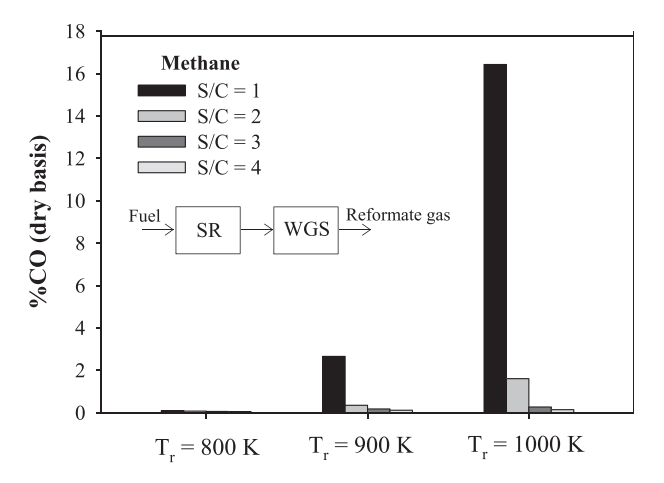


Fig. 8. %CO in the reformate gas from methane steam reforming with a water-gas shift reactor at different operating conditions.

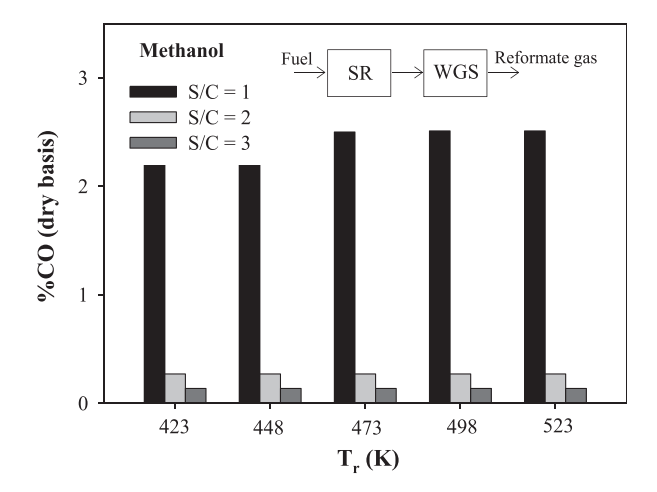


Fig. 9. %CO in the reformate gas from methanol steam reforming with a water-gas shift reactor at different operating conditions.

at low current density, but has slight effect on the fuel cell at high current density.

To determine the optimal operating conditions of the steam reformer, the efficiency of the HT-PEMFC system fed by different fuels at various operational conditions is considered. Fig. 11 indicates that the HT-PEMFCs integrated with the steam reforming processes of glycerol, ethanol and methane shows similar trends. At low current density, the efficiency of the HT-PEMFC system is enhanced when the steam reformer is operated at high temperatures and low S/C ratios. In addition to the hydrogen and CO fractions, the system efficiency also depends on the energy consumption. Because CO has a small effect on cell performance at low current density, the operation of the reformer at a high S/C ratio, at which a high level of energy consumption is required to diminish the formation of CO, would be unnecessary. However, the system efficiency is reduced at high current density when the

steam reformers are operated at high temperatures and low S/C ratios. This is because CO significantly affects the HT-PEMFC performance when operated at high current density. For the HT-PEMFC integrated with methanol steam reforming, a change in the reforming temperature has no effect on the system efficiency because of low CO content in the reformate gas obtained from the methanol steam reformer. In addition, increasing the S/C ratio to prevent the occurrence of CO is unnecessary. The reformer operated at an S/C ratio of one provides the highest system efficiency. It can be seen that the amount of CO containing in the reformate gas from the methanol reformer has an insignificant effect on HT-PEMFC performance and this result is in agreement with the previous study on HT-PEMFC run on synthesis gas from the reforming of methanol [32].

When considering the efficiency and performance of the HT-PEMFC system with the WGS reactor, the simulation results show that changing the reformer temperature and S/C ratio exerts an insignificant impact on the HT-PEMFC performance, even when different types of fuel are employed. This is because the fraction of CO at the outlet of the WGR reactor is lower than 3%, and thus, the CO poisoning effect on the HT-PEMFC system is small. In addition, the hydrogen content in the reformate gas at the outlet of the WGR reactor is almost the same. However, the efficiency of the HT-PEMFC system with a WGS reactor fed by different fuels varies with the operational conditions of the steam reformer, as shown in Fig. 12. The energy consumption values under different reforming conditions are the main reason underlying the variation of the system efficiency.

The optimal operating conditions of the steam reformer with the highest system efficiency when the HT-PEMFC is operated at voltage of 0.65 V are shown in Table 3. It is seen that the methanol steam reformer can be operated at lower temperatures and S/C ratio. The hydrogen fraction obtained under such optimal conditions is shown in Fig. 13. The methanol and methane reformers achieve the highest hydrogen concentrations when the WGS reactor is not considered in the system, whereas the glycerol

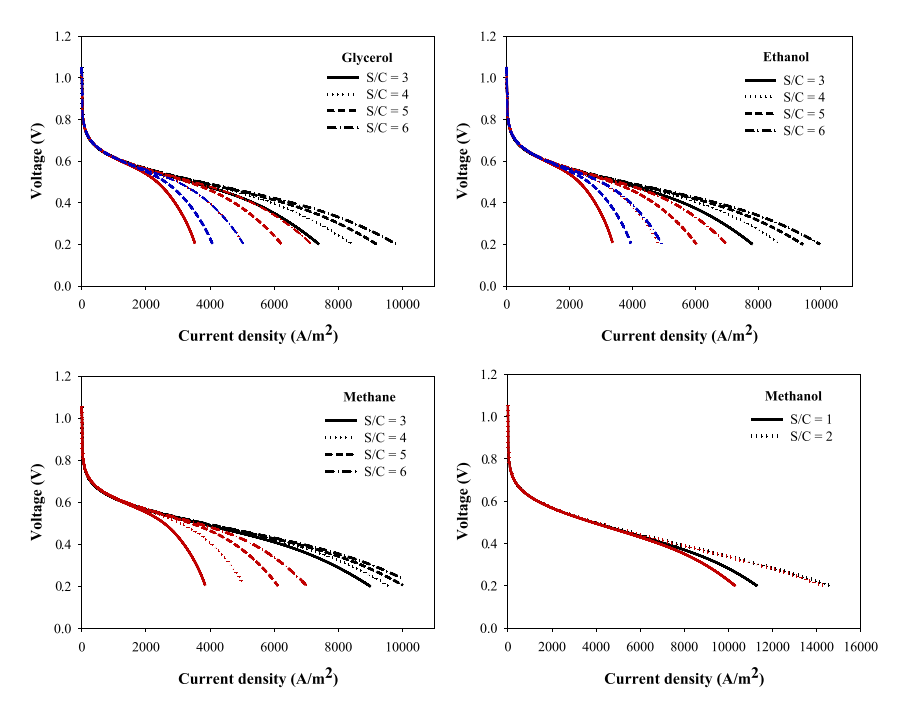


Fig. 10. Polarization curve of the HT-PEMFC fed by the reformate gas from the steam reformer (without the WGS reactor) operated at different S/C ratios and temperatures (for glycerol, ethanol and methane, the black, red and blue lines represent temperatures of 800 K, 900 K and 1000 K, and for methanol, the black and red lines represent temperatures of 448.15 K and 473.15 K, respectively). (For interpretation of the references to colour in this figure legend, the reader is referred to the web version of this article.)

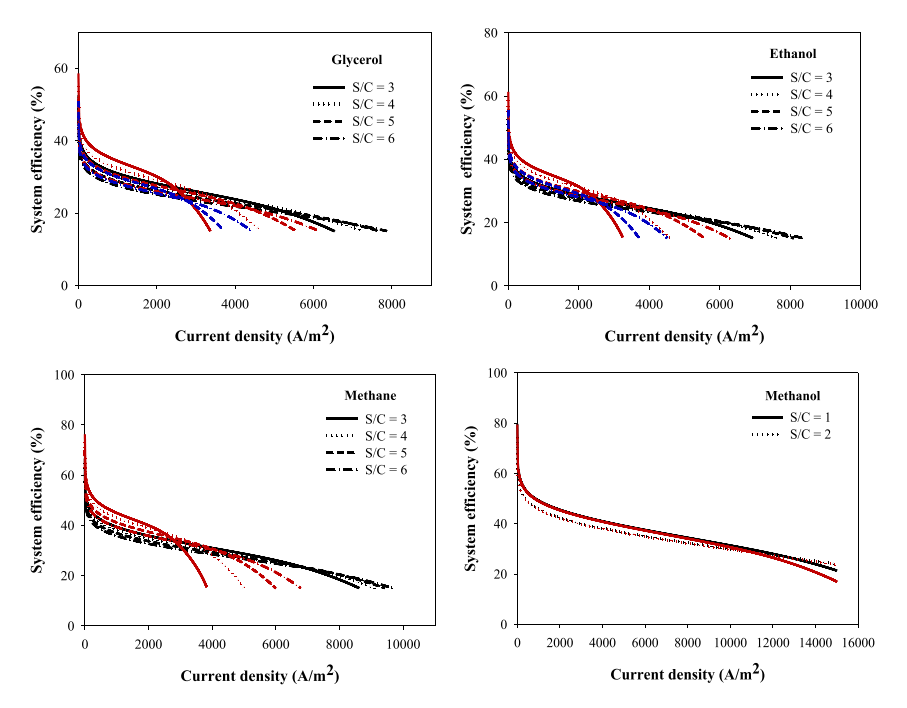


Fig. 11. Efficiency of the HT-PEMFC system fed by the reformate gas from the steam reformer (without the WGS reactor) operated at different S/C ratios and temperatures (for glycerol, ethanol and methane, the black, red and blue lines represent temperatures of 800 K, 900 K and 1000 K, and for methanol, the black and red lines represent temperatures of 448.15 K and 473.15 K, respectively). (For interpretation of the references to colour in this figure legend, the reader is referred to the web version of this article.)

reformer produces the lowest hydrogen fraction. In addition, the hydrogen fraction is increased when the WGS reactor is included in the fuel-processing process and glycerol, ethanol and methane are used as reactants. However, the hydrogen obtained from the methanol reformers with and without WGS reactors is the same. In conclusion, the methane reformer with the WGS reactor provides a higher hydrogen fraction than the other case studies.

The efficiency of the HT-PEMFC system with and without a WGS reactor is shown in Fig. 14. For the HT-PEMFC system without the WGS reactor, the HT-PEMFC system integrated with methanol steam reforming shows the highest efficiency, followed by methane, ethanol and glycerol reforming. Although the steam reforming of methane produces reformate gas with a high CO fraction, the energy consumption of this process is lower (no heat of

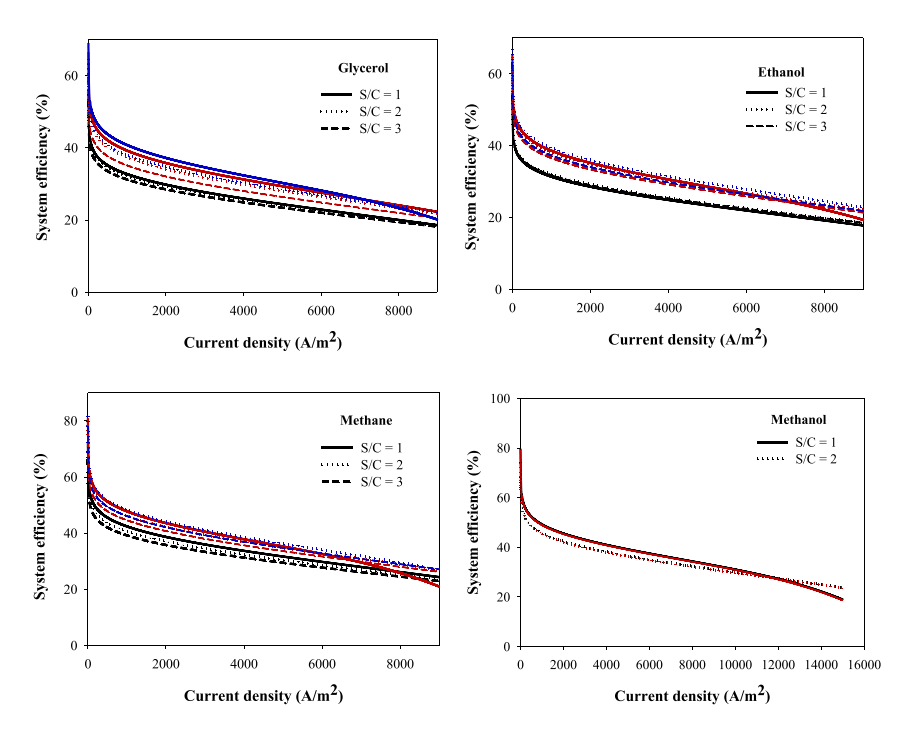


Fig. 12. Efficiency of the HT-PEMFC system fed by the reformate gas from the steam reformer (with the WGS reactor) operated at different S/C ratios and temperatures (for glycerol, ethanol and methane, the black, red and blue lines represent temperatures of 800 K, 900 K and 1000 K, and for methanol, the black and red lines represent temperatures of 448.15 K and 473.15 K, respectively). (For interpretation of the references to colour in this figure legend, the reader is referred to the web version of this article.)

Table 3Summary of the optimal conditions of the steam reformer in the PEMFC system.

Fuels	HT-PEMFC system without WGS reactor		HT-PEMFC system with WGS reactor	
	T (K)	S/C	T (K)	S/C
Glycerol	900	3	1000	1
Ethanol	900	3	1000	2
Methane	900	3	1000	2
Methanol	448.15	1	448.15	1

vaporization is consumed by this process), and the hydrogen fraction is higher than is observed in the reforming of other fuels. In the case of methanol steam reforming, the HT-PEMFC system without the WGS reactor shows higher efficiency than the system with the WGS reactor, and therefore, the WGS reactor is unnecessary for the methanol steam reforming integrated with the HT-PEMFC system. However, the performance of the HT-PEMFC system is enhanced when the WGS reactor is included in the steam reforming processes of glycerol, ethanol and methane. In addition, the HT-PEMFC system, including the steam reformer and the WGS reactor, provides the highest efficiency when methane is used as a fuel. Regarding all of the studied cases, the integrated methanol steam reforming and HT-PEMFC system without the WGS reactor and the integrated methane steam reforming and HT-PEMFC system with the WGS reactor exhibit the highest system efficiency values.

5. Conclusions

In this study, the HT-PEMFC system integrated with the steam reforming of different fuels, i.e., glycerol, ethanol, methane and methanol, is investigated to analyze effect of CO and hydrogen fraction in different reformed fuels on cell performance and find the suitable fuel for this system. The steam reforming of methanol results in the lowest CO fraction. The reformate gas obtained from the methanol reformer over the range of studied operating conditions can be fed directly to the HT-PEMFC without the need for a CO purification process; the quantity of CO is below the operational limit of the HT-PEMFC. When considering the reforming of glycerol, ethanol and methane, high S/C ratios and low temperature operation are needed to produce reformate gas with CO contents below the specified limit. A similar trend is also observed for the HT-PEMFC system with a water-gas shift (WGS) reactor. Methanol is the most favorable fuel for the HT-PEMFC system as it results in low

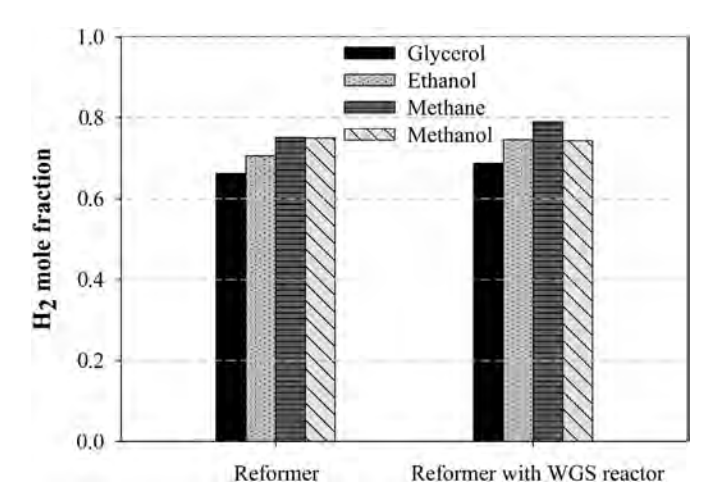


Fig. 13. Mole fraction of hydrogen at the optimal conditions of the reformer with and without the WGS reactor.

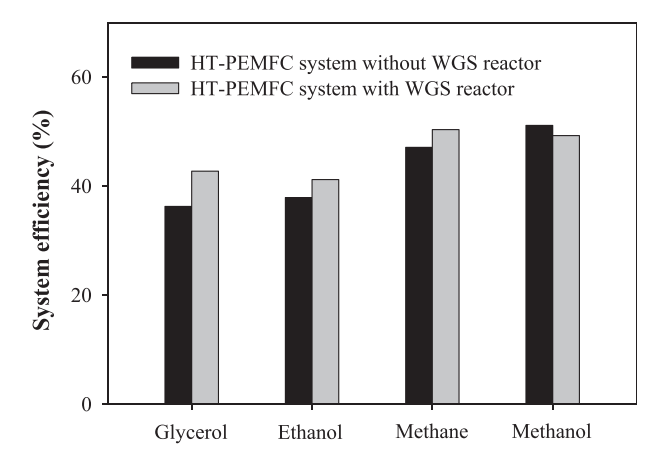


Fig. 14. Comparison of the HT-PEMFC systems with and without the WGS reactor.

CO formation. The reformer operations of glycerol, ethanol and methane strongly affect the HT-PEMFC performance, especially at high current density. The inclusion of the WGS reactor in the reforming processes of glycerol, ethanol and methane can improve the efficiency of the HT-PEMFC system, whereas the WGS reactor is unnecessary for methanol steam reforming integrated with HT-PEMFC. The integrated methanol steam reforming and HT-PEMFC system without the WGS reactor and the integrated methane steam reforming and HT-PEMFC system with the WGS reactor achieve the highest system efficiency values.

Acknowledgments

Support from the Srinakharinwirot University, the Ratch-adaphiseksomphot Endowment Fund of Chulalongkorn University (RES560530067-EN) and the Thailand Research Fund is gratefully acknowledged.

Nomenclature

HOIIICII	inter c
$C_{\rm dissolve}$	equilibrium concentration, mole cm ⁻³
C_{Pt}	concentration on the catalyst surface, mole cm ⁻³
$C_{ ext{Pt}}^{ ext{ref}}$	reference concentration on the catalyst surface,
	mole cm ⁻³
$D_{ij}^{ m eff} \ E_{ m cell}$	binary diffusion coefficient, m ² s ⁻¹
E_{cell}	cell voltage, V
$E_{\rm r}$	reversible cell potential, V
F	Faraday constant, 96,485 C mol ⁻¹
G	Gibb free energy, J mol ⁻¹
Н	enthalpy, J mol ⁻¹
Km	proton conductivity of LT-PEMFC, S cm ⁻¹
L_{c}	catalyst loading, mg cm ⁻²
LHV	lower heating value, kJ mol ⁻¹
N	molar flux, mol s^{-1} m ⁻²
P	pressure, atm
P_{FC}	power output of fuel cell, W
Q_{ref}	heat required for the steam reforming process, J s ⁻¹
Q_{rec}	heat recovery for the steam reforming process, J s ⁻¹
R	gas constant (=8.314), J mol^{-1} K ⁻¹
RH	relative humidity
S_{Pt}	real platinum surface area
T	cell temperature, K
X	mole fraction
i	current density, A m ⁻²
i_0	exchange current density, A m ⁻²
$l_{\rm m}$	membrane thickness, m
m	molar flow rate, mol s^{-1}

Greek letters

 α transfer coefficient γ reaction order λ water content

 $\begin{array}{ll} \theta_{\text{CO}} & \quad \text{CO coverage} \\ \theta_{\text{H}} & \quad \text{H}_{2} \text{ coverage} \end{array}$

 $\sigma_{\rm m}$ proton conductivity, S cm⁻¹

 η_{ohmic} ohmic loss, V activation loss, V η_{act} system efficiency

Subscripts and superscripts

a anode c cathode m membrane

i,j components "i" and "j"

in inlet stream out outlet stream

References

- Ouzounidou M, Ipsakis D, Voutetakis S, Papadopoulou S, Seferlis P. A combined methanol autothermal steam reforming and PEM fuel cell pilot plant unit: experimental and simulation studies. Energy 2009;34:1733–43.
- [2] Chutichai B, Authayanun S, Assabumrungrat S, Arpornwichanop A. Performance analysis of an integrated biomass gasification and PEMFC (proton exchange membrane fuel cell) system: hydrogen and power generation. Energy 2013;55:98—106.
- [3] Zhang J, Xie Z, Zhang J, Tang Y, Song C, Navessin T, et al. High temperature PEM fuel cells. J Power Sources 2006;160:872–91.
- [4] Xing L, Mamlouk M, Scott K. A two dimensional agglomerate model for a proton exchange membrane fuel cell. Energy 2013;61:196–210.
- [5] Kumar PM, Parthasarathy V. A passive method of water management for an air-breathing proton exchange membrane fuel cell. Energy 2013;51:457–61.
- [6] Asensio JA, Gomez-Romero P. Recent developments on proton conducting poly(2,5 benzimidazole) (ABPBI) membranes for high temperature polymer electrolyte membrane fuel cell. Fuel Cells 2005;5:336–43.
- [7] Li Q, Jensen JO, Savinell RF, Bjerrum NJ. High temperature proton exchange membranes based on polybenzimidazoles for fuel cells. Prog Polym Sci 2009;34:449-77.
- [8] Bellows RJ, Marucchi-Soos EP, Buckley DT. Analysis of reaction kinetics for carbon monoxide and carbon dioxide on polycrystalline platinum relative to fuel cell operation. Ind Eng Chem Res 1996;35:1235–42.
- [9] Arsalis A, Nielsen MP, Kær SK. Modeling and off-design performance of a 1 kWe HT-PEMFC (high temperature-proton exchange membrane fuel cell)based residential micro-CHP (combined-heat-and-power) system for Danish single-family households. Energy 2011;36:993—1002.
- [10] Oh SD, Kim KY, Oh SB, Kwak HY. Optimal operation of a 1-kW PEMFC-based CHP system for residential applications. Appl Energy 2012;95:93–101.
- [11] Leo TJ, Durango JA, Navarro E. Exergy analysis of PEM fuel cells for marine applications. Energy 2010;35:1164–71.
- [12] Falco MD. Ethanol membrane reformer and PEMFC system for automotive application. Fuel 2011;90:739–47.

- [13] Agrell J, Birgersson H, Boutonnet M. Steam reforming of methanol over a Cu/ZnO/Al₂O₃ catalyst: a kinetic analysis and strategies for suppression of CO formation. J Power Sources 2002;106:249–57.
- [14] Oliva DG, Francesconi JA, Mussati MC, Aguirre PA. Energy efficiency analysis of an integrated glycerin processor for PEM fuel cells: comparison with an ethanol-based system. Int J Hydrogen Energy 2010;35:709—24.
- [15] Lopes DG, da Silva EP, Pinto CS, Neves NP, Camargo JC, Ferreira PFP, et al. Technical and economic analysis of a power supply system based on ethanol reforming and PEMFC. Renew Energy 2012;45:205—12.
- [16] Rossetti I, Biffi C, Tantardini GF, Raimondi M, Vitto E, Alberti D. 5 kW_e + 5 kW_t reformer-PEMFC energy generator from bioethanol first data on the fuel processor from a demonstrative project. Int J Hydrogen Energy 2012;37: 8499–504.
- [17] de Lima SM, Colman RC, Jacobs G, Davis BH, Souza KR, de Lima AFF, et al. An integrated fuel processor comprising ethanol steam reforming and preferential oxidation of CO. Catal Today 2009:146:110—23.
- [18] Demirbas A. Biodiesel from waste cooking oil via base-catalytic and supercritical methanol transesterification. Energy Convers Manag 2009;50:923–7.
- [19] Byrd AJ, Pant KK, Gupta RB. Hydrogen production from glycerol by reforming in supercritical water over Ru/Al₂O₃ catalyst. Fuel 2008;87:2956–60.
- [20] Pompeo F, Santori G, Nichio NN. Hydrogen and/or syngas from steam reforming of glycerol. Study of platinum catalysts. Int J Hydrogen Energy 2010:35:8912–20.
- [21] Chen H, Ding Y, Cong NT, Dou B, Dupont V, Ghadiri M, et al. A comparative study on hydrogen production from steam—glycerol reforming: thermodynamics and experimental. Renew Energy 2011;36:779—88.
- [22] Smith JM, Van Ness HC, Abbott MM. Introduction to chemical engineering thermodynamics. 6th ed. McGraw-Hill International Edition; 2005.
- [23] Samuel DJ, Luke MN, Helena EH. Steam reforming of methanol using Cu–ZnO catalysts supported on nanoparticle alumina. Appl Catal B 2008;84:631–42.
- [24] Lima SM, Colman RC, Jacobs G, Davis BH, Souza KR, Lima AFF, et al. Hydrogen production from ethanol for PEM fuel cells. An integrated fuel processor comprising ethanol steam reforming and preferential oxidation of CO. Catal Today 2009:146:110–23.
- [25] Adhikari S, Fernando SD, To SDF, Bricka RM, Steele PH, Haryanto A. Conversion of glycerol to hydrogen via a steam reforming process over nickel catalysts. Energy Fuel 2008;22:1220–6.
- [26] Olivieri A, Vegliò F. Process simulation of natural gas steam reforming: fuel distribution optimisation in the furnace. Fuel Process Technol 2008;89:622— 32
- [27] Authayanun S, Wiyaratn W, Assabumrungrat S, Arpornwichanop A. Theoretical analysis of a glycerol reforming and high-temperature PEMFC integrated system: hydrogen production and system efficiency. Fuel 2013;105:345–52.
- [28] Mamlouk M, Sousa T, Scott K. A high temperature polymer electrolyte membrane fuel cell model for reformate gas. Int J Electrochem 2011;2011:1– 18
- [29] Authayanun S, Mamlouk M, Scott K, Arpornwichanop A. Comparison of hightemperature and low-temperature polymer electrolyte membrane fuel cell systems with glycerol reforming process for stationary applications. Appl Energy 2013;109:192–201.
- [30] Mamlouk M, Scott K. The effect of electrode parameters on performance of a phosphoric acid-doped PBI membrane fuel cell. Int J Hydrogen Energy 2010;35:784–93.
- [31] Jiao K, Alaefour IE, Li X. Three-dimensional non-isothermal modeling of carbon monoxide poisoning in high temperature proton exchange membrane fuel cells with phosphoric acid doped polybenzimidazole membranes. Fuel 2011;90:568–82.
- [32] Pascual ER, Soler J. Modelling of an HTPEM-based micro-combined heat and power fuel cell system with methanol. Int J Hydrogen Energy 2014;39: 4053—9.